Volume 1 | Issue 1 | 2019

Technical Journal

Engineering excellence around the globe

N LAVALIN

Foreword

Chris Hendy

Editor-in-Chief

FREng, MA (Cantab) CEng FICE Eur Ing
Technical Director, Atkins Fellow,
Professional Head of Bridge
Engineering
Engineering, Design and Project
Management
Epsom, UK

Welcome to the first issue of our new SNC-Lavalin Technical Journal, established to showcase the fantastic depth and breadth of our engineering technical excellence.

This issue reflects what SNC-Lavalin really excels at: we extend the safe and economic operation of existing assets and we plan, design and construct new assets for a safe and sustainable future.

The papers highlight our impressive credentials across all of our Sectors. We have monitored deflections and strains in structures over water, rail and road using our pioneering contactless digital image correlation expertise. We have developed innovative techniques to anticipate and prevent problems in oil and gas production processes, eliminating costly shut-downs. We have mapped geohazards using publicly-available satellite imagery to improve preparedness for flooding events. As well, we have brought our structural expertise to bear in Ecuador in rapidly assessing damage to buildings following the 2016 earthquake.

Our design capability is equally impressive and it's clear that designing for safety and whole life performance is embedded in our organisation. We have advanced the efficiency and buildability of integral bridges and brought innovation to the design of metro ventilation systems and platform edge screens. We also play a key role in transport safety, such as by checking the design integrity of aircraft landing gear and the design crashworthiness of trains through complex numerical simulations.

The above examples provide only a small insight into the wealth of innovative papers presented in this journal and the contribution that SNC-Lavalin makes every day to build what matters.

I hope you enjoy this selection of papers.

Editor-in-Chief

Chris Hendy

Editor-in-Chief

FREng, MA (Cantab) CEng FICE Eur Ing
Technical Director, Atkins Fellow,
Professional Head of Bridge
Engineering
Engineering, Design and Project
Management
Epsom, UK

2018-2019 Editorial Board Members

Ramy Azar

Ph.D, Ing.

Vice-President, Engineering & Chief
Technology Officer
Clean Power
Montreal, Canada

Vinod Batta

Ph.D., P.Eng.

Vice-President, Engineering & Chief
Technology Officer, Hydro
Clean Power
Vancouver, Canada

Eric Chui Hon Man

BEng CEng ACGI MHKIE MIMM MICE
MIStructE RPE(GEL, CVL, STL)

Divisional Director
Tunnel and Ground Engineering, EDPM
Hong Kong, China

Chad Gvozdenovic

P. Eng.

Vice President, Global Technical Lead
Oil & Gas
Calgary, Canada

Donna Huey

GISP

Atkins Fellow and Sr. Vice President,
Client Technology Director
Engineering, Design and Project
Management
Orlando, FL, USA

Matt Keys

PhD BEng CEng

Fellow, Technical Director, Global
Technical Authority – Offshore
Structures
Oil & Gas
Perth, Australia

Samuel Fradd

Technology Manager
Engineering, Design and Project
Management
Epsom, UK

Adrian Lindon

BA(Hons) Dip. Arch, ARB, RIBA

Managing Director, Design and
Engineering (Middle East)
Engineering, Design and Project
Management
Dubai, UAE

Navil Shetty

PhD, DIC, FIAM

Atkins Fellow and Technical Chair for
Asset Management
Centre of Excellence for Digital Asset
Management & Operations
Bangalore, India

Patrick Sikka

P. Eng

Vice-President, Engineering
Mining & Metallurgy
Toronto, Canada

Akshaye Sikand

MS, P.Eng.

Manager, Knowledge Management
Global Projects Support
Toronto, Canada

Production Team

Dorothy Gartner

MLIS

Librarian
Global Projects Support
Montreal, Canada

Graphic Design Team

Montreal, Canada

Volume 1 | Issue 1 | 2019

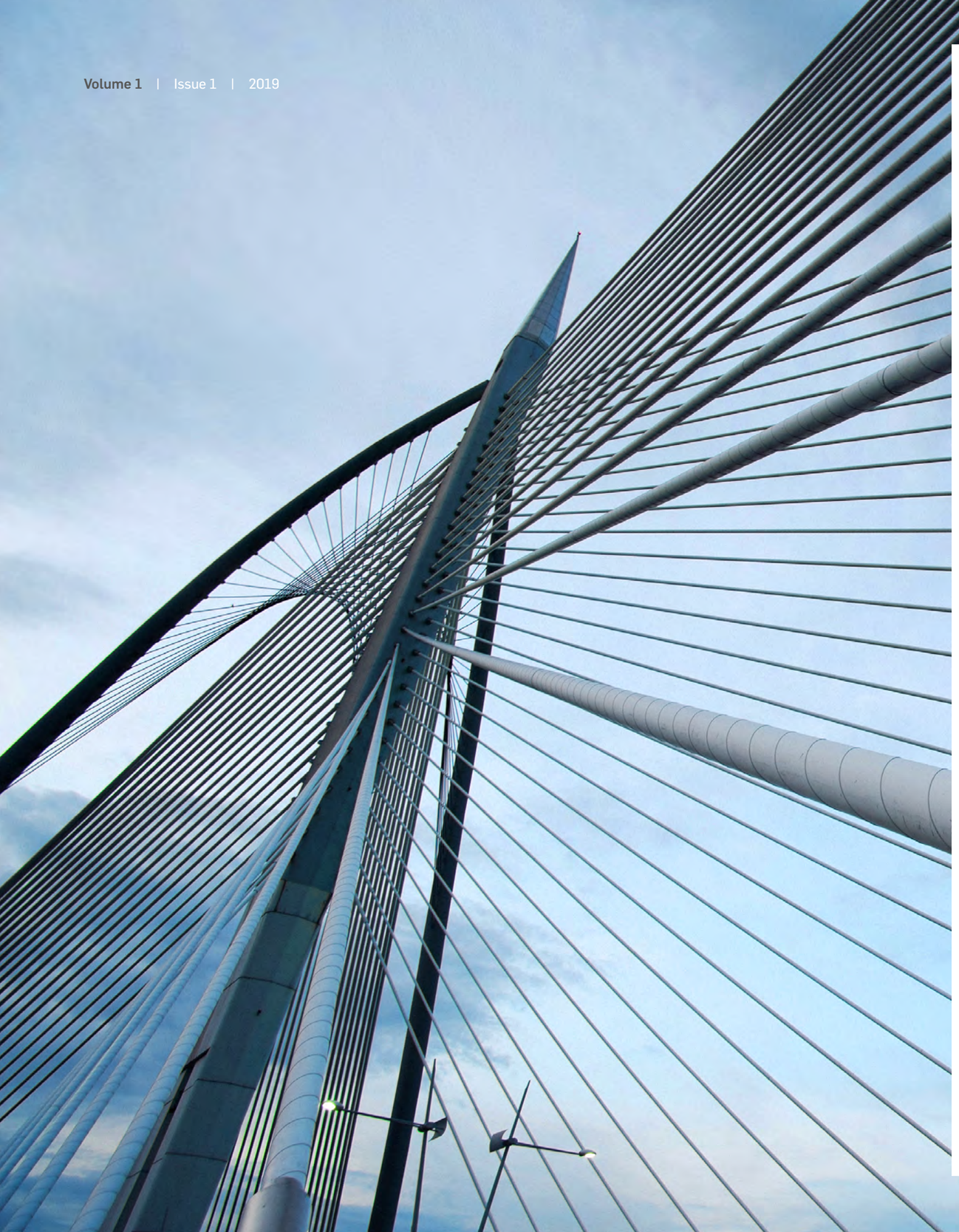

Remote Monitoring & Non-Destructive Testing

Structural Design

Structural Assessment

Safety

Mechanical and Electrical Design

Geotechnics and Tunneling

Water Management

Adapting Ultrasonic Inspection of Structural Steel Welds for Use With Distance-Amplitude Techniques

Paul Holloway

Holloway NDT & Engineering Inc.
Georgetown, ON, Canada

Sean Keay

Contract Engineering Lead
Infrastructure, O&M
St. John's, NL, Canada

Andrew Crawford

Buffalo Inspection Services
Edmonton, AB, Canada

Viwek Vaidya

Techno Vogue Inc.
Beaconsfield, QC, Canada

Abstract

Ultrasonic testing (UT) of welds to CSA W59 is based on techniques dating back the late 1960's with the original inception of UT into AWS D1.0. Since the original development, there has been significant progress in UT technologies, yet North American codes have failed to keep pace. The foundation of the W59/D1.1 approach is to manually or programmatically calculate attenuation using a linear approximation of 2 dB per inch. This approach places restrictions on equipment, incurs calibrations indicative of the analog era, and uses prescriptive procedure tables and angle-specific acceptance criteria. The protocols associated with these procedures have outlived their usefulness, and unnecessarily inhibit progress in adapting to more suitable transducers and newer technologies such as phased array. An overview of the proposed changes to W59 currently under review are presented. The differences between the 2 dB factor and actual attenuation are determined through simulation and experiment, providing the basis of the corrections applied to the existing acceptance tables, adapted for use with distance amplitude techniques. The new technique is shown to improve repeatability, and allows for a broader range of transducers while still maintaining equivalent quality levels. It also offers schedule advantages when correctly applied.

We are at a point in our civilization where the rate of change of technology is fast heading vertical; to stay with the status quo will ultimately render us uncompetitive and compromise our national supply chain. Adoption and advancement are the future that we must pursue.

This was written prior to the release of CSA W59-18.

Keywords

Time-Corrected Gain (TCG); Distance-Amplitude Curve (DAC); Phased Array Ultrasonic Testing (PAUT); Weld Inspection

1. Introduction

The ultrasonic testing techniques in the Canadian code for welded steel construction, CSA W59, are found in Clause 8.2 [1]. These techniques have served the industry well for nearly 50 years, and are virtually identical to those of AWS D1.1 Clause 6 [3]. They were developed in the late 1960s and first appeared as part of AWS D1.0 (1969) Appendix C[2]. At the time, this represented a major shift forward in providing an alternative to industrial radiography for volumetric weld inspection. However, these techniques have remained largely unchanged while ultrasonic technology and other codes have advanced significantly. The existing techniques are based on outdated equipment and approximations , making it impossible to conform to modern practices. CSA W59, AWS D1.1 and AWS D1.5[4] all use a "one size fits all" large, low frequency transducer and 2 dB/inch estimate of attenuation. They remain only major codes worldwide to assume this approach to transducers and attenuation. The equipment limitations, prescriptive procedures, and sizing calculations make inspection time consuming and confusing for the inspector, oftentimes resulting in shortcuts and use of improper transducers. The existing technique has reached the end-of-life, and has for many years been restrictive towards progress.

This paper details the pending changes to ultrasonic inspection of structural steel welds as part of Canadian code CSA W59 in 2018. The technical limitations related to the use of the 2 dB per inch model for attenuation are highlighted. It describes the adoption of the Time Corrected Gain (TCG) technique for sensitivity calibration, common in most other weld inspection codes. The advantages of using a TCG, and how the existing acceptance criteria were adapted for its use are also discussed. Other changes to the code under review including flaw length sizing [5], calibration schemes, and updated terminologies are not addressed in this paper.

Because of the international nature of these techniques, metric and U.S. units are used interchangeably throughout.

2. Need for Change

The question prior to any change to a long-standing practice is: "why fix what ain't broke?". Whilst workmanship acceptance criteria are conservative and have a successful history, modern fabrication methods require a more flexible approach that does not repair what are essentially harmless defects that have been sentenced through subjective engineering assessment rather than empirical evaluation. The system is indeed "broken down" as it pertains to practicality and repeatability, resulting in numerous shortcuts taken in the field and a lack of understanding by the common inspector.

Many inspectors shy away from structural work due in large part to the archaic fixed attenuation estimates requiring the "D = A – B - C" calculation for indication rating. Many do not understand the correlation between the large probe and the 2 dB/inch attenuation estimate, hence different probes are substituted in the field. The 2 dB/inch estimate has its shortcomings (Section 4.1), and substitution with a different probe only makes things worse. There are many idiosyncrasies in W59 that can simply be replaced by modern, sensible processes that are easier to understand and to practice.

Advancements in ultrasonic testing now enable us to size things three-dimensionally rather than simply in one dimension. The proposed advances in the code pave the way for adoption of these newer technologies.

It is stressed that the changes presented do not adversely affect the conservative practices and acceptance levels of the code as practiced for decades. The revisions proposed herein are intended to provide a more practical approach to the test procedure, which is intended to result in more precise and accurate examinations.

3. Elements of the Existing Technique

The existing techniques in CSA W59 are based on a workmanship approach in which indications are graded based primarily on their amplitudes. It is well known that indication amplitude may have little correlation to flaw size due to the anisotropic and fractal nature of real weld flaws. Misconceptions regarding workmanship based criteria have been presented before, and as a reminder it should be stressed that the actual function of a workmanship approach is to assess weld quality, not integrity [6]. Workmanship inspections are fundamentally conservative, oftentimes calling for the removal of innocuous slag or porosity colonies posing little or no threat to weld integrity. Ironically, the act of repairing of such defects could be more detrimental than the defects themselves. However, a workmanship approach is much easier to apply than a fracture mechanics approach where defect characterization and height measurements are required.

The existing technique (herein referred to as the "fixed attenuation" or "FA" technique) utilizes a relatively large, low frequency transducer coupled to a correspondingly large wedge. The size, shape and frequency ranges are restricted to keep attenuation close to an assumed rate of 2 dB/inch. The reference level is then conveniently set at a single point: the 1.5 mm (0.06 inch) hole in the IIW-Type block. For examination, the user must adhere to procedure tables dictating the refracted angle(s) used based on the weld thickness category, and refer to tables for scanning gains according to sound path. During evaluation of indications, the indication rating is calculated by subtracting the indication level from the reference level, then subtracting 2 dB/inch (after the first inch of sound path). The resulting severity rating is then compared to a table for classification as "Large", "Minor" or "Small" for disposition (or Class A, B, or C is AWS).

Regardless of weld geometry, the code assumes 70° as the "most desirable" angle [2] and enlists it as the primary angle for thicknesses up to 90 mm (3 ½ inches).

4. Drawbacks

In the past 50 years since the FA technique was developed, digital equipment has replaced analog, and ultrasonic inspection is now commonplace in industry. The main advantage of the technique is a one-point calibration for sensitivity. But this simplification comes at a cost: bulky search units, prescriptive procedure tables and angle-specific acceptance criteria.

The drawbacks of the FA technique can be placed in two general categories (Table 1) and are detailed in the sections that follow.

4.1. Error Incurred by the 2 DB Per Inch Approximation

Attenuation of ultrasonic waves is not a linear function. It is presumed that the authors of the original FA technique were aware of this, and decided upon a constant value of 2 dB/inch based on empirical results. Computer simulation shows that attenuation from the standard 5/8 inch square, 2.25 MHz transducer is indeed about 2 dB/inch if taken over very long sound path distances [10]. However, over the distances typically used during inspection, using 2 dB/inch will underestimate actual attenuation. The implications of this are discussed in Section 6.

4.2. Large Search Units Inhibit Inspection Access

At present, the FA technique prescribes a relatively narrow range for allowable transducer sizes and frequencies. Often, the typical selection is the square 5/8" or ¾" transducer mated to a "big red brick" or "snail" wedge. These wedges are difficult to maneuver in tight quarters, and the large surface areas may make coupling difficult.

Besides their cumbersome nature, they are simply unsuitable for the full range of thicknesses required (8 to 200 mm). The large wedge size prohibits access close to the weld cap, oftentimes requiring the weld root be inspected on the 3rd leg (1.5 skips). This is something generally avoided in ultrasonic testing.

4.3. Preference for 70° Angle

The selection of the 70° as the "most desirable angle" is based on direct reflection from the face of a discontinuity "most detrimental to the weld structure"[2]. In most circumstances, this would likely be a surface breaking crack or other vertical notch-like flaw producing high stress concentrations under load. Certainly, the generous beam spread afforded by using a large, low frequency transducer at a 70° angle maximizes reception of the direct reflection. However, this premise is based on optimistic expectations of scatter from the vertical face and fails to take into consideration the low reflection efficiency of beams greater than 57°.

Figure 1 (adapted from Krautkramer [11]) shows the reflection efficiency of shear waves off a vertical flaw. At an inspection angle of 70° (incident on the flaw at 20°), nearly half of the energy is lost. At 60°, only about 15% remains. These losses are primarily due to generation of mode-converted longitudinal waves. At inspection angles at or below 57° (33° incident on a vertical flaw), the shear wave reflects at maximum efficiency and generates no mode converted waves.

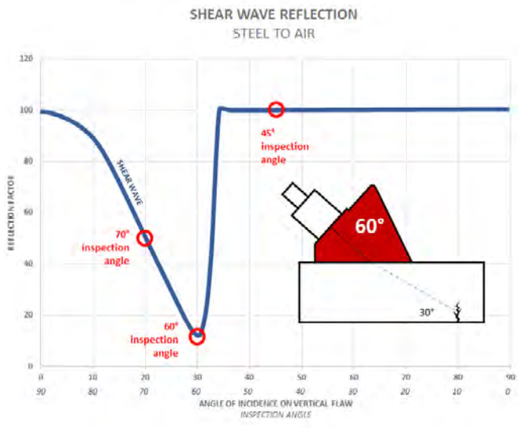

Figure 1: Reflection Efficiency of Shear Wave on Vertical Flaw

This is not to say that 45° is always a more desirable angle, nor that 60° is a poor choice. Inspection angles should be selected based on weld geometry, including bevel angle and thickness, to achieve full coverage and ensure a good POD.

Placing narrow restrictions on equipment and forcing use of prescriptive techniques, not based on science or attributable to weld geometry, is counter-productive. It harms POD and restricts inspection to a short, ineffective selection of compromises.

Table 1: Main Drawbacks of the Existing FA Technique

CATEGORY	REASON	REQUIREMENT	DRAWBACK	RESULT	SEC.
Attenuation = 2 dB/inch	Simplified sensitivity calibration	Fixed transducer size & frequency	Inaccurate for typical sound paths used	Underestimates attenuation	4.1
			"One size fits all" search unit is impractical, especially on thin welds	Wedge size too large to accommodate suitable approach distance	4.2
Angle-specific procedures and acceptance criteria	"To attain consistent results in ultrasonic weld testing it is necessary that a consistent procedure be used." [2]	Assumes 70° is the "most desirable angle", producing maximum reflection from a vertically oriented flaw (e.g. crack)	Max indication from a crack is typically the corner trap (surface breaking), maximum at angles less than 70°	Preference given to 70° ignores advantages of other angles and fails to consider weld geometry	4.3
			Many procedures require scanning from the top side (with ground profile) for detection of top side flaws - vice versa for bottom side	Low probability of detection for surface breaking flaws such as cracks	4.4

4.4. Low Probability of Detection for Near-Surface Flaws

In many places, the existing procedure table calls for near-side detection of flaws using direct reflection as shown in Figure 2.

The extremely short sound paths involved and reliance on advantageously oriented flaw surfaces make it unlikely that an inspector would be able to correctly discern a relevant indication from the wedge/steel interface echo (Figure 3). Surface breaking flaws are much more likely to be detected by reflection from the corner at half-skip or full-skip distances (Figure 4).

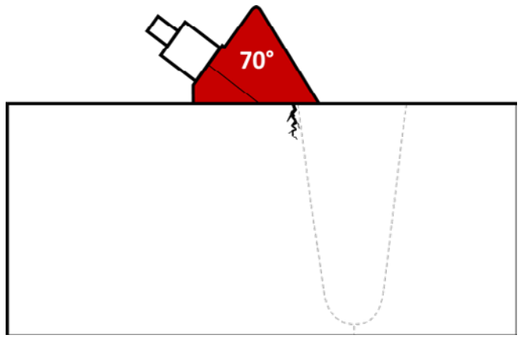

Figure 2: Procedure 6, Inspection of Top Quarter With 70°

5. Elements of the Proposed Alternate Technique

An alternate technique is proposed based on sensitivity calibration utilizing a Time Corrected Gain (TCG). This type of calibration is common in many other codes, and uses a series of reference reflectors at varying distances to accurately measure attenuation. A TCG varies from a Distance Amplitude Correction (DAC) by the fact that the reference heights are electronically normalized at a consistent screen height, aiding in identification and sizing of indications (Figure 5, Figure 6). The use of a TCG is generally preferred over a DAC for this reason.

5.1. Accurate Calibration for Sensitivity

The TCG technique is not unlike that used in ASME Sec. V Article 4 for non-piping applications. However, while ASME uses blocks with different reflector sizes based on weld thickness, the TCG technique for W59 would base sensitivity calibrations for all thicknesses on the standard 1.5 mm SDH reference reflector.

One calibration block may satisfy a range of weld thicknesses, and multiple backwall reflections may be utilized to construct a TCG over a longer sound path distance [7].

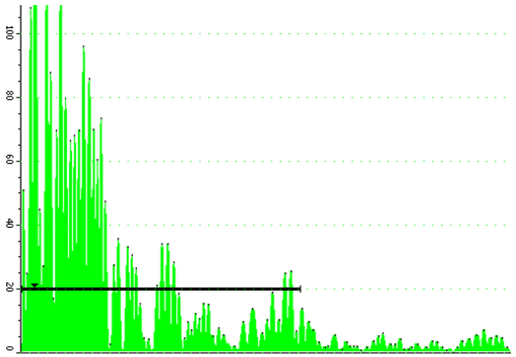

Figure 3: Inspection of Near-Side Crack Attempted as Per Figure 2. Crack Indication Obscured by Wedge-Steel Interface Echo.

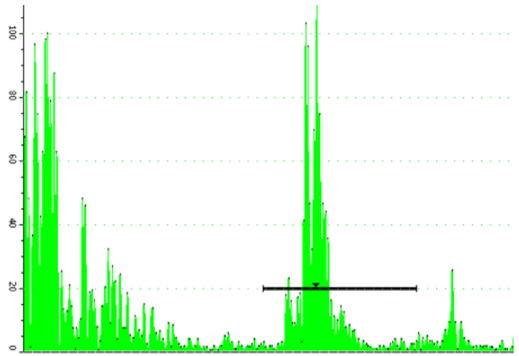

Figure 4: Inspection Performed From Opposite Face. Crack Indication Easily Resolved at Half-Skip Distance.

5.2. Wide Transducer Selection

By using a TCG for measuring attenuation, fixing the size and frequency of the transducer to fit a linear attenuation model is no longer required. A wide variety of transducers may be utilized, from sizes of 6.4 to 25 mm (1/4 to 1 inch) diameter and frequencies of 2.25 to 5 MHz.

5.3. Transducer Parameters Based on Application

As highlighted in section 4.3, a 70° angle may not always be the "most desirable". The most appropriate transducer frequency, size and angle will vary depending on weld thickness, preparation and access. Like most other codes, the operator will select the search unit to fit the needs of the inspection.

5.4. New Acceptance Criteria

The acceptance criteria have been adapted for the TCG technique to provide equivalent quality levels to the existing tables. The criteria are not bound to specific angles, and thus there is one value per rating class and weld thickness category. Development of new criteria is described in detail in Section 6.

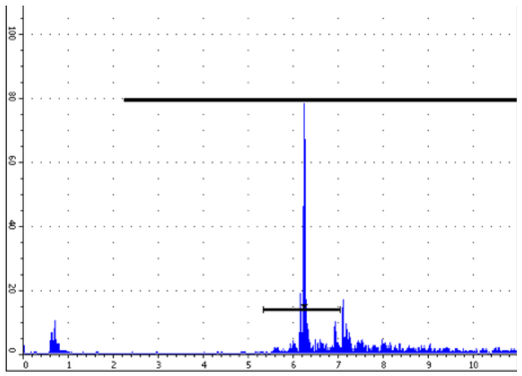

Figure 5: Time-Corrected Gain (TCG)

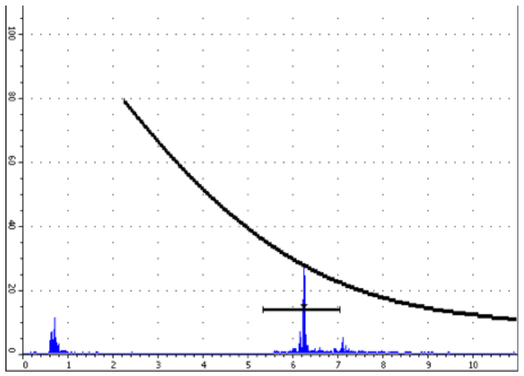

Figure 6: Distance-Amplitude Curve (DAC)

5.5. Sensible Sign Convention for Ratings

The existing FA technique uses the "low score wins" approach, i.e. a -3 dB indication represents more sound reflection than +3 dB. This is counterintuitive for ultrasonic technicians coming from any other code of practice, and is a source of confusion.

The TCG technique adopts the industry-standard "higher means bigger" sign convention. This is a more sensible approach and less prone to misinterpretation.

5.6. Possibility of Manual Phased Array

Without restriction on inspection angle, the TCG technique permits adoption of inspection using manual phased array (PAUT). PAUT provides the distinct advantage of being able to inspect with many angles at once, allowing for improved POD, geometric discrimination, and a reduction in false calls.

5.7. Other Changes

The proposals in the revised code contain numerous other corrections and improvements. These include updated periodic calibrations (horizontal and gain control linearity) as well as updated terminologies. The scope of changes is too expansive to review in full, however changes to the indication class names to match AWS D1.1 (Class A through D) is noted and used in the following sections.

6. Adapting the Acceptance Criteria

Maintaining equivalence with the existing acceptance criteria is vital to ensure portability between the FA and TCG techniques. The existing acceptance levels (CSA W59 Tables 11.3 and 12.5 [1]) are used with attenuation fixed at 2 dB/inch; a factor which is based on a specific transducer. The task at hand was to develop general acceptance criteria for any transducer by removing the influence of the 2 dB/inch model.

Adapting the criteria for use with the TCG technique was performed by first modeling the real attenuation of the standard search unit. This was then compared to the 2 dB/inch model to generate plots showing the differences between the two. Modeling was performed using CIVA simulation and verified experimentally. The procedures defined in W59 Table 8.3 (identical to AWS D1.1 Table 6.7) were compared to the acceptance criteria in Tables 11.3 and 12.5 and error values for each angle and thickness category were computed by finding the average over the sound path distances used. New tables were then generated by subtracting the error from the existing levels.

The following sections explain the process in detail.

61. CIVA Modeling of Actual Attenuation Vs. the 2 DB/Inch Model

To adapt the acceptance criteria for use with the TCG technique, the error incurred by using the 2 dB/inch model was quantified. From this, an accurate model of the standard transducer was made, and the error calculated [10].

Figure 7 shows the error incurred at 60° up to a depth of 200 mm. The discrete error values are then applied as correction factors in the construction of new tables. Using the existing procedure tables, the range of sound paths used for each angle and weld thickness are determined and the average corrections calculated.

Attenuation with the standard transducer at 45°, 60° and 70° were modeled. All models were normalized to 0 dB at a depth of 15 mm to simulate sensitivity calibration on the 1.5 mm standard reference reflector.

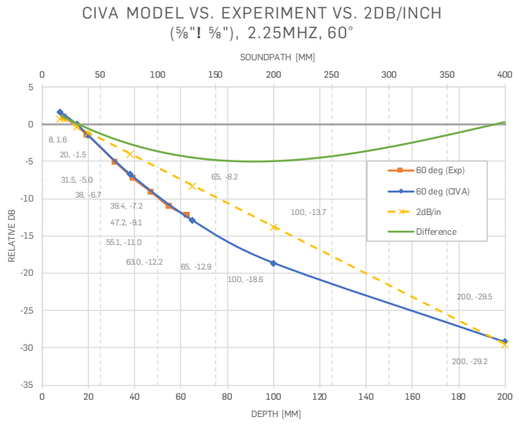

Figure 7: Example of Actual Attenuation at 60° Vs. 2 DB/in

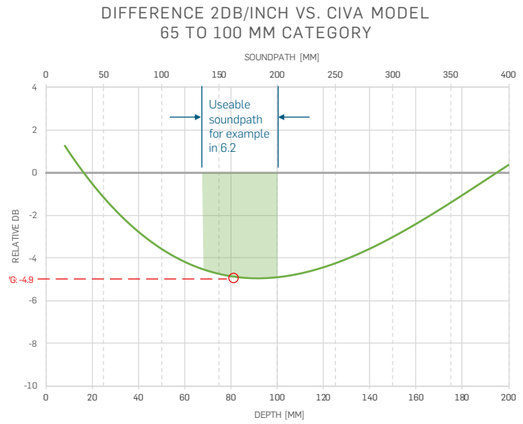

Figure 8: Determining Average Correction (60°, 65 to 100 Mm Category)

6.2. Determining Correction Factors for Each Weld Category

The differences between actual attenuation and the 2 dB/inch model are dependent upon sound path distance. As seen in Figure 7, the difference is not linear. However, it can be approximated into fixed values and applied over discrete sound path limits based on the angles of inspection prescribed in the existing procedure tables.

As an example, consider a 60° angle used on a 65 to 100 mm weld. According to the existing procedure chart in W59 and D1.1, procedures 1, 5, 6, and 7 may be used. Only procedures 6 and 7 involve a 60° angle, inspecting the bottom and top quarters from Face A and Face B. And procedures 6 and 7 are applicable only to welds over 90 mm. These procedures involve distances from 75% to full thickness, spanning a sound path of 135 to 200 mm.

The error in the 2 dB per inch approximation is displayed in Figure 8, with the area shaded in green representing the sound path limits under investigation. The average error over this range is -4.9 dB, meaning that actual attenuation is 4.9 dB more than what 2 dB per inch assumes.

Thus for a 60° angle, the 65 to 100 mm thickness category ratings are corrected by 4.9 dB, generating ratings that may be used with the TCG technique.

All angle and thickness categories are corrected in this fashion, with sound path limits based on the procedure chart as shown below in Table 2:

6.3. Removing Angle Dependency

One key improvement in the development of the TCG technique is freedom from angle-specific procedure and acceptance tables. Angle limitations were born from the idea of a "most desirable angle". As shown in 4.3, this approach likely harms probability of detection (POD) more than it helps to produce consistent results.

Removing the angle-specific nature during the development of the TCG tables was performed by taking the average of the resulting 45°, 60° and 70° levels for each thickness category. The range of values was carefully considered to ensure that averaging was appropriate for each case.

The process is shown in Table 3, up to the application of the correction values and removal of angle-dependency.

6.4. Manual Adjustments

The deconstruction and mathematical rebuilding of new tables revealed some minor inconsistencies between thickness categories. As weld thickness increases, it is logical that the indication levels would either remain the same or increase. By observing the bottom two rows in Table 3, the ratings for Class C and Class D indications decrease in the third category.

Minor +1 dB corrections are made to correct these inconsistencies (Table 4).

6.5. Revised Tables

The same corrections used in 6.3 and 6.4 are used for the criteria for statically- and cyclically-loaded structures. The final, revised acceptance criteria tables for the TCG technique are shown in Table 5 and Table 6. These are also presented graphically in Figure 11 and Figure 12.

Table 2: Calculation of Corrections Per Thickness Category

	70°					60°			45°		
Min legs:	0	0	0	0	0	1.75	0.75	0.25	1.75	1.75	0.25
Max legs:	2	2	2	1	0.75	2	1	1	2	2	1
Primary procedure(s)	1	1	1, 4, 5	1, 5-7	6-9, 11 12, 14, 15	4	6, 7	6-10	5	5	9, 11-14
Thickness Category Range											
Min:	8	20	38	65	100	38	65	100	38	65	100
Max:	20	38	65	100	200	65	100	200	65	100	200
Sound path distance											
Min:	0	0	0	0	0	133	135	55	94	161	57
Max:	117	222	380	263	395	260	200	260	184	283	283
Error (per thickness cat.)											
Min:	-2.9	-3.7	-3.7	-3.7	-3.7	-5.0	-5.0	-5.0	-1.4	-1.1	-1.4
Max:	+3.4	+3.4	+3.4	+3.4	+3.4	-4.1	-4.6	-1.6	-0.7	+0.9	+0.9
Range:	+6.3	+7.1	+7.1	+7.1	+7.1	+0.9	+0.4	+3.4	+0.7	+2.0	+2.3
Std.Dev:	+1.9	+2.0	+1.6	+1.9	+1.6	+0.2	+0.1	+0.9	+0.2	+0.6	+0.7
Avg:	-0.4	-2.0	-2.1	-2.2	-2.0	-4.7	-4.9	-4.2	-1.1	-0.1	-0.5

Table 4: Manual Corrections

	mm	8 to 20	>20 to 38	>38 to 65	>65 to 100	>100 to 200
A	Large	0	0	0	0	0
B	Small	0	0	0	0	0
C	Minor	0	0	+1	0	0
D	(N/A)	0	0	+1	0	0

Table 5: Ultrasonic Acceptance Criteria for Statically-Loaded Structures (TCG Technique)

	Weld thickness range				
	8 to 20 mm	> 20 to 38 mm	> 38 to 65 mm	> 65 to 100 mm	> 100 to 200 mm
Class	(5/16 to 3/4 in)	(> 3/4 to 1 1/2 in)	(> 1 1/2 to 2 1/2 in)	(> 2 1/2 to 4 in)	(> 4 to 8 in)
A	-5 & above	-4 & above	-3 & above	0 & above	+2 & above
B	-6	-5	-4 to -5	-1 to -2	+1 to 0
C	-7	-6	-6	-3 to -5	-1 to -5
D	-8 & below	-7 & below	-7 & below	-6 & below	-6 & below

Table 6: Ultrasonic Acceptance Criteria for Cyclically-Loaded Structures (TCG Technique)

	Weld thickness range				
	8 to 20 mm	> 20 to 38 mm	> 38 to 65 mm	> 65 to 100 mm	> 100 to 200 mm
Class	(5/16 to 1/4 in)	(> 3/4 to 1 1/2 in)	(> 1 1/2 to 2 1/2 in)	(> 2 1/2 to 4 in)	(> 4 to 8 in)
A	-10 & above	-10 & above	-9 & above	-6 & above	-3 & above
B	-11	-11	-10 to -11	-7 to -8	-4 to -5
C	-12	-12	-12	-9 to -10	-6 to -7
D	-13 & below	-13 & below	-13 & below	-11 & below	-8 & below

Table 3: Applying Correction Factors and Category Averaging (Cyclically-Loaded)

Original Table 12.5

		Minimum Acceptance Levels (dB)										
		Weld Thickness and Transducer Angle										
mm		8 to 20	>20 to 38	>38 to 65			>65 to 100			>100 to 200		
inch		5/16 to 3/4	>3/4 to 1 ½	>1 ½ to 2 ½			>2 ½ to 4			>4 to 8		
AWS Class	CSA Rating	70°	70°	70°	60°	45°	70°	60°	45°	70°	60°	45°
A	Large	+10	+8	+4	+7	+9	+1	+4	+6	-2	+1	+3
B	Small	+11	+9	+6	+9	+11	+3	+6	+8	0	+3	+5
C	Minor	+12	+10	+8	+11	+13	+5	+8	+10	+2	+5	+7
D	(N/A)	+13	+11	+9	+12	+14	+6	+9	+11	+3	+6	+8

Values Inverted

	mm	8 to 20	>20 to 38	>38 to 65			>65 to 100			>100 to 200		
	Angle	70°	70°	70°	60°	45°	70°	60°	45°	70°	60°	45°
A	Large	-10	-8	-4	-7	-9	-1	-4	-6	+2	-1	-3
B	Small	-11	-9	-6	-9	-11	-3	-6	-8	0	-3	-5
C	Minor	-12	-10	-8	-11	-13	-5	-8	-10	-2	-5	-7
D	(N/A)	-13	-11	-9	-12	-14	-6	-9	-11	-3	-6	-8

Corrections (CIVA minus 2dB/inch)

	mm	8 to 20	>20 to 38	>38 to 65			>65 to 100			>100 to 200		
	Angle	70°	70°	70°	60°	45°	70°	60°	45°	70°	60°	45°
	Correction	-0.4	-2.0	-2.1	-4.7	-1.1	-2.2	-4.9	-0.1	-2.0	-4.2	-0.5
A	Large	-10.4	-10.0	-6.1	-11.7	-10.1	-3.2	-8.9	-6.1	-0.0	-5.2	-3.5
B	Small	-11.4	-11.0	-8.1	-13.7	-12.1	-5.2	-10.9	-8.1	-2.0	-7.2	-5.5
C	Minor	-12.4	-12.0	-10.1	-15.7	-14.1	-7.2	-12.9	-10.1	-4.0	-9.2	-7.5
D	(N/A)	-13.4	-13.0	-11.1	-16.7	-15.1	-8.2	-13.9	-11.1	-5.0	-10.2	-8.5

	mm	8 to 20	>20 to 38	>38 to 65	>65 to 100	>100 to 200
A	Large	-10	-10	-9	-6	-3
B	Small	-11	-11	-11	-8	-5
C	Minor	-12	-12	-13	-10	-7
D	(N/A)	-13	-13	-14	-11	-8

7. Validation

The equivalency of the TCG acceptance criteria to the existing criteria was proven mathematically and is shown graphically in Figure 9 and Figure 10. On the left, Figure 9 shows the existing criteria overlaid with box and whisker plots demonstrating the rating variance of a 1.5 mm SDH positioned at any point within the weld. This is an effect from the of the mathematics the fit of the 2 dB/inch model, and not a function of human or equipment variance. On the right, Figure 10 shows the marked improvement in variance by using a TCG for determining attenuation. The 1.5 mm SDH reference reflector will present the same rating regardless of sound path when a proper TCG is established during calibration. The charts shown are graphical representations of the cyclic acceptance criteria, but the variability is the same for the static criteria.

There is some question as to the value of trials on welds with realistic flaws. Numerous previous trials have been conducted [12, 13, 14] that show the complexities of ultrasonic evaluation of real weld flaws and the difficulty in obtaining accurate and repeatable measurements. No two flaws are the same, and variations are expected from equipment, method, and human elements. The variation between measurements, even on those in well controlled studies, have such significant scatter that a direct comparison of the FA technique to TCG using trial samples would be inconclusive. Manual UT requires operators to manipulate the probe to obtain the optimum angle of reflection and maximize the indication height. Hand pressure on the transducer, couplant viscosity, and very minor changes in oscillation angle may make substantial differences in indication height. The normal operator-to-operator variance of amplitude-based UT, particularly on real weld flaws, far exceeds the narrow margin that would satisfy a test of equivalence. "For many ultrasonic techniques, there is no direct correlation between signal amplitude and flaw size." [19]. Comparison of workmanship techniques, with real operators inspecting real weld flaws is a bit like trying to hit a moving target. As such, mathematical modeling provides the better comparison of techniques.

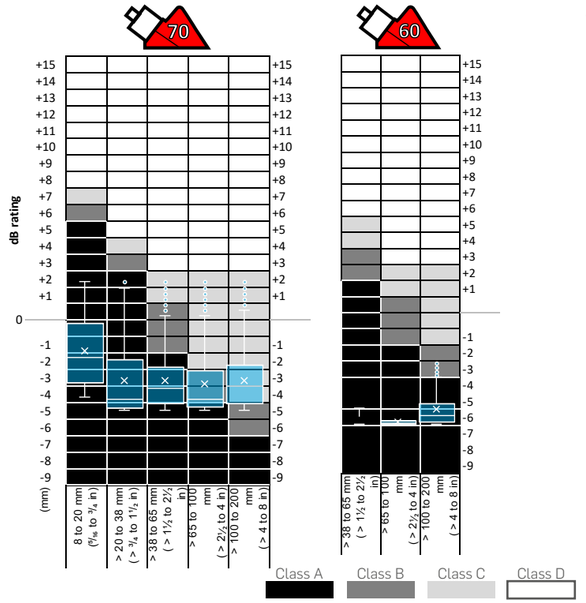

Figure 9: Existing Cyclic Acceptance Criteria and Inherent Variance From Ideal Reference Reflector Due to 2 DB/in Approximation

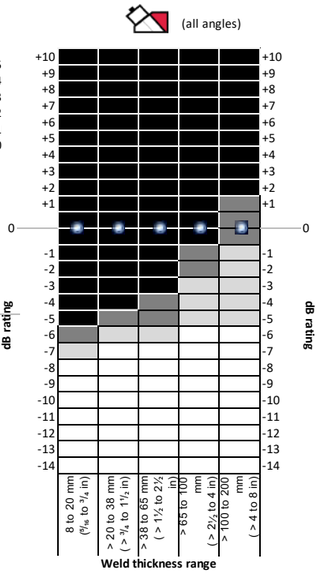

Figure 10: TCG Cyclic Criteria on Ideal Reference Reflector (Zero Variance)

8. Comparison to AWS Codes

Both AWS D1.1 and D1.5 include informative Annexes for UT examination by alternative/advanced techniques. The same acceptance criteria applied to both, and similar calibrations for sensitivity are utilized.

In 2015, AWS D1.1 Structural Welding Code [3] included informative Annex Q for manual, conventional shear wave with a DAC calibration. The annex allows for transducers up to 6 MHz and as small as ¼ inch diameter. AWS D1.5-2015 Bridge Welding Code [4] added normative Annex K for encoded phased array examinations. This annex proposes a TCG calibration for sensitivity.

Both Annex Q (D1.1) an Annex K (D1.5) propose the same acceptance criteria, using a 1.5 mm SDH used as the standard reference reflector. Similar length limits to the existing criteria apply for the various indication classes, with slight differences between static and cyclic loading.

A graphical comparison between the proposed W59 TCG technique criteria and the criteria in AWS D1.5 Annex K Table K.1 and Figure K.4 are shown below: The AWS rating levels are the same regardless of weld thickness, which is a marked change from the existing criteria. The AWS criteria in D1.1 Annex Q and D1.5 Annex K are substantially less conservative than the existing criteria. As well, the criteria are the same for PAUT and manual UT, yet manual UT allows for probe oscillation and rastering to further maximize signals.

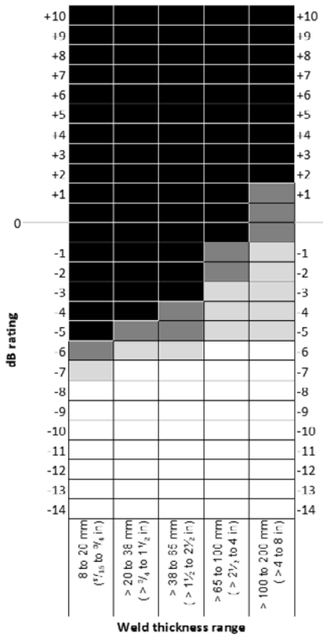

Figure 11: CSA W59 TCG Static Criteria

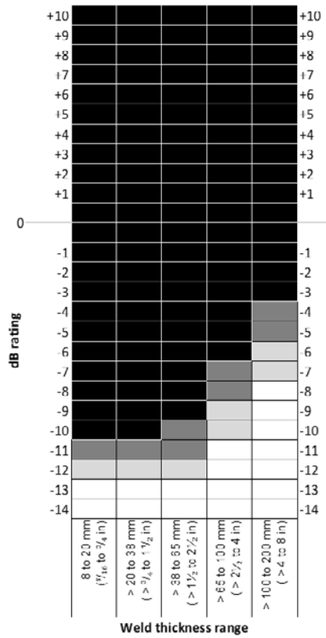

Figure 12: CSA W59 TCG Cyclic Criteria

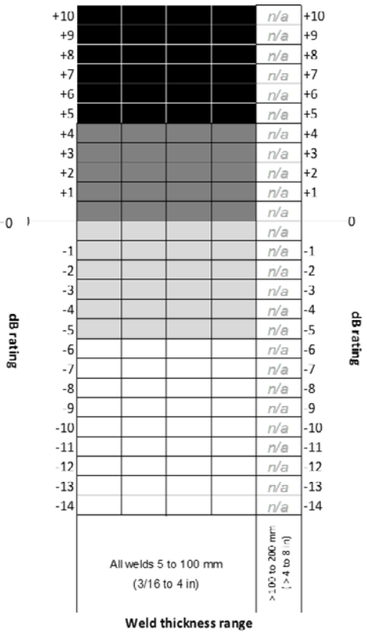

Figure 13: AWS D1.1 Annex Q and AWS D1.5 Annex K Criteria

9. Impact on Production

Costs associated with the addition of advanced ultrasonic inspection techniques to CSA W59 are difficult to quantify. In industry, the cost of inspection is typically based on cost per length of weld. Using this metric to compare the various UT techniques would be highly subjective and not provide significant information to the end user. While advanced techniques may take longer to calibrate or set up equipment, the resulting scanning speeds are faster, resulting in little difference in labour costs.

POD for PAUT (80%) is in fact higher than manual UT (50%) [20]. To compare the costs of the UT techniques one must examine the ability for the UT techniques to provide consistent information to the owner, fabricator and engineer about the weld quality being evaluated. As such, the implications on the repairs costs associated with the technique must be considered. It is for this reason that providing equivalence in acceptance criteria is of utmost importance when introducing a different technique.

Consider the results of a global survey performed by the TWI with their membership in 2012 [17] related to welding industry repair rates. While the report is not specific to Canada, the repair rates found in the survey are consistent with the experiences of the authors of this paper on recent Canadian projects. Two of the results provide indicators on the cost implications of the addition of new UT techniques. First it was noted that 96% of respondents to the TWI survey had the opinion that inspection methods had no impact on repair rates. Secondly, it was shown that the repair rates between structural and pressure equipment welded fabrication varied from 1 to 3%. Reviewing the results and the feedback on inspection methods, the variation in repair rates is likely due to the amount of volumetric inspection in the applicable industry rather than the technique. A reasonable hypothesis given that repair rates increase with the amount of inspection required by their associated codes, noting that standard structural steel has the lowest volumetric inspection requirements and pressure piping the highest.

Correlating the TWI results to the addition of new UT techniques suggests that the repair rates for the fixed attenuation method used in structural steel are consistent with repair rates using the DAC method used in pressure equipment.

While the TWI survey provides a qualitative indicator that repair rates are not a function of UT technique, it is not quantitative. A comparison of RT, UT and PAUT was performed by the Florida Department of Transportation Research Centre [18] in a study designed to evaluate the adoption of PAUT by the AWS D1.5, "Bridge Welding Code" committee. This study was quantitative. The results of investigation were that inspection using PAUT, RT and UT achieved similar results and concluded that there would not be an increase in risk of unnecessary rejection. The authors recommended to adopt PAUT as part of AWS D1.5.

Based on the above, the addition of these inspection techniques to CSA W59 should not cause an increase in repair rates and remediation costs. Rather it should improve their costs by allowing more productive technologies and improving the reliability of the current technique. The newer UT techniques allow productive inspections without changing current acceptance criteria. As such any increases in inspection costs will likely be a function of expenses born by the inspection agencies related to adoption of the newer digital technologies, training and procedures that will provide better value to their clients.

To reiterate, there have been no changes to the amount of volumetric inspection defined in CSA W59. The amount of inspection and methods of inspection are determined by the design codes. The quality and effectiveness of the chosen ultrasonic method will still depend on the inspection organization management [15] and the competency of the technician(s).

10. Conclusion

To evolve, as an industry we need to adopt methods and processes that fit the faster, better, cheaper model. The improved POD of modern UT systems could drive a reduction in the imposed safety factors thus reducing costs for the Canadian industry, simultaneously improving productivity and safety.

Improving upon the technique, yet maintaining quality levels, is paramount to enabling integration and maximizing the benefits of newer inspection technologies.

References

1. CSA W59 Welded Steel Construction (Metal Arc Welding), CSA Group, Mississauga, Ontario (2013)

2. Shenefelt, G.A., "Ultrasonic Testing: Requirements of the AWS 1969 Building Code and Bridge Specifications", Welding Journal, (May 1971)

3. AWS D1.1: Structural Welding Code – Steel, American Welding Society, Miami, Florida (2015)

4. AWS D1.5: Bridge Welding Code, American Welding Society, Miami, Florida (2015)

5. Holloway, P. “Improving on the 6 dB Drop Technique for Determination of Flaw Length”, ASNT Materials Evaluation, Vol. 74, No. 9, September 2016, pp. 1225-1232

6. Ginzel, E., “Misconceptions about NDT Workmanship Acceptance Criteria for Quality Control”, The e-Journal of Nondestructive Testing - ISSN 1435-4934, Vol. 19 No. 03 (March 2014)

7. Ginzel, E., Petersen, B., “Civa Modelling of Distance Amplitude Correction Curves on Flat Calibration Blocks”, NDT.net Vol.20 No.5, (May 2015)

8. Furr, P., “AWS D1.1 and D1.5 Phased Array Examination”, 2014 ASNT Conference

9. Wilkinson, S., “Comparative Testing of Radiographic Testing, Ultrasonic Testing and Phased Array Advanced Ultrasonic Testing Non Destructive Testing Techniques in Accordance with the AWS D1.5 Bridge Welding Code”, Mechanical Engineering Department, University of South Florida, February 2014

10. Holloway, P., “Structural UT: Variables Affecting Attenuation and Review of the 2 dB per Inch Model”, CINDE Journal, Vol. 38, No. 03, May/June 2017

11. Krautkramer, J., Krautkramer, H., “Ultrasonic Testing of Materials”, Second Edition, 1977

12. Visser, W., “POD/POS curves for non-destructive examination”, prepared by Visser Consultancy Limited for the Health and Safety Executive, 2002

13. “Information for the Procurement and Conduct of NDT - Part 4: Ultrasonic Sizing Errors and Their Implication for Defect Assessment”, Health and Safety Executive, 2008

14. Lingvall, F., Stepinski, T., “Ultrasonic Characterization of Defects - Part 4 Study of Realistic Flaws in Welded Carbon Steel”, prepared by Uppsala University for the Swedish Nuclear Power Inspectorate (SKI), SKI Project Number 97040, 2009

15. Krishnamoorthy, K., “Quality Assurance in NDT”, Atomic Energy of Canada Ltd., 2009

16. McGrath, B., “Programme for the assessment of NDT in industry (PANI 3)”, prepared by Serco Assurance for the Health and Safety Executive, 2008

17. “Repair Rates in Welded Construction – An Analysis of Industry Trends”, Welding and Cutting Journal, 2012 Issue 1

18. Wilkinson, S., “Comparative Testing of Radiographic Testing, Ultrasonic Testing and Phased Array Advanced Ultrasonic Testing Non Destructive Testing Techniques in Accordance with the AWS D1.5 Bridge Welding Code”, prepared by Mechanical Engineering Department, College of Engineering, University of South Florida for the Florida Department of Transportation, February 2014

19. Kurz, J., Dugan, S., Jungert, A., “Reliability Considerations of NDT by Probability of Detection (POD) Determination Using Ultrasound Phased Array – Results from a Project in Frame of the German Nuclear Safety Research”, 5th European-American Workshop on Reliability of NDE (Lecture 16), Germany 2013

20. Georgiou, G., “Probability of Detection (PoD) curves - Derivation, applications and limitations”, prepared by Jacobi Consulting Ltd. for the Health and Safety Executive, Research Report 454, 2006

Acknowledgements

The authors would like to thank the tireless dedication of the entire W59 committee, and those in industry who reached out to provide some of the history behind the original technique. Special thanks go to Ed Ginzel who performed all the simulations using CIVA, and Luc Mauzeroll at Torngats for his technical expertise.

Originally published as: Holloway P, Crawford A, Keay S, Vaidya V. Distance amplitude techniques and their adaptation to structural steel weld inspection. AWS Welding Journal, March 2018

Improved Structural Assessments Assisted by Digital Image Correlation

Jan Winkler

Chief Specialist, DIC Team Leader
Engineering, Design and Project Management
Copenhagen, Denmark

Chris R. Hendy

Technical Director, Atkins Fellow, Professional Head of Bridge Engineering
Engineering, Design and Project Management
Epsom, UK

Abstract

As our transportation infrastructure ages and the challenge of keeping it serviceable grows, the need for improved condition information on which to make good cost-effective maintenance decisions becomes ever more vital. Gathering this condition information requires structural health monitoring and inspection on a grand scale and, for it to be useful, it must be accurate, inexpensive, easy to interpret and avoid interfering with traffic flows - whether rail or highway. Digital image correlation (DIC) is a non-contact photogrammetry technique that can be used for monitoring by imaging a bridge periodically and computing strain and displacement from images recorded at different times or operating conditions. This paper discusses the use of DIC for monitoring a variety of bridges in service with the primary objective of better understanding the real behavior and avoiding the need for strengthening when appropriate or designing earlier interventions before problems become more serious. In majority of cases throughout the monitoring the structures were left untouched and were in full service operation.

Keywords

Bridge Monitoring, Performance and Damage Assessment; Digital Image Correlation (DIC); Deformation Measurement, Asset and Fatigue Management.

1. Introduction

1.1 Bridge Monitoring – Challenges

The principal difficulty with adding lots of monitoring systems to bridges is that they produce vast quantities of data. Bridge operators typically do not know what to do with this data unless there are very clear trigger levels defined associated with this data and clear interventions defined if they are exceeded. This means that the structural engineer needs to identify what the most likely deterioration mechanisms are for the particular bridge and design bespoke monitoring that can be used to specifically measure performance in such a way that an acceptable level can be set and checked e.g. movement at a bearing or joint, tensile crack lengths/ widths at particular discontinuity regions, wire breaks in a cable, fatigue cracking at a steelwork detail, tilt of a column or pylon or deflection of a deck where a bridge is very sensitive to creep variations and other material parameters. This may require the use of many different systems.

Instruments such as strain gauges, accelerometers, fiber optic sensors and displacement transducers are becoming increasingly common in structural health monitoring. These types of sensors can however possess drawbacks such as the need for external power and cabling/antenna for data transmission, high data acquisition channel counts and the limitation of only measuring at discrete points or along a line, so it is necessary to have an idea of where to expect damage when placing the instrumentation. These sensors can be used effectively to continuously monitor for abnormalities that indicate damage, but the type and severity of the damage can still be difficult to identify from discrete point measurements.

1.2 Digital Image Correlation (DIC)

DIC represents a photogrammetry technique used for accurate measurements of surface deformation. The digitized images (e.g of a bridge deck) are compared to match facets from one image to another by using an image correlation algorithm (Fig. 1a, b). Image analysis involves capturing a reference image of a bridge component surface in its undeformed state. As the load is applied (e.g truck load), additional images are collected. The algorithm (which can either run in real-time or post-process), involves a stage-wise analysis, in which each stage consists of one image resulting in a description of displacements occurring on the surface of the bridge component. The evaluation of a correlation measurement results in coordinates, deformations and strains of the surface (Fig. 1c, d). DIC method allows high precision surface deformation measurement that can reach the accuracy of a few micrometers.

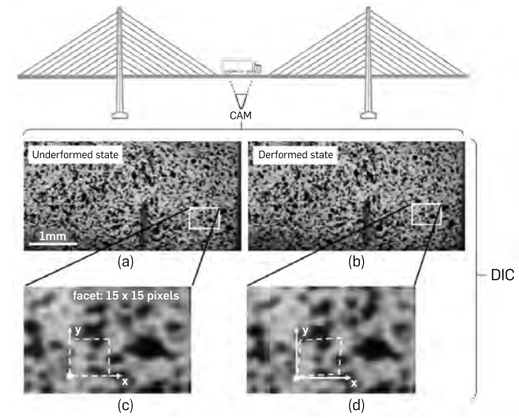

Figure 1: Digital Image Correlation Method

DIC measurement can provide information about strain (all directions), vertical and horizontal displacement, crack size, rotation and acceleration. DIC is independent of scale (local & global monitoring) and material (concrete, steel) and is especially helpful in monitoring of bridge components with a difficult access. Real time operation, off-line analysis, remote access to equipment and live reporting of results is also possible. As the technology stands, DIC can be operated with as little as one individual and does not have to be in contact with the bridge therefore avoiding any potential conflicts with traffic or difficult geography. Also, DIC takes a fraction of the time to setup compared to traditional instruments.

This paper discusses a number of case studies where DIC has been used for monitoring with a view to informing asset management decisions and, in some cases, using the evaluation of real behavior to avoid the need for remedial measures.

2. Docklands Light Railway (DLR) Bridges - Fatigue Assessment

Docklands Light Railway (DLR) has implemented the running of three-car trains on the DLR network between Poplar station and Stratford station, known as the north route. The 'DLR Capacity Enhancement & 2012 Games Preparation Project' report identified that the fatigue life of some of the underbridge structures should be reviewed. Atkins has been commissioned to prepare a fatigue management strategy for a number of DLR structures including the Warton Road Bridge, located close to the Olympic Stadium (Fig. 2). The bridge structure had its own site constraints and monitoring challenge. DIC monitoring was used to compare deck deflections to those expected from assessment global analysis and to calibrate the assessment model.

2.1 Measurement Methodology

The DIC system comprised a camera mounted on a geared head on top of a surveyor's tripod and the pan. Lens was adjusted to provide required field of view. The sampling frequency was +20 Hz. The normalized grey-scale correlation tracking algorithms were used for the image analysis. Calibration was achieved by measuring a distance within the image. The existing features on the bridge surface were used as the tracking objects. No editing of the raw data has been undertaken. All 'processing' was related to optimizing contrast levels and exact positioning of reference points for the virtual gauges.

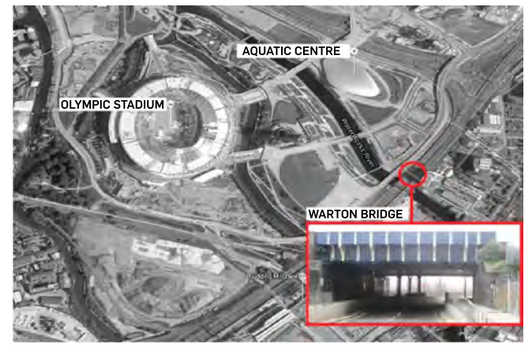

Figure 2: Docklands Light Railway (DLR) - Warton Road Bridge

2.2 Warton Road Bridge

The structure is a single span half through simply supported bridge constructed in 1937. The span of the longitudinal girders is 13.56 m. A plan view of the structural layout taken from as-built drawing records is shown in Fig. 3a. The structure consists of two longitudinal girders and a concrete slab with encased steel beams. Each longitudinal girder is formed from flange and web plates that are riveted together using angle sections.

Figure 3: Plan View (a) and Cross Section (B) of the Warton Road Bridge

In addition to the DLR track the southern girder also supports a walkway cantilevered from the girder top flange. The typical cross-section is shown in Fig. 3b. The structure carries a single DLR track and the alignment is effectively straight in plan. Three-car trains are in operation on this line. The abutments are brick abutments founded on spread footings.

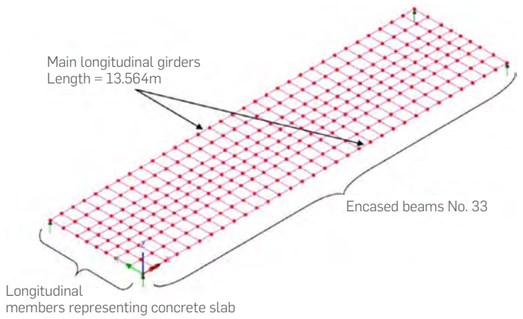

Figure 4: A Simplified FE Model of the Warton Road Bridge

2.3 FE Model of the Bridge

The bridge structure was analysed with a grillage model using a proprietary analysis computer program (LUSAS). The model is shown in Figure 4.

A grillage model is necessary to analyse axle load distribution between the transverse beams encased in the concrete slab. Cracked section properties were initially conservatively used for the members representing the longitudinal concrete and the members representing the encased transverse beams. With these properties, there was a small predicted fatigue deficiency in the edge girders. However, if some tension stiffening was available then the fatigue stresses reduced sufficiently to demonstrate adequate residual life. The main purpose of the DIC measurement was therefore to demonstrate that some such tension stiffening was occurring and that fatigue strengthening was not required.

2.4 Global DIC Monitoring of the Bridge (Displacement Measurement)

DIC was employed to capture the deflection of the main beam (Fig. 5), without instating a road closure to the road underneath which was a main route used for a large nearby shopping centre,

and compare this to the deflection calculated under the fatigue assessment loading. The camera was located 30 m away from the bridge. The measured peak deflections at mid span (Fig.5c) were of similar magnitude to the deflections obtained from the FE analysis under the real train loading, allowing for real passenger numbers, when the FE model girder stiffness was adjusted to lie roughly mid-way between fully cracked and un-cracked values.

This slight measured increase in stiffness was sufficient to demonstrate that the fatigue stresses seen by the bridge gave adequate residual fatigue life with the new 3-car trains. In the case of the Warton Bridge, it was possible to set up, record data on deflections, pack up and leave site within a few hours.

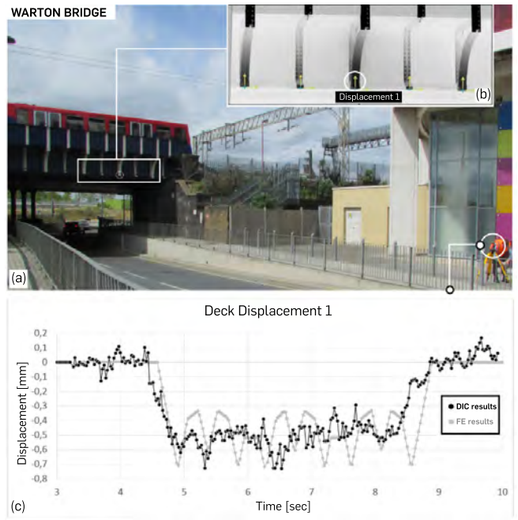

Figure 5: Warton Bridge (a), Close Up on Main Beam and DIC Measurement (B), Analysis of DIC Data (C)

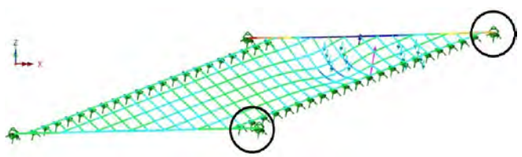

Figure 7: FE Model of the French Horn Bridge

3. French Horn Bridge

French Horn Bridge comprises a pair of edge girders with cross girders supporting a concrete deck and a high skew of 65 degrees across the rail line below. Inspection of the bridge had identified corrosion of the bearings and some spalling to the abutment. It was this suspected that the bearings may have seized and were no longer rotating, thus causing unacceptable pressures on the foundations and potentially also on the deck steelwork. It was thus necessary to monitor the bearings under load to determine how they were articulating in reality.

DIC dynamic monitoring of the bearing rotation and deck displacements was therefore undertaken to hopefully demonstrate satisfactory performance and hence to avoid the need for strengthening. The principal reason for selecting DIC measurement, rather than a more conventional measurement with attached displavement transducers, was to enable the measurements to be carried out without the need for either rail possessions or road closures. The camera was therefore mounted adjacent to the railway line with a clear line of sight to the bearings as shown in Figure 6. Displacement monitoring was additionally carried out solely for validation of the DIC model against the finite element model. Night works and working at height were avoided and all setting up, data capture and packing away was completed within 4 hours.

The camera operated at 9Hz with a resolution of 5Mpix. The results showed that the bearings were rotating freely and the behaviour was therefore as expected. The displacement measurements showed agreement to within 15% of the finite element model (Figure 7) with the true behaviour being stiffer than the finite element model predicted, as might be expected due to the unmodelled tension-stiffening effects of deck concrete and potential composite action with surfacing.

Figure 6: French Horn Bridge

4. Humber Bridge

The Humber Bridge is a 2220 m long suspension bridge with a main span of 1410 m – Figure 8. The north (Hessle) tower is sited on the high-water line and the south (Barton) tower founded in shallow water 500m from the shore. The bridge comprises reinforced concrete towers aerial-spun catenary cables and a continuously-welded, closed box road deck (dual two lane carriageway plus separate paths) supported by inclined hanger cables. The bridge carries an average of 120,000 vehicles per week.

As a part of a scheme to investigate the need or otherwise for future hanger replacements, DIC was used to provide information on the structural behavior of typical hangers and the overall deck. The purpose of the monitoring was to use the results to verify the behaviour predicted by the global finite element model (Figure 8b), to validate the predicted fatigue stresses in the hangers and hence validate the assumptions made with respect to selecting trial hangers for further destructive testing and replacement.

Figure 8a: Humber Bridge

Figure 8b: 3D FE Model of the Bridge

The DIC monitoring scheme was carried out in May 2017 and was divided into day and night measurements to capture effects caused by everyday traffic and also by a known vehicle of 11 tonnes driven across the bridge. The day and night measurements each measured deck deflection and hanger strains. The day measurements were conducted under normal traffic while the nightime mesuremement were carried out with the known vehicle.

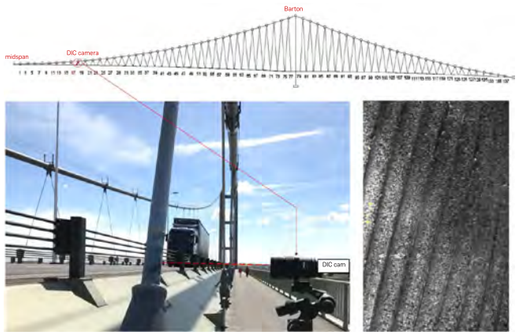

Figure 9: Traffic Load Applied to the Bridge and Camera Position for Hanger Strain Monitoring

The hanger strain mesurements utilised a camera mounted on the footpath and located close to the hanger being monitored (Figure 9).

The results of the nighttime strain monitoring under the 11T vehicle for a hanger are shown in Figure 10 after conversion to stress.

Figure 10: Nighttime Strain Monitoring of a Hanger Under Known Load

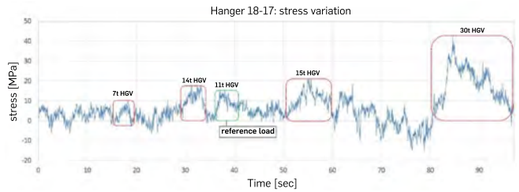

Figure 11: Daytime Strain Monitoring of a Hanger Under Normal Traffic

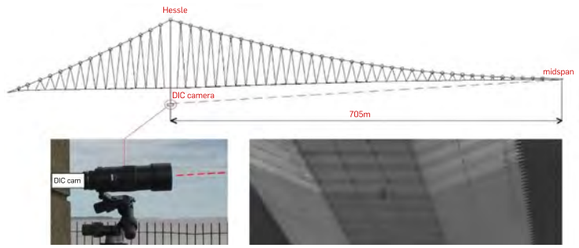

Figure 12: Camera Position for Midspan Deflection Monitoring

The peak stress recorded was around 15 MPa which was in near exact agreement with the results from the finite element model for the same loading case.

Strain monitoring was also carried out during the day under normal traffic and Figure 11 shows a typical trace of stress against time with estimated vehicle weights marked on the plot.

Figure 13: Spotlights for Nighttime Midspan Deflection Monitoring Under Known Load

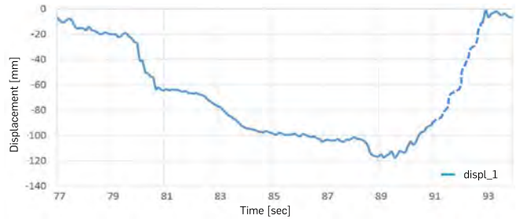

Figure 14: Nighttime Midspan Deflection Monitoring Under Known Load

The midspan deck displacements and rotations were measured using a camera positioned at the Hessle tower, some 705 m from the target midspan location (Figure 12). The nighttime measurements utilised spotlights to higlight the midspan target location as shown in Figure 13.

The outcome of the nighttime midspan deflection monitoring is shown in Figure 14. A very high precision of measurement (millimetre accuracy) performed from 705 m was achieved.

The overall conclusions from the DIC monitoring were that the finite element model was providing a good prediction of the real behaviour of the bridge and hence the choices made with respect to selection of hangers for trial replacement were apropriate. In addition, data was captured on inter-wire fretting behaviour to inform predictions of cable residual life.

5. Gade Valley Viaduct

Gade Valley Viaduct (Figure 15) is an 11 span composite box girder structure with a total length of 440 metres carrying the east and westbound M25 over the Grand Union Canal, River Gade and West Coast Mainline. The viaduct comprises of continuous twin curved decks. The superstructure for each carriageway is composed of 4 open top steel box girders with an in-situ reinforced concrete deck slab cast on permanent precast concrete plank formwork with bespoke precast soffit panels in the central reserve area.

Assessment had predicted a potential fatigue deficiency in a number of the the cross frames due to distortion of the boxes under eccentric live loading, caused by load cases with traffic in a lane adjacent to the cross frame being considered on one side of the box only. A typical cross frame is shown in Figure 15. The assessment was commissioned because a physical crack had been found in one cross frame a few months earlier. The assessment predicted that the crossframes in the midspan region of each span were most at risk where the distortional forces were greatest; towards the supports, the distortional warping stiffness of the box carries a greater share of the distortional forces and the cross frames are hence less heavily loaded.

Figure 15: Gade Valley Viaduct and a Typical Internal Crossframe

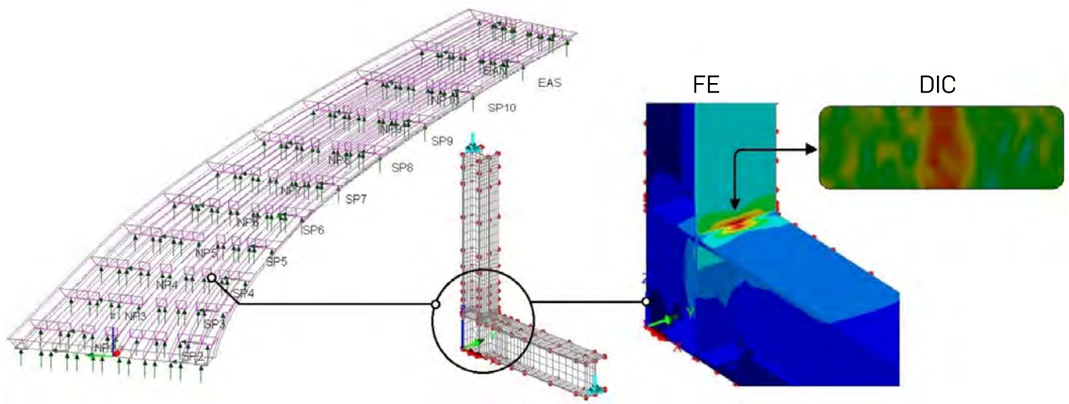

Figure 16: Finite Element Model and Corresponding DIC Strain Map

As many previous projects, such as the fatigue assessment of the Midland Links box girders (reference 1), have shown that the true distortional stresses in the real structure are less than those predicted by finite element modelling, in March 2017, as part of the overall assessment strategy, Digital Image Correlation was used to measure the strain and stress at the corner of a typical midspan cross frame via a camera was set up inside the box. Similar to the process used in reference 1, a vehicle of known weight (32T) was driven along marked lanes under temporary lane closures and the DIC technology was used to measure stresses occurring at the corners of the cross frame detail for comparison with, and to calibrate, the detailed FE model of the cross frame under the same applied load cases. A unique feature of the measurement was that the algorithms used considered a rosette of strains at each point in order to find the principal strain direction (see Fig.16). A strain/stress map was plotted live in the direction showing highest tensile/compressive strain.

In this case, the DIC results showed close agreement with the finite element results, indicating that the FE model was a good predictor of the cross frames that are most at risk and hence a strengthening solution has been planned accordingly.

6. Conclusions

Monitoring of the bridge structures discussed in this paper using traditional methods would have required construction of access platforms, working at height and road and/or rail closures. These were all avoided with DIC measurement and the setting up, data capture and packing away were completed much quicker than by conventional contact measurement techniques. The ability to capture a bridge's behaviour with DIC and calibrate a structural model with the collected data provides bridge designers and managers with an easy-to-collect objective measure of bridge performance and the examples presented have shown that capturing the true behaviour cannot often lead to avoiding expensive interventions that are predicted to be required solely by structural analysis of the idealised structure.

DIC is becoming very versatile and cost effective due to the dramatic improvement in digital cameras and is therefore a promising solution to low-cost structural monitoring of existing infrastructure. DIC should therefore be considered in combination with other monitoring technologies to provide the information we need to make effective whole life management decisions that keep our assets in service in a cost-effective way.

References

[1] Hendy CR, Chakrabarti S, Fatigue Management of the Midland Links Box Girders, ICE Bridge Engineering, June 2014

[2] Winkler, J., Georgakis, C.T., Fischer, G., Wood, S., and Ghannoum, W. 2015, Structural response of a multi-strand stay cable to cyclic bending load . Journal of Structural Engineering International 2/2015. (DOI: 10.2749/101686614X14043795570138).

Acknowledgements

Originally presented and published as: Winkler J, Hendy CR. Improved Structural Assessments Assisted by Digital Image Correlation. Structural Faults & Repair 2018 and European Bridge Conference 2018, May: Edinburgh, UK.

Single Row Piles in Integral Bridge Foundations: Challenges and Solutions

Debabrata Mukherjee

CEng MICE
Senior Group Engineer, Discipline Lead (Bridges)
Engineering, Design and Project Management
Bangalore, India

Abhishek Jain

PE, GMICE, MASCE
Design Manager
Engineering, Design and Project Management
Bangalore, India

Manju Balaji

CEng MICE
Senior Engineer
Engineering, Design and Project Management
Bangalore, India

Abstract

This paper presents the challenges and their solutions adopted for the design of two-span continuous integral overbridges supported by single row pile foundations without any interfacing pile cap elements, as part of A14 Cambridge to Huntingdon development. The paper highlights the geotechnical modelling limitations, construction requirements, contractor's preferences, and other constraints placed on pile configuration due to load demands and form of superstructure. With respect to structural aspects of design, the paper discusses the design challenges and solutions associated with reinforcement detailing within the abutment and pier walls in absence of interfacing pile cap elements. It also touches upon use of strut and tie approach, to propose a safe and buildable detail around the pile reinforcements, and the reinforcements of the substructure element.

Keywords

Integral Bridges; Strain Ratcheting; Continuous Flight Auger; Strut & Tie; Buildability.

1. Introduction

The 'A14 Cambridge to Huntingdon' is the first project of its kind being delivered under Collaborative Delivery Framework (CDF) for the client, Highways England, UK. The client has appointed Atkins and CH2M, as the collaborative design delivery partners for the scheme.

The client has engaged the contractors early, to work together with the design consultants: review, advice for safe buildability and advice on construction related issues. All these were addressed at detailed design stage, so that the construction stage is streamlined.

As is evident from the CDF set up, the key stakeholders in the scheme works together collaboratively, with a single objective of delivering the project successfully; to quality, cost and time.

The project scope under bridges and structures was delivered in the form of "good for construction" drawings during the detailed design duration. The work was closely monitored by the client, and the final deliverables incorporated the recommendations, observations, best practices, buildable and safe solutions identified from both client and the contractor's involvements.

The design consultants checked each other's deliverables and shared best practices, thereby furthering the quality of deliverables, from collective experience.

The bridges and structures scope was broadly categorised under the following:

Figure 1: A Typical Standard Overbridge Arrangement in 3D

- Standard Overbridges over A14
- Bridges carrying the A14 over other roads
- Pedestrian and equestrian Bridges
- Gantries

This paper particularly covers the eight Standard Over Bridges grouped together and their foundations proposed therein.

2. Structural Form and Arrangement

2.1 Standard Over Bridges

The proposed structural arrangements for the standard overbridges in this scheme are a combination of: best design practices followed by the consultants, with practical, buildable and safe construction advice arising from the contractor.

The design proposal taken forward for each standard overbridge, entails two-span continuous, integral structure with a wall type pier within the central reserve and half-height abutments at ends.

This not only gave a more efficient design approach, but also has the benefit of providing a scheme consistent aesthetics.

The foundations at the abutments and pier comprise of 900 mm diameter piles. While the proposal for this foundation arrangement was being firmed up, the design delivery team, in consultation with the contractor's team, explored the option of using single row of piles as foundation, directly connecting with each abutment wall and the pier wall. The contractor preferred this proposal as this would eliminate a major structural element, the pile cap, from the construction programme.

A 3D computer aided model indicating the structural arrangement of a typical standard overbridge is indicated in Figure 1.

2.2 Other Bridges and Gantries

There are several other bridges on this project carrying the A14 over, with conventional piles and pile caps as foundations. A few significant ones are namely the two non–motorised user, landmark overbridges to carry pedestrian, cyclists, equestrian and the East Coast Main Line Bridge and its approach viaduct.

Apart from the bridges, there are other highway structures in forms of MS3, MS4, ADS and portal gantries.

This paper however does not focus on these other structural forms and their arrangements, final proposals and or their design.

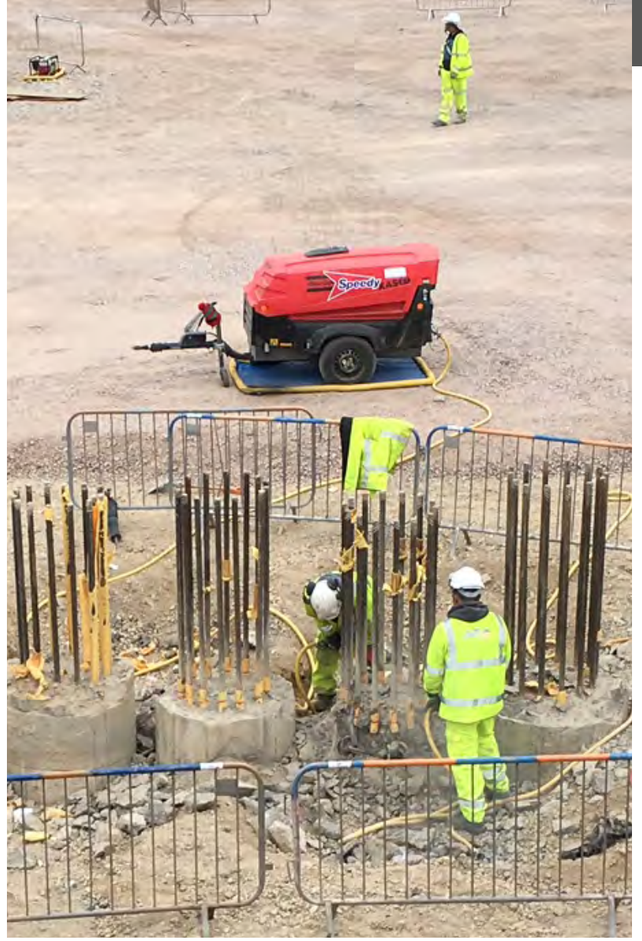

Table 1: Summary of Characteristic Geotechnical Properties for Predominant Cohesive Soil Layers

Soil Type	Dry Unit Weight, γ_d (kN/m^3)	Bulk Unit Weight, γ (kN/m^3)	Plasticity Index (%)	Undrained Shear Strength (C_u, kPa)	Drained (E') / Undrained (E_u) Stiffness (Medium Strain)
Glacial Till	0-4m: 15.7; >4m: 18.2	0-4m: 19.6; >4m: 21.1	0-4m: 18 - 50; >4m: 25	0-15m: 12.6z+80; >15m: 270	$200 – 300C_u / 1.25E'$
Oxford Clay	16.2	19.6	35	0-20m: 10z+30; >20m: 230	
Ampthill Clay	15.2	19.1	45	6z + 40	
Note: 'z' is measured from the top of the stratum.					

3. Geotechnical Analysis and Design

3.1 Geology and Ground Conditions

The approximately 38 km long project alignment is underlain by number of superficial deposits of varying thickness comprising: topsoil, made ground (engineered fill), alluvium, head deposits, river terrace deposits and terrace gravels, overlying glacial till, oxford clay, ampthill clay, gault clay, kimmeridge clay and lower greensand.

The standard overbridge foundations are predominantly within the underlying cohesive soil deposits. Groundwater was generally encountered within 1 m to 2 m below the existing ground level. For design purposes, the groundwater level was conservatively assumed to be at the existing ground level at 'fill' locations and at the proposed road level below the bridges at 'cut' locations. Only one of the eight standard overbridges will be constructed in 'cut' condition.

For the eight standard overbridges, the foundations are terminating in Glacial Till (for three), Oxford Clay (for four) and Ampthill Clay

Table 2: Summary of Results of Geotechnical Analysis

Design Situation →			DA1C2		DA1C1								Frequent SLS	Char SLS	Frequent SLS
			Maximum Pile Reaction (kN)		Max. Resultant BM (kN-m)				Max. Resultant SF (kN)						
Abut Piles (number)	Pier Piles (number)	Predominant Underlying Soil Layer	Abut	Pier	Abut	Critical Case	Pier	Critical Case	Abut	Critical Case	Pier	Critical Case	Settlement Pier (mm)	Max. Differential Settlement (mm)	Lateral Deflection Abut (mm)
8	7	Glacial Till	1705	3469	1277	ULS Char	1192	ULS Acc	890	ULS Char	643	ULS Acc	3.9	3.2	9.7
3	2	Glacial Till	1310	3400	946	ULS Char	1337	ULS Acc	500	ULS Char	918	ULS Acc	7.5	5.0	8.4
4	3	Glacial Till	1544	3002	874	ULS Char	2209	ULS Acc	596	ULS Char	1242	ULS Acc	7.0	3.6	9.2
4	3	Oxford Clay	1485	2953	910	ULS Acc	1794	ULS Acc	562	ULS Char	1046	ULS Acc	7.1	3.1	9.2
8	7	Oxford Clay	1680	3415	1145	ULS Char	1230	ULS Acc	625	ULS Char	605	ULS Acc	6.0	2.0	10.5
7	6	Oxford Clay	1625	3375	1216	ULS Char	508	ULS Acc	665	ULS Char	274	ULS Acc	3.9	3.4	11.5
7	6	Oxford Clay	1548	3309	571	ULS Char	428	ULS Acc	524	ULS Char	212	ULS Acc	5.8	0.3	8.3
7	6	Ampthill Clay	1660	3401	1236	ULS Char	494	ULS Acc	680	ULS Char	265	ULS Acc	7.0	2.0	11.4

Notes: Char – Characteristic; Abut – Abutment; Max. – Maximum; Acc – Accidental

(for one). The site-wide geotechnical properties of Glacial Till, Oxford Clay and Ampthill Clay are summarized in Table 1. The site-specific properties used for design, though differing slightly, were generally similar to those of the site-wide properties.

3.2 Pile Design Methodology

The pile foundations were designed in accordance with BS EN 1997-1:2004 (Eurocode 7, EC7)[1] and National Annex (NA) to EC7[2] considering Design Approach 1 for Load Combinations 1 and 2 (DA1C1 and DA1C2).

The pile lengths were determined based on maximum axial loading expected to be experienced over the design life, represented by the 'frequent' combination of actions; and meeting vertical settlement, differential settlement between abutment and pier piles, and lateral deflection criteria. The internal bending moments and shear forces in the pile, for use in its structural design, were evaluated based on the critical loading represented by the 'characteristic' and 'accidental' combination of actions. Serviceability of piles is being determined by pile load testing at the time of writing this

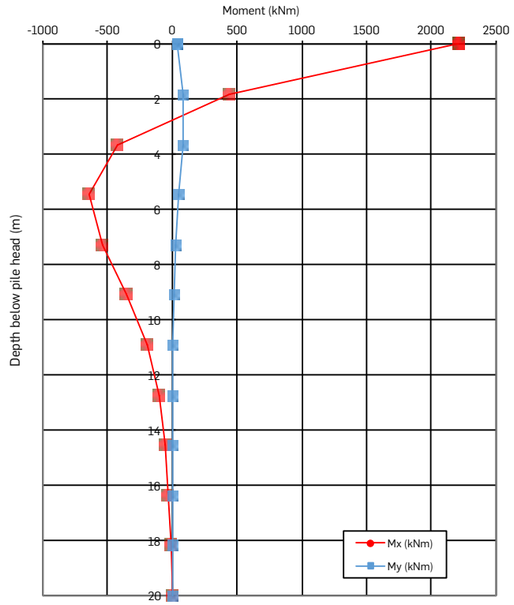

Figure 2: Typical Bending Moment Profile of a Critical Pier Pile

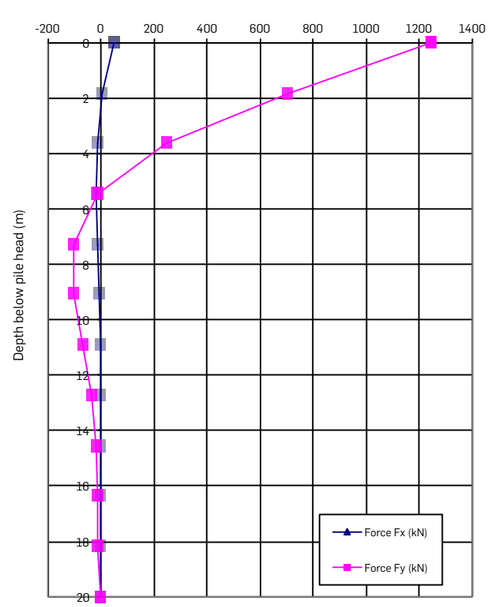

Figure: Typical Shear Force Profile of a Critical Pier Pile

paper, hence a reduced 'model factor' of 1.2 was used for pile design instead of the higher factor of 1.4 which is typically used in the absence of pile testing.

Being predominantly in cohesive (fine-grained) soils, pile foundations were designed using conventional pile design methods as described in Tomlinson et al.[4]

3.3 Pile Group Analysis and Design

The pile group analysis was performed using a proprietary software as it presents the ability to model multiple soil layers and models the pile group behaviour using Boundary Element Method (BEM). Soil was assumed to be linear elastic that was considered sufficient for the project needs as the design criteria did not allow for large lateral deflections and settlements of piles. Since the soil profiles were generally similar at both abutment locations for a bridge, only one of the two abutments along with the pier location were considered for pile group analysis.

The superstructure load effects were applied at the bottom of abutments and pier walls for abutment and pier piles, respectively. The load effects and their signs as output of the structural analysis software were matched to the sign convention of the geotechnical analysis software before application.

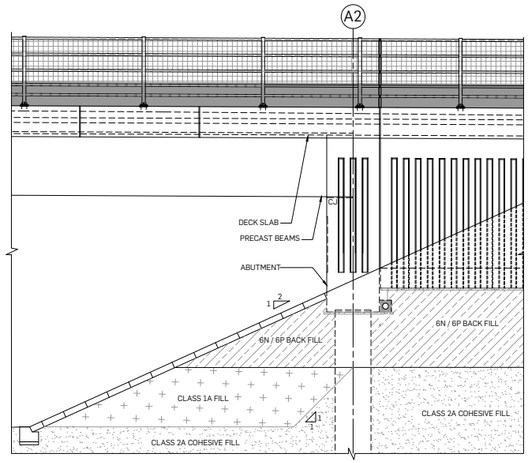

Figure 4: Typical Elevation at Abutment Location

To obtain equivalent cantilever properties for modelling piles, flexibility matrices were derived. These were derived with lower bound and upper bound soil properties, with long term and short term stiffness properties of concrete to facilitate the modelling of flexible and stiff pile group behaviours. Pile reactions, Shear Force and Bending Moment profiles, settlements and lateral deflections were obtained for each pile in relevant design situations with site-specific characteristic soil properties. A typical result summary of geotechnical analyses is presented in Table 2.

The maximum resultant bending moment and shear force for abutment piles and that for pier piles are presented in Table 2. Typical BM and SF profiles are presented in Figures 2 and 3, respectively. The BM and SF profiles obtained were generally similar in nature to those shown by Tomlinson et al.[4] The authors, however, did not observe any consistent trend between the maximum SF and BM at different overbridges, potentially due to number of variables, such as, different soil profiles, varying pile numbers and differing superimposed loads.

3.4 Design and Construction Challenges and Solutions

Continuous Flight Auger (CFA) Piling

For the standard overbridges, the contractors indicated their preference for Continuous Flight Auger (CFA) piles over bored piles very early in the project due to several advantages: fast and a relatively 'quiet' construction method, and suitability in a wide range of subsurface strata. However, CFA piling is generally feasible up to 30 m - 32 m of depth and for maximum 1200 mm pile diameter. Hence, the design team was constrained to find suitable solutions within these limiting criteria in terms of: pile configuration with adequate centre-to-centre spacing (approximately at least two times the pile diameter).

The pile may have large enough diameter to provide adequate reinforcement that would be feasible during construction on site. The design team could meet these limiting criteria with 900 mm diameter piles with lengths shorter than 30 m, which may be further optimised based on the ongoing pile load testing results.

Reduced Soil Stiffness

Although the proprietary geotechnical analysis software allowed modelling of the uniformly sloping ground around the piles, it does not allow modelling a berm, a condition that was present at abutment locations of half-height abutment locations as shown in Figure 4.

A reduced soil stiffness was therefore considered for the extent of soil depth between the pile cut-off level and berm toe level. The reduction in stiffness was assumed to be proportional to reduction in coefficient of passive earth pressure (K_p). The reduction in K_p was approximated to be one-half based on the graphical approach proposed for evaluation of K_p for 'retaining walls with inclined retained surface' within Annex C of EC7. Being on the conservative side, the reduction was assumed to be acceptable for the circular piles with clear spacing approximately equal to one pile diameter. Further, the reduction would be for limiting passive pressure condition that is not anticipated to be mobilized at abutment location during the design life of the project. Alternatively, a free-standing length of the piles starting from the berm toe level to pile cut-off level could have been considered for pile group analysis, but such a condition was too conservative, and was therefore not adopted for design.

Strain Ratcheting Considerations Due to Fill Regime around Abutment Piles

In granular soils, the year-on-year repeated expansion and contraction of abutments next to them leads to mobilization of passive soil pressure termed as 'strain ratcheting'[5].

As is evident from the typical elevation view of half-height abutment overbridges in Figure 4, the abutments retain Class 6P/6N granular fill material behind them. Additionally, the single row of piles will be surrounded by approximately 1.5 m thick Class 6P/6N granular material below their cut-off levels necessitated by the requirement of having granular fill underneath the wing wall next to the abutment. Additional lateral pressures due to strain ratcheting were therefore considered acting at the top of the piles.

Spacing of Piles

Many previous empirical studies, such as the one conducted by Mello[6] indicate that the efficiency of pile groups in cohesive soils decreases considerably when pile spacing is less than two pile diameters, and is therefore not desirable. Although the group efficiency was not explicitly considered in geotechnical design of pile groups, the pile group analysis software program implicitly considers soil-pile interaction including the effect of pile spacing. Based on the analysis, a centre-to-centre spacing of approximately two times the diameter of piles was found to be feasible for half-height abutment overbridges supported by a single row of piles.

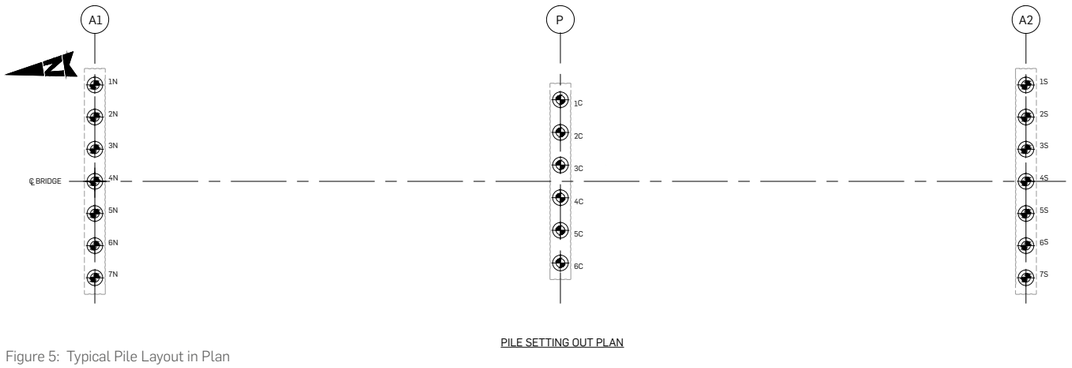

Figure 5: Typical Pile Layout in Plan

4. Structural Analysis and Design

4.1 Structural Challenges

Pile Foundation

Pile foundations represented by simple springs will not capture accurately the rotation and displacement due to the moment and shear that are applied from the above structural element. To obtain the correct behaviour, a flexibility matrix was generated using an equivalent cantilever, where the displacements and rotations at the pile cap are matched through the selection of suitable cantilever properties of the piles.

Abutment Wall and Pier

The superstructure comprised of precast prestressed W-beams and in-situ reinforced concrete deck that connects to pier and abutment through a rigid reinforced concrete diaphragm.

As no physical pile cap element is present at the abutment and the pier, the design team ensured that the forces from the substructure bases were distributed safely to the foundation (pile group) with careful and adequate reinforcement detailing.

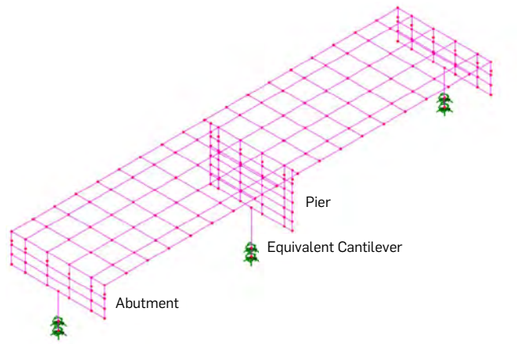

Figure 6: Idealisation of Typical STOB

Challenges: Piles and Substructure

The structures team and the geotech team worked together, conducting the required number of analysis; one for obtaining flexibility matrix and another to obtain the pile loads.

The pile design was carried out with the design loads and detailed to satisfy the contractors advice, on minimum reinforcement spacing, and type of shear links. The substructure element was idealised considering:

- Strain ratcheting as outlined under section 3.4.3 above was calculated as per PD6694-1[5].
- The bottom zone of the walls was designed using Strut and Tie methodology, though obtaining the expected tension and compression forces in strut and tie members were not straight forward. Idealising the model based on the proposed pile group arrangement involved engineering judgement and prior experience. The analysis was further conducted based on the designer-contractor agreed construction sequence.

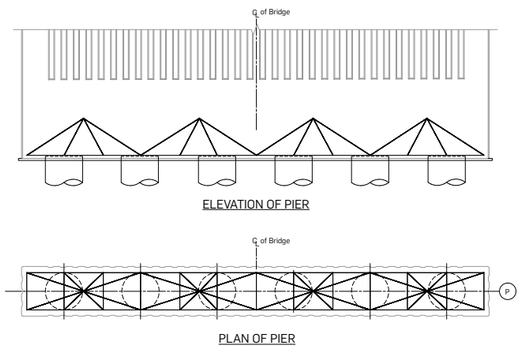

Figure 7: S&T Idealisation at Pier

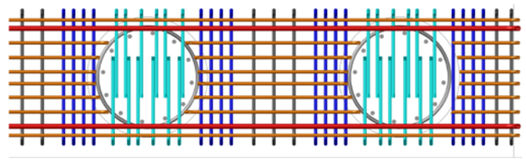

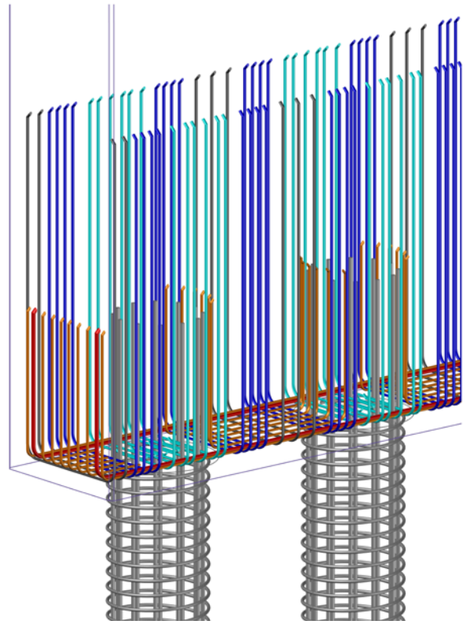

Figure 8: Tie Reinforcements

4.2 Solutions: Analytical and Design

Pile Analysis

It was necessary to prepare four numbers of model to cover the different ages of young's modulus of concrete and the extreme soil parameter the lower and upper bound. The four flexibility matrices obtained from the geotech team were then used to obtain the equivalent cantilever to represent the pile group stiffness, one for major axis and another for the minor axis. A typical pile layout arrangement for a standard overbridge is indicated in Figure 5.

Figure 6, indicates an idealised model of the standard over bridges (STOB) as prepared in the structural analysis software. The different elements of the overbridge like deck, girders, pier, abutments and foundations were idealised through grillage models.

Load Transfer from Wall Base to Piles

The bottom zone of the abutment/ pier wall is considered to transfer the loads to the piles. The Strut and Tie (S&T) approach was used to determine the steel ties around piles at the base of the section.

The design team considered the followings during the S&T idealisation:

- The S&T model was developed to achieve a "buildable reinforcement cage" details around the piles at pier as shown in Figure 7.
- The tie rebar's are taken in two direction, one around the pile reinforcement cage (indicated in red) and another set of rebar's connecting these ties transversely (indicated in blue) as shown in Figure 8.
- An appropriate height for the compressive struts within two times the width of the wall was considered. This allows to retain the strut angle ranges between 30 degree and 70 degree.
- To resolve the S&T model, load from beam was applied as nodal forces at each top truss location.

4.3 Solutions: Buildability

The design proposals, were made keeping in mind the buildability aspect and the safety of the personnel involved in the construction process.

In agreement with the contractor, choice of CFA piles for the smaller 900 mm diameter piles for the STOB's meant that the reinforcement cage may be lowered with ease.

The proposal of single row piles, directly connected to the abutment/ pier walls, meant the requirement of the structural element "pile cap" was eliminated. The contractor therefore will have to build one element less in each bridge, resulting in ease of construction, faster build up time and less exposure to site activity to the construction personnel.

The zone at the bottom of the abutment / pier walls has reinforcements from both the walls and the piles that are necessary as per the design / detailing requirements. Therefore, this zone required thoughtful detailing to avoid congestion and provision of safe and buildable details.

In keeping up with the good and practical practices of such detailing, the pile reinforcements are advised to be bent inwards, thus avoiding the chances of site accidents by impaling. The starter bars for the abutment / pier walls are detailed as shorter "L-bars", thus making it easy for the fabricators to build up the reinforcement cages. The design reinforcement as outcome of the "strut & tie" model as outlined above, are placed on the outside of the pile

reinforcements, thereby making it easier to handle and place at site. The horizontal wall reinforcements are placed at the outside of the vertical reinforcements in the walls, making it easier to place and fix in position. Suitable advises from the contractors, were sought, and the client's observations on safe detailing were discussed and followed.

Following the CDM-2015 regulations, safety workshops were conducted. Design teams and the contractor's representative discussed the safety issues related to the construction of each type of bridges. The risks were captured in the risk logs and the residual risks were captured in the relevant drawings under the SHE boxes.

One significant and practical addition to the conventional deliverables, which was agreed during the discussions with the contractor was to include the "reinforcement weight summary report" as part of the bending schedule. This will allow the contractor to understand and record along with the "Construction Drawings" the requirement of the reinforcement tonnage both bar diameter wise as well as in totality.

While detailing reinforcements, the designer followed a few more good practices. All the bars were detailed keeping the shorter leg length of the bar less than 2750 mm. This dimension is arrived keeping in mind the generally used truck dimension which may be used for transport of bars.

The designer also detailed the structural elements as much as possible with lengths of the bars that were easy to handle and in case required manual handling.

5. Conclusions

The geotechnical design of pile foundations was constrained by several design and construction requirements including: single row of piles, limitations on length of CFA piles preferred by the contractors, modelling challenges due to software limitations, and restrictions on pile spacing due to load demands and width of superstructure.

Viable design solutions were proposed by the design team satisfying the design and construction requirements. These are adopted in final design proposal through means of construction drawings, which are now accepted by all project stakeholders.

References

[1] BS EN 1997-1:2004, Euro code 7- Geotechnical design.

[2] NA to BS EN 1997-1, UK National Annex to Eurocode 7 – Geotechnical design – Part 1: General rules.

[3] NA to BS EN 1990:2002+A1:2005 – UK National Annex for Euro Code – Basis of structural design.

[4] Tomlinson, M. J and Woodward, J. Pile Design and Construction Practice, 6th Edition. London and New York: Taylor and Francis, 2014.

[5] PD 6694-1:2011, Recommendations for the design of structures subject to traffic loading to BS EN 1997-1:2004; Section 9. British Standards Institution.

[6] de Mello, V. F. B. Foundations of Buildings on Clay. State of the Art Report: p. 49-136 Proc. 7th International Conference S.M. & F.E., Mexico City, 1969.

Acknowledgements

[1] This paper was previously presented at the 2017 IABSE Symposium in Vancouver and formed part of the proceedings.

[2] All the structures and CAD team members working on the project, ably led by Andy Tye.

[3] Check team members of collaborative partner CH2M.

[4] The Geotechnical colleagues from Atkins who helped shape this up.

[5] Project representatives from Highways England.

[6] Representative of Stakeholder Engagement & Communication team.

[7] Representative of Communications & Engagement Manager.

[8] Project leaders, especially Alastair Moore and Suzanne Moore.

[9] Chris Hendy, David Smith and Gajanan Wagle, for the encouragement to see this through.

Originally presented and published as: Mukherjee D, Jain A, Balaji M. Single Row Piles in Integral Bridge Foundations: Challenges and Solutions. IABSE Symposium Report, IABSE Symposium Vancouver 2017: Engineering the Future; 8: 3484-3491.

Structural Design | 004

Engineering Design of the Platform Edge Screens for Crossrail's Mined Stations

Julian Birbeck
CEng, MIStructE
Associate
Engineering, Design & Project Management
UK

Rosemary Smiley
MEng
Engineer
Engineering, Design & Project Management
UK

George Stowell
RIBA, MRIAI
Architect
Engineering, Design & Project Management
UK

Ed Newman-Sanders
CEng, MICE
Technical Director
Engineering, Design & Project Management
UK

Abstract

This paper covers the engineering design of Platform Edge Screens for the five mined Crossrail stations in central London. Full-height platform edge screens are a signature feature of Crossrail's mined station platforms, and their design presented many challenges. To gain maximum uniformity, for the purpose of economies of scale in construction, quality finishes and low cost, safe maintenance the edge screens were developed as a common reference design, which was then issued to the each of the contractors for the mined stations. This paper describes the technical challenges from the point of view of a structural engineer, but in doing so, it draws in interfaces with disciplines as diverse as tunnel ventilation, electrical engineering, and rolling stock procurement. The reference design approach allowed features of the PES to be prototyped and tested before issuing to the station contractors.

1. Introduction

The term Platform Edge Screen (PES) as used in this paper describes a complete assembly, comprising screen doors, an upper 'service wall' supporting lighting, communications, and cabling, plus a smoke-extract duct positioned over the track. The term PES-frame is used to describe the structural frame that supports all these elements. This PES-frame design applies to five stations; Bond Street, Tottenham Court Road, Farringdon, Liverpool Street, and Whitechapel.

From street level, the scale of Crossrail platforms, and the associated screens may not be apparent (Fig.1). Given that 9-car Crossrail trains are over 200m long, and each platform has some additional publicly accessible length to allow for 10-car trains in future, there is over 0.5 km of screen required at each station and the PES-frames described in this paper extend for over 2.5km. The PES-frame is designed around a 3m module, so there are over 830 of these modules across the network.

Figure 1: Illustration of the Length of the PES on a Typical Crossrail Platform

2. Contractual Set-Up

The PES was developed as a linewide design package to create passenger, maintenance and safety consistency in public areas. Components were drawn, performance-specified by Crossrail's designer comprising Atkins, Grimshaw, Maynard and GIA Equation, then mocked-up, prototyped and tested by Crossrail's Chief Engineer's Group as generic solutions. Once approved, these common designs were passed on for station-specific design, manufacture and installation. The Platform Screen Doors (PSDs) including the glazed infill panels, are specialist mechanical elements, common to all sub-surface Crossrail Stations and delivered by a separate contract (Fig.2).

A part of the overall design strategy was to undertake stakeholder engagement with the organisations operating the stations and railway. This involved reviewing drawings, 3D BIM models, and physical prototypes. Thereafter, a coordinated Access and Maintenance Strategy was issued to station contractors alongside the RIBA F1 design: the objective being to create a harmonised maintenance strategy

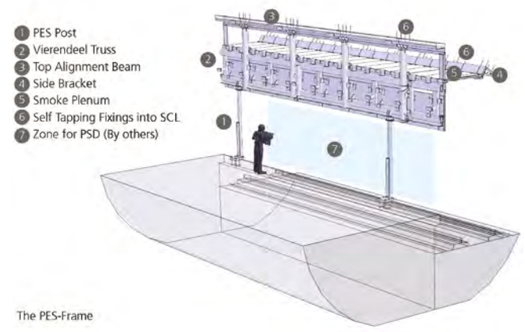

Figure 2: BIM Model of the PES-Frame Reference Design

3. The Purpose of Platform Edge Screens

Platform edge structures are uncommon in the UK being first used on the Jubilee Line extension in 1999. Nonetheless, such structures can be found on many metro systems, and fall into three categories (Fig.3):

1. Platform Edge Doors (PED): Balustrade-height edge structures with automatic doors aligned to the train doors. Their sole function is to prevent passengers falling onto the track.

2. Platform Screen Doors (PSD): Doorway-height structures with automatic doors aligned to the train. They have the same safety function as PEDs, also providing a degree of screening to passengers from air movement.

3. Platform Edge Screens (PES): Platform-to-ceiling structures providing more extensive screening than PSDs, and separating the platform and track environments.

Figure 3: Classification of Platform Edge Structures

For Crossrail, the early decision to use Platform Edge Screens transformed the tunnel ventilation strategy. Since air leakage through stations was effectively eliminated, the need for six additional ventilation shafts and head-houses in Central London was removed.

The simplest approach to design the PES would be to collect all station systems on the platform side and all rail systems on the trackside. Stations require extract ducting for the full length of the platform – both for the day-to-day managing of platform ventilation, but critically to provide smoke extract in the event of a fire.

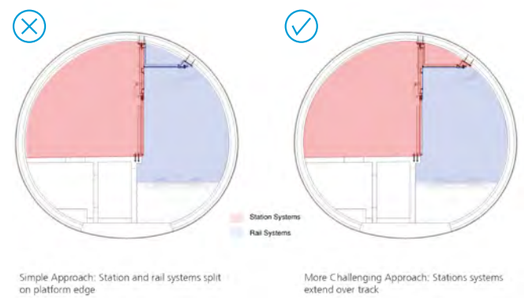

Figure 4: Platform Tunnel Space Planning: Station and Rail Zones

[1]The benefits of the common-components approach on large-scale infrastructure projects are described in more detail in papers by McClements, N. ICE 2012 and Moxon, S; Atherton S. ICE 2012

Figure 5: The Crossrail Platform Environment

4. Development of the Structural Diagram

The most obvious way to support a PES is to suspend it above the platform screen doors: the PSD providing the screen for passengers up to door height, and the PES frame supporting lighting, cabling and smoke duct above (as well as restraining the head of the PSD). However, construction demands prevented adoption of that solution. Firstly, during fit-out, the system-wide contract passes through each platform with track-laying plant requiring an unobstructed zone along the platform edge, meaning that a straightforward suspended solution could not be used. Secondly, Crossrail stations differ from existing tube stations in their use of Sprayed Concrete Lining (SCL) reinforced with fibre for profile stabilisation.

Spray linings are not suited to the accurate placing of reinforcement. Hence rebar is used sparingly, only at critical junctions. Furthermore, multi-stage lining build-up raises a risk of delamination between layers under radial point loads. Overall this meant that the concrete lining could not be designed with sufficient long-term capacity to support a suspended PES. The alternative was to support the PES from below with posts placed onto the platform edge, however, posts passing down to platform level would need to coordinate with the door positions on the PSD. At the time of design and initial tunnel construction, the rolling stock had not been ordered, moreover for competitive tender, train bids were placed with multiple suppliers, each with different door configurations. Even when this procurement sequencing issue was resolved, there remained a need to provide future flexibility in the PES, including the option to extend trains in the future with different door configurations.

A structural diagram was therefore planned around a sequence of fixings into the tunnel crown at 3m centres: these fixings provided vertical and horizontal restraint temporarily, but reverted to horizontal restraint only in the permanent condition (Fig.6). The crown fixings support a continuous Vierendeel truss with a 1.5m module. The truss is designed so that it may be supported at any point with pin-ended posts onto the platform edge below (subject to some basic setting-out constraints). Horizontal props at a 3m module, provide lateral restraint. To complete the system, the smoke duct soffit is formed in precast planks, spanning from the top of the truss onto a continuous side-bracket, fixed to the SCL on the track-side.

This structural arrangement provides alternative load-paths, giving the PES-frame an inherent robustness. Should a PES-post be accidentally removed, the slotted-hole connections at the crown would reach their limit of travel and the frame would revert (short term) to a hanging structure.

[2]Coughlan, D, Diez, R, Comins, J and Stark, A, ICE 2016.

The decision was taken to place the extract duct over the track (Fig.4), allowing the platform space to take on a unique character, resulting in a very different passenger experience. The tunnel cladding curves over the passengers' heads to the tunnel apex with all lighting, signage, public address and associated cabling then located on the vertical face of the PES above the screen doors. This concentrates electrical and mechanical services in one place to support maintenance efficiency. Light from the light boxes reflects off the tunnel cladding to create a soft, diffuse ambience (Fig.5).

Consequently, the structural engineer is in a pivotal position; not only designing a structure which is critical to the overall master-planning and land-take, but which also underpins the platform architectural concept and the passengers' experience.

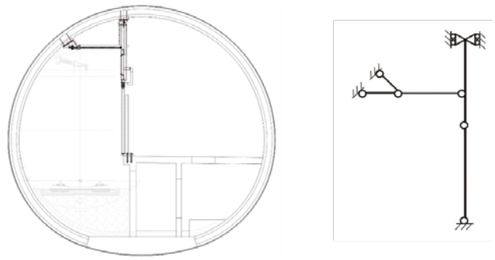

Figure 6: PES Structural Diagram – Permanent Condition

Figure 7: 6m Length of PES Vierendeel Truss Being Lifted Into Place at Farringdon Station (Note Top and Side Alignment Beams Already in Position)

Given the length of the PES, longitudinal movement was an additional consideration. Expansion joints are provided at 15m centres along the platform. Between these movement joints, it was necessary to provide moment-splices in the continuous truss, allowing it to be installed in 3m, 6m, or 9m lengths (Fig.7). Setting-out rules for were devised allowing the reference design to be adapted to any permutation of rolling stock and train stopping position.

The PES is not fire-rated to withstand a full train fire, but it does need to function in the event of a small baggage fire. To this end, computational fluid dynamic analysis was undertaken confirming a need for the PES to resist smoke temperatures of 200°C for up to one hour. This temperature does not critically affect steel strength, but does create a significant degree of thermal expansion, which needs to be accommodated at the movement joints

5. Tolerances

The SCL has a large construction tolerance envelope of 100mm, whereas the PSD and the cladding fixtures and fittings have an installation tolerance of +/-5mm. It was thus clear that due to multiple interfaces between the structural frame and the supported elements, this too would need to be erected to cladding tolerances. Consequently, the connection into the SCL was required to take up the major portion of the SCL tolerance.

The solution was to use grout infills running longitudinally along the tunnel at the two upper connections into the SCL: the top connection at the tunnel crown, and the side connection at the trackside edge of the smoke plenum. A folded-plate alignment beam was placed at the apex of the tunnel, and a similar folded plate detail was used for the side bracket (Fig.9). In this way, the erector was required to line and level these elements which were delivered to site in 6m or 3m lengths. Once positioned within tolerance, grout infills were poured and the required tolerances were locked in for the subsequent frame erection.

As there are the large tolerances involved at the SCL interface. the anchors needed to be through-fixings, allowing the PES brackets to be offered up, lined and levelled, with holes drilled using the brackets as templates. The anchors were threaded studs, with two nuts clamping so allowing the PES bracket to be held firmly in position whilst grout was poured.

Anchor choice was also influenced by the Boston Tunnel ceiling collapse of 2006 (consequent on creep in chemical fixings). Crossrail's technical standards prohibit such anchors working in direct tension in overhead fixings. The adopted anchors were therefore self-tapping anchors, used extensively for secondary fixings on the Channel Tunnel Rail Link. These offered the advantage of achieving full shear and tension capacity, without needing to be torqued-up or 'set'. The load capacity of these

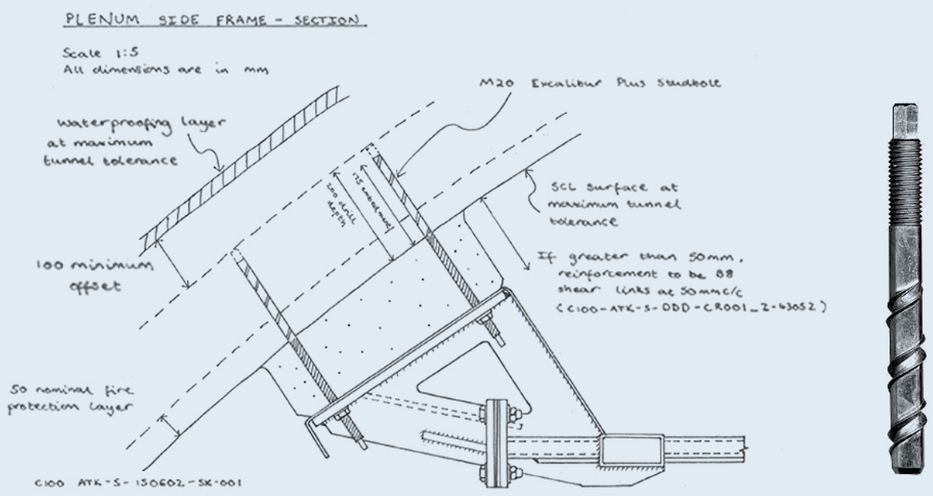

Figure 9: Design Development Sketch – Showing Grout Infill and Stud Anchors and Self-Tapping Threaded M20 Stud-Anchor

anchors when fastened into the SCL was verified by pre-contract testing, specified by the linewide designer.

6. Durability, Design Life, and Maintenance

The permanent and variable loads applied to the PES appear small, and the spans short. On the platform elevation, the PES is required to support lighting, signage and other items of equipment, totalling no more than 1 kN/m^2 (i.e. a typical cladding load). Even the smoke plenum soffit, formed in precast concrete, weighs no more than 2.2 kN/m^2 on plan.

As far as variable actions are concerned, crowd load is represented by a 3.0 kN/m line load. In addition, piston loads from train movement create pressure changes, with a typical value of 0.8 kN/m^2, and an extreme case of 1.2 kN/m^2. Although load magnitudes are small, they do cycle frequently creating a fatigue condition. Over the 120-year design life, 24 million cycles are forecast.

A key issue is demand for ongoing inspection and maintenance. This task is to check steel and corrosion protection condition and assure nuts remain tight albeit all nuts are secured with locking washers. To aid inspection, all connections were designed with the bolts visible, a condition verified by using a 3D BIM model (Fig.10). Anchor capacity was verified by testing

The corrosion protection system needed to be a minimum-maintenance solution. Stainless steel structure was considered, but adequate life was achieved from a cheaper galvanised finish (typically 140 microns)

7. Electrical Isolation

Electric train traction relies on the return current from the overhead lines passing through the rails. Over the distances involved, rails have significant electrical resistance with the net result that earth voltage on a train is 'floating' relative to its surroundings and can be in the order of 50 volts. This is of no

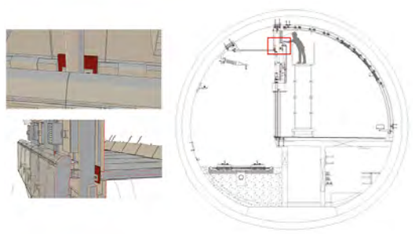

Figure 10: BIM Model Used to Develop the Access and Maintenance Strategy

concern when the train is moving and the passengers are separated from the surroundings. However, when the train stops, it is imperative that passengers cannot touch the train or any surrounding metallic infrastructure located on a separate electrical earth.

The platform edge structure therefore has to be electrically bonded to the adjacent rails and isolated from the surrounding station earthing system.

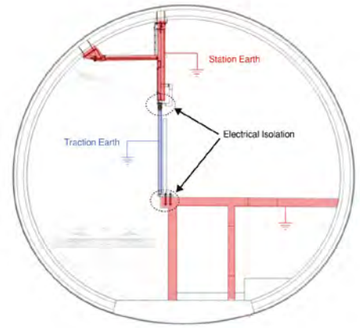

Figure 11: Summary of Earthing and Bonding Strategy, and the Need for Electrical Isolation Within the PES Frame

This is achieved by electrically isolating the PSD and the adjacent PES-posts from the remainder of the PES-frame above and the platform edge rebar below (Fig.11). The latter isolation was achieved by locally reinforcing the platform edge with non-conducting GFRP rebar. The former isolation, however, presented a challenge. The PSDs and the PES-frame form a wall bounding the platform space. As such, they are subject to the Subsurface Station Regulations, which originated in response to the Kings Cross fire disaster in 1988. These regulations stipulate that any material used in the construction of a wall in a public place must be of limited combustibility and this cannot be achieved with a polymer. Consequently, three ceramic isolator materials were short-listed and tested for mechanical properties. It is anticipated these will require periodic replacement and frame detailing was developed with this in mind.

8. Construction

The linewide design team prepared the PES-frame reference design for a generic, straight run of tunnel platform to RIBA Stage F1. As such, the station contractors were presented with an assured steelwork design, including full connection design, as well as precast planks for the plenum soffit with full reinforcement design. In this way, a common design approach undertaken by the linewide designer created a major saving in design and coordination effort, compared to each contractor working up a PES themselves

9. Conclusions and Lessons Learnt

When the Elizabeth line opens to the public, there will be a completely new sub-surface environment on the London Transport network. The 250m-long platforms with 5m unobstructed headroom will change passengers' expectations of sub-surface rail, made possible by the gathering of lighting, signage, communications, and services distribution onto the vertical plane of the PES with the smoke-extract plenum concealed behind. The delivery of the PES design by linewide designer brought undoubted design efficiencies. Given the complexities of the interfaces with the tunnel lining, electrical isolation, coordination with the door locations, and offsite testing, the level of design supervision required would have been significantly greater, had these issues been tackled independently by the station teams.

From the structural engineer's perspective, the PES design is intriguing. A cursory glance at the structural spans and the applied loads suggests that the PES is a simple element of secondary steel. Challenges have arisen, however, from the interfaces with other systems and are inherent in a heavily-serviced, spatially-constrained railway. The key to unlocking these challenges has been a structure with built-in flexibility. Adaptable geometry allows the location of support posts to be varied, and adaptable load-paths allow the structure to be hung as well as propped. In this respect, the development of such 'smart' structural components, with parameters that can be 'flexed' to suit local, temporary, or future conditions may become increasing common for large infrastructure projects.

Acknowledgements

Dr Sunday Popo-Ola, who oversaw the material testing of the isolator components and threaded anchors at Imperial College London, and led the subsequent analysis of the results.

Originally published in: Birbeck J, Smiley R, Stowell G, Newman-Sanders E. Engineering design of the platform edge screens for the Elizabeth line's tunnel stations. The Structural Engineer, 2018 Jul; 84-89.

Solfec Validation for Large Arrays of Radially Keyed Bricks: Comparison of Experimental Measurements and Computational Predictions

Benjamin Cannell

Senior Engineer
Nuclear
Bristol, UK

Steve Brasier

Senior Engineer
Nuclear
Bristol, UK

Neil McLachlan

Graphite Core Engineer
EDF Energy Generation
Bristol, UK

To ensure safe and reliable operation of the UK's Advanced Gas-cooled Reactors (AGRs), seismic qualification of the graphite cores is required to demonstrate safe shut down during an infrequent seismic event. Existing seismic assessments of the AGR cores use a finite element modelling approach called GCORE, modelling the behaviour of the graphite core components using a "stick and spring" finite element model. The experimental computational code, Solfec is designed to simulate multi-body contact dynamics of large systems and as such predict the consequence of component interactions beyond the capability of GCORE. This paper focuses on the validation of Solfec predictions against the measured dynamic responses for large arrays containing intact and simulated double axially cracked bricks, produced during rig tests at the University of Bristol.

Keywords

Solfec; Dynamics; Contact.

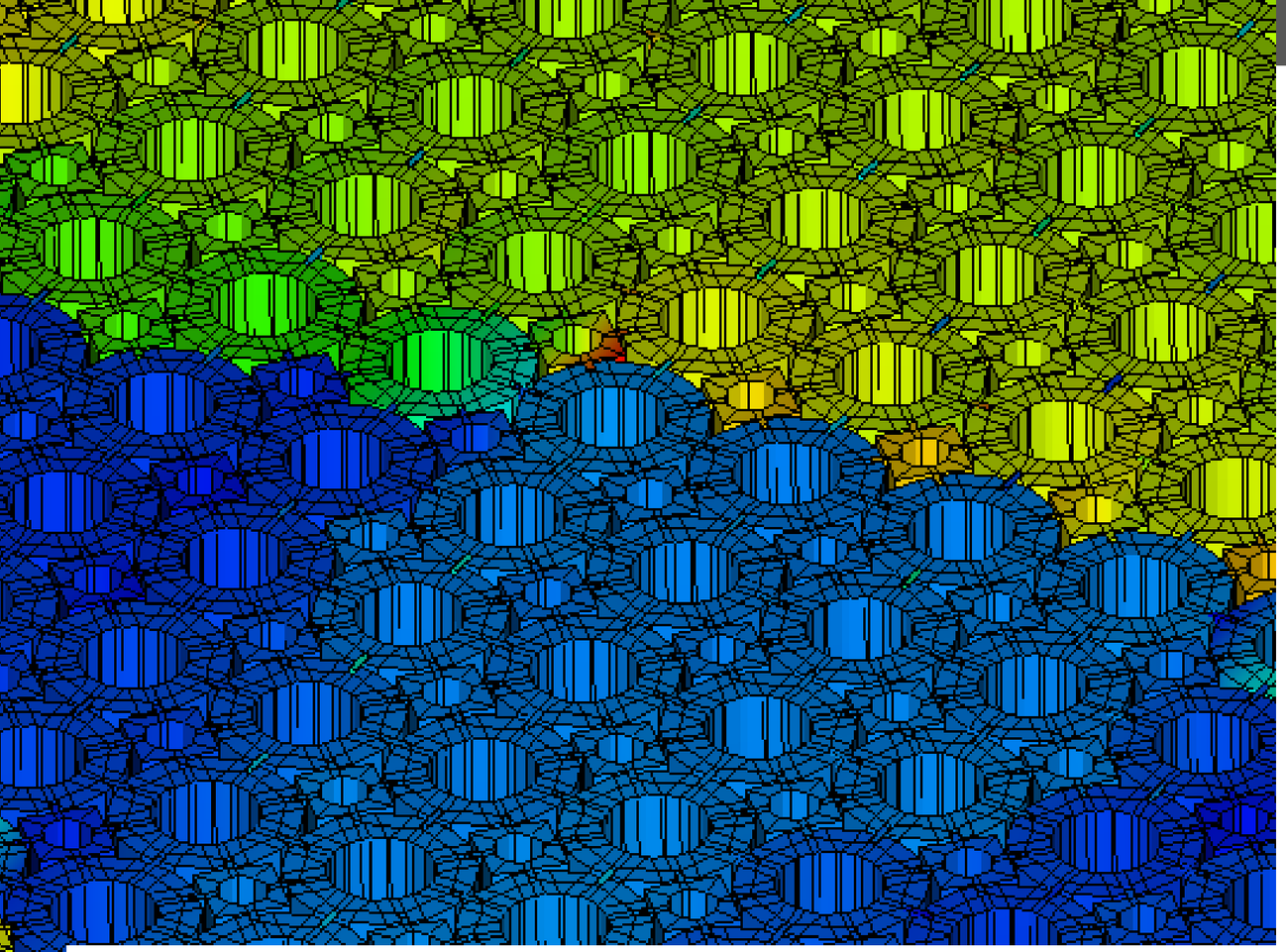

1. Introduction

The experimental Solfec computational code, (Koziara, 2015), is designed to simulate multi-body contact dynamics of large systems. It is a research code being developed by Dr. Koziara (formerly of Durham University) with funding from EDF Energy, with a view to use in analysing the seismic response of Advanced Gas-cooled Reactor (AGR) cores. Atkins have carried out various pieces of work to assess and improve the suitability of the Solfec code for AGR seismic analyses, and to develop the tools and methods needed to use it for this purpose.

As part of a wider programme of work on seismic assessments, the University of Bristol have been commissioned by EDF Energy to carry out dynamic shaker-table testing of arrays based on quarter scale geometry of a late-in-life AGR core. This test programme is on-going using both a single-layer array (SLA) and a multi-layer array (MLA) test rig.

The focus of this paper is to compare Solfec simulations and experimental results for the first two sets of tests carried out with the single layer array, SLA1 and SLA2. These tests utilised both uncracked and cracked arrays with applied haversine (asymmetrical single-pulse), sine dwell and seismic driving motions. The comparisons are not claimed to provide complete validation of Solfec, but provide a first assessment of Solfec's accuracy for large array type configurations which are representative of AGR seismic assessments.

2. Solfec Overview

A detailed description of the Solfec software and a general overview of the available functions which may be applicable to seismic assessments of AGR graphite cores is provided in (Brasier, 2014) and (Koziara, 2015).

As for most commercial general-purpose Finite Element (FE) codes, Solfec provides a number of options and input parameters which must be appropriately chosen by the user. In particular, the selection of appropriate meshes, time-step and damping values is complex as these do not have direct physical origins. Previous work by both Dr. Koziara and Atkins, showed that in Solfec simulations of unrestrained collisions between individual deformable bodies, these three parameters can have a large effect on energy loss and therefore the coefficient of restitution of the collision. This behaviour is complex and depends on the mesh, time-step and damping used, as well as on other simulation parameters such as the choice of contact constraint, and physical parameters such as the material properties and collision velocity. However, it has not been clear whether the variability in coefficient of restitution seen in these free collisions is relevant to the aggregate behaviours of large arrays, i.e. the behaviour of interest for seismic assessment of AGR cores. The availability of physical results from the SLA tests allowed this aspect of the simulation behaviour to be explored.

The effect of friction coefficient on the simulation results was also investigated. This was in part due to the limited friction data available for the SLA, but also to support future AGR analyses where the actual friction coefficient of irradiated graphite is likely to have significant uncertainty.

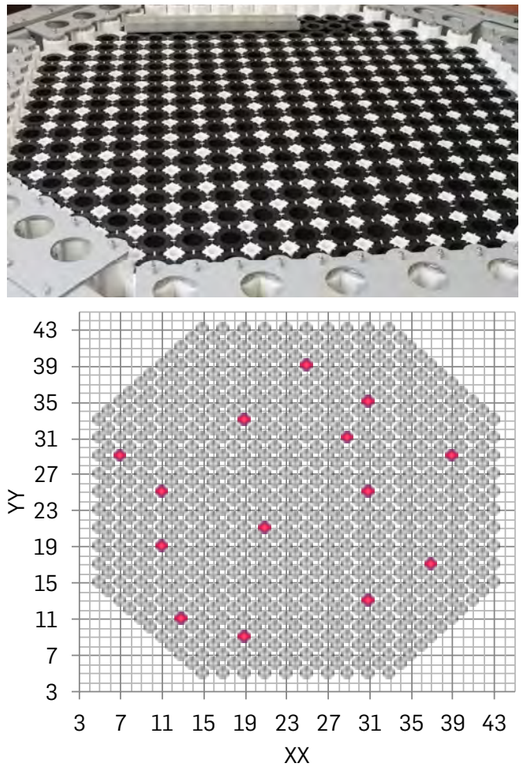

FIGURE 1: General view of the Single Layer Array and restraint frame and location of DCBs

3. Test Rig Single Layer Array Overview

3.1 Array Configuration

The experimental rig, shown in Figure 1, consists of an octagonal array of Acetal bricks and keys mounted within a restraint frame attached to a large shaker table, (Dihoru, 2015).

The overall configuration is broadly modelled on a ¼-scale Hinkley Point B (HPB) / Hunterston B (HNB) core design, although it is smaller at 20 columns across (c.f. 24) and octagonal rather than 16-sided. It includes lattice bricks, interstitial bricks and loose keys. The brick and key geometries (including key/keyway clearances) are based on simplified ¼-scale predicted geometry for the HPB/HNB reactors late in life. The restraint frame is a heavy steel structure which is considered effectively rigid, and is attached to the shaker table. The array is driven at its outer edge by partial bricks which are fixed to the restraint frame. The array components sit on a layer of glass beads which in turn rest on a smooth machined steel base. This provides a low-friction interface between the Acetal array components and the base.

The array X and Y axes are shown in Figure 1 and individual components within the array are identified by their position on the array grid, given in the format YYXX. The location of doubly cracked bricks (DCBs) included during the cracked rig tests is also presented in Figure 1.

3.2 Driving Motions

A variety of single-pulse sine-dwell and seismic-type input motions were applied to the array during the SLA tests series, with all motions along either the array X or Y axes. For seismic-type inputs both "full-scale" time-histories as would be applied to an AGR model and dynamically scaled "quarter-scale" time-histories (with displacements reduced by a factor of four and the time-axis compressed by a factor of two) were used. Only a sub-set of the tests carried out in these series were simulated for the comparisons described here.

3.3 Rig Instrumentation

As reported in (Dihoru, 2015), the motion of a selection of components and the rig restraint frame was recorded using an infra-red vision system. This IR vision system used calibrated cameras to track markers attached to selected bricks and keys and the restraint frame. The origin of the IR vision system's coordinate system was located at an arbitrary location fixed relative to the laboratory (i.e. not moving with the shaker table); review of frame marker IR data indicated that the IR system's coordinate system was parallel with the YY and XX axis of the shaker table. The motion of a number of DCBs was also tracked within the IR vision system using three IR markers located on each half of the DCB.

4. Solfec Single Layer Array Model

4.1 Geometry and Meshing

The Solfec model of the SLA included all Acetal components within the test rig, i.e. the lattice and interstitial bricks and the loose keys. These were modelled using the mid-tolerance geometry from the appropriate drawings. The partial bricks attached to the restraint frame were modelled as standard bricks

All SLA components were modelled using deformable finite element meshes. The model was assessed using two different mesh densities, presented in Figure 2. Sensitivity analyses indicated that combined with an appropriate time step of 1x10-5s, the coarse mesh produced acceptable results within reasonable analysis durations.

Note that all components are located at their "on-pitch" position at the beginning of each simulation. This differs from rig tests where the initial location of components is their resting location from the previous test.

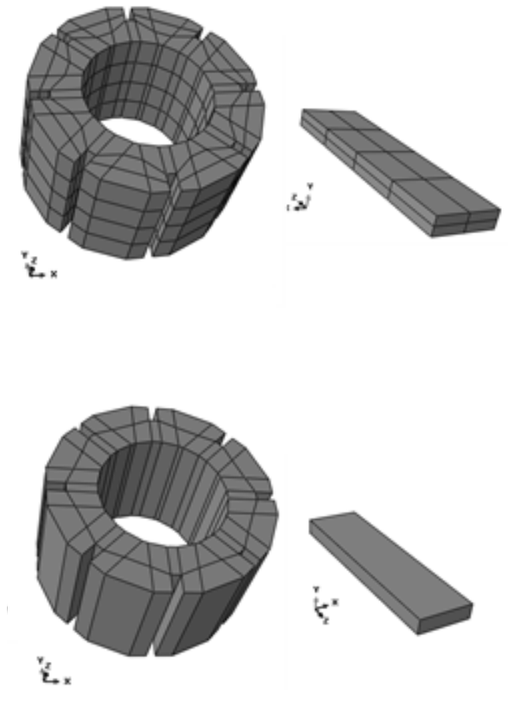

FIGURE 2: Comparison of fine and coarser meshes

4.2 Driving Motions and Boundary Conditions

A sample of SLA2 rig tests covering haversine, sine dwell and seismic driving motions, were simulated within SOLFEC. Array driving motions were extracted from the displacement time histories of frame IR markers measured during the rig test being simulated. As such, the SOLFEC input motion is identical to that experienced by the table, as opposed to the demanded table motion.

Driving motions were applied to the restraint bricks along with boundary conditions to prevent rotation around the vertical axis. Vertical boundary conditions were applied to all components, effectively modelling a frictionless base.

4.3 Damping and Friction

Solfec implements stiffness-proportional body damping with a user-selected coefficient. Initial simulations of a single Acetal bar impacting a rigid surface showed considerable sensitivity to choice of damping parameter with coefficients of restitution ranging from 0.41 to 0.79 for damping coefficients in the range 1x10-5 to 1x10-4.

In contrast, simulations of the SLA showed that the range in peak displacement of the central lattice brick LB2525 (e.g. Figure 3) was not particularly sensitive to the choice of damping parameter. As such, it does not appear necessary to "tune" the damping parameter for analyses of large arrays.

However, the behaviour of the SLA simulation did appear to be sensitive to the choice of friction coefficient. This is less problematic as it is a measurable parameter and the results

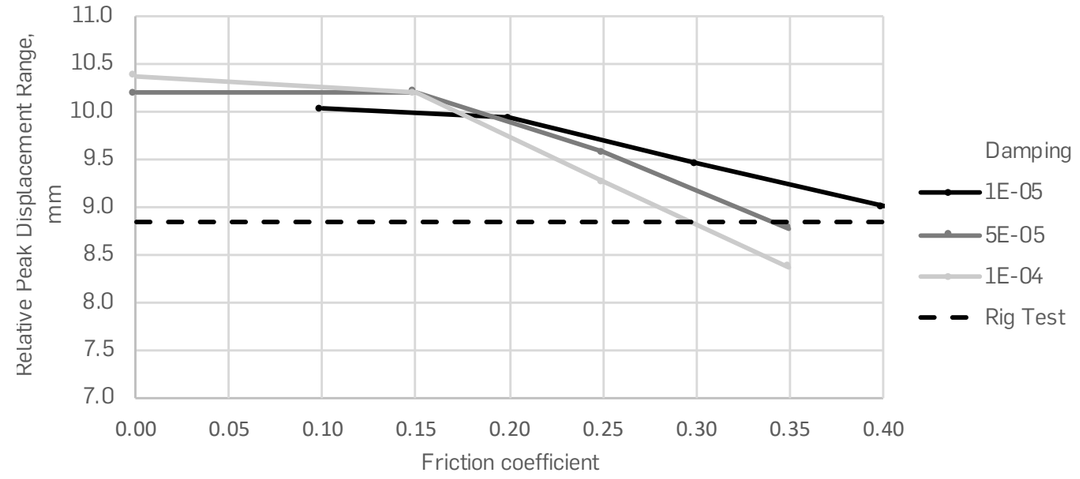

FIGURE 3: Sensitivity to damping and friction coefficients for 3Hz sine dwell motion

presented in Figure 3 indicate that the manufacture's quoted value of static friction coefficient, 0.35, appears to be appropriate for SLA simulations.

5. Rig Test And Solfec Simulation Comparisons

5.1 Haversine Driving Motions

Direct comparison of the test rig and Solfec simulation array relative X displacement of LB2525 is presented in Figure 4 for an uncracked array. The results show good agreement beyond 0.2s once the effect of the different starting locations of the brick is washed out.

A key observation is that the motion of LB2525 within the test rig appears to be heavily damped. This is illustrated in Figure 4 by the lack of motion of LB2525 after the table has stopped moving. Comparison with results of the Solfec simulation suggests that, for the SLA configuration, the Solfec simulation also appears to be heavily damped even when using a relatively low value of body damping. These observations suggest that the damping in the Solfec SLA model is primarily due to the contact interactions, supporting the observation that SLA simulations are unaffected by the choice of body damping.

An important configuration at which to compare simulations and rig-tests is when the array is "locked-up", i.e. it is loaded such that clearances are taken up between adjacent components. This state is important because it determines the maximum relative displacements of components in the array and the loadings in the keying system.

To compare the "lock-up" behaviour of the test rig and Solfec, three simulations were completed of haversine input motions with peak table displacements of 10mm, 29mm and 53mm. The peak positive and peak negative array relative displacement of LB2525 were then compared against the equivalent values from haversine rig tests, Figure 5. Note that the maximum array relative displacement is reached following the peak table displacement being achieved whereas the minimum array relative displacement occurs once the table comes to rest.

For driving motions of greater than ~10mm, the array appears to experience "lock-up" at both the positive and negative end of the cycle, indicated by the relatively consistent values of minimum and maximum array relative displacement. There is a slight increase in maximum array relative displacement and decrease in minimum array relative displacement as the table peak displacement increases beyond ~10mm due to the bricks experiencing an increasing force as the table accelerates and decelerates.

Note that the method of post-processing rig test data assumes that the "lock-up" behaviour is symmetrical. In reality, the difference in loading between the peak and end of the cycle is likely to result in larger maximum array relative displacements than minimum displacements and is considered to contribute to the slight difference in results presented in Figure 5.

5.2 Sine Dwell Driving Motions

Comparison of rig test and Solfec simulation results of an uncracked array for a 1Hz sine dwell driving motion show very good agreement and are not presented here. Comparisons of a cracked array are of more interest and a comparison of results is presented in Figure 6 for a 1Hz sine dwell with an amplitude of 10mm.

Comparison of the array relative displacement behaviour of LB2525 indicates that the rig test and Solfec simulation generally show good agreement although Solfec appears to predict a greater range in array relative displacement than the rig. Notably the behaviour predicted by Solfec is non-symmetrical, i.e. the displacement achieved during positive "lock-up" is greater than that achieved during negative "lock up" (the presented rig displacement behaviour is forced to be symmetrical as a consequence of the assumptions used to post process rig test results).

A contributing factor to the difference in displacement range results may be due to the 1Hz sine dwell driving motion only resulting in a peak table displacement of ~10mm, which may not be large enough to lead to "lock-up" of the array, Figure 6, given the freedom of movement due to the inclusion of DCBs. It was also observed that the array relative displacement in the Y direction, perpendicular to the driving motion direction, was considerably greater in the Solfec simulation than the test rig. Figure 7 presents a time history of the X and Y relative displacement of the centre of LB2525 illustrating this difference in behaviour.

The behaviour illustrated in Figure 7 is considered to be as a result of cracks orientated at 45° to the driving motion direction introducing forces at the end of the motion cycle orthogonal to the driving motion direction. The (low) friction between the test rig array components and test rig base may be enough to resist this force and hence resist this orthogonal motion. In contrast the SOLFEC model has zero friction between the array components and test rig base, and hence cannot resist the orthogonal motion.

Interestingly, disengagement of a single loose bearing key was recorded in the rig test and predicted in the Solfec simulation at the same position within the array.

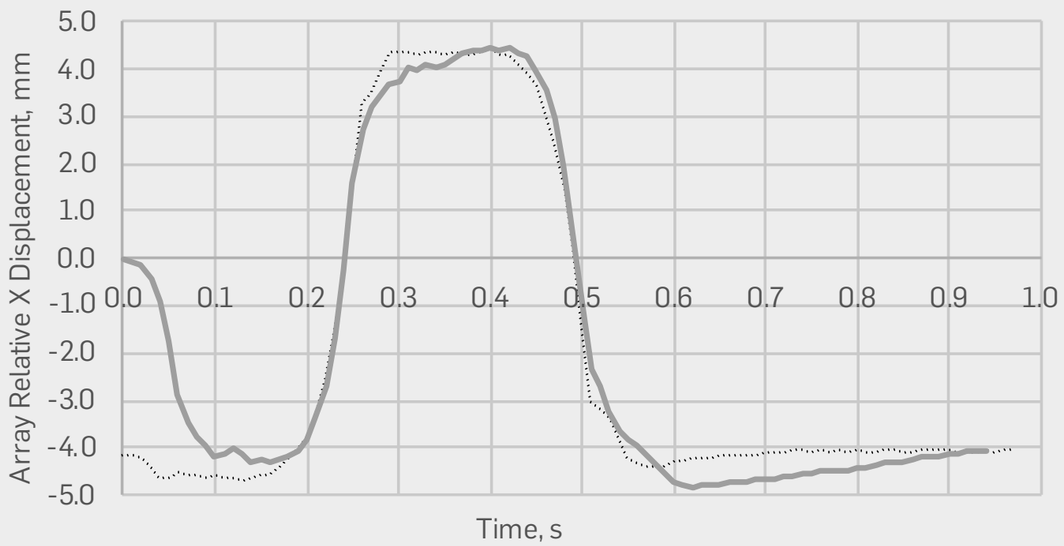

FIGURE 4: Comparison of LB2525 displacement during a haversine driving motion, uncracked

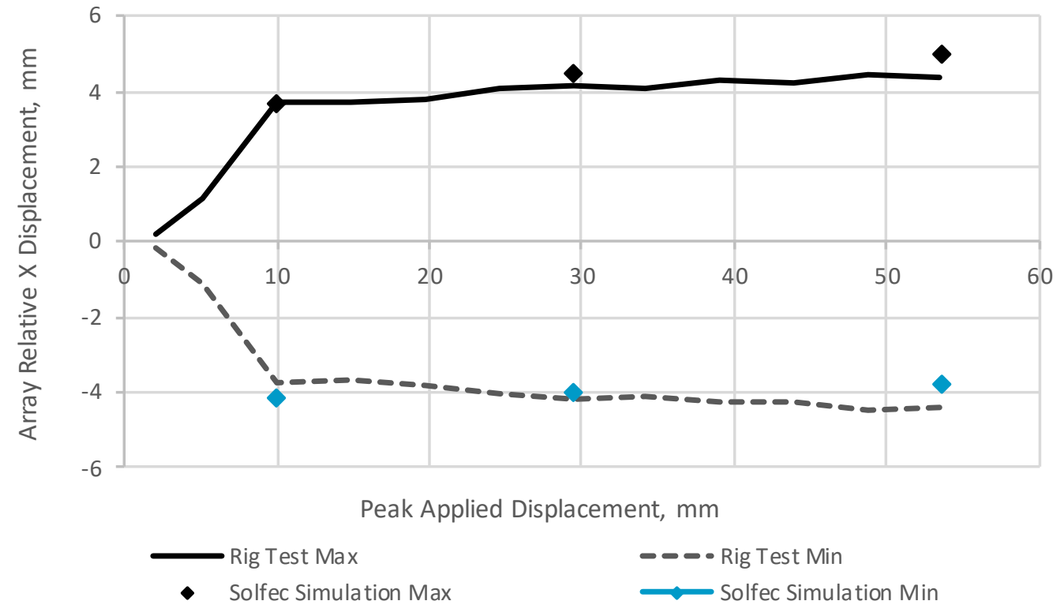

FIGURE 5: Comparison of LB2525 "lock-up" displacement during a haversine driving motion, uncracked

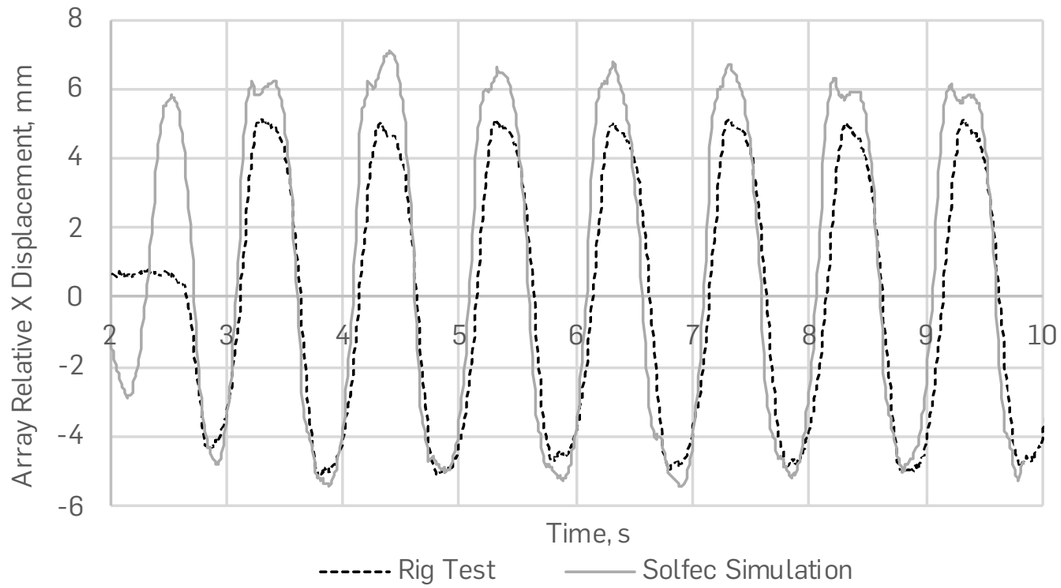

FIGURE 6: Comparison of LB2525 displacement during a 1Hz sine dwell driving motion, cracked

Seismic Driving Motions

Both quarter scale and full scale seismic HPB driving motions were applied in rig tests and Solfec simulations. Comparisons with quarter scale motions were typically poor, which is considered to be largely due to the peak displacement of the rig table being very low, <4mm, considerably less than the >10mm displacement required to cause “lock-up”. Since the initial position of the rig lattice bricks is not captured in the Solfec simulation, comparisons of these quarter-scale motions are not expected to be useful and are not discussed further here.

Figure 8 presents a comparison of the array relative displacement of LB2525 for a cracked array subject to a full scale seismic input motion. The simulation shows good agreement with the rig during the “strong” portion of the driving motion between 5s and 8s. During this portion of the motion the array experiences large displacements and accelerations and hence is likely to be “locking-up”. Agreement of LB2525 motions after the “strong” portion of the motion (post 8s) is worse suggesting that Solfec is less capable of predicting brick motions whilst in free-flight. This is possibly due to the body damping parameter not being “tuned” for the SLA components and giving inaccurate restitution coefficients between individual bodies. Since the intention is to use Solfec to simulate multi-layer arrays, within which components are not anticipated to experience extended periods of free-flight, this disparity in behaviour has not been investigated further. Friction between the Acetal bricks and test rig base may also be a contributing factor.

Note that uncracked full scale seismic comparisons exhibit similar behaviour to the cracked assessment described above.

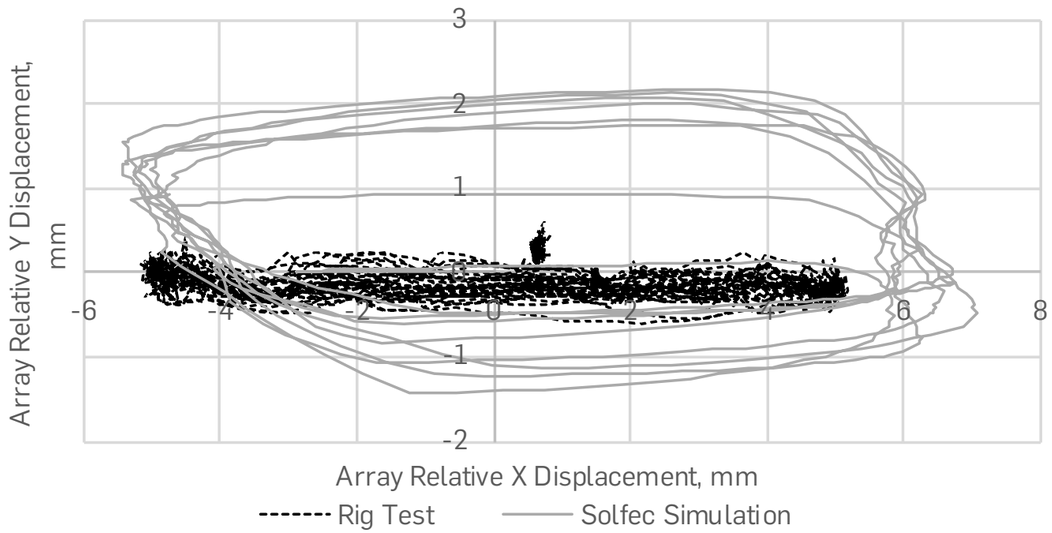

FIGURE 7: Comparison of LB2525 displacement during a 1Hz sine dwell driving motion, cracked

6. Summary

A solid-body approach to AGR seismic simulations could significantly extend the behaviours which can be simulated with current methods. The experimental computational code, Solfec is designed to simulate multi-body contact dynamics of large systems and as such predict the consequence of component interactions beyond the capability of current methods.

Assessments have been completed to contribute towards the validation of Solfec against the measured dynamic responses for large single layer arrays containing intact and simulated double axially cracked bricks. Motion comparisons of the central lattice brick within uncracked and cracked arrays generally show good agreement with Solfec being particularly capable of accurately predicting “lock-up” displacements and brick motions during the “strong” motion of a full scale seismic signal. The increased mobility of bricks within a cracked array appears to result in Solfec over-predicting brick motions compared to the test rig. It is noted that this may be attributable to Solfec not modelling friction between the Acetal components and the test rig table, and the choice of body damping. Additional validation assessments of large multi layer arrays would provide more confidence in the ability of Solfec to predict the behaviour of arrays representative of an AGR graphite cores.

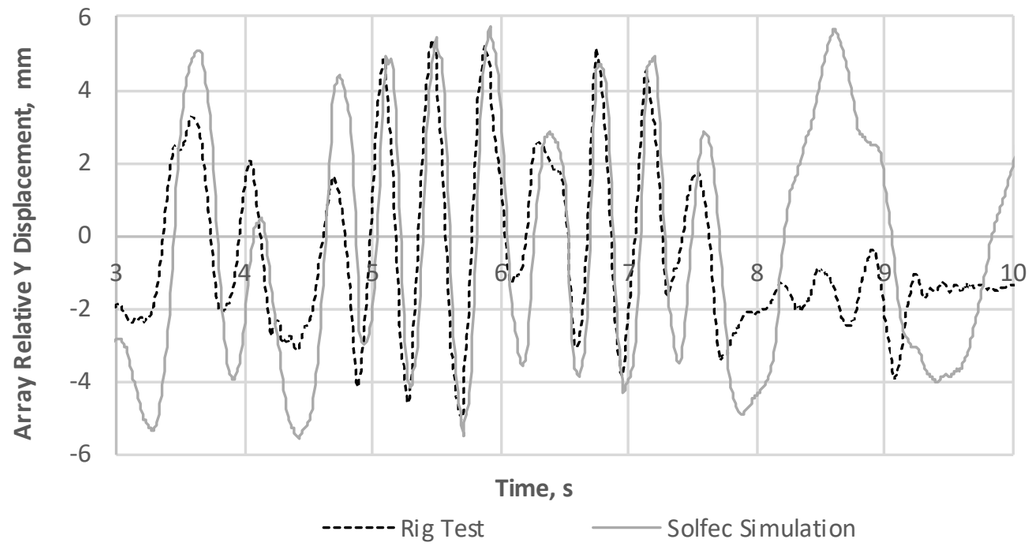

FIGURE 8: Comparison of LB2525 displacement during a full scale seismic driving motion, cracked

References

Brasier, S., Dey, S. and Kumar, R. (2014). Future methodologies for seismic assessment of AGR graphite cores. The 4th EDF Energy Nuclear Graphite Symposium. Engineering Challenges Associated with the Life of Graphite Reactor Cores, EMAS Publishing 2014.

Dihoru, L., Oddbjornsson, O., Brasier, S., Crewe, A., Taylor, C., Steer, A. (2015). A Single Layer Rig for Exploring the Dynamics of an Advanced Gas Cooled Reactor Graphite Core: Commissioning and Proposed Validation Studies, Earthquake Risk and Engineering towards a Resilient World, Proceedings of SECED 2015 Conference held in Cambridge, United Kingdom, 9-10 July 2015.

Koziara, T. 2015. Solfec. [ONLINE] Available at: https://github.com/tkoziara/solfec. [Accessed 12 April 2016].

Acknowledgements

Originally presented and published as: Cannell B. , Brasier S., McLachlan N., Solfec Validation for Large Arrays of Radially Keyed Bricks: Comparison of Experimental Measurements and Computational Predictions. The 5th EdF Energy Nuclear Graphite Conference, May 2016, Southampton, UK.

Reduced Partial Factors for Assessment in UK Assessment Standards

Chris R. Hendy

FREng, MA (Cantab) CEng FICE Eur Ing
Technical Director, Atkins Fellow,
Professional Head of Bridge Engineering,
Transportation
Engineering, Design and Project
Management, Epsom, UK

Louisa S. Man

MEng CEng MICE
Senior Engineer
Engineering, Design and Project
Management, Epsom, UK

Rachel P. Mitchell

MEng CEng MICE
Senior Engineer
Engineering, Design and Project
Management
Epsom, UK

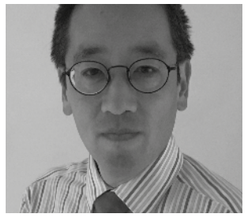

Hideo Takano

BEng ACGI CEng MICE MCIHT
Highways England
Guildford, UK

Abstract

Design standards are based upon a range of input variables for resistance, action and modelling. The distribution type and parameters for each determine the partial factors appropriate to achieve a defined reliability level over a specified reference period. For assessment a reduced reliability level may be accepted due to the greater cost of providing reliability through strengthening when compared to the cost of providing it at design. This would allow the use of lower partial factors, although they are still limited by the need to provide a minimum level for human safety. Adoption of this approach for assessment would have significant benefits for an ageing UK infrastructure by reducing the need to carry out costly strengthening and retrofitting schemes whilst still ensuring appropriate structural reliability levels are maintained. This paper presents a study investigating appropriate reduced partial factors to be applied through UK assessment standards, the sensitivity of these values to input distribution model assumptions, and how they could be implemented in industry.

Keywords

Bridges; Codes of Practice and Standards; Concrete Structures; Risk and Probability Analysis; Steel Structures; Assessment; Partial Factors

1. Introduction

1.1 Background

Assessment codes usually utilise the same partial factors as design codes, which have been specified to achieve a desired reliability. However, for assessment a reduced reliability is acceptable justified by the greater cost of providing reliability through strengthening and retrofitting when compared to the cost of providing it at design. Subsequently, lower partial factors can also be utilised. However, the reduction in reliability is still limited by the need to provide a minimum level for human safety. This approach of reducing partial factors for assessment is already implemented in the Netherlands through NEN 8700 (2011) and NEN 8701 (2011).

In the United Kingdom existing highways structures are assessed using BD21 (2001) 'The Assessment of Highway Bridges and Structures'. This standard defines the partial factors to use for actions and resistances. Following the adoption of this approach in the Netherlands, Highways England commissioned a study to investigate how partial factor reduction could be implemented in the United Kingdom through the DMRB.

This paper presents the detail of this study, focusing on the calculation of appropriate partial factor reductions, their sensitivity to input assumptions, and how the approach can be implemented through the DMRB assessment codes.

The method described in this paper focuses on reduced reliability levels for assessment without the need for detailed knowledge of the real statistical distributions of actions and resistances. Since drafting this paper, *fib* Bulletin 80 has been published which provides guidance for partial factor reductions for concrete structures accounting for measured statistical distributions of input variables and for residual life and is complementary to this paper.

1.2 Objectives

The study firstly defined the appropriate reliability levels to use, as there are a number of different recommendations for different reference periods in available literature. Using these reliability levels partial factor reductions were then calculated for a number of variables.

Different assumed input variable distribution models were used to determine how this affects the partial factor reductions calculated, and therefore the sensitivity of the method to the assumed distributions. This was a key objective as when undertaking assessments the input distribution characteristics are usually unknown, such as the distribution of concrete compressive strength, so sensitivity to these assumptions would limit the extent to which a single reduction factor for each partial factor could be recommended.

The limitations on applicability of the method are also discussed, and finally recommendations are made on how the method of reducing partial factors can be implemented within the UK assessment codes and an example given in section 9.

2. Relationship Between Partial Factors, Reliability And Probability Of Failure

Explanation on the inter-dependence of partial factors, reliability and probability of failure can be found in Eurocode 0 Annex C. However, a brief summary is given here to aid understanding.

2.1 Relationship Between Partial Factors and Reliability

Reliability is defined by the reliability index β, which is related to the probability of failure P_f by $P_f = \Phi(-\beta)$, where Φ is the cumulative distribution function of the standardised Normal distribution. Typical values are given in Table 1 below.

Table 1. Probabilities of Failure and Corresponding Reliability Indices.

P_f	10^{-1}	10^{-2}	10^{-3}	10^{-4}	10^{-5}	10^{-6}	10^{-7}
β	1.28	2.32	3.09	3.72	4.27	4.75	5.20

If a performance function g is defined as: -

$$g = R - E, \quad (1)$$

where R=Resistance,

and E = Effects of actions,

then failure is defined as when g becomes negative, so that P_f = Probability($g \leq 0$).

If the function g is normally distributed then: -

$$\beta = \mu_g / \sigma_g, \quad (2)$$

where μ_g is the mean value of g, and

σ_g is the standard deviation of g,

when no partial factors are applied. By applying partial factors to R and E the function g altered, so the partial factors determine the reliability level and hence probability of failure.

Input variables for resistance, actions and modelling have distribution types, means and standard deviations associated with them. The assumed distribution models for the inputs impact on the reliability level determined and therefore partial factor reductions calculated later in this study.

2.2 Consequence Class and Cost of Safety Measure

The target reliability levels specified in design codes can vary according to the consequence of failure and relative cost of safety measure. The target β indices in the International Federation for Structural Concrete (*fib*) Model Code 2010 (2013) are given in Table 2.

Table 2. *fib* Model Code 2010 Reliability Indices for a 1 and 50 Year Reference Period.

	Cost of safety measure	Consequence class (CC)		
		Some (CC1)	Moderate (CC2)	Great (CC3)
50 year reference period	High	1.5	2.3	3.1
	Moderate	2.3	3.1	3.8
	Low	3.1	3.8	4.3
1 year reference period	High	3.0	3.5	4.1
	Moderate	3.5	4.1	4.7
	Low	4.1	4.7	5.1

Where the consequence class is high the reliability index is high, which equates to a lower acceptable probability of failure due to the catastrophic implications of failure. Similarly, where the cost of safety measure is high the reliability index is low, reflecting a higher acceptable probability of failure due to the high cost associated with strengthening.

At design stage the cost of additional safety measures are low, and hence partial factors are determined on the basis of producing a high level of reliability, or low probability of failure. The approach of reducing partial factors for assessment is therefore based upon the cost of retrofitting safety measures being higher, so a reduced reliability or higher probability of failure is acceptable. A lower target reliability level allows the use of lower partial factors.

3. Selection of Appropriate Reliability Levels for Use

3.1 Use of *fib* Model Code 2010 Reliability Levels

Based on a literature review there are several sources from which reliability levels can be taken to calculate partial factor reductions. To determine which of these sources to use, the annual probability of fatality by structural failure was calculated as below, and compared to a level of $1x10^{-6}$, which is generally accepted as a reasonable safety level within the industry. This was carried out assuming a high cost of safety measure, as this has the lowest reliability justified by the highest cost of remedial works. The assumed conditional probability that structural failure will cause fatalities was taken from values suggested by Vrouwenvelder (2010) and Sykora et al. (2011).

$$P_d = P_f \times P_c$$

P_d = Probability of death by structural failure

P_f = Probability of structural failure

P_c = Conditional probability that failure leads to fatality

From this calculation, it was decided to use the reliability indices from the *fib* Model Code 2010 presented previously in Table 2, as these produced a level of human safety comparable with the industry accepted level over all three consequence classes.

3.2 Distinction Between Constant Annual Probability of Failure and Constant Lifetime Probability of Failure

Before discussing the choice of baseline reliability levels for a 120-year design life, the importance of differentiating between a constant annual probability of failure and a constant lifetime probability of failure is first explained. Where the annual probability of failure is kept the same during the lifetime of the structure, the lifetime probability of failure will subsequently increase with increasing design life. This is appropriate where human safety considerations govern, where it is desirable to keep the annual probability of failure constant at a level which produces an acceptable level of human safety within the industry.

Where the lifetime probability of failure is kept the same regardless of the design life, the annual probability of failure will subsequently decrease with increasing design life. This is appropriate if economic considerations govern, where it is desirable to keep the lifetime probability of failure constant so that all structures have the same probability of failure over their lifetime. Figure 1 below gives the graphical representation of this differentiation between a fixed annual probability of failure and a fixed lifetime probability of failure.

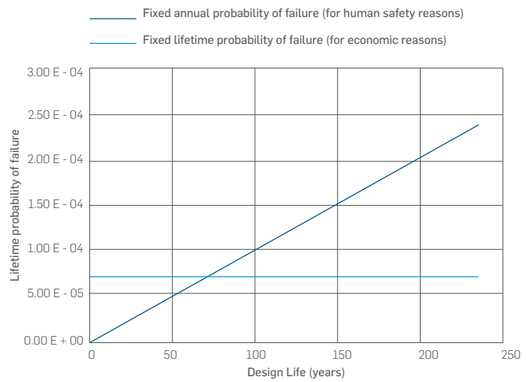

Figure 1. Graphical Representation of Fixed Annual and Fixed Lifetime Probability of Failure.

Economic considerations are assumed to govern when reducing target reliability for assessment. So the target lifetime reliability is fixed and independent of the reference period or design life.

It is noted that at the crossover point in Figure 1, there is a design life below which the fixed annual probability of failure (for human safety reasons) is less than that derived from a fixed lifetime probability of failure (for economic reasons). Over these shorter design lives the approach of reducing partial factors is not valid, as human safety factors govern. This limitation is discussed in further detail in section 6.1.

3.3 Choice of *fib* 1 Year or 50 Year Reliability Levels

As the *fib* Model Code 2010 presents two sets of reliability indices at 1 year and 50 years, one set must be chosen which remains constant for any reference period, including the 120 year design life. To determine the appropriate set to use the annual probabilities of fatality by structural failure for a 120 year reference period has therefore been calculated based on the 1 year and then the 50 year reference period reliability levels, assuming a high cost of safety measure and a fixed lifetime probability of failure.

It is not appropriate to use the 1 year reliability levels, as once the lifetime probability is divided by 120 the annual probability of fatality by structural failure would be extremely low, leading to higher reliability levels than required.

In contrast, taking the 50 year reference period reliability levels as being applicable to a lifetime of 120 years, gives probabilities of fatality by structural failure which achieve an industry accepted safety level. Therefore the 50 year *fib* Model Code 2010 reliability indices are used in this study to calculate reduced partial factors.

4. Calculation Of Reduced Partial Factors

4.1 Method for Determining Partial Factors

The partial factor reductions were calculated assuming the variables are independent, and hence an individual partial factor reduction can be calculated for each variable. This makes it possible to determine how the reduction is dependent on different input distribution assumptions.

A brief explanation of the method for reducing partial factors is given in this section. Further detail can be found in Melchers (1999).

1. Determine the baseline reliability level for the partial factor being considered for an assumed consequence class and cost of safety measure.

2. Determine the target reliability level for the partial factor considered by assuming the same consequence class but a higher cost of safety measure.

3. Calculate the ratio of reliability levels.

4. For the input variable being considered decide upon the assumed distribution model and distribution characteristics.

5. Calculate the factor to be applied to the mean of the distribution to obtain the characteristic value, as the DMRB partial factors are applied to the characteristic value.

6. Calculate the baseline partial factor $\gamma 1$ (applied to the mean value) associated with the baseline reliability level, which is a function of the DMRB partial factor (applied to the characteristic value) and the factor applied to the mean of the distribution to obtain the characteristic value.

7. Calculate the revised partial factor $\gamma 2$ (applied to the mean value) based on the following relationships between reliability and partial factor, which depend on the distribution type assumed.

$$\textit{Normal distibution: } \gamma_2 = 1 - \frac{\beta_2}{\beta_1}(1 - \gamma_1) \quad (4)$$

$$\textit{Lognormal distribution: } \gamma_2 = e^{\left(\frac{\beta_2}{\beta_1}\ln \gamma_1\right)}$$

$$\textit{Gumbel distribution: } \gamma_2 = \frac{\beta_2}{\beta_1}\gamma_1 \quad (5)$$

(6)

8. Calculate the revised DMRB partial factor (applied to the characteristic value) which is a function of the revised partial factor (applied to the mean value) and the factor applied to the mean of the distribution to obtain the characteristic value.

9. Calculate the partial factor reduction by taking the ratio between the revised DMRB partial factor and the original DMRB partial factor.

It is assumed that partial factors in the DMRB are set for CC2 and low cost of safety measure.

4.2 Distinction Between Different Partial Factors

Use of this method allows individual partial factor reductions to be calculated, and hence it must be known which partial factors account for which uncertainties. Uncertainties in inputs fall generally into the groups described in Table 3.

Table 3. Uncertainties Accounted for in DMRB Partial Factors.

1.Uncertainty in actions	1a. Statistical and geometrical uncertainty in representative values of actions e.g. Density of material, section size
	1b. Model uncertainty in action effects e.g. idealisation of supports, non uniform distribution of live load
2.Uncertainty in resistances	2a. Statistical and geometrical uncertainties in material and cross-section geometry e.g. strength of material, bar diameter
	2b. Uncertainty in resistance model used to describe the physical behavior of the element

The DMRB accounts for these uncertainties through the following partial factors; γ_{fL} accounts for 1a, γ_{f3} accounts for 1b and γ_m accounts for 2a and 2b. Therefore, when calculating reduced partial factors the input variable distributions must be accounted for within the appropriate partial factor.

4.3 Dealing With Variables Which Are a Function of Several Other Variables With Different Distribution Models

As discussed in the previous section, partial factors allow for uncertainties in a number of different contributing variables. For

example, although γ_m is a single partial factor which is applied to the material resistance, it accounts for statistical uncertainty in the material strength, as well as uncertainty in the dimensions of the cross section and also uncertainty in the resistance model being used. Each of these will have their own distributions. As the method of partial factor reduction assumes a single input distribution, several contributing input distributions must be combined into a single distribution with its own mean and coefficient of variation.

Where a distribution is the product of other distributions it has been mathematically found as detailed in Riley et al. (2006) that the distribution will tend to a lognormal distribution with the following values for mean and coefficient of variation, regardless of the input distribution types: -

$$E[X_1 * X_2 \ldots * X_n] = E[X_1] * E[X_2] \ldots * E[X_n]$$

$$COV[X_1 * X_2 \ldots * X_n] = \sqrt{(COV[X_1])^2 + (COV[X_2])^2 \ldots + (COV[X_n])^2}$$

Where $E[X_n]$ is the mean of distribution n,

and $COV[X_n]$ is the coefficient of variation of distribution n

Using the above expressions a combined variable with its own distribution model can be defined, and therefore a partial factor reduction can be calculated. For the purposes of the calculation it is assumed that the combined variable is a product of the individual component variables. The assumption of a product function is accurate for the loads, as they are a multiple of the dimensions and material densities. It is a simplification for the resistances though, where the resistance model is some function of the component variables. The appropriate model depends on the failure mode being assessed, for example a strut may fail in squashing or buckling. It is difficult to find guidance on the distributions of different failure modes or material properties, and so there was limited value in looking into other functions in this study.

It is also noted at this point that it is obviously possible to take samples from existing structures to determine statistical distributions for the actual loading, materials and geometry and these could be used in the derivation of partial factors following the same approach if a sufficiently large sample were to be available. Often it will be a challenge to get such a sample and therefore this paper focusses on adjusting partial factors based on required safety levels without including the additional potential benefits of using bridge-specific data.

4.4 Typical Input Distributions Assumed

The list below of model distributions assumed is not exhaustive, but includes some of the assumptions made for key variables used in this study. These distributions were collated from a variety of published work including: JCCS Probabilistic Model Code (2006), Melchers (1999), Vrouwenvelder, T. and Siemens, T (1987) and Caspeel R., Sykora M., Allaix D. & Steenbergen R. (2013).

Table 4. Assumed Distribution Models for Input Variables.

Variable	Distribution type	Coefficient of variation	Probability of exceeding characteristic value
Concrete compressive strength	Lognormal	0.1-0.2	95%
Concrete dimensions	Normal	0.04-0.1	50%
Concrete resistance (except shear)	Lognormal	0.1-0.2	95%
Concrete density	Normal	0.03-0.10	50%
Structural steel yield stress	Lognormal	0.05-0.13	95%
Steel section dimensions	Normal	0.01-0.04	50%
Steel resistance checks	Lognormal	0.05-020	95%
Steel density	Normal	0.01-0.03	50%
Traffic load	Gumbel	0.18-0.38	5%
Wind load	Gumbel	0.2-0.3	5%

5. Results And Discussion

5.1 Calculated Partial Factor Reductions

The calculated partial factor reductions are summarised in Table 5.

The results show that the average reduction in partial factor over all variables is 0.94 for medium cost of safety measure, and 0.89 for high cost of safety measure. It is highlighted that these values are calculated for each input, and hence the net effect on the outcome of the assessment is significantly greater, as will be apparent through the assessment test cases reported in section 5.3. This highlights the benefits that reduced partial factors could have for assessment.

5.2 Sensitivity to Input Distributions

Where ranges are given in the partial factor reduction value, these result from assuming a minimum and maximum value for the coefficient of variation, based on values available from a literature review. Where the maximum coefficient of variation was assumed, this led to a greater reduction in partial factor compared to when the minimum coefficient of variation was assumed. The range in the variations though is not sufficient to cause a large difference in the partial factor reductions, at less than 5%. Importantly this shows that codified partial factor reductions could be used over a range of assessments without detailed knowledge of the distribution models specific to each, as they are not particularly sensitive to assumptions made about these distributions. This is important for the application of partial factor reduction for assessments, as usually little is known about the distributions of the variables involved.

The results also show that variables with a greater coefficient of variation have a partial factor which is more sensitive to changes in reliability, and hence the partial factor reductions calculated were greater. For example, the reduction calculated for concrete resistance is 0.85 assuming high cost of safety measure, compared to 0.98 for steel resistance which has a lower variation. Likewise the same differentiation is made between variable actions compared to permanent actions, which have a lower coefficient of variation. As most bridge assessments are governed by highly variable traffic loads this highlights how partial factor reduction could have significant benefits when used for assessment of existing structures.

5.3 Implications on Assessment Results

In order to gain a better understanding of how partial factor reduction affects different assessments, the overall partial factor reduction was calculated for seven different test cases as listed in Table 6, which represent different possible assessments. All calculations have been carried out using partial factor reductions reported in Table 5 for high cost of safety measure.

The overall reduction in partial factor varies between 0.64-0.77, averaging at 0.71. This gives an indication of the significant benefits that would be obtained using partial factor reduction if individual reductions were applied to γ_{fL}, γ_{f3} and γ_m in accordance with the values being proposed.

It also justifies the recommendation of a single 0.77 reduction factor to be applied to the overall utilisation assuming a high cost of safety measure. This would be a conservative reduction that could be applied at the end of an assessment, as opposed to more accurately reducing each partial factor by the amounts in Table 5. Applying the same test cases using reliability levels at a medium cost of safety measure leads to reduction factors which vary between 0.77 and 0.91 with an average of 0.84. A conservative overall partial factor reduction of 0.91 could therefore be used for a medium cost of safety measure.

5.4 Sensitivity to Structural Type

Tests 1 to 3 where the ratio of steel to concrete is varied show that the reductions are greatest for the concrete (test 1) and smallest for steel (test 2), showing that the method of partial factor

Table 5. Calculated Partial Factor Reductions.

Variable	DMRB partial factor	Assuming medium cost of safety measure $\beta_2 = 3.1$ $\beta_1 = 3.8$ $\beta_2/\beta_1 = 0.82$	Assuming high cost of safety measure $\beta_2 = 2.3$ $\beta_1 = 3.8$ $\beta_2/\beta_1 = 0.61$
Concrete resistance (except shear)	1.5	0.92	0.84-0.85
Concrete resistance in shear	1.25	0.95-0.96	0.90-0.91
Rebar resistance	1.15	0.97	0.94
Steel resistance	1.05	0.99	0.97-0.98
	1.2	0.96-0.97	0.92-0.93
Welded connections	1.2	0.96-0.97	0.92-0.93
Bolts in shear	1.1	0.98	0.96
Bolts in tension	1.2	0.96-0.97	0.92-0.93
Friction in HSFG	1.3	0.95	0.89-0.90
Concrete dead load	1.15	0.96	0.92
Steel dead load	1.05	0.98	0.95
Surfacing dead load	1.75	0.89	0.79
SDL	1.2	0.95	0.90
Traffic	1.5	0.82	0.67
Wind	1.4	0.82	0.71
Thermal	1.3	0.82	0.77
Modelling uncertainty	1.1	0.99	0.97
Average		**0.94**	**0.89**

reduction will be most beneficial for reinforced and prestressed concrete structures as opposed to steel. This follows on from the earlier finding in section 5.2 that variables with a greater variation, such as concrete when compared to steel, are more sensitive to changes in reliability and hence calculated partial factor reductions are greater.

5.5 Sensitivity to governing load

Tests 4 to 7 where the permanent load as a proportion of the total load is varied between 20-80%, shows that as the proportion of permanent load increases the partial factor reduction decreases. The method of partial factor reduction therefore will be most beneficial for shorter span concrete structures, where variable loads from traffic make up a significant proportion of the total load. This also follows on from the earlier finding that variables with a greater variation, such as live load when compared to dead load, are more sensitive to changes in reliability and hence calculated partial factor reductions are greater.

Table 6. Overall Reduction in Partial Factor for 7 Assessment Test Cases.

Test No.	Ratio of concrete to steel	Permanent load as a proportion of total load	Overall reduction in partial factor (or utilisation)
1	100:0	50%	0.68
2	0:100	50%	0.75
3	50:50	50%	0.70
4	50:50	20%	0.64
5	50:50	40%	0.68
6	50:50	60%	0.72
7	50:50	80%	0.77
		Average	**0.71**

6. Limitations On Use

6.1 Minimum Design Life

As previously mentioned there is a design life where the lifetime probability of failure plots intersect from human safety and economic considerations. At a design life shorter than this value the lifetime probability of failure derived from a fixed annual probability of failure required for human safety is more onerous than that required from a fixed lifetime probability of failure required for economic reasons. Therefore at these shorter design lives reducing the partial factors by reducing the reliability for economic reasons becomes invalid, as human safety requirements govern.

A graphical representation of this crossover point is given in Figure 2, and shows that partial factor reduction methods are not valid where the original design life is less than 107 years. This assumes a CC2 consequence class and a high cost of safety measure.

The exact position of the crossover point depends on the assumptions made on the lifetime reliability level, the industry accepted level for annual probability of fatality due to structural failure, and the conditional probability that structural failure will lead to fatality. Subsequently it is recommended that the DMRB conservatively only allows partial factor reductions where the structure design life is equal to or greater than 120 years.

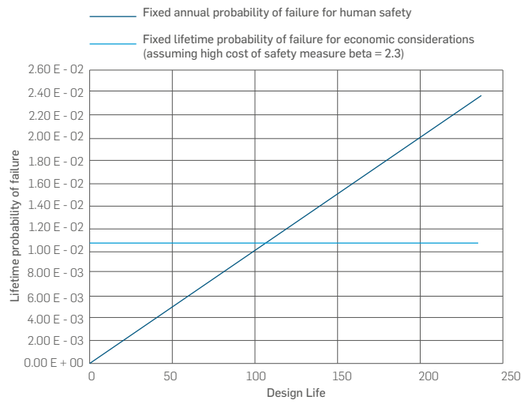

Figure 2. Graphical Representation Of Crossover Point Between Probabilities Of Failure For Human Safety And Economic ConSiderations, With Accompanying Calculation Of Crossover Point.

For fixed annual probability of failure for human safety reasons:

- Industry accepted level for annual probability of fatality due to structural failure = 1×10^{-6}
- Conditional probability that structural failure will result in fatality = 0.01 (assuming CC2)
- Annual probability of structural failure for human safety reasons = $1 \times 10^{-6} / 0.01 = 1.00 \times 10^{-4}$

For fixed lifetime probability of failure for economic reasons:

- Lifetime reliability index for CC2, high cost of safety measure = 2.3, equating to a lifetime probability of failure of 1.07×10^{-2}

Design life at crossover point = $1.07 \times 10^{-2} / 1.00 \times 10^{-4}$ =107 years

6.2 Maximum Span Length

It is highlighted that the crossover point discussed in the previous section occurs at an increasing design life as the consequence class increases, due to an increasing conditional probability that structural failure will result in fatality.

For long span structures this is significant because many people could be present on the structure at the same time, so any failure could lead to multiple losses of life. This increases the conditional probability that structural failure leads to fatality, and for long span bridges was taken as 0.77. In turn the annual probability of failure for human safety decreases, reducing the gradient of the plot for fixed annual probability of failure. As a result the crossover point below which human safety factors start governing occurs at a reference period of 372 years. This exceeds the design life of the structure, and hence partial factor reduction is not recommended for long span bridges, as they are governed by human safety requirements rather than economic considerations.

Note the conditional probability of 0.77 was simplistically derived from a review of long span (>50m) road bridge collapses that have occurred since 1950 whilst the structure was in operation. This review showed that 27 of the 35 bridge collapses resulted in fatalities, giving a 0.77 conditional probability that failure leads to fatality.

7. Summary of Key Findings

The key conclusions from this paper and the relevant section references are listed below: -

- Partial factor reductions calculated individually for different variables and overall for assessment results show that there would be significant benefits to using this approach. Individual partial factor reductions averaging 0.94 for medium cost of safety measure, and 0.89 for high cost of safety measure could be applied. (Section 5.1)
- Where the coefficient of variation for an input is greater, partial factors are more sensitive to reliability level changes. Hence the reductions calculated for variable loading and concrete resistance are greater than those calculated for permanent loading and steel resistance respectively. Use of the partial factor reduction methods should therefore have more significant benefits for shorter span reinforced concrete and composite structures governed by traffic loading, which are prevalent on the UK Highways Network. (Sections 5.4 and 5.5)
- Different resistance checks are based on different material behaviour models, which are a function of different components including material properties and resistance models. Hence it is recommended that different partial factor reductions are recommended for different checks, depending on the component distributions they are based upon. (Section 5.2)
- In general the partial factor reductions do not vary greatly over the range of variations for the input distributions. Hence the calculated reductions can be applied with confidence without any detailed knowledge of the input distributions or material testing, as is often the case when carrying out assessments. (Section 5.2)
- The *fib* Model Code 2010 reliability levels at 50 years are appropriate target values to use for the calculation of partial factor reductions assuming a 120 year design life. (Section 3)
- Partial factor reduction is not suitable where the design life of the structure is less than 120 years, as for periods less than this reliability levels and hence partial factors are governed by those required for human safety. (Section 6.1)
- Partial factor reduction based on the target reliability index values used in Table 2 is not suitable for long span bridges (taken as those with spans greater than 50 m in this paper) due to the increased consequence of failure for human safety; larger values of target reliability index are required because more fatalities can be expected as the collapsed span length increases. Since this paper was first drafted, *fib* Bulletin 80 has been published which contains guidance on suitable target reliability index to use as span length increases.

8. Recommendations For Implementation In DMRB Assessment Standards

Considering the key findings reported in the previous section, the following recommendations are proposed for inclusion into the DMRB assessment standards to enable partial factor reduction methods to be used:

- A reduction to the overall assessment usage factor of 0.91 can be applied where remedial works would represent a medium cost of safety measure. A reduction of 0.77 can be applied where a high cost of safety measure is assumed.

These factors are the minimum values calculated over a range of assessment test cases and are therefore conservative.

- Individual partial factor reductions can instead be applied to each partial factor, which will result in an overall reduction that is greater than 0.91 and 0.77 for medium and high cost of safety measure respectively. The reduction values recommended are presented in Table 5 and the minimum values calculated should be taken for conservatism.
- If a large amount of test data is available, the resulting knowledge of the input variable distributions could be used to calculate partial factor reductions which are specific to the input variable distribution models for that structure. Approval should be sought from the Technical Approval Authority if this is proposed.

The method of reducing partial factors described in this paper, based on reduced reliability, is not valid in totality for the following cases: -

- Structures other than those consisting of reinforced concrete, prestressed concrete and steel
- Structures where traffic loading is restricted and hence the designed traffic load does not follow an extreme type distribution. Partial factor reduction methods are still applicable but must be calculated for the traffic load model that was designed for.
- Structures where the original design life is less than 120 years.
- Long span structures, assumed to be those with a span length greater than 50m where the target reliability index may need to be taken as greater than the values assumed in Table 2.
- Assessments which are governed by serviceability or fatigue limit states, which are subject to different reliability levels.
- Assessments which have been based on non-linear finite element methods.

9. Application To A Real Structure

The simplified methodology, comprising a single reduction to the overall assessment utilisation, was applied to the assessment of Barton High Level Bridge as a Departure from Standard for Highways England. The bridge, which carries the M60 across the Manchester Ship Canal, was being assessed for normal operating conditions combined with predicted settlement caused by adjacent highway construction works as part of the Western Gateway Improvement Scheme (WGIS). The bridge is 737 m long with a main span of 94 m across the Manchester Ship Canal and approach spans of mostly 35 m in length (13 spans) and two spans of 41 m and two of 53 m.

The bridge has a multi-girder steel-concrete composite deck with cross-bracing between the main girders. The cross-bracing is essential to guarantee the adequacy of the main girders through the transverse distribution provided under live load, but the predicted settlement induces additional forces in it. The net effect for the assessment was that the cross-bracing was found to be overstressed by 10% which would have either led to a significant live load restriction being required or a very extensive strengthening programme being undertaken. However, by applying the simplified reduction factor of 0.91 for medium cost of safety measure proposed in section 8, both load restrictions and strengthening were avoided.

For the critical bracing unit, the traffic load accounted for 40% of the total force in the bracing members while structural concrete weight accounted for the majority of the remaining 60%. Table 5 shows that for medium cost of safety measure the design traffic load can be reduced by a factor of 0.82 and the design structural concrete weight can be reduced by a factor of 0.96; this alone, without consideration of adjustments to resistances, would have led to a reduction in utilisation by a factor of 0.90, so the simplified reduction factor of 0.91 is conservative here. If the reduction applicable for the resistance partial factor and the modelling factor are also applied this becomes further conservative.

This simple example illustrates the huge potential for reducing the costs of managing existing UK infrastructure by taking a reliability-based approach to assessment.

10. Conclusion

The study carried out showed that the method of reducing partial factors for assessment based upon reducing reliability can offer significant reductions in the overall assessment utilisation factor. Although the exact partial factor reductions depend on the distribution models of the input variables, the study has found that the reductions are not particularly sensitive to these assumptions. Therefore, the calculated reductions for each partial factor could be implemented in the DMRB standards, and used over a range of assessments without detailed knowledge of the distribution models specific to each. This is important for the application of partial factor reduction for assessments, as usually little is known about the distributions of the variables involved unless extensive testing has been specified.

It was also found that where the coefficient of variation is greater, partial factors are more sensitive to reliability level changes. Hence the reductions calculated for variable loading and concrete resistance is greater than those calculated for permanent loading and steel resistance respectively, which are less variable. Use of the partial factor reduction methods should therefore have more significant benefits for shorter span reinforced concrete and composite structures governed by traffic loading, which are prevalent on the UK Highways Network.

Considering the age of the UK infrastructure and increasing need for assessment work, implementation of reduced partial factors through the DMRB could avoid the need to carry out costly strengthening schemes, whilst still ensuring structural reliability is maintained at acceptable levels.

References

BSI (2002) BS EN 1990: 2002 Eurocode – Basis of structural design. BSI, London, UK.

Caspeel R., Sykora M., Allaix D. & Steenbergen R. (2013) The Design Value Method and Adjusted Partial Factor Approach for Existing Structures, Structural Engineering International 2013, pp. 386-393

Ciria Report 63 (1977) Rationalisation of Safety Factors in Structural Codes. London, UK

fib Bulletin 80 (2016), Partial factor methods for existing concrete structures, DCC Document Competence Center Siegmar Kästl e.K., Germany

fib Model Code for Concrete Structures 2010 (2013), Ernst & Sohn, Germany

Highways Agency (2001), BD 21/01 The Assessment of Highway Bridges and Structures, Design Manual for Roads and Bridges, Volume 3, Highway Structures: Inspection and Maintenance, Section 4, Assessment, UK

Highways Agency, Design Manual for Roads and Bridges, http://www.standardsforhighways.co.uk/ha/standards/dmrb/, UK

Joint Committee on Structural Safety (2006) Probabilistic Model Code, http://www.jcss.byg.dtu.dk/Publications/Probabilistic_Model_Code

Melchers, R, E (1999) Structural Reliability Analysis and Prediction, 2nd Edition, Wiley, UK

NEN (2011) NEN 8700, Assessment of existing structures in case of rec onstruction and disapproval- Basic rules, Netherlands Normisatie-instuut, Netherlands

NEN (2011) NEN 8701, Assessment of existing structures in case of reconstruction and disapproval- Actions, Netherlands Normisatie-instuut, Netherlands

Riley K.F, Hobson M.P. & Bence S.J (2006) Mathematical Methods for Physics and Engineering, Cambridge University Press, UK

Sykora, M., Holicky, M. & Markova, J (2011) Target reliability levels for assessment of existing structures. M.H. Faber, J. Kohler & K. Nishijima (eds.), Proc. ICASP11, ETH Zurich, 1-4 August 2011. Leiden: CRC Press/Balkema

Vrouwenvelder, T (2010) Safety philosophy for existing structures and partial factors for traffic loads on bridges. Heron: 123-139, Deft, the Netherlands

Vrouwenvelder, T. & Siemens, T (1987) Probabilistic calibration procedure for the derivation of partial safety factors for the Netherlands building codes, Heron, Vol. 32, no 4, Deft, the Netherlands

Bigaj-van Vliet, A & Vrouwenvelder, T. (2013) Reliability in the performance-based concept of *fib* Model Code 2010. Structural Concrete Volume 14, Issue December 2013, Pages 309–319, Wiley

Acknowledgements

Originally presented and published as: Hendy CR, Man LS, Mitchell RP, Takano H. Reduced partial factors in UK standards for assessment of bridges and structures. Proceedings of the Institution of Civil Engineers - Bridge Engineering 2018; 171:1, 3-12.

Structural Assessment | 007

Parametric Studies of Bridge Specific Assessment Live Loads and Implications for Assessment

Nick Benham

MEng GMICE
Assistant Engineer
Engineering, Design and Project Management
UK

Chris Mundell

MEng (Hons) PhD CEng MICE
Principal Engineer
Engineering, Design and Project Management
UK

Chris R. Hendy

FREng, MA (Cantab) CEng FICE Eur Ing
Technical Director, Atkins Fellow, Professional Head of Bridge Engineering, Transportation Engineering, Design and Project Management
UK

Abstract

A number of UK long span suspension bridges now require routine inspection, assessment and maintenance to ensure their continued durability. The UK Design Manual for Roads and Bridges (DMRB) has explicit guidance on the traffic loading for assessment lengths up to 50m, however beyond this the assumptions become conservative. In these instances, the assessment of these structures requires a Bridge Specific Assessment Live Load (BSALL) to be derived. Although a number of methodologies exist to derive BSALLs, there are several parameters that may significantly affect their results and there is little published guidance on the subject.

Through recent work covering the calculation of suspension bridges, Atkins have completed many parametric studies, considering different distribution methods and the relative importance of the various parameters involved. This paper discusses the above themes and outlines the advancements made by Atkins in this field, highlighting the critical parameters to consider, the advantages and limitations of the various approaches, and a recommended approach based on our findings to date.

Keywords

Bridge, Assessment; BSALL; Partial Factors

1. Introduction

In the UK, the Highways Agency[1] Design Manual for Roads and Bridges (DMRB) includes extensive guidance for the assessment loading criteria for bridges spanning up to 50 m. For the assessment of long-span bridges, the use of such assessment loading becomes excessive and not representative of real traffic loading conditions. Instead, a bridge-specific assessment live load (BSALL) can be determined, giving an assessment loading derived from a probabilistic assessment of the actual traffic flows.

The authors have determined BSALLs for three of the UK's iconic suspension bridges: The M48 Severn Bridge, The Forth Road Bridge and the Humber Bridge, built in 1966, 1964 and 1981 and spanning 1600m, 2512m and 2220m respectively. The methodology used to complete this process, outlined by Hendy et al.[2], involves using a probabilistic distribution of recorded traffic data to extrapolate to the characteristic load effect that is defined as having a 5% probability of being exceeded in a 120-year period.

In order to further develop understanding of the sensitivity of BSALL results to the methodology used, investigation in to a number of independent parameters has been completed. This paper explores the types of probability distribution that are commonly used to undertake the derivation of BSALLs, highlighting the advantages and disadvantages of each. It then discusses the parametric studies that have been completed to assess the impact that these variables have on the derivation of a BSALL. Upon discussion of the findings, the recommended approach based on the research undertaken to date is provided.

It is also noted that a study of the statistics of live loads allows not only characteristic values to be determined but also design values and hence partial factors for loading. Further comment on this aspect is provided in section 6.

2 BSALL Derivation

2.1 Commonly Accepted Approach

The Transport and Road Research Laboratory report CR016 [3] was a study to develop interim rules for the design of vehicular loading for long span bridges that are 75 to 1600 metres in length. In the report, the total loading on a given length of carriageway is calculated by considering a row of vehicles called a 'load train' passing over the bridge. The statistical distribution for sets of vehicles was said to be normal for sets of 10 or more vehicles.

Building on the findings of this report, the authors developed a method for deriving BSALLs that is based on the formation of load trains passing across a structure in order to determine the required load effects. As outlined by Hendy et al.[2], traffic data is recorded with the use of Weigh-in-Motion (WiM) sensors which are commonly used to monitor the traffic flow on long span bridge structures. The traffic model is simulated by forming a load train for each lane of traffic for each hour of WiM data. Once the traffic queue has been formed for each lane, the load train is progressed over the loaded length to determine the critical position for the queue depending on the output requirement. The deck length assessed is modelled as simply-supported for simplicity of the calculation, and the resulting maximum mid-span bending moment, shear force at supports and total load are used to derive an equivalent uniformly distributed load (UDL); the most appropriate being selected for the particular structure being assessed. The maximum UDLs for each hour are then tabulated, giving a Gumbel distribution that is formed in to a cumulative frequency distribution.

As outlined in BS EN 1990:2002 [4], additional to the use of a Gumbel distribution, Normal and Lognormal distributions can alternatively be used when undertaking probabilistic analysis to determine nominal and characteristic design values. Their advantages and limitations in relation to the calculation of BSALLs are presented in the following sections.

2.2 Gumbel Distribution

Previous BSALL derivation undertaken by the authors has consisted of normalising the data to provide Gumbel probabilities and then extrapolating to the characteristic load effect that is defined as having a 5% probability of being exceeded in a 120-year period. The full method of undertaking this process, with associated calculations, is provided in Hendy et al.[2].

Whilst the derivation of BSALLs using this methodology has been proven to produce accurate approximations of characteristic traffic loadings at longer loaded lengths, one of the key limitations of using this method is the accuracy of the results at shorter lengths. Recent investigation identified that BSALL approximations do not agree well with DMRB loading curves for bridge lengths of less than 200m, being more onerous than the design code values which is evidently not correct. This is a product of the Gumbel distribution approach, whereby the influence of Heavy Goods Vehicles (HGVs) becomes dominant for the hourly maximum values at shorter lengths. As the load train progresses, it is entirely likely that in some instances a convoy of multiple HGVs will exist in any given hour. HGVs are regularly recorded as 20-25m in length, and when combined with the applied vehicle spacing, it only takes a convoy of three large HGVs to effectively fill a 100m loaded length, with only one or two required for a 50m length. During periods of high light-vehicle traffic (i.e. cars and small vans), it is probable that within each hour there will be instances of HGV convoys, and during off peak hours the percentage of HGV traffic increases with respect to light traffic. As the Gumbel methodology takes the most onerous load combination for each hour, at these shorter lengths the values obtained will therefore reflect almost entirely HGV traffic on the structure. The worst recorded values at shorter lengths could therefore themselves represent almost the highest loading possible. Extrapolating these results to a 120-year, 5% chance of exceedance value is based on HGV traffic alone, rather than the mix of traffic present at the longer lengths, results in traffic loads that represent unrealistically large HGV loads akin to Special Order vehicles rather than standard traffic. Such traffic would not normally be allowed across the structure without prior notice and escort, and as such do not represent normal operating conditions.

2.3 Normal Distribution

To investigate the issues presented by the Gumbel Distribution, a normalised distribution has also been used. Studies have been undertaken in which BSALLs have been derived using independent methodologies, and compared to the commonly-adopted Gumbel approach.

To undertake the derivation of a BSALL using a normalised distribution, an initially similar methodology to that previously described by Hendy et al.[2] is adopted to determine the maximum load effects for each hour of traffic. With the worst-case load effects from each hour of traffic identified, a normalised distribution is then applied to each of the load effects (shear force, bending moment and UDL). In the instance of UDLs, the maximum UDLs for each hour of traffic within the reference period are grouped in to suitably sized intervals. The mean UDL (x) and the total number of UDLs that fall within each interval i.e. the frequency (f) are then calculated. The frequency within each interval is plotted against the mean UDLs which represents a roughly bell-shaped curve associated with Normal distributions. An example plot can be seen in Figure 1, where a dataset of 656 maximal UDLs were grouped in to intervals of 0.5kN/m ranging between 0 to 24kN/m.

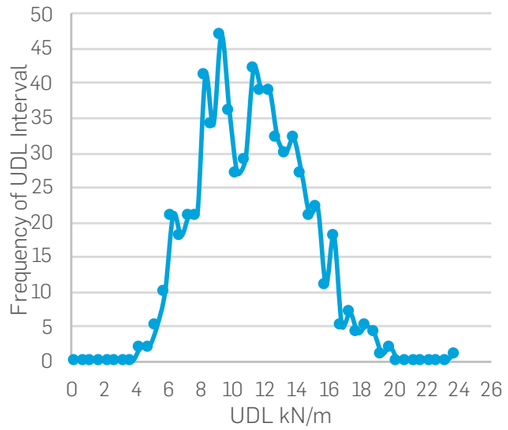

Figure 1: Example Traffic Distribution Plot

The characteristic BSALL, F_k, can be calculated by summing the mean of the hourly UDLs with the product of the standard deviation of the mean and the number of standard deviations:

$$F_k = mean + s \times n \quad (1)$$

The weighted mean UDL of the full data set, X', is calculated as follows:

$$X' = \frac{\Sigma Xf}{\Sigma f} \quad (2)$$

The standard deviation of the data set, s, is calculated as follows:

$$s = \sqrt{\frac{\Sigma (X - X')^2 f}{\Sigma f}} \quad (3)$$

The cumulative frequency for a 5% probability of exceedance in 120 years is calculated as:

$$P = (1 - P_{120}) \quad (4)$$

Where the 5% probability of exceedance in 120 years, P_{120}, equates to:

$$= \frac{hourly\ probability\ of\ exceedence\ of\ 5\%}{total\ hours\ in\ 120\ years \times f} \quad (5)$$

Where the probability of a queue forming, f, is derived as a function of the hourly traffic in accordance with TRL report CR016 [3].

$$f = \frac{2 \times hourly\ flow}{1200} = 1.93\% \quad (6)$$

The probability for each number of standard deviations, n, is determined from the following equation for a one tailed distribution:

$$P = 1 - \frac{(1 - e^{-1.4n}) e^{\frac{-n^2}{2}}}{1.135 n \sqrt{2\pi}} \quad (7)$$

The 5% probability of exceedance in 120 years is then converted to a number of standard deviations, 4.55 in this case, to use when calculating the characteristic BSALL. For use with UK assessment codes, the nominal BSALL is then calculated by dividing the characteristic BSALL by 1.2 in accordance with BD 50/92 [5]; this is needed because the nominal load is accompanied by a higher partial factor than a characteristic value would be.

As a result of the previously described methodology, both the Gumbel and Normal distributions have been used to derive BSALLs for a range of loaded lengths. This provides a set of results that are directly comparable to the recommended BD 37/01 [6] nominal UDLs for lengths in excess of 50m but less than 1600m. It is clear from Figure 2 that at shorter spans, between 200m and 1000m, the use of the Normal distribution provides more efficient results in comparison to the more onerous Gumbel distribution. Whilst both methods potentially extrapolate from a value that may itself be already close to a realistic maximum at short loaded length, the Normal distribution extrapolation is less severe.

2.4 Lognormal Distribution

Although it has been proposed in notable sources, such as fib bulletin 80 [7], that the use of a Lognormal distribution is the most appropriate approach, it has been shown in section 2.2 that the use of the Gumbel distribution is appropriate when assessing long loaded lengths. However, because of the previously described limitations of the Gumbel distribution approach for shorter spans, it is more appropriate to use a Normal or Lognormal distribution when assessing a wide range of loaded lengths.

To further explore the differences between the Normal and Lognormal model, an investigation has been undertaken with the data used in sections 2.3 and 2.4. As in Figure 2, it has been shown to have only marginal difference on the resulting BSALL (an average of 4.5%) for spans between 50m and 1823m in comparison to the use of a Normal distribution. Given that it is statistically impossible to extrapolate in the negative direction when using a set of Lognormally distributed data, it is therefore recommended that the adoption of the Lognormal distribution offers the most appropriate approach for general use.

3. Parametric Studies

3.1 Sensitivity to Sampling Period

In addition to the investigation in to which type of statistical distribution to use when deriving BSALLs, a number of other

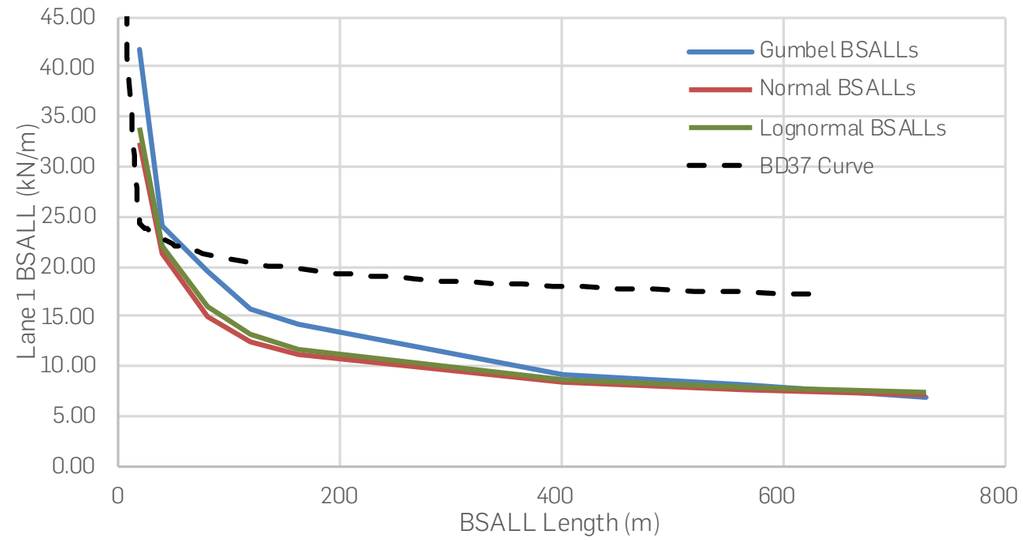

Figure 2: Gumbel/Normal/Lognormal BSALL Comparison

parameters have been explored to assess their relative importance with regards to the overall determination of the BSALL. The outcomes of the previous investigations have provided the impetus to explore other parameters and to identify what level of impact the modification of them will have.

Within this study, the most significant parameter considered was the decision of whether to include the hourly maximum load effects from the load train within the cumulative frequency distribution, or to include load effects as a result of each incremental movement of the load train; the latter using the data in a continuous way, rather than sampling maximums in a discrete period. Continuous use of data implies sampling by very short time periods, whilst using maximum hourly values clearly implies sampling over an hour. The sensitivity to this sampling period has therefore been studied.

A key consideration, particularly at longer loaded lengths, is how the progression of the load train is considered. It can consider actual queues in the time period or theoretical queues, formed by simple squashing of real vehicle trains into the loaded length within the sampling period. The above raises the question, particularly for long loaded length, of what to do when this is not enough traffic within the sampling period to fill the entire loaded length as this can distort the statistics.

3.2 Hourly Maximums Vs. 'All Data' Approach

As previously described, the methodology the authors have formerly used to derive BSALLs involved the progression of a load train of vehicles over a specified loaded length to determine the critical position for the queue of vehicles for each hour. The maximum load effects for each hour were then extracted and formed in to a cumulative frequency distribution. The aim of this parametric study was to determine if the BSALL is sensitive to this sampling period. Therefore, an alternative approach was investigated whereby the load effects from each incremental movement of the load train within the time period of one month was included in the cumulative frequency distribution.

It is important to note that the extrapolation to the 5% exceedance in 120 years is independent of the sample size of data. I.e., even with 120 years of data to process, an extrapolation would still be required to determine the 5% exceedance value. The approach described in this paper explains how the various statistical parameters are obtained; having a larger dataset would only increase the accuracy of those parameters, but in all likelihood, would not substantially change the values derived from a much smaller sample (e.g. 1 month of data).

To undertake the comparison between the hourly maximums and the 'all data' approach, a dataset of Normally distributed traffic against various lengths as described in Section 2.3 was used as the benchmark. For the 'all data' approach the process was repeated, however rather than outputting the maximum load effects for each hour of traffic, the load effect from each 'increment' was recorded. This produced a pool of data that included 659,052 UDL's within the one month time frame (rather than 656 for the hourly maximum approach). The data was then tabulated and formed in to a cumulative frequency distribution and the approximate increment time step estimated based on the total number of increments in the dataset. For this example, it equates to a time step of 3.58 seconds per increment.

In contrast to section 2.3 where the 5% probability of exceedance in 120 years was calculated based on an extrapolation using hourly maximums (with a number of standard deviations of 4.55), the extrapolation using this approach was undertaken using the instantaneous movements of the load train (with a number of standard deviations of 5.83) in order to calculate the nominal BSALL from a much larger sample size with a much smaller time step. The process of calculating the BSALL was undertaken for both sets of data for a total of 8 different loaded lengths in order to produce a set of results comparable those recommended in BD 37/01 [6].

Figure 3 shows the results obtained using both methods and the nominal UDL curve as recommended in BD 37/01 [6].

As shown in Figure 3, the use of the 'all data' approach has produced a loading curve with BSALLs of smaller magnitude throughout each of the loaded lengths calculated. The reasoning behind the difference in results between both methods is due to assumptions that have been made within the methodology used. The 'all data' approach involves forming a load train of traffic which is progressed along the loaded length in increments of 50m, which is independent of time. As described above, to allow extrapolation to a 120-year BSALL, a time reference is required for each data point. This was accomplished by estimating the time step of each increment, based on the total number of recorded increments (usually in the order of 650,000) and the amount of time in the reference period (one month, or 2,592,000 seconds), leading to the increment time step of 3.58 seconds as previously described.

This assumption however leads to potential ambiguities in the data, as the realistic time step for each data point is not constant and varies for each data point, based on a number of factors. The time reference is different for each lane of traffic, for different hours of the day, and for different days of the week; therefore, adopting a constant time reference for an entire month of traffic data is potentially an erroneous assumption. Splitting the data in to more manageable time periods with a set time frame (e.g. datasets of hourly groupings of traffic) avoids this issue, and allows for a more consistent approach, and to a large degree invalidates the 'all data' approach.

3.3 Variation in Time Step

Further to the investigation undertaken in section 3.2, the second parameter explored was the use of different time steps for which to extract the maximum load effect rather than the previously selected time step of 1 hour. This was to determine if the previously adopted assumption of using an hourly maximum load effect within the cumulative distribution function was suitable, or if a time step that had not yet been investigated was in fact more appropriate.

As with the experiment in Section 3.1, a month of WiM data using a Normal distribution was used as the benchmark data. Investigation was to be undertaken with the use 9 different time steps: 5 days, 2 days, 1 day, 8 hours, 4 hours, 1 hour, 30 minutes, 20 minutes and 10 minutes. As described in section 3.1, the load effects from each incremental movement of the load train were recorded. With this data, the maximum UDL values were recorded within each of the specified time steps for the full period of 30 days. This resulted in,

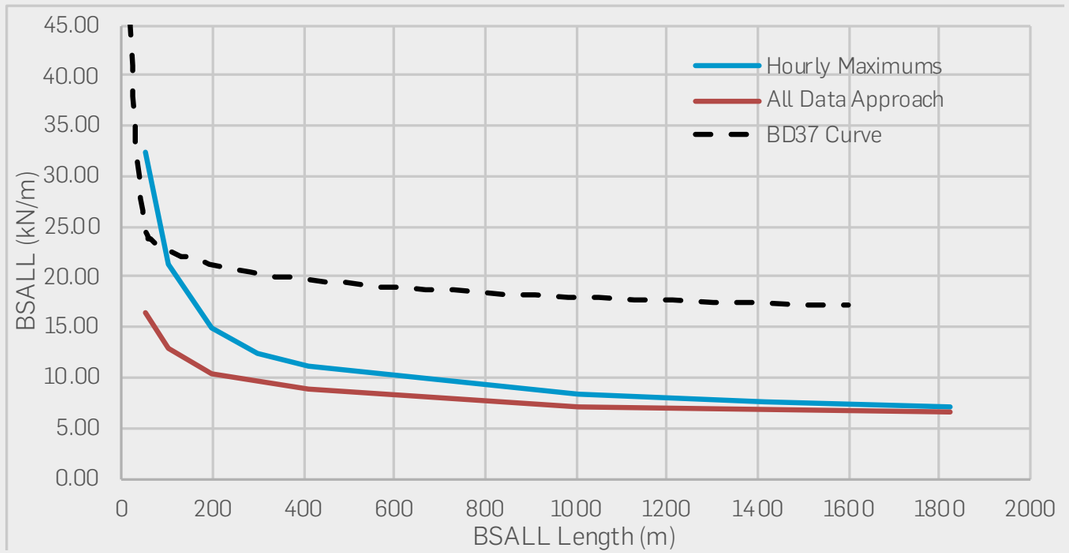

Figure 3: Hourly Maximums/'All Data' Approach BSALL Comparison

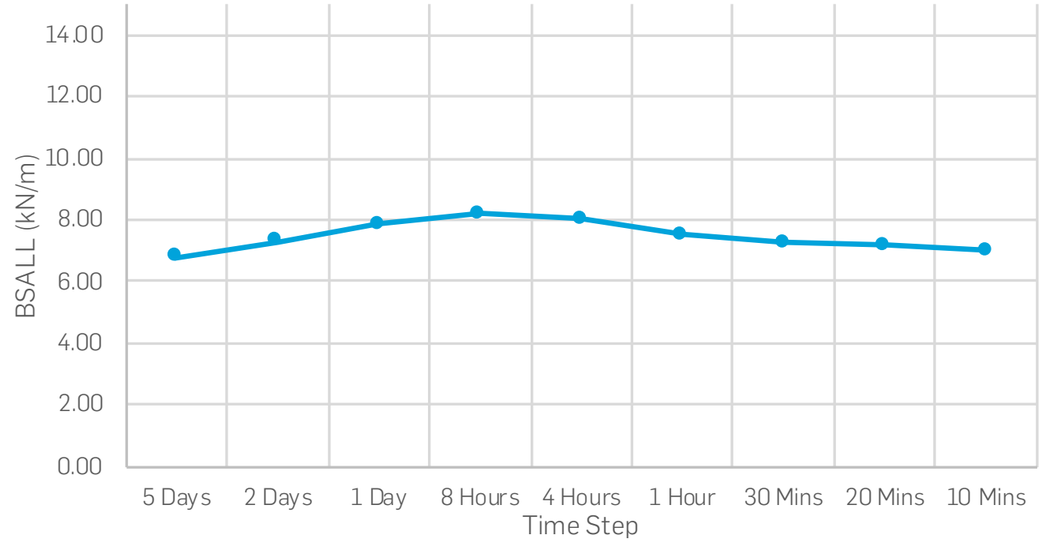

Figure 4: BSALL Results for Various Time Steps

for example, 30 maximum UDL values when using a time step of 1 day, and 90 maximum UDL values when using a time step of 8 hours. With a set of maximum UDL values for each of the time steps, the values were then used to derive the BSALLs for a loaded length of 1823m following the Normal distribution approach outlined in section 2.3. The results of this study are outlined in Figure 4.

As can be seen from Figure 4, it generally appears that the use of a shorter time step results in a BSALL of a marginally smaller magnitude. The reasoning for this is because when short time steps are used, there are instances in which the load trains of vehicles that are assessed do not completely fill the loaded lengths. This is exaggerated at longer loaded lengths and will reduce the resulting BSALL.

The downward trend in BSALLs as the time step increases is due to the total size of the dataset used. With the monthly datasets available to the authors, the BSALL calculated when using a time step of 5 days is only made up of 6 maximals, which does not offer a sufficient number in order to produce accurate results. A time step that is a smaller proportion of the overall dataset is therefore required. As described in Section 3.2, the benefits of using a larger dataset are only in allowing a more refined set of statistical parameters. If enough data was available to enable the use of time steps in excess of several days, the BSALL derivation would be of a similar magnitude to those generated from the hourly time step data.

From the Figure above, it is clear that the time step of 1 hour provides a good balance of an efficient BSALL, whilst ensuring that the traffic lanes are full for the assessment.

4 Summary of Findings

Parameter	Findings
Use of Gumbel Distribution	Conservative at shorter loaded lengths; best at longer loaded lengths.
Use of Normal Distribution	Realistic at shorter loaded lengths. Possibly slightly unconservative at longer loaded lengths.
Use of Lognormal Distribution	Realistic at shorter loaded lengths; similar to Gumbel at longer loaded lengths. Recommended approach.
'All data' approach	Potential for erroneous assumptions. Inferior to hourly maximum approach.
Variation in time step	1 hour confirmed as a suitable time step.

5. Recommended Approach

Based on the research Atkins has undertaken to date, it is therefore recommended that if deriving a BSALL for a significant loaded length (e.g. over 200m), any of the Gumbel, Normal or Lognormal distribution approaches can be adopted and similar results will be obtained. However, if deriving a BSALL for a loaded length of less than 200m, it is recommended that the Lognormal distribution approach should be adopted to produce the most efficient results. With that in mind, the use of the Lognormal distribution approach can therefore be recommended to ensure an efficient BSALL is calculated at all times.

Following the parametric studies, it is additionally recommended that the method of extracting hourly maximums is suitable within the derivation of the BSALL. This offers the assessor a less complex approach of derivation, which still makes use of the whole dataset but in a way which ensures it can be sensibly extrapolated to a suitable remote value for exceedance in 120 years.

6. Additional Considerations for the Selection of Partial Factors

There is a great advantage to having a statistical set of data when conducting an assessment, and that is twofold. First, characteristic values, typically with 5% chance of exceedance in the reference period (120 years for bridges), can be calculated directly for the real structure. These can be used together with prescribed partial factors from design or assessment codes. But, second, the statistical data can be used to go direct to a design or an assessment ULS value based on the required probability of exceedance at ULS. This may be different for design (where economic considerations tend to dominate as it is cheap to increase reliability through the addition of a little more material at the design stage) and assessment of existing structures (where retrofitting strength to provide improved economic reliability is very expensive and a minimum level of human safety becomes the dominant consideration).

This principle is illustrated in the accompanying paper to this conference “Reduced Partial Factors for Assessment in UK Assessment Standards “by Hendy et al., but also within fib bulletin 80 [7].

7. Conclusion

Through this work, the authors have greatly improved their understanding of BSALL derivation and the importance of a variety of factors that are involved throughout the process of the calculation. The studies completed have validated the work which has been completed to date and additionally offered new avenues of research to develop further understanding in this field.

References

[1] Highways Agency et al. Design Manual for Roads and Bridges - BD21/01 The Assessment of Highway Structures and Bridges. 2001. Available from: Standards for Highways.

[2] Hendy C.R, Mundell C, Bishop, D. Management of the Severn Bridge Suspension Bridge. Multi Span Large Bridges. 2015. ISBN: 978-1-315-68719-3.

[3] TRL Contractor Report 16. Interim Design Standard: Long Span Bridges. 1986.

[4] BSI. BS EN 1990:2002 Eurocode – Basis of structural design. 2010. ISBN: 978-0-580 71374-3.

[5] Highways Agency et al. Design Manual for Roads and Bridges - BD50/92 Technical Requirements for The Assessment and Strengthening Programme of Highway Structures. 1992. Available from: Standards for Highways.

[6] Highways Agency et al. Design Manual for Roads and Bridges - BD 37/01 Loads for Highway Bridges. 2001. Available from: Standards for Highways.

[7] fib. fib Bulletin No. 80. 2016. ISBN: 978-2-88394-105-2.

Acknowledgements

Originally presented and published as: Benham N, Mundell C, Hendy CR. Parametric Studies of Bridge Specific Assessment Live Loads and Implications for Assessment. IABSE Conference 2018 – Engineering the Past, to Meet the Needs of the Future, June 25-27 2018, Copenhagen, Denmark.

Structural Assessment | 008

UK Earthquake Engineering Assessment Team's Response to the M7.8 Muisne Earthquake, Ecuador 2016

Mark Scorer

Principal Engineer
Engineering, Design and Project Management, UK
USAR Engineer and Technician, SARAID, UK

Anna Pavan

Lead Engineer for Latin America
Build Change
Medellin, Colombia

Francisco Pavia

Program Manager
Bridges to Prosperity
Matagalpa, Nicaragua

Abstract

On 16th April 2016, a M7.8 earthquake struck the coastal provinces of Esmeraldas and Manabi in northwest Ecuador. The epicentre was approximately 27km south-southeast of the town of Muisne and 168km from the capital Quito. In response to this event UK-AID through the Department for International Development (DFID), organised an Earthquake Engineering Assessment team that deployed to Ecuador on the 22nd April. The team, comprised all co-authors of this paper, were based in the town of Pedernales, one of the worst affected areas for ten days.

The main task of the team was to provide damage assessments and surveys which were carried out based on the methodology presented in ATC-20-1. These included both 'Rapid' and 'Detailed' Assessments. Working closely with the Ecuadorian Army, the team initially focused on the community and municipality buildings including banks, churches and the town hall; before dedicating much of the mission to the assessment of schools and educational facilities in the area. This information was shared with the EUCPT and communicated to the Ecuadorian Army, the Ministry of Education and to UNICEF.

The paper provides details of activities carried out by the assessment team with several photographic examples to provide evidence of the damage and destruction caused by the earthquake. They indicate where deficiencies in building design and construction were identified and therefore where improvements in future construction can be made. Some of the key findings from the mission are summarized, with lessons learnt and potential areas for improvement noted.

Keywords

Earthquake; Ecuador; Muisne; Damage Assessments; ATC-20-1;

1. Introduction

Ecuador is located at the interface where the Nazca plate is subducting eastwards beneath the South American plate at a velocity of about 61mm/yr (USGS 2016). Throughout its history, the country has experienced a number of large earthquakes greater than magnitude 7 related to this subduction zone. On 16th April 2016 at 18:58 local time (23:58 UTC), another large earthquake (M7.8) struck the coastal provinces of Esmeraldas and Manabi. The epicentre, at 0.382°N, 79.922°W, was approximately 27km south-southeast of the town of Muisne and 168km from the capital Quito (Figure 1); with a hypocentral depth of 20.6km.

The shaking on the Modified Mercalli Intensity (MMI) scale experienced in many coastal towns including Muisne, Tosagua and Pedernales was severe (VIII) (USGS 2016) reflecting the considerable damage and collapse of buildings. The maximum peak ground acceleration (PGA) recorded by the Instituto Geofisico was 1.407g (13.803 m/s2) (Figure 2) at a location close to the town of Pedernales (Singaucho et al., 2016)

In the weeks following the main event, a number of significant aftershocks with magnitude greater than 6 occurred in the region with notable events on 20th April (M6.1) and 18th May (M6.7 and 6.9).

Figure 1. Epicentre of 2016 Muisne Earthquake With PAGER Modified Mercalli Intensity (MMI) Contours (USGS 2016)

2. Response

In response to the main event on 16th April, UK-AID, through the Department for International Development (DFID), organised a response mission of engineers to provide technical assistance to the Ecuadorian Army. The three authors of this paper were selected as a team of specialist earthquake engineers and deployed to Ecuador on the 22nd April 2016, linking up with Humanitarian Coordinator, Andy Wheatley. On arrival in Quito, prior to deployment into the field, the team met with the British Ambassador Mr Patrick Mullee and the Deputy Head of Mission, Mr Piers Craven to better understand the immediate need for response. Collaboration also took place with the European Union Civil Protection Team (EUCPT) which had arrived in country and were subsequently based in Portoviejo, to ensure knowledge share and consistency in approach between the respective missions.

Following high level discussions, the authors were deployed to the coastal town of Pedernales (0.071°N, 80.052°W), in the province of Manabí where they were based for ten days. This was one of the worst affected towns, close to where the highest PGA was recorded (Figure 2). More than 50,000 people in the canton of Pedernales were affected by the earthquake and it was the focus of much attention as the British, American and Canadian Ambassadors visited the area. As a result of the significant damage sustained in Pedernales, the team were accommodated in the small town of Cojimies (0.366°N, 80.037°W) approximately 35km to the North.

Upon arrival in Pedernales, the team's input was coordinated by Major Manuel Querembas, director of the Ecuadorian Army's Corp of Engineers. Major Querembas and his superiors helped facilitate the logistical challenges of working in a disaster zone and ensured the expertise being provided gave the most benefit. It should be noted that the support provided by Major Querembas and his team was invaluable to the assessments and surveys completed on the mission. The relationships established under the challenging conditions were vital and helped facilitate the subsequent Earthquake Engineering Field Investigation Team (EEFIT) Reconnaissance Mission of May 24 – June 7 (Franco et al., 2017).

The team also registered their presence and coordinated with the sub On-Site Operations and Coordination Centre (OSOCC) that had been established by the UN Disaster Assessment and Coordination (UNDAC) mechanism. The main OSOCC had been set up in Portoviejo but the sub OSOCC provided a platform for coordination with some cluster stakeholders and an opportunity to liaise with UNICEF. This resulted in the team focusing and prioritizing the assessment of educational buildings.

The main tasks undertaken by the team in Pedernales were to verify structures identified by the Ecuadorian Army for demolition and conduct damage surveys and structural assessments on a variety of critical community and educational buildings.

3. Methodology

In order to provide an internationally recognized and standardized approach, that provided clear, easily understood guidance and recommendations to both the local residents and authorities, the team performed the assessments in accordance with the Field Manual: Post-earthquake Safety Evaluation of Buildings (ATC-20-1, 1989). The purpose and scope of this manual is to determine whether 'damaged, or potentially damaged buildings are safe for continued use, or if entry should be restricted or prohibited.' Whilst it primarily deals with structural safety, it also offers guidelines for dealing with other hazards including hazardous material spills and downed power lines (ATC-20-1, 1989). In the immediate aftermath of an earthquake, being able to provide this information to authorities and locals can relieve a massive burden on the community. Two main methods of evaluation are prescribed in the document and both were utilized by the team in Pedernales:

- Rapid Evaluation Method
- Detailed Evaluation Method

The majority of the inspections completed were done using the 'Rapid Evaluation Method' which assesses six basic criteria that are primarily observable from the outside of the structure. Where, necessary any interior inspections were typically of short duration and limited scope, whilst no obviously unsafe buildings were entered. Through completion of the assessment forms, sufficient evidence was obtained to classify the building as 'Unsafe'; 'Restricted Use' or 'Inspected' and the respective placard was posted on the structure. It is important to ensure the placards are clearly visible and well attached.

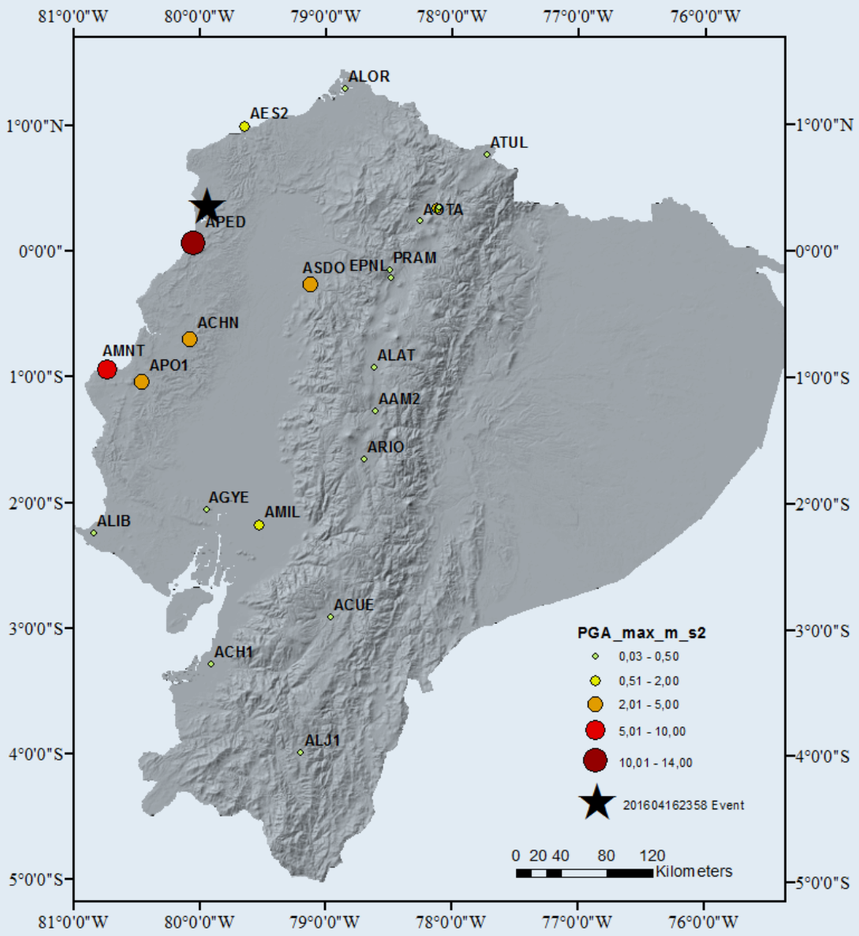

Figure 2. Peak Ground Acceleration Registered on the Ecuadorian Seismograph Network (Singaucho Et Al., 2016)

If the safety of the building is deemed to be questionable then a 'Restricted Use' posting is given and the recommendation made for the 'Detailed Evaluation Method' to be applied to the structure. In a few cases, the team classified buildings as 'Restricted Use' and 'Detailed Evaluations' of the structures were completed, including inspection to the inside of the buildings where safe to do so.

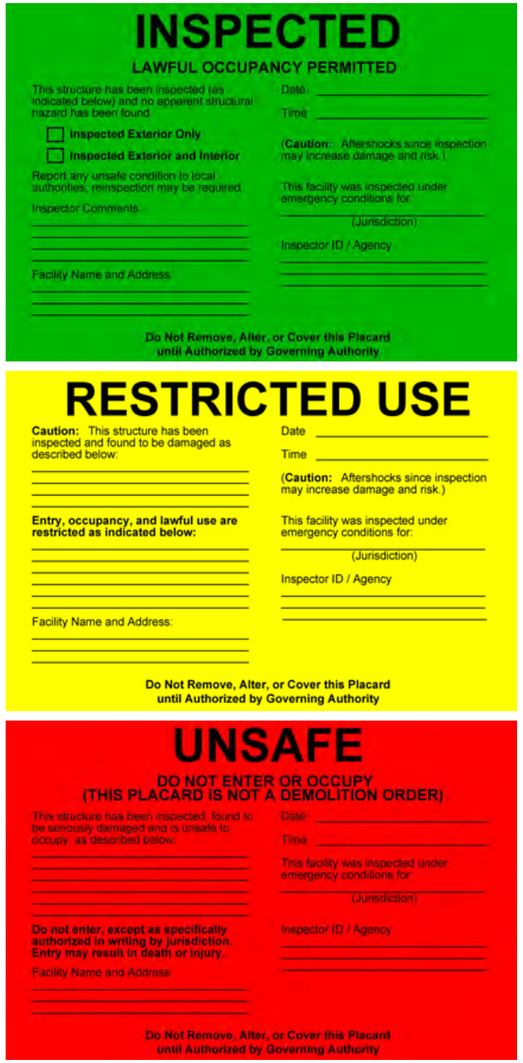

Figure 3. Examples of ATC-20-1 Assessment Placards

During the planning and preparation phase of the mission whilst the team was in Quito, the opportunity was taken to translate the assessment placards that were posted onto the buildings into Spanish. This was done to ensure they could be clearly understood by the local population and authorities. Examples of the classification placards from ATC-20-1 are shown in Figure 3.

4. Evaluations

4.1 Demolition Verification

In the days immediately following the main earthquake on the 16th April and prior to the team's arrival in Pedernales, the Ecuadorian Army Corp of Engineers had identified a total of 24 structures for demolition. The locations of these structures were provided to the team (Figure 4), however details of the assessments undertaken or criteria used were not available. The team's initial tasking was to visit these locations and provide technical assessment and advice on potential repairs or demolition. A number of the structures had been demolished before a follow-up evaluation could be made, but where possible additional assessments were undertaken. In most of cases, it was found that those buildings identified for demolition by the Army Corp had partially or totally collapsed during the earthquake and demolition was essential.

4.2 Critical Facilities

Priority was given to assessing a number of critical and communal buildings including the town hall, central church, Police station, local bank, water tanks and sports venues. These focal points within the community are vital in the response and recovery process to return daily life to pre-disaster conditions.

The most common building type evaluated in Pedernales was reinforced concrete (RC) structures with bricks or concrete block masonry infill walls. However, the design, construction and materials used for these buildings varied greatly in terms of quality, and it's likely the majority were non-engineered structures. Evidence of slender masonry panels comprised of brittle blocks with no reinforcement ties were commonly observed.

Other types of construction observed and assessed included timber frame with and without masonry infill; and informal timber or bamboo structures with traditional 'quincha' (bamboo covered with mud) walls. These light weight, more flexible structures typically performed relatively well in the earthquake.

A variety of photos of the damage observed during the evaluations are provided in Figures 5 to 8.

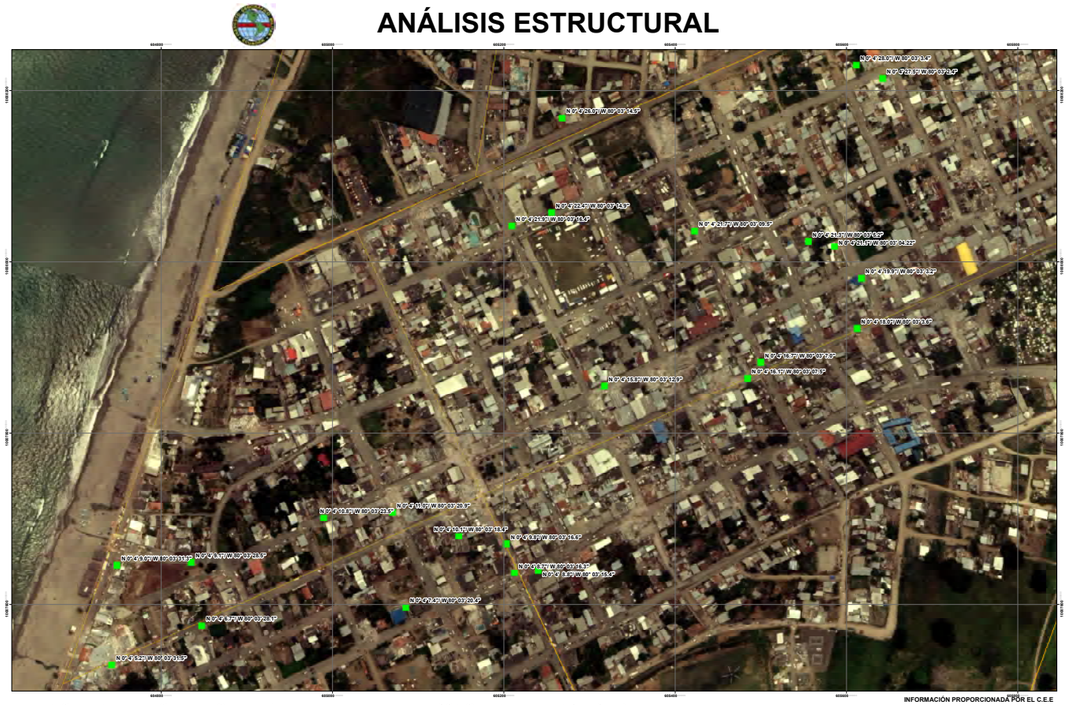

Figure 4. Satellite Image Showing Central Pedernales and Locations of 24 Structures Identified for Demolition

Figure 5. Maria Auxiliadora Church in Plaza Central, Pedernales

4.3 Educational Facilities

A significant proportion of the time in Pedernales was dedicated to the assessment of educational facilities including schools, colleges and universities. Fortunately, the main earthquake struck on a Saturday evening otherwise the consequences could have been significantly worse. Post-earthquake, these structures represent key facilities as their spaces, if safe to do so, can be used as shelters or operational centres for the response. To enforce this point, the Ecuadorian Army Corp of Engineers based themselves in the Atahualpa school in downtown Pedernales. As noted in Section 4.2, schools also represent important focal points for the communities as they are intended to be congregation spaces, and places of progression and development. In this sense, having schools back in operation as soon as possible after an earthquake represents a fundamental step in the long process of recovery for a community that suffered a natural disaster. As a means of expediting this process further, the team was also asked to provide advice on proposed locations for temporary schools.

Following discussions with Mario Calderon, the Team Leader for UNICEF in Pedernales, the team were provided with a list of 50 educational facilities (both public and private) in the canton of Pedernales. It was understood that the Ministry of Education had already performed a first round of assessments on the public institutions but exact details of the methodology used or results of the evaluations were not available. However, it was communicated that the schools were broadly separated into three different levels, based on the number of days required to repair and refurbish them as follows:

- Level 1: 0-30 days
- Level 2: 30-90 days
- Level 3: 90 days or more

With regards to these levels, it was not clear what level of resource was required during these repair periods.

In order to provide a more detailed and practical assessment for these facilities, evaluations using the ATC-20-1 methodology discussed in Section 3 were completed. For facilities with multiple buildings (i.e., classrooms, toilets, kitchen, etc.), each structure was assessed and marked independently. This approach enabled the local stakeholders (i.e. Ministry of Education and UNICEF) to understand which institutions or parts of them could be used immediately or in the short term. To optimize the limited time of the mission the team took the decision to prioritize those establishments that served the greatest number of students.

There were a number of different structural design types identified for the schools in Pedernales and their behavior during the earthquake varied significantly. On the whole, the single-story buildings performed well (Figure 9), with any damage typically limited to the non-structural elements such as masonry walls or window-grates.

Figure 6. Severe Damage to Hotels and Other Commercial Buildings to Be Demolished in Pedernales

Figure 7. Cojimies and Settlement of the Malecon in Pedernales

Figure 8. Significant Internal (Non-Structural) Damage Apartments

The two-storey structures, typically rectangular, with detached or integrated staircases performed less well. Significant damage was observed to the infill panel walls (Figure 10); from pounding between the staircase and classroom blocks; from the collapse of un-reinforced or un-tied parapets (Figure 11) and resulting from the short column effect (Figure 12).

Figure 9. Un-Damaged Classrooms Block (Escuela Fausto Molina)

5. Key Findings

The total number of structures assessed during the team's mission to Pedernales was 144 and the numbers and percentage of those classified 'Unsafe', 'Restricted Use' and 'Safe' are presented in Table 1.

Table 1. Total Number of Evaluations in Accordance With ATC-20-1 Completed by the Team in Pedernales

ATC-20-1 Classification	No. of Buildings Evaluated	Percentage (%)
UNSAFE	48	33
RESTRICTED USE	40	28
SAFE	56	39
TOTAL	**144**	**100**

The results of these evaluations were provided on a daily basis to the EUCPT for incorporation into their daily reports to Brussels (Goretti et al., 2017). Of these, 22 were educational facilities serving the needs of over 10,000 students from the canton of Pedernales. All the information collected in the field during the mission was transmitted to the Ecuadorian Army, the Ministry of Education and to UNICEF for their own records.

The vast majority of damage observed was due to poor seismic detailing, in particular the lack of appropriate ties and anchors between different structural elements. This lead to the collapse of numerous infill walls, staircases and parapets etc., and in some cases of complete multi-story buildings. Serious damage was also caused by configuration vulnerabilities that lead for example to the short column effect and pounding failures and poorly designed architectural features.

6. Lessons Learnt

During all phases of the team's mission, from response and deployment to the information sharing and de-brief, there were valuable lessons to be learnt. A summary of some of these lessons is provided here with a view to aiding and supporting future missions.

In the pre-deployment and travel phase, it is important to maximize any available time to ensure the team can be as focused and efficient as possible once in the field. Research and information on local design and construction techniques (World Housing Encyclopedia) should be obtained and having a regional office (Arup, Bogota, Colombia) provided valuable information and support.

Figure 10. Diagonal Shear Cracks and Damage to External Un-Reinforced Block-Work Walls

Coordination with local and international authorities can be complicated and time-consuming. It requires full-time dedication during deployment and should not be done by the engineers, whose skills can be better used in the field. For this mission, Andy Wheatley, our Humanitarian Coordinator from UK-DFID mainly focused on reporting to local contacts (e.g. the British Embassy in Quito, representatives of UK-Government in field) and briefly reporting key-points to the head-office in London. This approach is more efficient than reporting directly to Europe, especially where there is a significant difference in time zone.

The damage assessments and structural evaluations are a key activity during post-disaster intervention and should be initiated immediately, overlapping with the search and rescue phase. The assessments in accordance with ATC-20-1 provided a fast, efficient repeatable methodology that could be implemented and coordinated by both local authorities and other evaluation teams. Whilst the address of each building is required by AT20-1, a GPS location for each structure should also be mandatory. Often street names are unknown and building numbers have been lost or damaged, so to enable accurate assessments of the data and return evaluations (if required), this information should be recorded.

Figure 11. Un-Reinforced Parapets Collapsed at UEM Pedro López Ramos and Escuela Carlos Maria De La Condamine

It is vital that the ATC-20-1 classifications are understood and emphasized that Unsafe does not mean demolition. There were instances where this was the perception and may have been exacerbated by reports contractors were payed per unit quantity of material disposed of. In some cases, building owners were interested in having their properties demolished as quickly as possible to obtain the insurance payout, which may not have been available for repair or retrofit.

Local language proficiency is strongly recommended and for this mission it was vital. Conducting the surveys and reporting in the local language is essential for them to be properly utilized. Local authorities may have some English skills that can help, however, fluent communication in the local language is fundamental to be effective and interact with different stakeholders at all levels. Regular meetings and workshops with local stakeholders and communities are recommended to engage them in the operations, ensure they understand the scope of the assessments and allow them to proceed in a more structured manner to next steps of recovery.

Depending on the scale of the disaster and available resource, it is recommended teams comprise a minimum of three engineers and have the logistical support of a local driver. Assessments should be carried out in pairs at all times to ensure the safety of the team members. The duration of the missions will depend on a variety of factors but a minimum of 10 days is preferable.

In tropical regions, high temperature and humidity can impact the team's performance. Careful consideration should be given to optimal working times for both climate and security; and a reasonable level of accommodation and subsistence can ensure the team's efficiency during the mission is maintained. Data collection in the field is only part of the process and significant time is also required for processing and communicating the results.

References

ATC-20-1 (1989). Procedures for post-earthquake safety evaluation of buildings. 2nd Edition. Applied Technology Council. www.ATCouncil.org

ATC-20-2 (1995). Addendum to ATC 20 post-earthquake building safety evaluation procedures. Applied Technology Council. www.ATCouncil.org

Franco, G., Stone, H., Ahmed, B., Chian, S.C., Hughes, F., Jirouskova, N., Kaminski, S., López, J., G. van Drunen, N. and Querembás, M. (2016). The April 16 2016 MW7.8 Muisne Earthquake in Ecuador – Preliminary Observations from the EEFIT Reconnaissance Mission of May 24 - June 7. 16th World Conference on Earthquake Engineering, 16WCEE 2017. Santiago Chile, January 9th to 13th 2017. Paper N° 4982.

Goretti, A., Molina Hutt, C. and Hedelund, L. (2017) Post-earthquake safety evaluation of buildings in Portoviejo, Manabí province, following the Mw7.8 Ecuador earthquake of April 16, 2016. International Journal of Disaster Risk Reduction. 24: 271-283.

Singaucho, J.C., Laurendeau, A., Viracucha, C. and Ruiz, M. (2016) Observaciones del sismo del 16 de abril de 2016 de magnitud Mw 7.8. Intensidades y aceleraciones. Informe Sísmico Especial N.- 18. Área de Sismología – Instituto Geofísico. Available at: www.igepn.edu.ec

USGS (2016): General Summary of the M7.8 Muisne Event. USGS, Reston, USA [ONLINE] Available at: https://earthquake.usgs.gov/earthquakes/eventpage/us20005j32#executive [Accessed December 2017]

World Housing Encyclopedia [ONLINE] Available at: http://www.world-housing.net/ [Accessed December 2017]

Acknowledgements

The authors would like to extend their thanks and appreciation to a number of people and organisations who made this technical assistance mission possible. The UK Department for International Development (DFID) and both Atkins (now part of the SNC-Lavalin group) and Arup who enabled and supported the team's deployment. Special thanks to the staff of the British Embassy in Quito led by Mr Patrick Mullee and Mr Piers Craven; and to Major Querembas and all in the Ecuadorian Army who welcomed us and assisted with vital logistical support during an extremely challenging time.

Originally presented and published as: Scorer M, Pavan A, Pavia, F. UK Earthquake Engineering Assessment Team's Response to the M7.8 Muisne Earthquake, Ecuador 2016. The 16th European Conference on Earthquake Engineering, Jun 2018, Thessaloniki, Greece.

Figure 12. Short Column Effect (UEM Pedro López Ramos)

Modern Rolling Stock Crashworthiness Engineering Using Numerical Simulations – Australian and International Context

Abstract

This paper presents an example project to demonstrate the process that has been undertaken to meet modern rolling stock crashworthiness requirements of European Standard EN15227. This project relates to a newly designed metro passenger fleet to be delivered to a large international client. The methodology deployed takes into consideration the big-picture train-on-train whole-consist collision performance as well as detailed structural design of the Crash Energy Management (CEM) structure.

Design standards of rolling stock are constantly evolving. A brief discussion on the current crashworthiness standards and their expected direction of evolution for various types of rolling stock will be presented.

This presentation will also provide a discussion on the mathematical theories behind finite element analysis, and more specifically the differences between implicit and explicit schemes, and how they can be used to solve engineering challenges and designing rolling stock to meet crashworthiness requirements.

Two philosophies of CEM will be discussed. One philosophy is that the deformation of the car body structure being relied upon as a mechanism for energy absorption during a collision. The other philosophy is that impact energy being primarily managed by bolt-on off-the-shelf crush tubes.

Apart from crashworthiness engineering of newly-designed rolling stock, project examples of retrofitting and engineering of existing fleets will also be presented. One example involves refurbishing and engineering an antiquated fleet in an effort to improve crashworthiness performance. By applying first-principles engineering, the safety and crashworthiness of the fleet have being demonstrably improved. Another example involves assessing a proposed external attachment on an existing fleet for the potential of damage to the host structure as well as the attachment becoming a potential hazard upon collision with infrastructure.

Dr. Jademond Kiang

Senior Consultant Specialist Engineering
Engineering, Design and Project Management
Sydney, Australia

Keywords

Crashworthiness; Rolling Stock; Finite Element Analysis

1. Introduction

Most forms of rolling stock have crashworthiness requirements that need to be addressed. This paper focuses on passive aspects of crashworthiness, more specifically the structural performance, should a collision occurs after all possibilities of preventing an accident have failed.

What is crashworthiness? Crashworthiness can be described as how well a piece of rolling stock performs in terms of its ability to mitigate severity of consequences in a collision in a controlled manner, and how well the passengers are protected during such an event.

Modern-day crashworthiness design standards apply to new rolling stock. Older or existing rolling stock may also have been designed with crashworthiness considerations, but may not necessarily offer the same level of protection as modern specifications.

This paper presents a discussion on the philosophies of rolling stock crashworthiness engineering, crashworthiness standards, as well as the theoretical background to virtual crash testing technology. Actual projects will be used to exemplify the application of virtual crash testing technology and crashworthiness engineering.

2. Different Philosophies of Crashworthiness Engineering

During a train collision, an enormous amount of energy is involved. The forces involved would be in the order or mega-Newtons and the energy levels involved would be in the order of mega-Joules.

Such high levels of collision energy and forces need to be managed appropriately in order to provide passengers with a better chance of survival should a collision is to occur.

Some of the generic objectives of rolling stock crashworthiness engineering are to ensure:

1. The energy is dissipated by the train rather than passing it onto the passengers (which would be detrimental to passenger survivability). This is managed by the train's Crash Energy Management (CEM) system;

2. The car body structure remains intact during a collision such that passengers' and drivers' occupancy spaces are not intruded by the deformed structure;

3. The decelerations are limited or reduced to a level that is considered acceptable;

4. The cars in the train would not over-ride one another as they decelerate and come into contact with one another during a collision.

To achieve these objectives, crashworthiness design generally follows two common philosophies. One philosophy is that the deformation of the car body structure being relied upon (usually in conjunction with the coupler system) as a mechanism for energy dissipation, occupancy space protection and deceleration control. The other philosophy is relying primarily on bolt-on off-the-shelf crush tubes.

Using the car body structure to achieve these objectives has the advantage of having inherent robustness and structural protection for passengers during a collision, even if the collision is more onerous than it is designed for. For example, if the train is designed withstand a head-on collision with an identical train at 25km/h, passengers may still have an inherent level of protection if it collides with a heavier freight train at 60km/h.

However, engineering a car body structure to achieve these objectives requires the structure to comply and deform in certain areas in a certain manner, which is often counter-intuitive and contradictory to the requirements of mass reduction, as well as strength and fatigue life performance. Due to these challenging requirements and attributes, crashworthiness engineering generally involves specialist expertise.

However the second approach, where collision energy is primarily managed by bolt-on off-the-shelf crush tubes, would not generally provide the same level of inherent passenger crashworthiness protection. This is because the structure itself would not be specifically engineered for crashworthiness. Therefore, if the collision is more onerous than the design scenario, the car body structure may not provide sufficient protection for passengers.

There are however some advantages with this approach to crashworthiness design such as a lower design and construction timeframe and cost.

3. Crashworhtiness Standards

There are various local and international standards in relation to whole-consist crashworthiness requirements. One of the most the most notable and prevalent standard today is the European Standard EN15227.

Examples of other international crashworthiness standards from various countries are listed in Table 1 below:

Table 1: Crashworthiness Standards From Various Countries

Country of Origin	Standard
Britain and Europe	EN15227
Australia	AS/RISSB7520
USA	FRA 2010

The RISSB standard AS/RISSB7520 applies to the Australian rail industry. However this standard references EN15227 for crashworthiness requirements.

One notable requirement of EN15227 is that full train-on-train collision is required to be assessed by FEA, which can involve impact speeds of up to 36km/h depending on the type of rolling stock. For areas of large deformation (such as the CEM structure), FEA needs to be validated by physical testing.

For the train-on-train assessment, some of the requirements that need to be satisfied are:

- Average deceleration is limited;
- Intrusion into occupant and driver's space is limited;
- The cars in the train consist must not override during a collision;
- Plastic deformation in the car body structure during a collision is limited;
- Absorb collision energy in a controlled manner.

4. Where Are Design Standards Heading in Australia?

Design standards of rolling stock are constantly evolving. The widely used EN15227 (which is directly referred to by Australian standard AS/RISSB7520 for crashworthiness requirements) is only applicable to new passenger rolling stock and locomotives.

Other forms of rolling stock such as road-rail vehicles and maintenance vehicles do also have a design standard that considers crashworthiness, but not to the extent of EN15227. Australian standard AS/ RISSB7502 has a section specific to road-rail vehicle crashworthiness and AS/RISSB7520.4 has crashworthiness requirements for maintenance vehicles.

It is expected that design standards for road-rail vehicles and maintenance vehicles will attract more focus in the future to more extensively address crashworthiness requirements similar to those stipulated in EN15227 for passenger rolling stock and locomotives.

It is also expected that crashworthiness requirements, especially for passenger rolling stock, will become more stringent in the future as engineering design and analysis technology becomes more mature and refined.

5. Designing and Validating Crashworthiness

One way to address modern crashworthiness requirements is by physical testing of various designs and/or modifications in an effort to assess or determine the most appropriate design.

Another way to address crashworthiness considerations is by virtual crash testing. In other words, crashing trains in a computer by undertaking finite element analysis (FEA) to assess structural performance.

Each of these are discussed below.

5.1 Method 1 - Physical Crash Testing

The most direct method of validating crashworthiness performance is physical testing of the car body structure or sub-components of the structure. Whilst physical testing can theoretically be done, it has a lot of undesirable attributes in practice. These include:

- Monetary cost associated with the preparation of the full-scale test article (a full train-consist or sub-component);
- Monetary cost in relation to test facility;
- Long timeframe between test cycles leading to an inefficient design process;
- Variance between as-built test specimen and actual production article leading to test results not reflective of actual performance;
- Safety risks associated with large collision energy magnitudes (in the order of mega-Joules);
- OH&S and insurance complications associated with full-scale physical testing.

5.2 Method 2 - Virtual Crash Testing

A lot of the undesirable attributes associated with full-scale physical crash tests would no longer be applicable if the process is performed virtually:

- Cost of preparing test articles and facility (FEA models) will be significantly reduced;
- Timeframe between 'test' cycles will be significantly compressed;
- No OH&S and insurance complications;
- And most important of all, there would be no safety risks.

6. Mathematical Theory of Virtual Crash Testing

As described earlier, virtual crash testing involves the use of FEA technology. This section provides a high level summary of the mathematics behind the finite element method.

Crash scenarios are dynamic events. Therefore the effects of mass, stiffness, inertia, acceleration/deceleration, velocity and damping all need to be taken into consideration.

During static or non-dynamic events, loading is either constant or is applied slowly onto the structure, hence the dynamic effects mentioned above is either non-existent or insignificant. In such a case, the mathematical relationship between loading and structural response is simply:

$$\{F\}=[k]\{x\} \qquad (1)$$

where

{F} is the external force vector
[k] is the stiffness matrix
{x} is the displacement vector

For a single degree-of-freedom (DOF) system (such as a linear spring loaded with a point force), all three quantities consist of single values. This is called a single DOF system.

For a more complicated system with 'n' DOFs, the force and displacement vector becomes a vector of dimension 'n×1'. The stiffness matrix would have dimension 'n×n'.

The above system of equation can be solved by inverting the stiffness matrix ([k]-1) and then re-arranging the equation as follows:

$$[x]=[k]\text{-}1\{F\} \qquad (2)$$

Once the displacement vector is calculated, stress distribution throughout the structural system can then be computed.

In a dynamic system, the system of equation now includes the additional dynamic quantities mentioned previously, thus turning it into the following differential equation:

$$[m][a]+[c][v]+[k][x]=\{F\} \qquad (3)$$

where:

[m] is the mass matrix;
[a] is the acceleration vector;
[c] is the damping matrix;
[v] is the velocity vector.

Now that time is in the system of equation, the system of equation needs to be solved in the time domain as well in the mechanical domain.

There are two mathematical schemes to solve this system of equation, namely the implicit and explicit schemes.

In the implicit scheme, the system of equation can again be solved by inverting the stiffness matrix and re-arranging the equation to obtain the structural response. For simplicity of discussion, if damping is taken out of the equation, the solution becomes:

$$[x]=[k]\text{-}1(\{F\}-[m][a]) \qquad (4)$$

This scheme is called the implicit scheme because the unknowns do not occur strictly on one side of the differential equation. An iterative approach is required to obtain the solution over both the time and mechanical domains.

One of the advantages of this scheme is its efficiency in solving the dynamic response of a system over a long timeframe because there is no theoretical limitation on the size of the time steps.

However one of the major drawbacks is that the stiffness matrix needs to be inverted. Whilst this is no major issue for systems with a small number of DOFs, it is computationally expensive for detailed FEA models with large number of DOFs. Combining this with the need for multiple iterations at each time step imposes a limitation on the amount of detail that can be captured in the FEA model in practice.

The explicit scheme on the other hand is more efficient at solving FEA models with greater details (such as full train-on-train collisions), provided that the timeframe of the dynamic event is short (such as for in a collision). This is because the explicit scheme does not involve the inversion of the stiffness matrix nor does it require iterations to find a solution at each time step. This makes it less computationally intensive than the implicit scheme (for a given amount of model detail).

Mathematically, unknown quantities in the explicit scheme are defined by known quantities and therefore the solution can be explicitly defined (hence the name). Therefore no iterations are required to obtain the solution at each time step.

In the explicit scheme, the differential equation is solved by re-arranging it into the following format and solving for acceleration directly (again, damping is taken out of the equation for simplicity of discussion):

$$[a]=[m]\text{-}1(\{F\}-[k][x]) \qquad (5)$$

The inversion of the mass matrix is a trivial task because a lumped mass matrix is usually used for explicit schemes.

Structural response of the system (such as velocity, acceleration, stress and strain distributions) can then be calculated from the acceleration vector at each time step.

The type of effects the explicit scheme can capture efficiently include (but not limited to) the following:

- Large plastic strains and geometry changes;
- Post-yield and material fracture;
- Stress wave propagation;
- Pre and post buckling response;
- Surface-to-surface contact and associated friction.

Further technical and theoretical details relating to the finite element method can readily be found in FEA literature such as Bathe (1982), Cook (1995) or in journals papers such as Kiang et al (2007, 2010).

7. Can FEA Accurately Predict Structural Response?

The output of crash analysis is largely dependent on the model's assumptions and accuracy of the input parameters.

Experienced engineers who are specialists in crashworthiness engineering and FEA would be able to make decisions on relevant assumptions, level of model detail and modelling methodology in order to achieve meaningful and accurate outcomes within a practical model run time.

Below is an example to demonstrate FEA being used to accurately predict physical testing results.

During a recent crashworthiness engineering project, the accuracy of FEA in predicting the crashworthiness behaviour of a structure was required to be demonstrated as part of the requirements of EN15227.

To achieve this, the major energy absorbing structure (in this case, the CEM structure in the leading-end underframe) was required to be crash tested and compared with FEA results.

The crash test set-up consisted of a sled (i.e. a train analogue onto which the test article is attached) that rolls on a section of straight and horizontal track.

The sled and test article were propelled into a solid concrete barrier which is fronted by a steel plate. Between the steel plate and the concrete barrier are load cells to measure the impact forces. The steel fronting plate has a layer of timber to provide some sacrificial protection and a small amount of damping at the impact interface.

To predict the structural behaviour of the tested scenario, a representative FEA model of the test set-up and the CEM structure was constructed using MSC Patran and solved using explicit dynamic solver LS-Dyna. The potential for self contact was defined for the entirety of the CEM structure as well as between the front of the structure and the rigid barrier.

A schematic representation fo the FEA model is shown in Figure 1 below.

Figure 1: Schematic FEA Model Representing CEM Structure Crash Test

Note that due to confidentiality requirements, the FEA model and structural performance of the CEM structure could not be shown. However, it can be said that deformation shape and structural response behaviour (such as the force-displacement curve) were in good correlation.

The key performance parameters of the CEM structure also correlated well. As shown in Table 2, energy absorption, compression stroke and average force predicted by FEA were all within 10% of the tested response, which satisfies the correlation requirements of EN15227.

Table 2: Comparison of FEA and Test Results

Parameter	FEA vs. Test
Energy absorption	<10%
Compression Stroke	<10%
Average Force	<10%

To further demonstrate the accuracy of FEA, a crush tube of 60mm×60mm×t2mm is used. The front of the tube is collided with a rigid mass weighing approximately 100kg travelling at approximately 27km/h. This scenario is analysed in a FEA model and compared with test data presented in Zarei (2008). The results of this comparison are presented in Figure 2 and Figure 3.

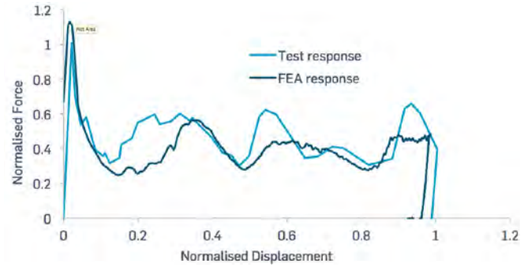

Figure 2: Force-Displacement Response of Test and FEA

Figure 3: Progressive Deformation of Crush Tube Predicted by FEA Compared With Test (Symmetric Half Shown)

As can be seen, both deformation shape and structural response of the test article and FEA prediction are in good agreement. The correlation would be even better if the exact material parameters of the test article are known.

In summary, the response of a structure in a collision, as predicted by FEA, can accurately represent the actual structure, provided that the FEA modelling approach is appropriate.

On the other hand, if the modelling approach is inappropriate, the structural response predicted by FEA would not be representative of the actual structure. An inappropriate approach may include the use of incorrect assumptions and simplifications, the use of incorrect finite element formulation altogether or even incorrect solver settings.

The engineer undertaking such a task needs to have the knowledge, expertise and experience in FEA and crashworthiness engineering in order ensure a positive outcome can be achieved.

8. Project Example 1 - Design of New Metro Fleet

A recent project undertaken involved the design of the car body and CEM structure of a new stainless steel metro passenger fleet that is to be delivered to a large international client.

As part of the crashworthiness requirements, the car body and CEM structure not only had to fulfil the requirements of EN15227 (such as those listed in Section 3), but also had to be compatible with existing fleets that are currently in service.

The compatibility requirement with existing fleets meant that in the event of a collision, the requirements of EN15227 can be satisfied for both trains.

8.1 Preliminary Design

During the preliminary design phase, the configuration and structural details of the new train were not yet available and yet some representative collision performance parameters were required to form part of the design input.

Some of the collision performance parameters included the answers to the following questions:

- What car body and CEM stiffness is desirable in order to satisfy the requirements of EN15227?;
- What is the appropriate stiffness for the leading-end auto-coupler and inter-car couplers?
- What is the ideal weight distribution throughout the consist for crashworthiness?;
- What are the likely compression strokes of the car body and CEM structure at the leading-end and inter-car ends?
- Is coupler shear-out going to occur?
- What are the likely deceleration levels on each car of the consist?;
- How much roll-back (if un-braked) or slide-back (if braked) would each car on the impacted train experience?

In order to answer these questions during the preliminary design phase, train-on-train collisions were analysed using a 1D approach.

With this approach, each major components of the train were simplified into discrete 1D finite elements with representative mass and stiffness properties.

These components include the car body, leading-end auto-couplers, inter-car couplers, CEM structure, bogies and the wheel-rail interface.

A schematic illustration of a single car represented by 1D finite elements is shown in Figure 4.

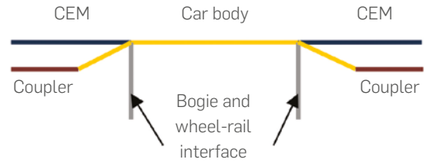

Figure 4: Schematic 1D FEA Representation of a Single Car

Multiple cars were then coupled together to form a train consist. Two consists were then assembled into straight linear alignment thus representing the head-on frontal collision scenario.

The nonlinear stiffness of the CEM structure of the existing train were obtained by a homogenisation process. This involved running a 3D FEA simulation of the CEM structure of the existing train (by following a similar methodology to that presented in Section 7) to obtain the force-displacement profile (or energy absorption profile). This profile is then used as input into the 1D analyses.

Correspondingly for the yet-to-be designed train, a series of different stiffness profiles for the couplers (which was information from the manufacturer) and CEM structure (which was dependant on the structural details yet to be designed) were used as input to the 1D analyses.

These 1D simulations were analysed using the implicit dynamic scheme (implemented via MSC Nastran). In this instance, the explicit scheme is not required because the number of DOFs were small (not a detailed model), even for a full train-on-train collision, and hence the use of the implicit scheme remains numerically efficient.

In consideration to answering the questions listed above and satisfying the requirements of EN15227, the most suitable combination of coupler and CEM was selected as the 'target' for the detailed design phase to achieve.

8.2 Limitations of 1D Approach

It should be noted that there are inherent limitations using a 1D analysis approach. Some of these limitations are noted below:

- Accelerations, velocities and forces in any direction other than in the longitudinal direction are restricted and not captured;
- Roll, pitch, yaw and bounce behaviours as well as displacement of the cars in directions other than the longitudinal direction are restricted and not captured;
- Although the stiffnesses of the car bodies are included, the 1D stiffness definitions do not allow flexing in any direction other than the longitudinal direction;
- The mass of the car bodies, couplers and collapse zones are lumped at discrete points, which limits the ability of the 1D model to capturing realistic inertial effects.

All of the aforementioned limitations in the 1D analyses affect the overall accuracy in simulating actual collision behaviour.

Therefore, the results from the 1D analysis approach should be considered as an indicative response of the system which is only appropriate for preliminary design input.

8.3 Detailed Structural Design

The detailed design phase involved the design of the CEM structure such that it would exhibit the 'target' energy absorption profile which was selected during the preliminary design phase.

The first step of this design task was to create a conceptual design that would be a good starting point. This initial concept design was created using a combination of first-principles engineering and hand calculations to work out approximate layout, section sizes and material requirements. A 3D FEA model of this concept was then constructed in MSC Patran and analysed in explicit dynamic software LS-Dyna.

Explicit FEA was used in this instance partly because of the large number of DOFs (a detailed model) and large plastic deformation involving surface-to-surface contact and friction, thus making the explicit scheme more practical and efficient than the implicit scheme.

Although the conceptual design turned out to be a good starting point, the design had to be fine-tuned in order to closely exhibit the target behaviour. During this fine-tuning process, numerous iterations were trialled and virtually tested. Each iteration involved the tuning of structural layout, material properties, sectional profiles and other details.

During the entire design process, it was important to keep in mind that the design had to be manufacturable and practical. More specifically the design had to be easy to fabricate (for example, it cannot have weld lines in places that are difficult to reach) and that the sections and materials can be readily purchased.

In total, over 10 iterations of the underframe structure were required to achieve the design objective. The timeframe for these 10 iterations was approximately 2 weeks. Imagine the amount of resources needed, the timeframe required and the safety risks involved if each of these design iterations were physically tested.

The target profile and the profile achieved by the final design are shown in Figure 5. Note that the response of the structure is not the same as shown in Section 7 (even thought they pertain to the same CEM structure design) because of differences in mass and impact velocity of the two analyses.

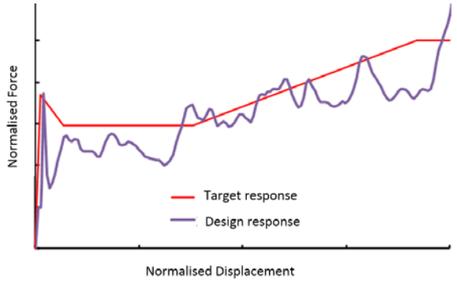

Figure 5: Target Energy Absorption Profile and Actual Achieved Profile

As evident in Figure 5, the achieved energy absorption behaviour of the CEM design closely matches the target profile. The structure was designed such that the actual profile is slightly below the target in order to account for the energy absorption contribution of other components of the car body which the CEM structure is attached to.

8.4 Features of the CEM Design

The CEM structure consists of five rectangular hollow sections arranged longitudinally in a parallel configuration. Two outboard and three internal longitudinal members constitute the CEM structure. Unfortunately pictures of the CEM structure cannot be shown due to confidentiality requirements.

The intent of these longitudinal members is to act as crush tubes, which compress longitudinally by folding of the faces as shown in Section 7. This is the collapse mode that would absorb the largest amount of energy for a given section.

The two outboard longitudinal members provide the initial force against compression, corresponding to the flat portion in the first half of the energy absorption profile in Figure 5.

The internal longitudinal members compress progressively as the compression stroke increases, each adding more resistance, thus providing the progressively increasing force against compression. This corresponds to the slope in the second half of the energy absorption profile in Figure 5.

To ensure the structure would collapse in a controlled manner, collapse initiators at the leading end of the outboard and internal longitudinal members have been introduced into the design. These initiators are made by having their four corners removed and the faces indented as depicted in Figure 6.

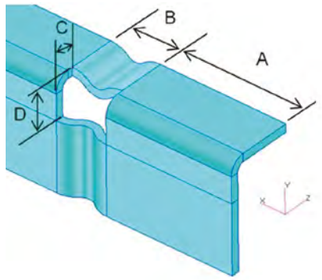

Figure 6: Schematic Illustration of Collapse Initiator Design (Quarter Section Shown)

The dimensions of these features (dimensions A, B, C, D, as well as the thickness of the section and indentation offset) have been meticulously designed and fine-tuned (with consideration to manufacturability) for two important functions:

- Firstly they serve to ensure collapse of the members would initiate at the leading-end thus ensuring controlled progressive collapse along their lengths, starting from the front (this helps the design to comply with the requirements of EN15227); and
- Secondly, they reduce the initial peak force against compression. This is the reason behind the low initial forces as each longitudinal member gets engaged, as well as the relatively smooth profile shown in Figure 5. Without the collapse initiators in the design, the response curve would contain large peaks similar to the one shown in the initial part of the curve in Figure 5.

8.5 Integration of CEM Structure Into Car Body

After the CEM structure had been designed, it was then integrated into the rest of the car body structure for performance validation prior to committing to train-on-train validation.

Spot welds and fusion welds provide structural integrity to the car body. They can have a significant influence on structural performance in a collision. The FEA models for the car body structure thus takes into account the strength of fusion welds and spot welds (which can fail and disconnect if overloaded) so that the appropriate level of accuracy is achieved.

8.6 3D Train-On-Train Crashworthiness Validation

Full-consist 3D train-on-train collision analyses are required to be undertaken to validate the final design's crashworthiness performance as per the requirements of EN15227.

This phase of the project is currently underway.

9. Project Example 2 – Retrofitting an Existing Fleet

Crashworthiness performance is not only important to new rolling stock. Quite often, older or existing fleets need to be retrofitted or upgraded to improve crashworthiness performance. An example of such a project has been undertaken for a fleet of older rolling stock in Australia.

It would be unreasonable in attempting to bring the fleet's performance to modern-day specifications. Instead, a first-principle approach was undertaken where the existing timber cab structure was replaced with a stiffer and stronger steel frame structure.

It should be noted that a stiffer and stronger cab may not always provide the best crashworthiness performance, but in this case it does because the existing cab did not have sound structural integrity to begin with.

The underframe structure was also redesigned to provide more integrity as it undergoes compression during a collision. This was achieved by the addition of lateral members in the underframe structure to stabilise the longitudinal members as they undergo compression during a collision.

The effectiveness of these modifications then needed to be validated. Instead of undertaking full-scale physical crash testing (there are undesirable implications associated with physical crash tests discussed in Section 3), the structural modifications were validated by FEA instead.

A FEA model of the car body was constructed in MSC Patran and analysed using explicit dynamic solver LS-Dyna. The model takes into consideration the strength of bolts and rivets (which can fail and disconnect if overloaded) at the appropriate locations as well as the effects mentioned in Section 6.

To validate the improvement to crashworthiness performance, the collision scenarios that were virtually crash tested included the collision of a retrofitted vehicle with an existing vehicle, with other types of vehicles on the network as well as with a rigid barrier at various impact speeds.

The FEA results of the existing and retrofitted vehicles colliding with a rigid barrier are shown in Figure 7. These deformations correspond to the same collision speed at the same snapshot in time.

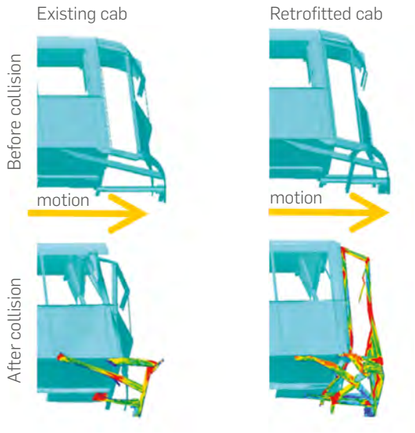

Figure 7: Improved Driver Occupancy Space Preservation in Retrofitted Vehicle (Underside View)

As shown by these virtual collisions, there is demonstrable improvement to driver protection as a result of these structural modifications because of better preservation of driver occupancy space.

After satisfactory validation of improved crashworthiness performance, these modifications have now been implemented by the client onto the fleet.

10. Project Example 3 - Investigation of External Attachment

Apart from full car body or train-on-train collisions, small components may also need to be validated for crashworthiness performance. For example, a project was undertaken for a fleet of rolling stock in Australia where the operator was proposing to attach a component to the external side of the car body by a series of fasteners. The operator wanted to ascertain whether the proposed attachment would become a safety hazard.

The potential hazards assessed included the potential of damage to the car body structure (such as bolt hole failure or section buckling and yielding) should impact with infrastructure is to occur, and the potential for the component turning into a projectile if it detaches from the car body (due to fastener failure).

A FEA model of the component and the relevant parts of the car body structure was constructed using MSC Patran. The FEA model is shown in Figure 8, which included seven sets of fasteners distributed along its length.

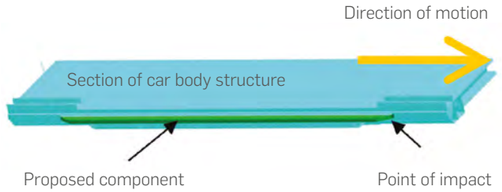

Figure 8: FEA Model of Component (Green) Attached to a Section of Car Body Structure

There are various reasons why hand calculations cannot provide an accurate assessment of the structural response.

Firstly, due to the dynamic nature of collisions, the distribution of deformation and stress in the component, as well as loads in the fasteners, would not be uniformly distributed along its length. This is partly because the stress wave that is generated at the impact zone may not have time to travel down the length of the component, and partly due to the effect of friction between the component and the car body. This would lead to higher loads near the impact zone compared to locations that are further down the length.

There is also a combination of alluminium, steel and rubber materials in the component and the car body structure. Having such large dfferences in material properties, coupled with the different dynamic behaviour of these materials at impact, would make it difficult if not impossible to be accurately assessed by hand calculations.

Instead, a combination of nonlinear static and explicit dynamic analyses were used to assess the response of the component and surrounding structure. Nonlinear static analysis was used to determine the outcome for slow speed impacts or pseudo-dynamic impacts, whereas explicit dynamic analysis was used for the assessment of higher speed impacts.

Nonlinear static analyses were performned using MSC Nastran and explicii dynamic analyses were performed using LS-Dyna.

Deformation of the component and the car body structure, as well as loading in the fasteners (which can fail and disconnect if overloaded) has been assessed for various impact speeds and scenarios.

The non-uniform distribution of stress in the car body during one of the higher speed impact scenarios is illustrated in Figure 9.

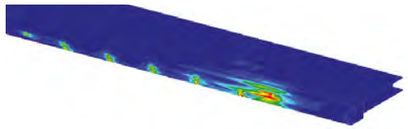

Figure 9: Non-Uniform Distribution of Stress Along a Section of Car Body Structure (Attached Component Removed From Image for Clarity)

The outcome of this project was that potential fastener failure (thus transitioning into a projectile hazard), as well potential damage to the car body structure, has been assessed and delivered to the client.

11. Conclusions

An overview of the process that was undertaken during a project on the crashworthiness design of a new fleet of rolling stock was discussed. Other project examples involving the retrofitting of existing fleets were also presented.

In the examples discussed, crashworthiness performance could not be validated accurately by hand calculations and therefore were assessed virtually using FEA.

A comparison between FEA and physical testing has been provided. It has been demonstrated that collision performance of a structure can be accurately predicted by FEA, provided that the modelling approach is appropriate for the task and that input parameters are accurate.

It has been demonstrated that the combination of sound engineering principles, FEA technology and implementation of crashworthiness standards has served the rail industry's crashworthiness performance needs.

Moving forward, this will continue to be the case as crashworthiness standards are expected to increase in stringency and coverage.

References

1. Australian Standard/Railway Industry Safety and Standards Board, 2012, 'Railway Rolling Stock - Body Structural Requirements ', AS/RISSB7520:2012

2. Bathe, K.J., 1982. Finite element procedures in engineering analysis, Prentice-Hall.

3. Cook, R.D., 1995. Finite element modelling for stress analysis, Wiley.

4. European committee for standardization, 2008, 'Railway applications - Crashworthiness requirements for railway vehicle bodies', EN15227.

5. Federal Railroad Administration, 1997, 'Transportation: Passenger equipment safety standards, 49CFR238'.

6. Federal Railroad Administration, 2010, 'Passenger Equipment Safety Standards; Front End Strength of Cab Cars and Multiple-Unit Locomotives; Final Rule', Federal Register, vol. 75, no. 5, p. 1180.m FRA 2010.

7. Hamidreza, Z., 2008. Experimental and numerical investigation of crash structures using aluminum alloys, Cuvillier Verlag.

8. Kiang, J., Tong, L., 2007. Three-dimensional constitutive equations for Ni-Mn-Ga single crystals. Journal of Magnetism and Magnetic Materials, 313, 214-229.

9. Kiang, J., Tong, L., 2010. Nonlinear magneto-mechanical finite element analysis of Ni-Mn-Ga single crystals. Smart Materials and Structures, 19(1), 1-17.

Acknowledgements

Originally presented and published as: Kiang J. Modern Rolling Stock Crashworthiness Engineering Using Numerical Simulations – Australian and International Context. CORE 2016: Maintaining the Momentum. Melbourne: Railway Technical Society of Australasia, 2016: 329-338.

Unsatisfied-Desire Lines: A Spatial Approach To Pedestrian Collision Analysis

Beatriz Campos

Principal Consultant
Engineering, Design and Project Management
London, UK

Jose Carpio-Pinedo

Universidad Politecnica de Madrid
Madrid, Spain

Abstract

Safety is one of the most important conditions for pedestrian activity and a principle that should underpin any public realm scheme. However, there is still a gap in understanding where collisions and pedestrian casualties happen and thus, a lack of tools to be applied from the urban design discipline to prevent them. Our initial hypothesis is implicit in pedestrian safety guidelines: collisions take place where there is an imbalance between high pedestrian demand (pedestrian desire lines[1]) and low public realm quality. This statement has the potential to be analysed systematically and as a prevention tool.

This paper presents the case study of Peckham Town Centre, London. Peckham Town Centre was selected as part of a Transport for London (TfL) initiative to develop transport strategies with the objective of improving pedestrian safety, promote walking and to improve the overall pedestrian experience in town centres.

Pedestrian desire lines were identified using the space syntax methodology, which has proven its capacity in understanding pedestrian route choices and flows through streets network configurational analysis. In a consistent way, Visibility Graphic Analysis (VGA) of spatial configuration added to land use data offered a detailed, weighted description of pedestrian route choices. Public realm quality was assessed using Pedestrian Environment Review System (PERS). The identification of 'unsatisfied desire lines', i.e., pedestrian routes which are not supported by good, adequate design, was subsequently compared to the collision data from 2011 to 2015.

The analysis found that there was a strong correspondence between spatial morphology and the location of collisions. Surprisingly, the analysis showed little correspondence between the quality of the public realm and collision locations. Lastly, the study tested the methodology applicability to development options without compromising on urban vitality, public space connectivity or community severance.

Keywords

Collision; Pedestrian Safety; Space Syntax Methodology; Urban Morphology; Visibility Graph Analysis (VGA)

[1] Pedestrian desire line is defined as the preferred route a person will take to travel from A to B. Often, this is the most direct and quickest route someone can take and does not necessarily follows a 'designated path'. Parks are a clear example where visitors walk across the grass, rather than using the available paths, when those paths are not aligned with the most direct, simplest route between locations.

1. Introduction

Safety is one of the most important prerequisites for pedestrian movement in the urban environment and, thus, should be considered at the heart of any public realm scheme or masterplan. Pedestrian safety is also a matter of public health: In Greater London alone, between 5,000 and 6,000 pedestrians are involved in a collision annually, of which nearly one hundred lose their lives (Transport for London, 2016). Pedestrian safety should also be safeguarded as part of all strategies seeking to encourage active, sustainable travel. Pedestrians are the most vulnerable group when looking at overall road safety. Furthermore, despite being involved in only 18% of all collisions, pedestrians accounted for nearly half (49%) of all fatalities in London (Transport for London, 2016).

It is, therefore, the responsibility of planners, designers, engineers and architects to plan and design safe environments. However, there is a general lack of methodologies to assess the degree of safety that a design provides prior to its implementation. Another challenge is the need to apply methods to analyse urban environments at a micro-scale, given that some studies have highlighted the important role of certain micro-scale factors, such as the location of crossings, bus stops or retail units, in the incidence of collisions.

Our study examines two cutting-edge methodologies – Visibility Graph Analysis (VGA), carried out using the Fathom software developed by Atkins Ltd, and Pedestrian Environment Review (PERS) – to understand the correspondence between urban environment variables and the location of collisions at the micro-scale of urban areas. These two methodologies correspond to two levels of practice: VGA analyses urban form, the impact of land use distribution and the location of transport services. These factors relate to the level of master planning and generally are not easily modifiable. In contrast, PERS addresses the perceived quality of physical elements such as the width of footways or crossings, which relate to the micro design level and are easier to modify. These relate two methodologies structure our study.

1.1 State of the Art: Where Collisions Happen or Where Pedestrians Go

Common pedestrian safety strategies to date have focused on both pedestrian and driver behavioural change through education, encouragement and law enforcement on the one hand, and innovations in road design, engineering and traffic calming strategies on the other hand. These strategies have been supported by studies that examine the influence of certain factors on collision risk, such as pedestrian characteristics, i.e., age, gender or ability or vehicle speed (Zegeer & Bushell, 2012). However, the environmental and contextual factors associated with the location of collisions involving pedestrians have been generally less investigated (Moudon et al., 2008).

Pedestrian safety strategies have incorporated some urban environment issues, such as road design, lighting, maintenance, speed limits or specific equipment such as safety cameras, crash-protective objects or countdown traffic lights (Transport for London, 2013). These can be framed into the field of public realm design and, therefore, can be easily modified in a 'quick-win' street re-design project.

Yet, Moudon et al. (2008) and Shawky et al. (2014) highlight that several factors, such as the crossing typology, have limited effectiveness to promote safety. In contrast, they suggest that the highest risk of collisions take place in areas where the concentration of retail activities takes place. However, as Moudon et al. argue, retail concentration might be just a proxy measure for pedestrian activity in a given area.

This statement leads the discussion towards a different approach: should we instead focus on the factors influencing pedestrian movement? The literature has identified consistent evidence pointing at urban morphology and land use distribution as the main drivers of pedestrian activity, strongly correlated with pedestrian counts.

Based on network analysis, space syntax methodology (Hillier & Hanson, 1989; Hillier et al., 1993; Hillier, 2007) analyses the street network from a configurational perspective. Space syntax variables, such as choice or integration, highly correlate with pedestrian flow volumes and distribution. These variables summarise relevant topologic and geometric patterns and develop the idea of natural movement and wayfinding due to visual connections. This methodology has succeeded in identifying the pedestrian 'desire lines' of movement, mapping the places with a higher pedestrian demand and the most common pedestrian routes.

Within the same theoretical basis, VGA allows the assessment of urban spaces at a more micro level (Turner et al., 2001; Desyllas & Duxbury, 2001; Turner, 2003). Space syntax representations such as axial lines (straight parts of the street network) and, street segments between two consecutive junctions (Hillier et al., 2010) provide a 'large' scale representation and quantification of urban spaces. In contrast, VGA enables a finer granularity and the analysis of different locations within the same street segment with a distinction between footways, if required. This level of detail results in improved correlation coefficients with pedestrian flows (Desyllas & Duxbury, 2001).

Including land use data and transport node locations into the analysis have the potential to improve the correlation even further (Desyllas et al., 2003). This seems evident as land use density, commercial activities and public transport nodes are clear pedestrian trip generators, even though their contribution to the correlation may not be as crucial as expected (Ozbil et al., 2011). However, regardless of its overall contribution to pedestrian collision risk, consistent studies suggest the importance of land use variables, such as population and employment density (LaScala et al., 2000; Graham & Glaister, 2003), in addition to the concentration of retail activities introduced before.

1.2 Research Questions and Goals

The literature illustrates that urban morphology, street network topology and geometry, land use distribution and density are variables that explain pedestrian volumes in the urban environment and thus the pedestrian exposure to collision risks. However, most pedestrian safety strategies deal with the urban environment at the micro level of design.

The goal of this study is hence to re-frame the subject of pedestrian collision location according to these two levels of spatial intervention: micro design versus urban form including land use. We, therefore, ask ourselves the following questions: What is the role of design quality in enhancing pedestrian safety? Are current pedestrian safety strategies correctly focusing their actions at the scale of the road and public realm design? Would a double approach (urban planning vs. design) support a stronger understanding of collision locational patterns? To that end, this study compares these two scales of interventions to inform, redefine and consolidate pedestrian safety strategies.

Opposing urban form and design quality leads to four space types: 'Successful pedestrian spaces' (high demand, good design quality), 'unsatisfied-desire lines' (high demand, poor design), 'back forgotten spaces' (low demand, poor design) and 'red-carpeted deserts' (low demand, good design), whereas demand relates to pedestrian flow volumes and design refers to the physical elements constituting the public realm[2] (Figure 1). All variables are analysed at the micro level of the collision location, which is also the micro level of intervention for some elements, e.g. crossings or pavements. However, the urban form variables are the consequence of urban planning decisions at a more macro scale of intervention, such as the scale of a masterplan. The four fundamental typologies used to frame the topic and discussion are summarised in the Space-Type Diagram below:

Figure 1: Space-Type Diagram: Urban Form Versus Design Quality

[2] There are a range of factors that can be used to assess the design and quality of the public realm. In this study, we based our criteria on the PERS methodology (refer to Section 2.4) including suitable materials, accessibility (gradient and dropped kerbs), lack of clutter, lighting, maintenance and quality of environment. We did also consider adequate footway width in line with Transport for London guidelines (2010). This does not exclude other important design elements such as street furniture, greenery, distinctive character and desirability.

2. Datasets And Methods

2.1 The Study Area: Peckham Town Centre

In line with Transport for London's 'Improving the Health of Londoners' Transport Action Plan, a safe and attractive urban environment can encourage people to walk and consequently to become more active. Similarly, there has been a wealth of studies (Gehl, 1987; Hart, 2015; Hillier, 2007) that reiterate how accessibility is crucial for the development and sustainability of local economies and to reinforce a sense of place and the welfare of local communities. Peckham Town Centre was selected by TfL as a pilot location based on the number of pedestrians Killed or Seriously Injured (KSI) in recent years and the pedestrian safety risk.

The study area consists of almost 2km of the TfL's Road Network (TLRN) and 3km of local authority roads. These links exhibit a wide variety of functions: the TLRN A202 providing a major east-west arterial route from Westminster to Greenwich; Rye Lane acting as the spine of Peckham and the centre for community activity and retail; and several side streets which serve as local routes to residential areas beyond. Further, the study area comprises a typically busy urban environment with mixed use, services and residential buildings, characterised by both high levels of pedestrian movement and demand for a sense of place where local people can make use of local retail, social and community facilities.

The Peckham streetscape has remained largely unchanged over recent years and, apart from routine maintenance and street works, there has been no significant change to the road layout.

Conversely, in Peckham town centre, there are several examples of community severance, i.e., the local infrastructure acts as a physical and/or psychological barrier to the movement of people. For instance, the entrance to Peckham Rye Station is confusing, its visibility across Rye Lane is poor due to multiple obstructions such as trader's stalls, wastes and street furniture on narrow footways, which also limit accessibility for less mobile people. Often people were observed walking on the road itself, increasing the risk of collisions. The access between Peckham Library, a hub of cultural activities, and Rye Lane, the shopping destination, is another example of community severance. Despite being a signalised crossing, the crossing at the junction of Rye Lane and Peckham High Street is far from safe, as highlighted by the number of casualties over the past five years.

2.2 Collision Data

Within the five-year period studied (April 2010 to May 2015)[5] , the annual collision frequency in the study area was relatively unchanged, although KSI collisions[6] of all types have reduced considerably. A total of 512 collisions were recorded in the study area, resulting in 576 casualties; of these, 118 (23%) collisions involved a pedestrian resulting in 121 casualties[7], which form the main database used in this study. It is also notable that Vulnerable Road Users (VRU's), i.e., motorcyclists, pedal cyclists and pedestrians, account for 62% of all casualties in the town centre. Further, the data also showed that:

- Pedestrians, as a user group, account for the highest proportion of KSI's in the town centre, demonstrating their vulnerability when involved in a collision.
- The proportion of pedestrians involved in collisions is increasing: from 20 in 2010-11 (19% of all collisions) to 25 in 2014/15 (26%) and averaging 24 over a five-year period.
- Pedestrian KSI's are reducing – from 2010-11 to 2014-15 there were 18 collisions with pedestrian KSI as a result (1 fatal and 17 serious casualties). Despite the increase in

Figure 2: Peckham Rye Station (Top) and Junction of Rye Lane and Peckham High Street (Bottom).

At first glance, one may think that pedestrian collisions are most likely to happen on 'unsatisfied-desire lines', where there is a high pedestrian demand in areas of poor design quality. Following the same logic, if design plays a crucial role in safety, one could assume that places with high design standards are overall very safe, regardless of the level of pedestrian activity hosted. Likewise, one should not expect many collisions where pedestrian demand and exposure are very low.

Pedestrian safety strategies seem to accept the implicit assumption that collisions are indeed most likely to occur in 'unsatisfied-desire lines' location types. This study however sheds light on this assumption.

[3] Defined as the rate of pedestrian KSIs per billion kilometres walked.

[4] https://tfl.gov.uk/info-for/boroughs/street-types.

pedestrian injury collisions overall, the number of pedestrian injury collisions whereby a KSI injury occurred has reduced from 7 (2010-11) to 3 (2014-15) and averages 4 in number (similar to the downward KSI trend in the study area overall).

While the focus of the study was pedestrian KSI's, due to their relatively low number and reducing trend overall within the study area, all pedestrian injury collision types were therefore considered in order to establish a greater evidence base.

Even if this initial study does not distinguish factors like day of the week, time of day, gender, age, type of vehicle, it is worth noting that the contributory factors were quite enlightening. Overall, pedestrian behaviour (and not the driver) was seen as the significant factor in pedestrian-vehicle collisions, suggesting that poor pedestrian behaviour, such as failing to properly look, failing to judge the vehicle's path, or walking speed, is the main cause of collisions[8] . Most significantly, 80% of all pedestrian collisions and 60% of KSI pedestrian collisions occur at junctions, of these most occur at give-way / uncontrolled junctions. Furthermore, approximately half of pedestrian collisions are classified as occurring at pedestrian crossings. All of these findings confirm the need to study the on-street pedestrian perception and the spatial/ design performance at the micro-scale.

A pedestrian collision 'hotspot' analysis (collision concentration[9]) has shown that out of the 18 pedestrian KSI collisions[10], the majority are concentrated on (or just off) the A202 Peckham Road/ Peckham High Street /Queen's Road corridor running east/west through the town centre comprising a total of 14 collisions (78%). Otherwise, there is no evidence to suggest that there are distinct pedestrian KSI collision clusters elsewhere. Figure 3 illustrates the location of collisions according to the severity: fatal, serious or slight.

2.3 Traffic and Pedestrian Flow Data

The levels of both vehicle and pedestrian flows at each location were also considered for the analysis.

Pedestrian flow data was collected manually by the authors and Atkins Ltd employees during lunchtime on a weekday in 2015 covering most of the street segments along Peckham Road, High Street, Queen's Road and Rye Lane providing enough information to consider pedestrian movement variability within the study area. Compatible traffic flow data was provided by the London Borough of Southwark.

2.4 Design Variables: PERS Survey

The Pedestrian Environment Review System (PERS) developed by The Transport Research Laboratory (TRL) provides a framework for assessing pedestrian provision in an urban environment. PERS has been applied to footways[11] and crossings, which were assessed on-site using an audit checklist to quantify the quality of the streetscape. The process aims to review the environment from the perspective of different users, including the elderly, people with disabilities, children and those with impaired mobility, in order to consider the inclusivity of the public realm[12]. Following the on-site survey, using the PERS v2 software, on-site scores were collected and weighted based on TRL weighting criteria, converting the assessment into quantifiable performance values[13].

Peckham High Street and Rye Lane formed the focus of the PERS survey. Formal crossings have been examined on these roads and adjacent roads. In total 45 junctions were assessed with more than 100 crossings included as part of the review. Also, 16 segments of footways were assessed. Overall scores have been noted alongside images documenting the full extent of the study area. Figures 4a and 4b illustrate the outputs of the PERS crossings and footways audit.

5 An excel table with the summary of all collision and casualty records between April 2010 to May 2015 (selected STATS19 fields only) and KeyAccident input files detailing all collisions, casualties and vehicle records between April 2010 to May 2015 for the study area.

6 Killed: A human casualty who dies within 30 days after collision due to injuries received in the crash. Serious injury: Injury resulting in a person being detained in hospital as an in-patient, in addition to all injuries causing fractures, concussion, internal injuries, crushing, burns, severe cuts, severe general shock which require medical treatment even if this does not result in a stay in hospital as an in-patient (iRAP International Transport Statistics Database - Safety Definitions).

7 Transport for London (TfL) 'Casualties in Greater London' Fact sheets 2012, 2013, 2014. Collisions might have more than one casualty.

8 Please note that the terminology such as 'poor pedestrian behaviour' or 'failed to look properly' is set by the policy while recording the collision.

9 The concentration of KSI collisions was defined when the physical proximity was less than 50 meters.

10 Fatal or serious cases only.

11 Footways (also referred as links) were divided according to segments of consistent character and, in particular: (A) a significant change in footway width and (B) a change in adjacent land use. These two factors have been selected as they were considered to be the most influential aspects of the street environment, impacting how pedestrians move through and across the street.

12 The assessment process for crossings looked at the following parameters: crossing provision, deviation from desire line, performance, capacity, delay, legibility, legibility for sensory impaired people, gradient, obstructions, surface quality and maintenance. The assessment process for footways looked at the following parameters: effective width, dropped kerbs, gradient, obstructions, permeability, legibility, lighting, tactile information, colour contrast, personal security, surface quality, user conflict, quality of environment and maintenance.

13 For both segments and crossings, the percentage scores attainable range from -100% to 100%, as follows: A) high quality (represented by green dots or lines): no immediate changes requires / only minor maintenance issues ranging from 34% to 100%; B) moderate quality (represented by orange dots or lines): generally operating satisfactory but could be improved ranging from -33% to 33% and C) low quality (represented by red dots or lines): critical issues identified requiring immediate attention ranging from -100% to -34%.

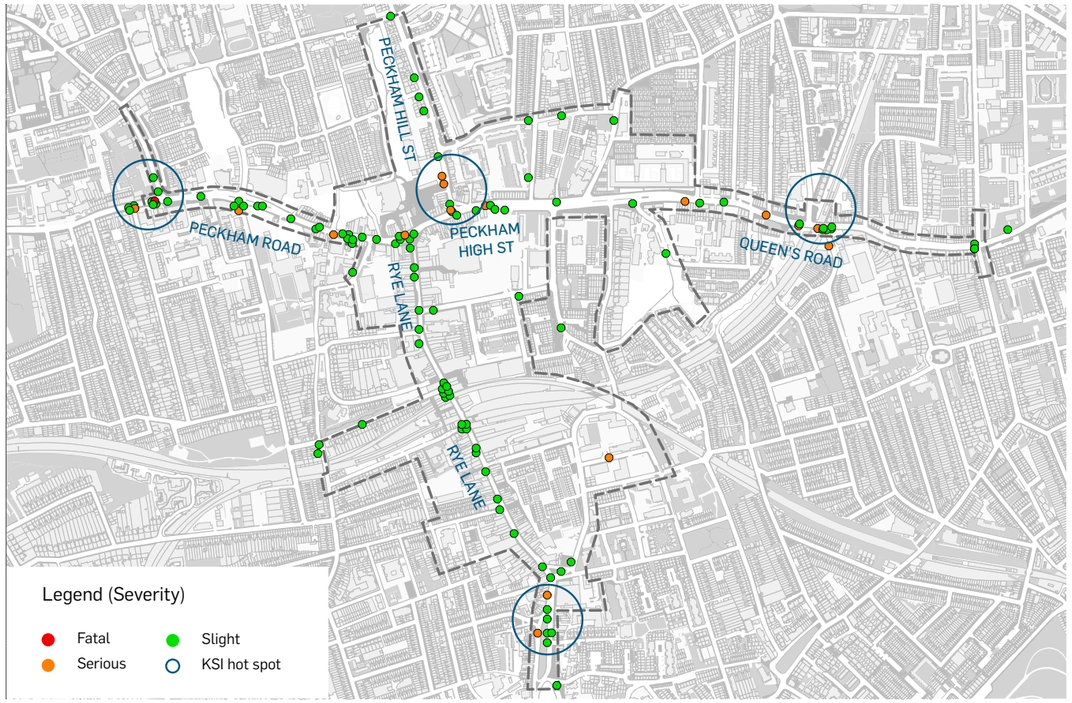

Figure 3: Location of Collisions Within the Study Area According to the Severity of Collisions. Study Area Represented by the Grey Dotted Line.

The results of the PERS assessment displayed a number of issues, such as several uncontrolled crossings on the side road of major intersections, e.g. Clayton Road and Lyndhurst Way. On Rye Lane, there are fewer controlled crossings and pedestrians generally walk informally across the road. The study also noted that materials used along the length of Peckham High Street and Rye Lane are of low quality. Moreover, for a given location, the quality of crossings and footways was not always consistent. Within the study area, one could find good quality crossings adjacent to poor quality footways and vice-versa, as well as locations with both crossings and footways with good or poor perceived quality. In short, all combinations exist, which makes this an ideal study area for this research.

2.5 Urban Form Variables: Visibility Graph Analysis

Visibility Graph Analysis is based on how much space pedestrians can see as they move around. In dense urban areas, where there are many possible origins and destinations and a complexity of routes for pedestrians, pedestrians tend to choose the simplest path. This means that movement flows tend to concentrate on those streets that offer the simplest visual links through the street grid. Visibility (the area of usable space visible to a pedestrian at any point in the street grid) is, therefore, one of the most important factors determining movement. Pedestrian movement flows tend to be greater on routes that provide clear and direct visual links through the built environment than on complex routes where people cannot find a clear line of travel.

It is possible to quantify this ease of natural wayfinding within a computer model, using a methodology known as 'Visibility Graph Analysis (VGA)'. The software calculates the visual field available to pedestrians at every step of any possible journey within the network. This creates an overall measure of visibility of pedestrian space for any urban area, which can be displayed using a spectral colour range, where red indicates the highest levels of visibility through to blue, representing the lowest levels of visibility. Because of the common correlation between visibility and pedestrian flows, VGA can be used as a representation for pedestrian flow levels and pedestrian demand.

In this study, VGA was carried out using the Fathom software developed by Atkins Ltd. Fathom calculates the visual field for a pedestrian standing at any point in the public space network. Taking accurate scale maps of an area as an input, a computer algorithm creates a 3x3 metre grid of sample observation points throughout the pedestrian movement space. The software then calculates the visual field and the number of points of interest at 360 degrees

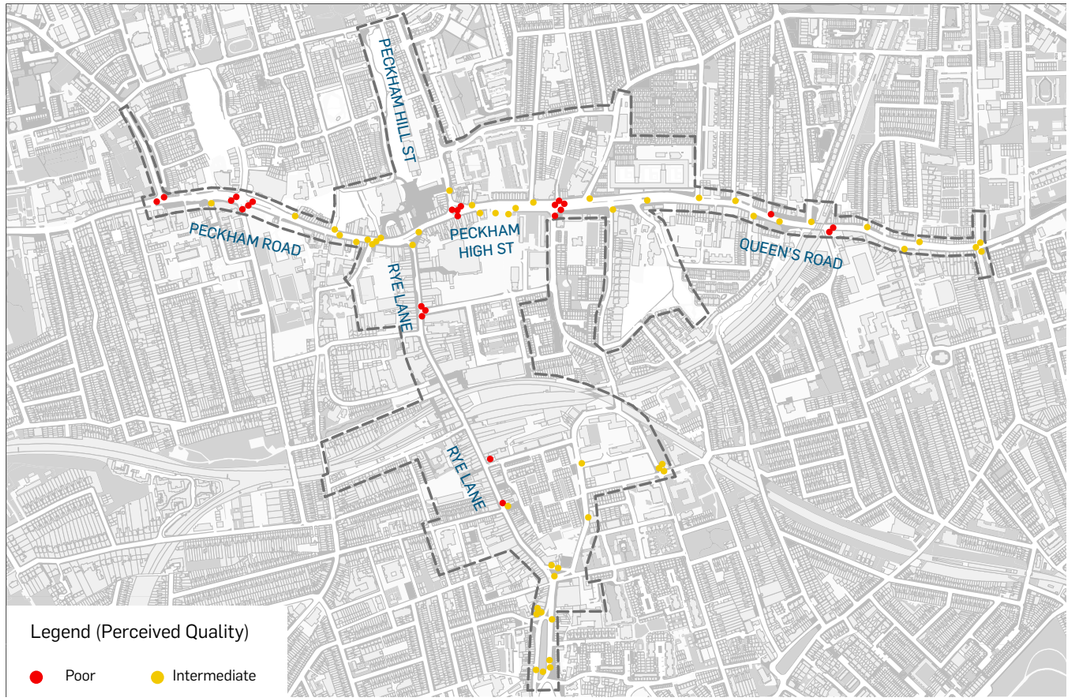

Figure 4a: PERS Crossing According to Perceived Quality. Study Area Represented by the Grey Dotted Line.

Figure 4b: PERS Footways According to Perceived Quality. Study Area Represented by the Grey Dotted Line

from each point in the grid by checking all directly visible points. The VGA outputs produced with Fathom were the following variables:

a) street network visibility (visible area at 50 and 500 metre distance);

b) spatial accessibility (visible area at 50 and 500 meters, directly or within one change of direction);

c) building entrances in view or natural surveillance[14];

d) retail and food/drink units in view;

e) access to bus stops; and

f) access to railway/overground stations.

The first two variables are expressed in square metres. The next two variables are the number of units in view and are calculated twice: directly in view only or within one change of direction. Finally, the last two variables start from 1 (direct visual connection) and sum up 1 unit for every necessary change of direction.

As discussed, the pedestrian desire lines, i.e., the routes of choice by pedestrians, can be identified based on the location of the most visible areas (represented by the red Or orange tiles) in the VGA processed maps. To that end, Fathom results highlighted important desire lines of pedestrian movement such as the diagonal route linking Rye Lane and Peckham Library across Peckham High Street (Black arrow in Figure 5a). Further, within the context of the study area, there is a clear retail centrality formed by Rye Lane and the central stretch of Peckham High Street, in sharp contrast with most back streets often lacking active frontages (Figure 5b). Finally, despite their role as key pedestrian drivers, neither of the two train stations are located at the most visible/accessible locations, an element that we have further explored regarding the location of collisions (Black dots in Figure 5c).

2.6 Linking and Comparing Collisions With Space and Design Data

Using Geographical Information Systems (MapInfo Pro 15.2 software), the collision data was plotted against all spatial information. A 25-metre buffer area around each collision location was drawn and intersected with all other data to capture their properties. In case of intersection with more than one element, the aggregation method was the average weighted by length or area.

A limitation of the study is that PERS results were not available for all collision locations. Also, some of the collisions did not happen near any crossing, so no crossing quality value could be associated. In contrast, urban form results were available for the whole study area[15].

Scatter plots have been used to display each pair of variables for total collisions. This type of diagram enables a combined comprehension of the two factors and their correlation. In this case, we compare urban form and land use variables with design quality values. This allows a quick visual understanding of the role of each variable.

We have produced a scatter plot for each pair of variables (Figures 7 and 8): one from the PERS design audit (x-axis) and one from the urban form analysis (y-axis). The minimum and maximum values in the study area are located at the ends of the axes, whereas both axes intersect at the study area average values (as in Figure 1). This chart allows a simple inspection of the distribution of collision locations according to those two variables and the four types of spaces in the study area.

[14] Not only is the location and visibility of building entrances an important factor in the concentration of pedestrian activity, but also an important aspect of the on-street safety perception. Building entrances provide a degree of natural surveillance of public spaces from building users themselves. Although windows also provide natural surveillance, building entrances offer the potential for a neighbour to intervene if a criminal act is being undertaken. The natural surveillance of an area is measured by the number of building entrances in view from every point within pedestrian areas.

[15] Regarding the missing data, for the urban form – design quality comparison, 39% of collision locations had no value for crossings, whereas 28% of them had no footway value. Instead of omitting these collision events, those were kept so that the urban form information would be displayed. Regarding representation in the scatter plots, they have been plotted on top of the axis as if they had average values.

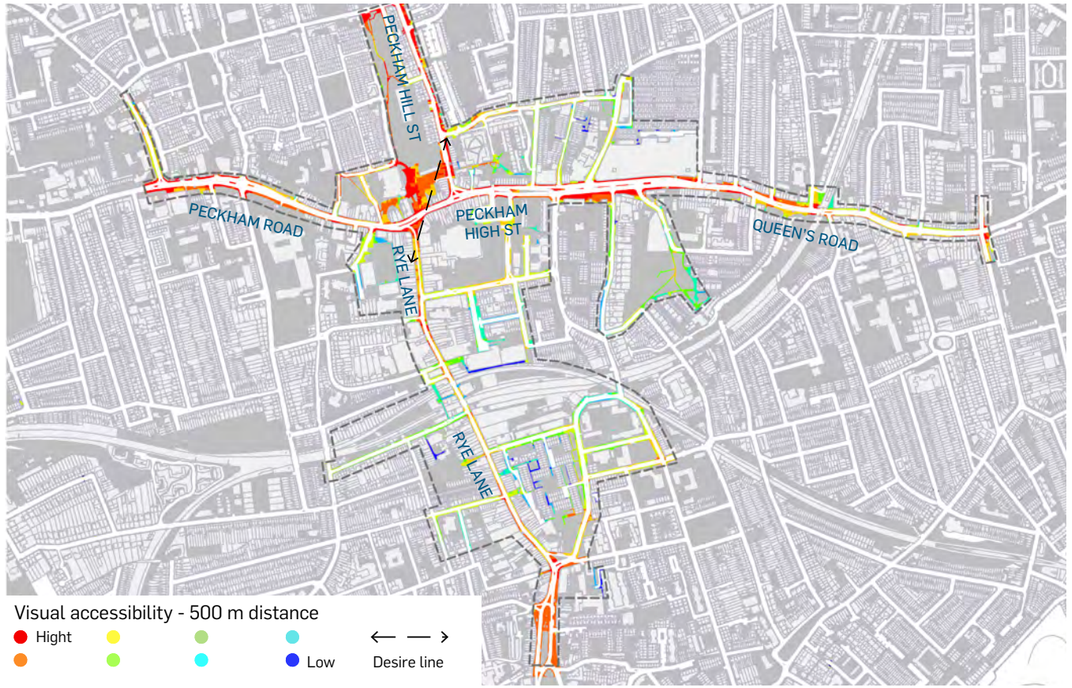

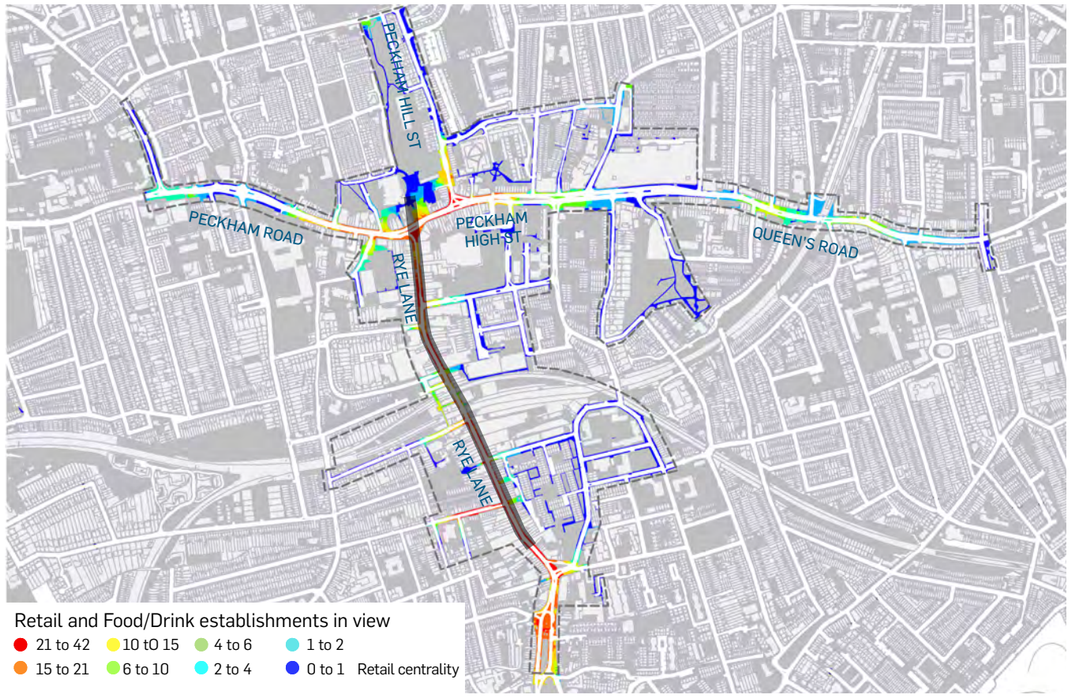

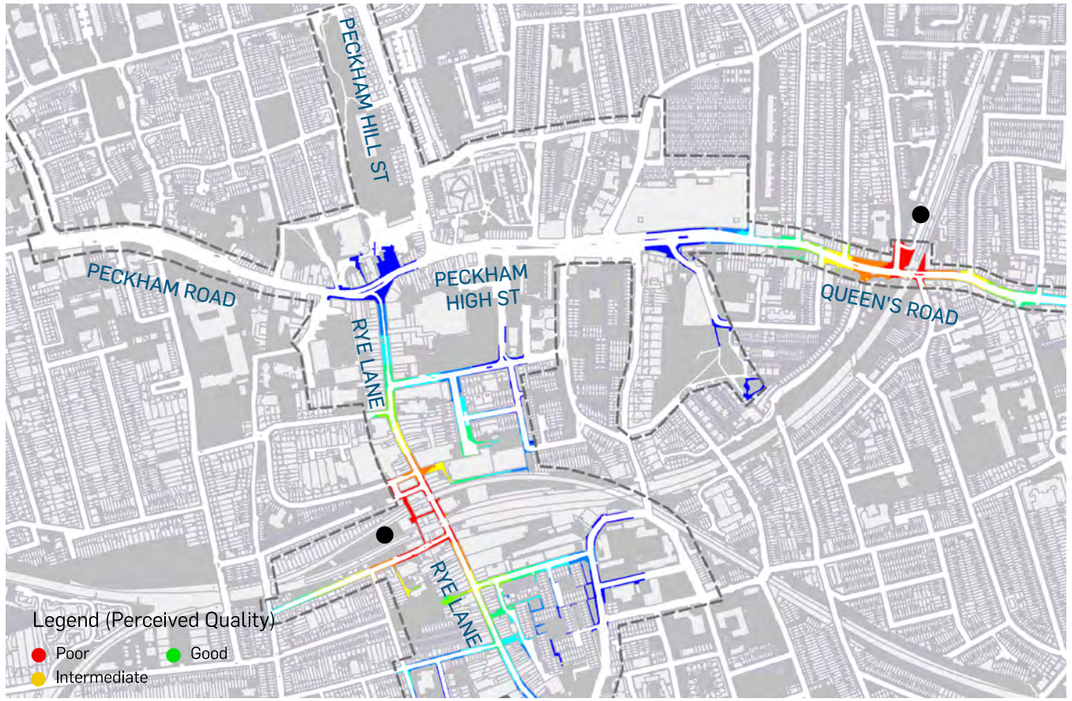

Figure 5: Three Examples of VGA Outputs. From Top to Bottom: A) Visual Accessibility (500m Distance), B) Access to Retail and Food/Drink Units (Direct) and C) Access to Stations. The Results Are Presented Using a Spectral Colour Scale From Red (Areas With the Highest Accessibility Levels or Number of Retail Establishments in View) to Blue (Areas With the Lowest Accessibility Levels or Number of Retail Establishments).

Finally, after describing the location of individual collisions, these were aggregated per street segments to allow the comparison with pedestrian and traffic flows. Two ratios were calculated: number of collisions per segment length (km) and per vehicle flow (daily number of vehicles) and number of collisions per segment length and per pedestrian flow (pedestrians per hour, total for both footways and direction of flow).

These two ratios were compared with all urban form and design variables using Pearson's correlations, in order to measure the degree of association between the collision ratios and the urban environment variables.

3. Results

Firstly, the comparison of urban form and land use (pedestrian demand) versus design quality has been shown in the scatter plots. As mentioned earlier this enables a quick understanding of the distribution of collisions. Following the discussion on the four typologies of urban form characterised as pedestrian demand versus design quality, the number of collisions for each type has been calculated[16] (Figure 6). It is evident that most collision points fall within the first two typologies: successful pedestrian spaces and unsatisfied-desire lines where there is high pedestrian demand, with a clearly lower importance of the design quality.

This is also further highlighted when reviewing the scatter plots (which follow the Space-Type Diagram typologies quadrants) and the consistent collision distribution pattern that is observed: whereas one can hardly see collisions plotted below the x-axis, they are common on either side of the Y-axis (Figures 7 and 8).

This means that all the urban form/land use variables showed a strong association with collision locations, with most collisions occurring in locations with a higher pedestrian demand potential than the average in the area. On the other hand, the design quality variables were not clearly associated with the distribution of collisions. Collisions took place in all sorts of locations along the design quality spectrum.

In sum, pedestrian collisions do not only occur on 'unsatisfied-desire lines' but also in the better designed 'successful pedestrian spaces'.

[16] Note that the collision points without PERS data have been counted twice within Q_1-Q_2 or Q_3-Q_4, depending on their urban form value, which explains why the sum of all percentages in Figure 9 exceeds 100%.

	Q1: Successful Pedestrian Spaces	Q2: Unsatisfied-desire lines	Q3: Back forgetten spaces	Q4: Red-carpeted deserts
CROSSINGS				
VIS_50M_AVG	45.8%	48.3%	20.3%	24.6%
VIS_500M_AVG	60.2%	57.6%	11.0%	10.2%
ACC_50M_AVG	56.8%	59.3%	9.3%	13.6%
ACC_500M_AVG	65.3%	63.6%	5.1%	5.1%
BIEV_1_AVG	63.6%	62.7%	5.9%	6.8%
BIEV_2_AVG	68.6%	66.9%	1.7%	1.7%
RIV_1_AVG	47.5%	44.1%	24.6%	22.9%
RIV_2_AVG	48.3%	44.1%	24.6%	22.0%
BUSSTOP_MINSTEP_AVG	66.1%	64.4%	4.2%	4.2%
STATION _MINSTEP_AVG	63.6%	57.6%	11.0%	6.8%
FOOTWAYS				
VIS_50M_AVG	49.2%	39.0%	28.8%	11.0%
VIS_500M_AVG	50.0%	56.8%	11.0%	10.2%
ACC_50M_AVG	53.4%	54.2%	13.6%	6.8%
ACC_500M_AVG	55.1%	62.7%	5.1%	5.1%
BIEV_1_AVG	53.4%	65.3%	2.5%	6.8%
BIEV_2_AVG	58.5%	67.8%	0.0%	1.7%
RIV_1_AVG	33.1%	53.4%	14.4%	27.1%
RIV_2_AVG	33.1%	54.2%	13.6%	27.1%
BUSSTOP_MINSTEP_AVG	55.9%	63.6%	4.2%	4.2%
STATION _MINSTEP_AVG	48.3%	65.3%	2.5%	11.9%

Figure 6: Percentage of Collisions According to VGA Measures and Space Type[17].

[17] Abbreviations stand for: VIS = street network visibility, ACC = spatial accessibility, BEIV = building entrances in view, RIV = access to retail and food / drinks units, BUSSTOP = access to bus stops, STATION = access to railway and/or over ground stations. 1=direct visibility, 2=direct visibility or within 1 turn, AVG = average value at location.

Figure 7: Scatter Plots: PERS Crossing (X) Versus Urban Form and Land Use Variables (Y).

Figure 8: Scatter Plots: PERS Footways (X) Versus Urban Form and Land Use Variables (Y).

To allow comparison between variables, another way to look at the results is the variation of the average value. What is the collision location average in comparison with the whole study area average? We have analysed the deviation for each variable range in the study area (Figure 9), using the formula below:

$$\text{Average value variation (as \%)} = \frac{\text{Average}_{COLLISIONS} - \text{Average}_{STUDY\ AREA}}{\text{Max}_{STUDY\ AREA} - \text{Min}_{STUDY\ AREA}}$$

Regarding the morphological variables[18], the results show that the more strategic configurational variables are (accessibility over visibility; 500m over 50m distance), the higher the variation (+18.63% for accessibility at 500m). The location of building entrances, retail units, bus stops and transport stations are all even more significant than the morphological variables, in that order of importance (+27.19%, +24.5%, +21.54% and +19.79% respectively). This is consistent with the literature in relation to pedestrian volumes, as described in the introduction.

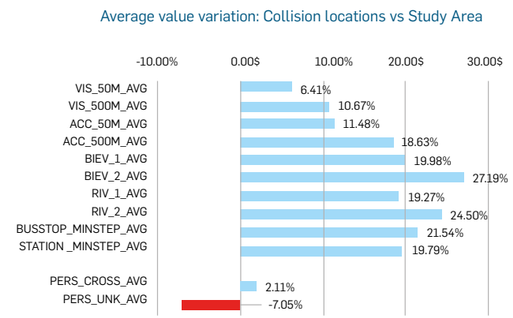

Figure 9: Average Value Variation: Collision Locations Vs Study Area

[18] They morphological variables are: street network visibility (visible area at 50 and 500 metre distance), spatial accessibility (visible area at 50 and 500 meters, directly or within one change of direction), building entrances in view or natural surveillance, retail and food/drinks units in view, access to bus stops and access to railway/over ground stations. Refer to Section 2.4.

The average value variation for the design variables is weaker. The quality of footways around collision locations is generally lower (-7.05%) than in the overall study area. Surprisingly, the quality of footways is slightly better (+2.11%) around the collision locations. This might be due to recent refurbishments at some of the busiest street segments, such as the northern end of Rye Lane.

Lastly, regarding the two collision-flow ratios and the correlation with the urban form and design variables (Figure 10), the results were not as consistent. Firstly, 14 out of the 24 correlations were not considered significant even at the 0.05 level (two-tailed). This could be expected given the low sample size (29 street segments)[19]. Further, quite relevant to note is that none of the correlations with design variables were significant (consistent with previous results), as welll as 'combined variables' such as pedestrian flows / vehicular flows ratio and pedestrian flows x vehicular flows. Looking at the significant results, we have (Figure 10):

a) For the similar levels of vehicular flows[20], the collisions per vehicle ratio shows that collisions are more likely to take place at locations with a higher number of building entrances (R=+0.39), retail units (R=+0.43) or close to a public transport station (R=-0.38) . This would be consistent with our previous hypothesis and results: all these variables are a proxy for higher pedestrian flows and subsequenlty the higher the likelyhood of a collision.

b) However, assessing separately the correaltion between number of collisions and similar levels of pedestrian movement, it seems that collisions are less likely to take place at locations with higher number of building entrances (R=-0.39), retail units (R=-0.45) or close to a station (R=0.47). This might seem contradictory to the previous results except that, in this case, the variability of these factors is not working as a proxy of pedestrian flows, given that the ratio is a relative measure per pedestrian. This points to the interrelationship of these variables and traffic flow: in locations with a concentration of retail units, freight traffic and / or operations often have traffic-calming and speed reduction measures and bespoke schemes to safetyguard pedestrians with a positive impact on pedestrian safety. This is the case of the north section of Rye Lane, where only buses are allowed, so overall traffic flow is very low and the collision probability is lower despite the high retail concentration.

It is suggested that this might be related to the traffic-calming and speed reduction measures inplemented in these areas, which considerably reduce the likelyhood of collisons and the severity of injuries.

						POSSIBLE INTERPRETATIONS
A	**SIMILAR TRAFFIC** (as ratio per traffic)	**MORE** BEIV, RIV, etc.	=	**MORE** COLLISIONS	→	Pedestrian flow can vary with BEIV, RIV, etc.] **Same** traffic + **More** pedestrians = **More** collisions.
B	**SIMILAR PEDESTRIAN FLOW** (as ratio per pedestrian)	**MORE** BEIV, RIV, etc.	=	**LESS** COLLISIONS	→	*Pedestrian flow variation is not reflected, even if BEIV/RIV/etc. rises.* Collisions may decrease because of: - Formal or informal traffic calming due to retail concentration, freight, etc. - Traffic constraints. **Same** pedestrians + **Less/slower** traffic = **Less** collisions.

[19] Further research with a larger data set (possibly including several areas in London and / or other urban areas) is needed to achieve more significant conclusions.

[20] As a stand anole variable, i.e., and disregarding vehicular flows.

Correlations

		Collisions per km / Traffic flow	Collisions per km / Ped flow
VIS-50M	Pearson Correlation	-.042	.024
	Sig (2-tailed)	.020	.900
VIS-500M	Pearson Correlation	-.294	.389*
	Sig (2-tailed)	.121	.037
ACC-50M	Pearson Correlation	.002	-.016
	Sig (2-tailed)	.993	.932
ACC-500M	Pearson Correlation	**-.402***	.165
	Sig (2-tailed)	.031	.393
BIEV-1	Pearson Correlation	.317	**-.372***
	Sig (2-tailed)	.094	.047
BIEV-2	Pearson Correlation	**.386***	**-.394***
	Sig (2-tailed)	.039	.035
RIV-1	Pearson Correlation	.365	**-.430***
	Sig (2-tailed)	.052	.020
RIV-2	Pearson Correlation	**.430***	**-.454***
	Sig (2-tailed)	.020	.013
BUSSTOP-MINSTEP	Pearson Correlation	-.248	-.074
	Sig (2-tailed)	.195	.704
STATION-MINSTEP	Pearson Correlation	**-.376***	**.466***
	Sig (2-tailed)	.044	.011
PERS-CROSSINGS	Pearson Correlation	.304	-.243
	Sig (2-tailed)	.123	.222
PERS-FOOTWAYS	Pearson Correlation	.023	.191
	Sig (2-tailed)	.907	.320

*. Correlation is significant at the 0.05 lvel (2- tailed)

4. Conclusions

Our analysis shows that there is a strong association between the location of collisions and urban form and its configurational measures, including the number of building entrances, retail and food/drink units in view and the location or transport nodes (bus stops and rail). This finding is consistent with previous research highlighting the key drivers for pedestrian movement that correlate with pedestrian flows and exposure to traffic. In sum, collisions are more likely to happen where people go.

However, the fact that design quality variables seemed to play no significant role in the location of collisions is surprising, especially if we consider that most pedestrian safety guidelines are very design-focused.

It could be argued that the PERS method might not adequately reflect the design characteristics affecting safety. In fact, previous literature has focused on the type of crossings, traffic lights and other elements, rather than the on-street perceived quality of design.

However, this study shows that 'unsatisfied desire lines' are not the only types of spaces in which collisions take place. Locations with the highest design quality also host collision events and are not necessarily safer. Consequently, pedestrian safety strategies based on design only may not have the expected level of impact and success.

Our research suggests that an analysis of urban form and land use is key to identify the pedestrian 'desire lines' and exposure to collisions. The holistic understanding of the spatial hierarchies of pedestrian movement in a given environment can guide other initiatives, such as the strategic location of design investment, traffic-calming areas or behavioural change programmes. It would also identify the areas where the highest traffic flow lines of travel are a threat and should be deviated.

Further research with a larger data set (possibly including several areas in London and / or other urban areas) is needed to bolster the initial findings of this research.

References

Atkins (2015), Peckham pedestrian town centre programme: Action Plan. London: Atkins Ltd.

Department of Transport (2011), Fatigue and road safety: A critical analysis of recent evidence. Road Safety Web Publication No 21. London: Department of Transport.

Desyllas, J. and Duxbury, E. (2001), 'Axial maps and visibility graph analysis'. In J. Peponis, J. Wineman & S. Bafna (Eds.), Proceedings of the Third International Space Syntax Symposium. Atlanta, U.S.A: Georgia Institute of Technology.

Desyllas, J., Duxbury, E., Ward, J. and Smith, A. (2003), Pedestrian demand modelling of large cities: an applied example from London, London: Centre for Advanced Spatial Analysis Working Paper Series – Paper 62.

Gehl, J. (1987), Life between buildings: Using public space, New York: Van Nostrand Reinhold.

Graham, D. J. and Glaister, S. (2003), 'Spatial variation in road pedestrian casualties: The role of urban scale, density and land-use mix'. In Urban Studies, Vol. 40(8), p. 1591-1607.

Grundy, C., Steinbach, R., Edwards, P., Wilkinson, P. and Green J. (2008), 20 MPH zones and road safety in London: A report to the London Road Safety Unit, London: LSHTM.

Hart, J. (2015), Towns and Cities: Function in Form, Farnham: Ashgate Publishing Ltd.

Hillier, B. (2007), Space is the machine: a configurational theory of architecture. London: Space Syntax.

Hillier, B. and Hanson, J. (1989), The social logic of space. Cambridge: Cambridge University Press.

Hillier, B. and Iida, S. (2005), 'Network effects and psychological effects: a theory of urban movement'. In: van Nes, A. (ed.), Proceedings of the Fifth International Space Syntax Symposium, Delft: University of Technology, Vol. 1, p. 553-564.

Hillier, B., Penn, A., Hanson, J., Grajewski, T. and Xu, J. (1993), 'Natural movement: or, configuration and attraction in urban pedestrian movement'. In Environment and Planning B: Planning and Design, Vol. 20(1), p. 29-66.

Hillier, B., Turner, A., Yang, T. and Park, H. T. (2010), 'Metric and topo-geometric properties of urban street networks: some convergences, divergences and new results'. In Journal of Space Syntax, Vol. 1(2), p. 258-279.

Hillier, B., Yang T. and Turner, A. (2012), 'Normalising least angle choice in Depthmap and how it opens up new perspectives on the global and local analysis of city space'.

In: Journal of Space Syntax, Vol. 3(2), p. 155-193.

LaScala, E. A., Gerber, D. and Gruenewald, P. J. (2000), 'Demographic and environmental correlates of pedestrian injury collisions: a spatial analysis'. In: Accident Analysis & Prevention, Vol. 32(5), p. 651-658.

Lassarre, S., Papadimitriou, E., Yannis, G. and Golias, J. (2007), 'Measuring accident risk exposure for pedestrians in different micro-environments'. In: Accident Analysis & Prevention, Vol. 39(6), p. 1226-1238.

Maxwell, A., Kennedy, J., Routledge, I., Knight, P. and Wood, K. (2011), Puffin pedestrian crossing study. Wokingham: TRL.

Moudon, A., Lin, L., Hurvitz, P. and Reeves, P. (2008), 'Risk of pedestrian collision occurrence: case control study of collision locations on state routes in King County and Seattle, Washington'. In: Transportation Research Record: Journal of the Transportation Research Board, Vol. 2073, p. 25-38

Ozbil, A., Peponis, J. and Stone, B. (2011), 'Understanding the link between street connectivity, land use and pedestrian flows'. In: Urban Design International, Vol. 16(2), p. 125-141.

Shawky, M. A., Garib, A. M. and Al-Harthei, H. (2014), 'The impact of road and site characteristics on the crash-injury severity of pedestrian crashes'. In: Advances in transportation studies, Vol. 1 (Special issue), p. 27-36.

The Royal Society for the Prevention of Accidents. (2012). Road safety engineering: Cost effective local safety schemes, Birmingham: ROSPA. Available from: http://www.rospa.com/rospaweb/docs/advice-services/road-safety/roads/road-safety-engineering-0912.pdf (Accessed: 31/01/2016).

Transport for London (2010), Pedestrian Comfort Guidance for London: Transport for London.

Transport for London (2013), Safe Streets for London The Road Safety Action Plan for London 2020. London: TfL. Available from: http://content.tfl.gov.uk/safe-streets-for-london.pdf (Accessed 17/01/2016).

Transport for London (2016), Casualties in Greater London during 2015. London: TfL. Available from: http://content.tfl.gov.uk/casualties-in-greater-london-2015.pdf (Accessed 17/01/2016)

Turner, A. (2003). 'Analysing the visual dynamics of spatial morphology'. In Environment and Planning B: Planning and Design, Vol. 30(5), p. 657-676.

Turner, A., Doxa, M., O'Sullivan, D. and Penn, A. (2001), 'From isovists to visibility graphs: a methodology for the analysis of architectural space'. In Environment and Planning B: Planning and Design, Vol. 28(1), p. 103-121.

Zegeer, C. V. and Bushell, M. (2012), 'Pedestrian crash trends and potential countermeasures from around the world'. In Accident Analysis & Prevention, Vol. 44(1), p. 3-11.

Acknowledgements

Originally presented and published as: Arruda Campos, M. B. and Carpio-Pinedo, J. (2017), 'Unsatisfied-Desire Lines: A Spatial Approach To Pedestrian Collision Analysis'. Proceedings of the 11th Space Syntax Symposium, London: University of Lisbon, p.54.

Safety | 012

Preventing Human Error in Crane Operations: a Case Study of Organizational and Design Elements

Jiun-Yin (Irene) Jian

Senior Human Factors Consultant
Oil & Gas
Houston, TX, USA

Gerry E. Miller

Self-employed Maritime Ergonomist

Sahil Shah

Graduate Student
Massachusetts Institute of Technology
Cambridge, MA, USA

Abstract

Between 2009 and 2016, 57 offshore crane-related incidents in the process industry resulted in numerous injuries and fatalities in the Gulf of Mexico region (Bureau of Safety and Environmental Enforcement, 2017) with estimated cost over 3.5 million US dollars. For this reason, crane incidents continue to be a major focus and of oil and gas industry concern. Despite the large progress made with crane technology and regulation (American Petroleum Institute, 2013, 2014), operators and workers remain exposed to risks due to inadequate consideration of human factors in design. This desk-based evaluation was conducted to address the human factors related to crane operations with a detailed focus on cabin display and control arrangements, identification of blind spots, safe lifting practices, and compliance with regulatory requirements. It was found that the one configuration of the two-lever controls recommended by API 2C was conducive to causing human error, and that a rearrangement of the labeling and color-coding could increase readability and legibility to the operator. A modification to this arrangement is recommended in order to further prevent exposures to crane hazards stemming from human error. In addition, the operator's field of view (FOV) or line of sight (LOS) was simulated using schematics, 3D models, and anthropometric data in order to identify blind spots during lifting and lowering activities. This strategy can be implemented in the preparation of lift plans which will subsequently facilitate adequate communication between the operator and flagman during blind lifts.

Keywords

Human Error; Human Factors in Design; Crane Operations

1. Introduction

Crane incidents in the process industry can be fatal along with damage to equipment as well as the facility, and impact on environment. Between 2009 and 2016, 57 offshore crane-related (excluding drilling) incidents resulted in a total of 47 injuries in the Gulf of Mexico region (Bureau of Safety and Environmental Enforcement, 2017). Of the 57 incidents, 48 were classified to be related to "human error" based on BSEE's classification. The total cost of those incidents is estimated more than 3.5 million US dollars (reported). In 2011, of the three fatalities, two were due to crane operations (Bureau of Safety and Environmental Enforcement, 2015). Over the period 2008 to 2015, crane associated incidents, among all incidents excluding fatalities within the Outer Continental Shelf (OCS), as reported to Bureau of Safety and Environmental Enforcement (BSEE), were approximately 20.2% (1103 of 5466 incidents) (BSEE, 2015). The primary focus of causes has been on crane operator and rigger errors as well as the influences on the loss of load control (i.e., inability to control the movement of a load) and the loss of load (uncontrolled or accidental dropping of a load) (Moore & Bea, 1992). However, other aspects, such as Human-Machine Interface (HMI) on controls and displays, cabin habitability, and maintenance accessibility should also be taken into account (American Bureau of Shipping, 2014; UK Health and Safety Executive, 2001). Possible causes that may lead to crane incidents or fatalities particularly defined for this case study are shown in Figure 1. They are as follows:

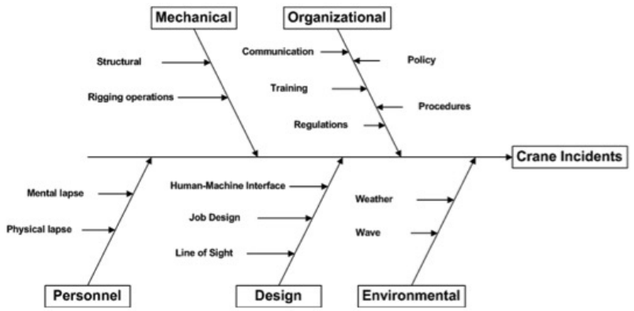

Figure 1:High Level Cause-and-Effect of Crane Incidents

1. Mechanical
   - > Pedestal or boom structural failure
   - > Rigging strap/chains or shackles failure at lifting points
2. Organizational
   - > Poor or mis-communication
   - > Lack of knowledge or training
   - > Violation of policies
   - > Violation of procedures
   - > Violation of regulatory requirements
3. Personnel
   - > Mental/Cognitive slips/lapses, mistakes, and violations
   - > Lapse/Re-adoption of physical activity
4. Design
   - > Inappropriate design or arrangements of controls and displays
   - > Inappropriate job design
   - > Limited or restricted Line of Sight (LOS)
5. Environmental
   - > Inclement weather
   - > Extreme or rogue wave

Among the five categories illustrated in Figure 1, this article will not center on the personnel element, (i.e., mental and physical lapses), mechanical failure, nor the environmental factors. This article intends to provide a case study that was conducted to address the human factors concern related to pedestal crane operations, in particular, the HMI controls and displays arrangement, maintenance access, safe lifting practices, and compliance with regulatory requirements.

2. Overview of an Offshore Pedestal Crane

Pedestal cranes are commonly used in the process industry, especially in an offshore environment to transfer personnel, equipment, and supplies between supply vessels and the facility. In order to operate a crane safely, it is important to understand the functionality of all the major components of a typical pedestal crane. Typical components of a pedestal crane, as illustrated in the Specification 2C by American Petroleum Institute (API) (API, 2013) are shown in Figure 2. Depending on the load capacity of the crane, anticipated operations, and Safe Working Load (SWL) (or load capacity), a lift, e.g., heavy versus light lift, would be planned and carefully executed.

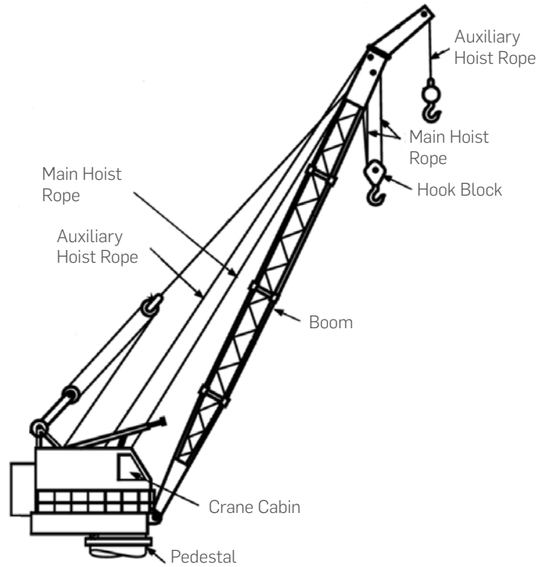

Figure 2: Typical Crane Components

The main six motions of a crane are as follows and illustrated in Figure 3:

1. Luff (Jib) up – To decrease the boom working radius;
2. Luff (Jib) down – To increase the boom working radius;
3. Hoist raise – To lift a load;
4. Hoist lower – To lower a load;
5. Slew left – To rotate the boom to the left; and
6. Slew right – To rotate the boom to the right.

These six motions are controlled by the operator from the crane cabin using a pair of joysticks. The operator is able to see through the cabin windows or utilizing CCTV (Closed-Circuit Television) whether the desired motion is carried out.

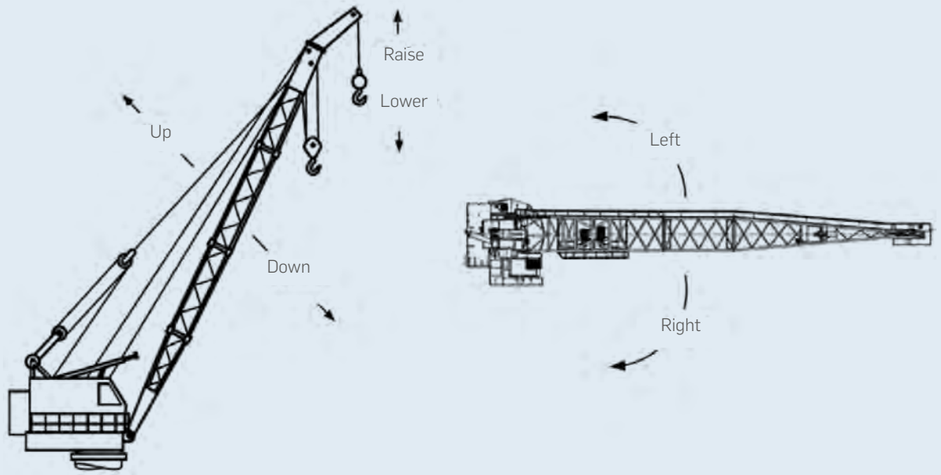

Figure 3: Six Main Crane Motions

3. Case Study

3.1 Objective

A case study was conducted which strives to explore risks that could potentially contribute to human error during crane operations, for instance, limited Field of View (FOV) from the crane cabin, poor arrangement of controls and displays, and restricted maintenance access.

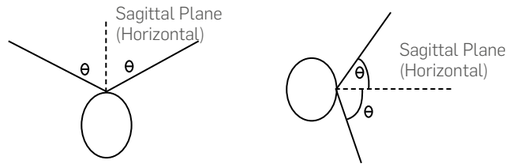

Figure 4: Field of View – Sagittal and Transverse Planes

3.2 Definitions and Assumptions

Field of View. Field of View is defined as the area that is visible by an operator for viewing only through eye and head movement (U.S. Department of Defense, 2012). FOV of a crane operator, i.e., visibility, may be restricted by the physical hardware of the crane cabin (e.g., window frames, display panels, communication equipment). It is assumed that view angle at each side of the sagittal (horizontal) plane is 60 degrees; at each side of the transverse (vertical) plane is 50 degrees (U.S. Department of Defense, 2012).

Controls and Displays. Selections, grouping, and arrangements of controls and displays should be established to allow effective human machine interfaces and to preclude system characteristics that will require extensive physical and sensory skills (e.g., a switch located out of normal work envelope; pressure gauge display face not color-coded) leading to the increase of both cognitive and physical workload (U.S. Department of Defense, 2012). Capabilities of users, task performance, and skill requirements shall be taken into consideration.

Assumptions. In order to limit the scope of the case study and the modelling purposes, the following assumptions were made:

1. Chair height in the crane cabin is assumed to be approximately 18 in (457 mm) off the floor level and not adjustable.

2. Operators do not use dynamic upper body posture for a better view to the load.

3. Sitting height and eye position of a crane operator who is medically fit are between the 5th percentile female and 95th percentile male North American working population

4. During crane operations, loads can be viewed by a crane operator at a seated position, without standing required, through only the front window.

5. Maximum main hoist outreach (reach distance) is 115 ft (35 m).

6. Crane boom does not move up or down; thus, the crane boom motions are limited to slewing left or right.

4. Findings

Identifiable human factors risks were reviewed using schematics and a 3D model. Study findings, including observation and recommendations, were then grouped and are described in the following four sections: Visibility, Controls and Displays, Communication and Procedures, and Ease for Maintenance.

4.1 Visibility

According to the guidance requirement (API, 2013), the visibility from a crane cabin "shall include a vertical range adequate to cover the boom point and load at all time." The following were observed, simulated, and/or recommended for this case study:

1. Wipers for the main forward window(s) shall be able to clear at least 90% of the glass area.

2. Slings, hoists, lines, etc. may be painted to provide visual contrast against surroundings and to allow crane operators for better differentiation and quick identification.

3. FOV was simulated for the 5th percentile female and 95th percentile male North American crane operators as shown in Figure 5 and Figure 6. The red shaded area indicates FOV being blocked by the crane cabin. Between the two, the view of the 5th percentile female is wider and more elongated. It is also found that the laydown area directly underneath the crane is mostly visually obstructed (Figure 7). Due to the potential for poor depth perception and occurrence of blind lifts, it is evident that during operations the crane operator would have to heavily rely on the video display on CCTV and radio communication with rigger.

4. The operator's chair needs to be adjustable.

5. Standard signals, including hand, voice, or audible, should be incorporated per United States Code of Federal Regulations (CFR) 29 CFR Part 1926 or API 2D (API, 2014).

6. Crane operator should have a clear view of the hook and load throughout the crane's full slewing circle.

7. Markers, where feasible and visible to crane operators, may be added at the proximity of a crane on structures such that the vertical travel distance of a load can be easily identified.

8. Rigger should be in full view of and always in direct radio communication with the crane operators.

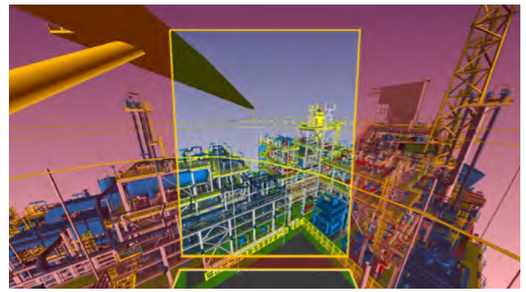

Figure 5: FOV of 5th Percentile North American Female

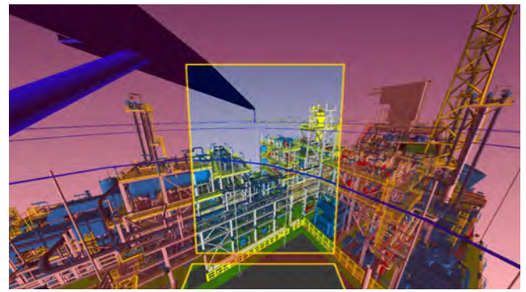

Figure 6: FOV of 95th Percentile North American Male

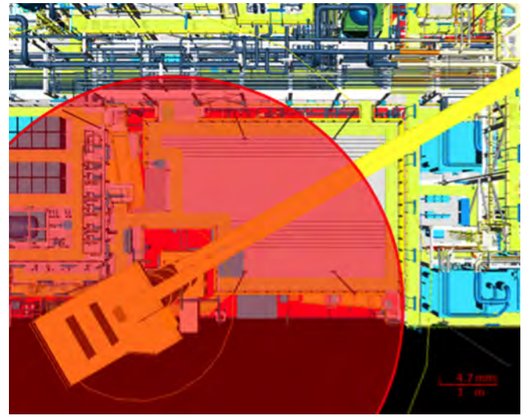

Figure 7: Obstructed View From Crane Cabin (Top View)

4.2 Controls and Displays

Inside the crane cabin, there are many controls and displays such as emergency stop, pressure gauge, hoist limiters, crane level indicator, etc. A crane operator would sit in a chair maneuvering two joysticks with both hands while observing the load being handled through the windows of the crane cabin. By observing the design of configuration on the chair arms (Figure 8), the following risks are identified:

1. Labels are placed below associated controls. Arms/hands potentially will block the labels leading to improper identification or utilization of the controls.

2. Emergency stop was not protected with a safeguard that will prevent the emergency stop from inadvertent use. In addition, the label for the emergency stop (Figure 8) should have white text on a red background per design guidance (American National Standards Institute, 2011a, 2011b).

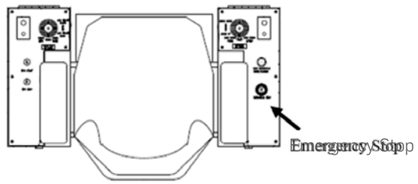

Figure 8: Chair in the Crane Cabin

3. The configuration of the two-lever control for crane motions (Figure 9), although is in compliance with API 2C (API, 2013), has a history of causing incidents due to human error. The control direction for lowering (push forward) or raising (pulling back) the auxiliary hoist joystick on the left hand (L.H.) is different from the raising (move left) and lowering (move right) for the main hoist joystick on the right hand (R.H.). This inconsistency for the same functional outcome has led to reported human error in the industry (Undisclosed Company, 2011). The right-hand joystick for the main hoist control furthermore violates or is counter to cultural stereotypical behavior as exhibited on the left-hand joystick in Figure 9 as well as in Figure 10 where a forward motion results in a lowering of the boom, main and/or auxiliary hoist and by pulling back on the joystick will raise the boom, main or auxiliary hoists. The alternate control configuration (Figure 10) is recommended to match cultural stereotypes and operator's expectations.

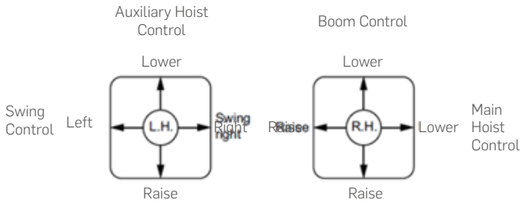

Figure 9: Designed Crane Motion Control Configuration (Source: API 2C (API, 2012))

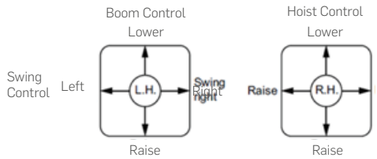

Figure 1:. Alternate and Recommended Crane Motion Control Configuration (Source: API 2C (API, 2013))

4. A footswitch for emergency shutdown (Figure 11) needs to be located within crane operator's reaching distance by his or her predominant leg, preferably for the 5th percentile female operator at a seated position. The construction of the footswitch should be such that the operator's foot will not readily slip off.

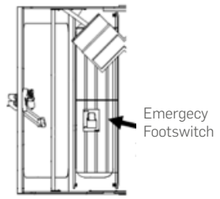

Figure 1:. Emergency Footswitch

5. Controls that deal with "settings" should be designed for non-predominant hand (i.e., left hand).

6. Boom slew rate control which is safe critical should be placed at the side for the predominant hand.

4.3 Communication and Procedures

Direct communication between a crane operator and flagman/rigger or supply boat crew is very critical and essential such that situation awareness is properly shared (Endsley & Jones, 2011). In this case study, it is observed that:

1. Warning and caution messages, including procedures and charts, need to be in compliance with industry standards such as American National Standard Institute (ANSI) Z535 (ANSI, 2011a and 2011b) or American Society for Testing and Materials (ASTM) F1166 (American Society for Testing and Materials, 2013). Based on the observation, the load chart and emergency release procedure chart that are safety critical are located at the back of the crane cabin door (i.e., behind the operator's chair) and are not easily accessible with an operator's view. These safety critical charts and procedures should be located within reach and afford optimum visibility (U.S. Department of Defense, 2012) when the crane operator is at a seated position facing forward.

2. Failure Mode Charts should be displayed on the screen, when possible, of the crane operator's choice of viewing with hard copies available and stored inside the crane cabin.

3. Labels for controls shall indicate function and direction of movement (U.S. Department of Defense, 2012).

4. There should always have two means of communications: radio and video. However, video display does not provide sufficient depth perception. Therefore, when one communication is down, the operation should be temporarily ceased until communications are re-established.

5. Crane operations should be certified (i.e., meeting competency requirements) and always follow a prescribed lifting plan or operations procedures that include how to lift and hoist safely.

4.4 Ease for Maintenance

Boom, machinery parts, and equipment require routine maintenance. Several maintenance accessibility issues were observed:

1. Because individuals are not protected on the inboard side, the crane lattice boom for a pedestal crane shall have a separate horizontal lifeline attached to the boom. This will allow easy movement along the walkway by a person wearing a full body harness to attach to the lifeline.

2. Panel and cabinet doors shall open fully without completely obstructing the main access.

3. Sufficient space should be provided for possible inclusion of a workbench or tool storage area inside engine house.

4. Crane boom shall be provided with a maintenance walkway running the full length of the boom. The maintenance walkway shall be equipped with a handrail, and a horizontal lifeline to serve as an attachment point for a fall arrest harness.

5. The head sheave access platform shall provide complete access to all sides of the boom tip and shall be accessible from the boom walkway. The sheave access platform shall provide access to the boom tip sheaves and the aircraft warning light for all maintenance tasks with the worker standing on the access platform decking.

6. Window wipers should be accessible from inside the crane cabin for repair or replacement.

7. Screen of windows should be allowed to be cleaned and/or replaced from inside of the crane cabin.

8. Defogging functionality should be considered and incorporated, when possible, for the forward window.

5. Conclusions

Exposure to crane hazards can be prevented. Human error due to design defects can lead to operations failure and subsequently loss of load control. The best approach to minimize human error and accomplish zero incidents is to build engineering controls into the design of the crane by complying with industry standards or best practice. However, even though this case study has indicated compliance with the standard's recommended design method, the review and outcome illustrate possible flaws if a design recommendation does not account for fundamental human factors design principles which are not always covered by industry standards.

References

American Bureau of Shipping. (2014). Guidance notes on the application of ergonomics to marine systems. American Bureau of Shipping.

American National Standards Institute. (2011a). ANSI Z535.1 American National Standard for Safety Colors.

American National Standards Institute. (2011b). ANSI Z535.2 American National Standard Environmental and Facility Safety Signs.

American Petroleum Institute. (2013). API Specification 2C Offshore Pedestal-mounted Cranes.

American Petroleum Institute. (2014). API Specification 2D Operation and Maintenance of Offshore Cranes.

American Society for Testing and Materials. (2013). F1166 Standard Practice for Human Engineering Design for Marine Systems , Equipment , and Facilities. https://doi.org/10.1520/F1166-07R13.2

Bureau of Safety and Environmental Enforcement. (2015). OCS Incidents/Spills by Category: CY2008-2015 ytd. Retrieved February 18, 2016, from https://www.bsee.gov/

Bureau of Safety and Environmental Enforcement. (2017). OCS Incidents Associated with Oil and Gas Operations - Outer Continental Shelf 2000. Retrieved June 8, 2017, from https://www.bsee.gov/stats-facts/offshore-incident-statistics

Endsley, M. R., & Jones, D. G. (2011). Designing to Support SA for Multiple and Distributed Operators. In Designing for Situation Awareness: An Approach to User-Centered Design (2nd ed., pp. 193–218). Boca Raton, FL: CRC Press.

Moore, W. H., & Bea, R. G. (1992). Modeling Human Errors in Operations of Marine Systems: Case STudy Examples. Report No. HOE-92-5, Management of Human Error in Operations of Marine Systems Project. Berkeley, CA.

U.S. Department of Defense. (2012). MIL-STD-1472G Design Criteria Standard: Human Engineering.

UK Health and Safety Executive. (2001). UK HSE Offshore Technology Report: Beyond Lifetime Criteria for Offshore Cranes.

Undisclosed Company. (2011). Learning from Incidents.

Acknowledgements

Special appreciation goes to Dr. Johan Hendrikse for his technical expertise to the work, and for his time and good-natured support.

Originally presented and published as: Jian JY, Miller GE, Shah S. Preventing Human Error in Crane Operations: A Case Study of Organizational and Design Elements. Proceedings of the Human Factors and Ergonomics Society Annual Meeting, 2017; 61(1): 1695-99.

Spark Ignition CHP: Great Performance, but Lots to Think About

Owen Elson

Principal Mechanical Engineer
Engineering, Design and Project Management
UK

Abstract

'Combined Heat and Power' systems have been commonplace on waste water treatment works for decades. The latest engine technology however offers significant gains in terms of efficiency and emissions. The ability to successfully integrate this type of engine, and hence access these benefits, relies upon the careful consideration of some key aspects:

- Sizing/utilisation – High capital cost makes redundancy uneconomic. These engines can 'ramp' to a greater extent, but constraints still apply.
- Gas quality – Spark ignition engines have increased sensitivity to contaminates in the biogas.
- Integrated control – ensuring that the site systems and proprietary engine systems can communicate without compromising network security.
- Load management – The low inertia of this type of engine makes them susceptible to trips in response to load steps. (A particular challenge if the CHPs are going to be used during power outages).

These aspects are discussed herein, with practical examples to illustrate, as required.

Keywords

Biogas; CHP; Efficiency.

1. Introduction

Asset planners and accountants can sometimes be forgiven for being so excitedly seduced by the prospect of step changes in OPEX opportunities that a high efficiency CHP installation can offer. When assessed simplistically based on the typical engine efficiencies, the numbers speak for themselves:

Table 1: Indicative OPEX Improvements

Engine Technology	Typical Electrical Efficiency	Notional kW/ Nm^3 'biogas'	£/year benefit*
Historic compression ignition	30%	1.80	£660k
Modern spark ignition	42%	2.55	£920k
			£260k improvement.

* Based exclusively on energy import offset @ £0.1/kWh for a site generating 10,000 Nm3/d of 'biogas'. Such a site would likely be at the mid to lower end of the spectrum in terms of CHP viability for municipal wastewater treatment plant applications.

These theoretical improvements can indeed become a reality. In many cases, opportunities to improve heat recovery system performance, and reduce maintenance down-time, means the benefits can be extrapolated further still.

However, any project to upgrade or install a spark ignition CHP engine must be carefully conceived if it is going to deliver successfully, and go on to return the anticipated 'operational expenditure' (OPEX) benefits. Some of the influencing factors are obvious, but others are more subtle. This paper seeks to explore some of the key aspects from a general perspective and is written in laymen's terms as far as is possible. The paper is written in the context of CHP at municipal wastewater treatment plants. This is due to circumstance, with the author's experience arising from projects in this sector. It is however suggested that the same challenges apply to varying degrees in other applications such as landfill or food waste processing.

2. Sizing/Utilisation Review

A consideration that certainly falls into the 'obvious' category is engine sizing; selecting the correct number and size of engines is by no means a new conundrum. The main difference compared to historic considerations appears to be that of budget provision as it is often the case that asset planners are no longer inclined to approve the inclusion of 'spare' or 'standby' engines. The predominant reason for this, as explained further in 4, is that spark ignition type CHP engines are seldom truly counted as part of a site's 'standby power provision'. As a result, the OPEX case for procuring units basically needs to justify the cost of installation. Even when maintenance outage cover is considered, any installed capacity that is not regularly generating is likely to tip the balance and extend the payback period significantly.

Static engines are generally intended to run at, or close to, 'maximum continuous rating' (MCR). If the gas is available, then of course an operator would want to run engines at MCR continually to maximise revenue. It also makes sense to run an engine at MCR as the maintenance intervals tend to be based on 'hours run'. (This is because your maintenance costs remain the same regardless of how many kWh you manage to generate over a time-based running interval). When operating more than one engine, it is also necessary to consider that ramping CHP engines together will increase the likelihood that they reach service intervals at the same time. This of course should be avoided if possible.

A modern spark ignition CHP is generally more flexible in terms of 'turn down' than an ageing dual fuel engine. The penalty paid in terms of an efficiency drop when running below MCR is certainly likely to be reduced when compared to an older engine. Acknowledging the maintenance cost impact and small efficiency penalty, the ability to better match gas consumption to gas production gives system designers a little wriggle room. However, limits of course apply. For example, the maximum 'turn down' is prescribed by the engine supplier but is typically say MCR x 60%. Also, for old and new engines alike, frequent stop/starts are not desirable. Suppliers often impose warranty linked limits to the number of permissible starts in a 24-hour period. (4 starts per 24-hour period might be considered typical). Therefore, at sites with limited gas storage, even the ability to reduce consumption rates will mean a poorly selected engine will stop and start with undesirable regularity. (Poorly selected in this context suggest the engine or engines are oversized). The compression ignition type engines as previously employed could typically be switched over (when already running on biogas plus a small proportion of 'pilot' diesel fuel) to run exclusively on diesel fuel. Rather than subject an engine to a stop, operators running dual-fuel engines have the option to switch engine(s) to full diesel fuel supply until the biogas supply recovers. As they will not run on diesel, this option is simply not available for spark ignition engine operators.

Losing the option to run CHPs on diesel fuel also has implications for the raising of process heat. In most municipal wastewater applications, the heat recovered off the engines is utilised for sludge treatment (e.g. anaerobic digestion/pasteurisation/thermal hydrolysis etc). Providing these processes with sufficient heat is often the key to overall process compliance. Although sites should theoretically have the means to satisfy this process heat demand using dedicated boilers, it is often the case that a combination of CHP engines and boilers will in fact be required to cater for peak demands. On occasions where the peaks in heat demand (during cold weather periods) coincide with low biogas production, dual fuel engine operators would again have the option to supplement CHP heat output by running engines on diesel fuel. Without this option, spark ignition engine operators will need to rely to a greater extent on any auxiliary boiler capacity to ensure sludge compliance is not compromised.

3. Fuel Gas Composition

As per the subject of Section 1, ensuring the fuel gas supply is appropriate for the CHP engines is clearly a fundamental consideration, as fuel gas supply pressure is perhaps the most common bugbear for operators of gas engines of any type. Moisture content normally comes in a close second. The presence of contaminates in the fuel gas has a more gradual impact on engine performance and health. None the less, this gradual degradation resulting from fuel gas contaminates can have devastating effects.

From a fuel gas pressure perspective, spark ignition engines are in fact easier to satisfy than compression ignition type engines. The primary difference being that the compression ignition type engines require a much higher supply pressure in order to operate. The capital and operational costs associated with supplying fuel gas at high pressure are significant in the first instance; the operating pressures invariably require that positive displacement compressors are needed. The hazard associated with operating gas equipment and pipelines at (relatively) high pressures is a further unwelcome headache. Generally speaking, systems serving spark ignition engines can utilise centrifugal type blowers. Not only do these blowers use significantly less power, but the system thermodynamics do not necessarily mandate that post-compression gas cooling is required. Booster machinery must still be carefully selected and system design is still highly critical. Fluctuations in fuel gas pressure can and do manifest in issues with spark ignition engine operation.

Spark ignition engines, or moreover, spark ignition engine suppliers, are more prescriptive about the moisture content of fuel gas. It is clear that condensate tends to carry the aggressive and damaging contaminates (discussed below) forward through fuel gas systems. It has hence always been the case that fuel gas systems for engines should be designed to incorporate facilities for collecting and removing condensate. However, apparently conservative relative humidity (%RH) limits are often prescribed by spark ignition engine suppliers, introducing the additional need to assess requirements for 'drying' of fuel gas. As a result, it is not uncommon to find gas dryers in modern CHP fuel gas systems. As well as increasing the capital cost of a new spark ignition installation, these active dryers also erode the OPEX benefit as a further 'parasitic loss'.

When it comes to contaminates in the fuel gas, there are a number of key risks that need to be considered. In wastewater treatment applications, the presence of significant quantities of hydrogen sulphide (H2S) in the fuel gas has historically been the main concern. Hydrogen sulphide (or sulphuric acid in condensate) can of course cause corrosion both in the gas train and within the engines themselves. This remains the case for spark ignition engines. Typically, the process of drying the gas to the requisite %RH helps to reduce the H2S concentration (as a quantity drops out in the condensate). By specifying a limit for H2S, spark ignition engine suppliers further force designers to consider the potential need for scrubbing.

Another clear limit stipulated by most engine suppliers concerns siloxanes. If present in significant quantities in the fuel gas, siloxanes leave a glass-like silica residue on the surfaces of internal engine components. These deposits accelerate wear and necessitate additional maintenance. Whether it is because modern engines are more sensitive to this type of contaminant damage, or whether this type of contaminant is becoming more prevalent in the waste water influent, there is now a clear need for system designers to address the presence of siloxanes and include filtration or absorption stages to protect engines (and comply with engine warranty conditions). Removing siloxanes again comes at a cost and the ongoing (subcontract) OPEX implications are particularly high.

Spark plugs (that are clearly not a problem for compression ignition engines) certainly have been observed to suffer if the fuel gas is not properly conditioned. Although they are essentially consumables, the cost associated with renewing spark plugs on these multi-cylinder engines is significant and should be considered.

4. Control, Control Integration & System Security

The main reason modern engines can offer such an efficiency increase is the sophistication of the engine control systems. These control systems are monitoring thousands of parameters in real time and adjusting the combustion to suit. Every CHP engine will have an 'engine control unit' (ECU), just like a modern car. Typically, CHP units also have a programmable controller that takes care of the ancillary items (such as the heat recovery systems and enclose ventilation etc). In tandem, these controllers will work to optimise and protect each engine. In most cases, the programmable controllers (rather than the ECUs) offer the control interface for site systems. It is ordinarily via this interface that the engine/engines are given information regarding the availability of fuel gas or site heat demands. (Some pertinent exceptions are discussed in Section 4).

As well as managing engine operation locally, it is common for both the engine ECU and engine controller to have the means to communicate via modem to the supplier's technical service teams. If either it detects a problem, or the site operator reports an issue, the supplier's off-site technical teams can interrogate and potentially rectify issues quickly and efficiently. Whilst this is a valuable feature, there are two significant aspects that need to be considered; safety and network security.

From a safety perspective, the implications of a remote team having the ability to start/stop/trim/adjust these large machines are clearly significant. Operators will admittedly be used to the fact that these engines are operated in an automatic mode. They might for example be automatically ramping up in response to a high digester gas level on site. However, under remote control, there is a possibility that the engines will operate in a way that is contrary to the local operator's expectations. Although there should be operational safeguards to prevent this from leading to a situation that might result in damage or harm, a residual risk remains. Further to such operational safeguards, system designers might consider the option to disable remote control functionality whilst the engines are running in regular 'auto' mode. It would then be necessary for the operational team on site to enable this functionality should the engine supplier's service team need to make changes. If agreed to be a requirement during design development, collaboration will be required in order to facilitate this type of discretionary access. The additional complexity of the solution is likely to attract additional cost.

With their modem connections, the ECU and/or the engine controllers are potential access points for malicious attempts to breach network security. As noted above, and it is certainly probable in the context of municipal wastewater installations, the engine controllers are likely to be connected to site systems for data transfer in some capacity. The specific arrangements for these connections are critical to ensure the engine modem/modems do not indeed become access points for malicious attacks.

If the engine controller/controllers are simply monitoring site field instruments or communicating with items like site alarm outstations via 'hard wired' signals, then there is no risk of a beach. However, if it is proposed that the engine controllers will be communicating with other networked controllers on site via a true communications network, the risk is very real. Dependant on the existing site systems, there may well be the need for a communications protocol conversion in order that the engine controllers can communicate with the site network. If such a protocol conversion is required, then this is the logical place to configure a firewall to protect against the possibility of a breach. If a protocol conversion is not required, then a dedicated firewall may need to be included. Again, the cost resulting from the added complexity must be factored in during the feasibility assessment.

5. Engine Stability and Load Management

The 'active load' on a generating engine is imparted by its alternator. As the active load increases or decreases, the engine governor and 'automatic voltage regulator' (AVR) react accordingly. All engines have limits with respect to the load steps that they are able to tolerate. Too great a step, and the protection on the engines will trip them to prevent damage due to stalling/over-speeding. When operating engines in parallel with a grid connection, such under or overloads are largely attenuated. When operating in 'island mode', engines are exposed to changes in site load resulting when electrical equipment is started or stopped.

Compression ignition type engines tend to have a high rotational inertia. They also tend to operate at high compression ratios. These features give them a robust nature. It is hence conceivable that a compression ignition engine will withstand reasonable over, or underload, whilst the engine governor and AVR adjust to suit. As such, these engines are relatively stable and can often be run in island mode operation to provide generation capacity (or supplementary generation capacity) should a site lose its grid connection. As noted in Section 1, compression ignition type engines can also typically be switched over to run on diesel fuel if required. Operating on diesel further improves the compression ignition type engine's ability to withstand load steps and perform in a stable way in island mode.

Spark ignition engine design seeks to maximise efficiency. The rotating inertia is reduced, allowing the engines to rev to a higher speed. They are also running 'leaner' at significantly lower compression ratios. These features tend to give them a more sensitive nature with respect to load steps. The protection settings for the engines need to be much tighter, limiting their ability to accept or reject load quickly. Again, when operating in parallel with a grid connection, this limitation is not a significant drawback. However, the option to run spark ignition type CHPs when a site is operating in island mode needs special consideration. It is certainly the case that spark ignition type engines should only be run in conjunction with regular diesel generators to support island mode operation. It is probable that, even if the CHP engines were running at the time, a loss of the grid connection would necessitate a 'black start' for the site. This black start must be managed with diesel engines. Only once the site is running again on the diesel generators might the option to run the CHPs be considered. Depending on the nature of the site load, the diesel generator capacity and the CHP capacity, it may still not be possible to run spark ignition CHPs due to their intolerance of load steps.

The manual management of island mode operation with CHPs would require detailed knowledge of the site load characteristics and engine performance criteria. At sites with an automated power management system (that will automatically start and stop generators ahead of permitting electrical load to change), there is an improved probability that CHPs can be run in conjunction with diesel generators in island mode. It should be possible to programme the power management system to recognise the limitations of the CHP engines, exposing them only to load steps that they are known to tolerate. Figure 1 is an example of permissible load steps for a 20 cylinder 2MW TCG2020 CHP supplied by MWM GmbH.

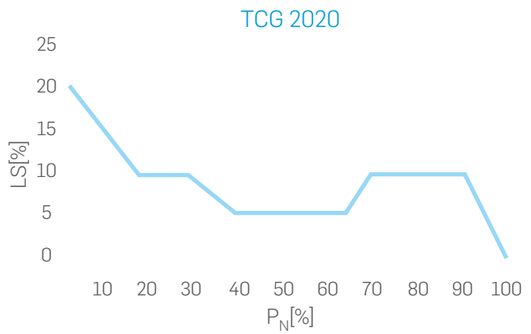

Figure 1: MWM TCG 2020 : Permissible Load Step Data

P_N Active Load	LS Load step	
P_N[%]	$t_{f,ln}$[s]	n[%]
0 - 20	15	11
20 - 30	15	10
30 - 40	15	9
40 - 45	15	9

$t_{f,ln}$ [S]	n Speed drop	
P_N[%]	$t_{f,ln}$[s]	n[%]
55 - 60	15	7
60 - 65	15	7
65 - 70	12	7
70 - 80	12	7

If spark ignition engines are replacing compression ignition engines, the standby power provision for the site needs to be reviewed. If the compression ignition engines had formed part of the standby provision, then an assessment of the practicality of counting the replacement engines in that provision needs to be made. Once again, the complexity and cost of making it possible to run CHPs during island mode operation and making said CHP installation resilient enough to be considered dependable in the event of an outage needs to be understood at feasibility stage.

6. Conclusions

In the main, the conclusions drawn below are pertinent for asset planners or teams tasked with feasibility assessments for new or upgraded CHP installations.

1. Designers should not be tempted to simply oversize CHP engines in an attempt to cater for current uncertainty or future increases in gas make.
2. When planning a CHP installation or upgrade, review the capacity and condition of the site's auxiliary boilers to ensure that the ability to meet process heat demands is not compromised.
3. A means to control the %RH of the fuel gas is likely to be required for a spark ignition system. The capital cost and OPEX impact of this aspect needs to be assessed.
4. A means to reduce contaminant levels in the fuel gas is likely to be required for a spark ignition system. Siloxanes are of particular concern. The capital cost and OPEX impact of this aspect needs to be assessed.
5. Remote (third party) control of CHP engine systems potentially constitute a H&S risk. Supplementary mitigation may be required.
6. Remote (third party) modem access to CHP controllers potentially constitutes a security risk. Additional security features may be required.
7. Spark ignition CHPs are significantly less tolerant of load steps when compared to compression ignition units. This compromise is required to access the improved efficiencies on offer.
8. If spark ignition engines are replacing compression ignition engines, the standby power provision for the site needs to be reviewed. If the compression ignition engines had formed part of the standby provision, then an assessment of the practicality of counting the replacement engines in that provision needs to be made.

Acknowledgements

Originally presented and published as: Elson O. Spark ignition CHP: Great performance, but lots to think about. Proceedings of the 22nd AquaEnviro European Biosolids and Organic Resources Conference 2017, November: The Royal Armouries, Leeds, UK.

Automated Coupling of Standard One-Dimensional and Three-Dimensional Flow Solvers for Simulation of Metro Ventilation Systems

Yinan Scott Shi

Tunnel Ventilation Engineer in Training
Infrastructure Engineering
Vancouver, Canadag

Conor Fleming

Tunnel Ventilation Engineer
Infrastructure Engineering
Vancouver, Canada

Chandan Sejekan

Tunnel Ventilation Engineer
Infrastructure Engineering
Vancouver, Canada

Eugene Wong

Tunnel Ventilation Co-op Student
Infrastructure Engineering
Vancouver, Canada

Mina Samimi

Tunnel Ventilation Lead
Infrastructure Engineering
Vancouver, Canada

Melissa Duckham

Tunnel Ventilation/Mechanical Group Manager
Infrastructure Engineering
Vancouver, Canada

Abstract

With increased globalization and the exponential growth of human population, underground transit systems have become a necessity in metropolitan areas around the world. In addition, there is an increasing awareness of human comfort and safety inside these complex structures, and the need for accurate numerical modelling and analysis has become a priority as part of the design process. This modelling is generally carried out both network-scale and station-scale. Network-scale phenomena include the piston effect of trains, longitudinal ventilation of tunnel fires, and the long-term thermal absorption of the tunnel lining and surrounding soil. One-dimensional network flow solvers are well-suited to network-scale modelling. Station-scale flow features include smoke migration through stations as well as flow separations and their corresponding pressure losses. These complex flows necessitate more sophisticated three-dimensional flow solvers. As the two scales are highly interdependent, achieving good consistency between the 1D and 3D models is essential especially since the boundary conditions for the 3D models are most often supplied by the 1D runs. However, the complicated 3D designs rarely translate well into accurate 1D models. Thus, the simplification and assumptions made while creating the models introduce inconsistencies. In this article, a novel coupling approach is proposed to mitigate these inconsistencies by optimizing the local pressure loss coefficients within the 1D models. This approach is validated and tested on representative station models. Results promise better flow distribution and prediction using the 1D model. Furthermore, this coupling method would not just be limited to 3D computational data but could also be used with field measurements.

Keywords:

Computational Fluid Dynamics; Tunnel Ventilation; Fire Life Safety

1. Introduction

Metro ventilation system designs are typically verified at the design stage using numerical models. Modelling is generally carried out at two scales: network-scale and station-scale. Network-scale phenomena include the piston effect of trains, longitudinal ventilation of tunnel fires, and the long-term thermal absorption of the tunnel lining and surrounding soil. 1D network flow solvers such as the Subway Environmental Simulation (SES) Program [1] are well-suited to network-scale modelling, and provide predictions of flow rates and temperatures which are adequate for network design purposes (refer to the validation cases reported in the SES User Manual [1] for examples). Station-scale flow features include smoke migration through stations as well as flow separations and their corresponding pressure losses (e.g. through doors and stairways). These complex flows necessitate more sophisticated 3D flow solvers, which may be based on Reynolds-averaged or filtered formulations of the Navier-Stokes equations.

Station-scale and network-scale flows are interdependent: the local flow pattern within a station is influenced by train motion and fan operation within the wider network, and air flow at the network scale is influenced by local pressure losses within stations. 1D and 3D numerical models of a metro system should be consistent with one another to reflect this interdependency of scales. Boundary conditions at tunnel interfaces in a 3D station model should represent the influence of the wider network. Local pressure losses in a 1D network model should reflect the actual pressure losses at corresponding locations in the 3D station model. This is a straightforward task for tunnel flows, where local losses for simple expansions, contractions and branches can be determined via coefficients based on experimental data [1, 6]. Difficulties arise for flow through more complex geometries such as metro stations, where experimental reference data is not available. It is often unclear how best to represent 3D features such as stairways, fare gates, escalator shafts or smoke baffles in a 1D model, and what values the corresponding loss coefficients should take.

As illustrated in Figure 1, the pressure loss through an open-style stairway is difficult to interpret as an equivalent pipe flow pressure loss. One approach would be to interpret the system as a combination of two turning elbows and an orifice. However, the elbows are ill-defined and hence their losses are difficult to determine from standard references. Additionally, there is an interaction effect between the three elements which must be accounted for. Prince et al [2] used a 3D computational fluid dynamics (CFD) model to demonstrate that the pressure loss across a duct with two elbows depends on elbow orientation, and the interaction effect depends on elbow separation distance. They found that 3D CFD can predict the pressure losses along complex flow paths reasonably well.

Another modelling approach for metro systems is to use a fully coupled 1D/3D flow solver, such as those developed by Collela [3] and Prince [4]. These methods, based on modified versions of the 3D flow solvers ANSYS Fluent and OpenFOAM respectively, directly calculate the local pressure losses at the station-scale, and automatically update boundary conditions at 1D/3D interfaces based on events at station-scale and network-scale. Of course, the successful calculation of complex pressure losses using a 3D numerical model is dependent on its quality and accuracy, the discussion of which is beyond the scope of this paper. Additionally, there is a significant computational cost associated with the 3D portions of the model. Hence, it is not suitable for network-scale modelling.

An alternative method of 1D/3D model coupling was developed using (but not limited to) standard versions of SES and the 3D flow solver Fire Dynamics Simulator (FDS) [5]. The method involves using an isothermal 3D CFD model to determine the pressure losses and flow rates in complex areas of the network (i.e. within stations) and adjusting the loss coefficients in an equivalent 1D model until local flow rates and pressure losses are matched. It is worth noting that this method could also utilize field measurements instead of 3D CFD predictions.

The resulting 1D network model has a reasonably accurate representation of stations, and therefore in addition to predicting network-scale flows with good confidence it is a useful and fast indicator of potential design failures at station-scale. Station-scale design scenarios, such as platform fires, are first simulated using the 1D model, and boundary conditions for subsequent 3D models are determined. The resulting 1D model also benefits network-scale non-emergency simulation where more accurate local air flow rate in stations will help determine potential violation of air velocity criterion. Furthermore, the model can be used to better predict air flow during testing and commissioning phase.

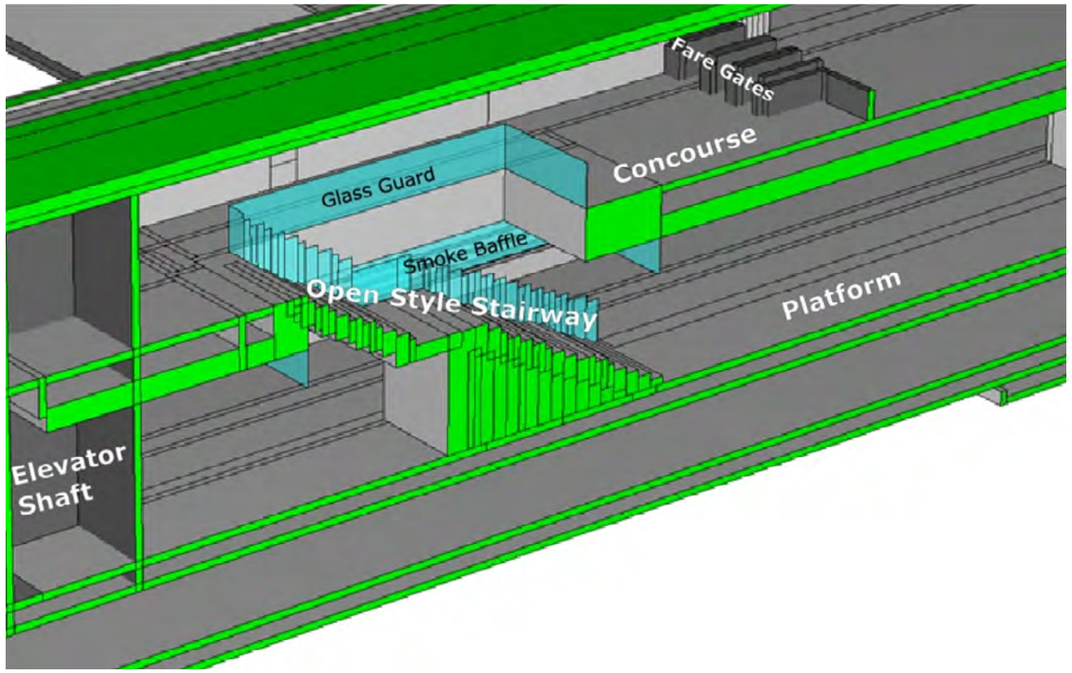

Figure 1: Example of an Open Staircase (Side Section View)

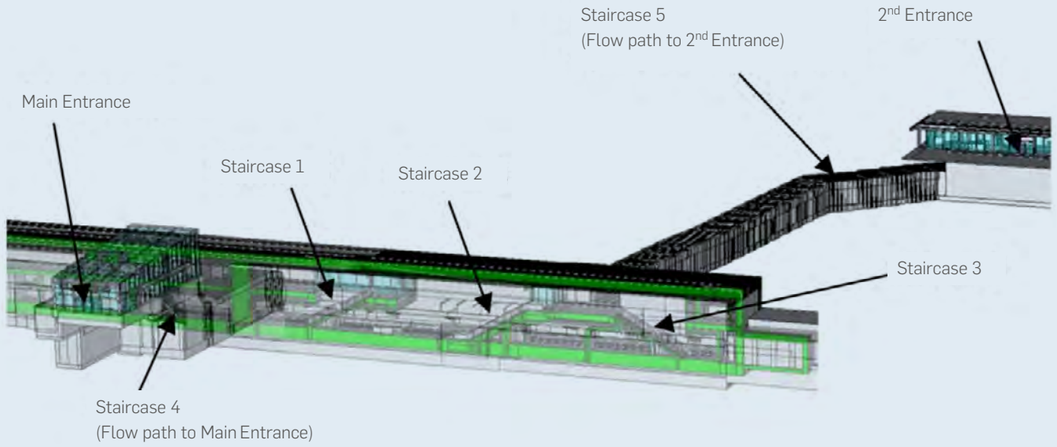

Figure 2: 3D Schematic Diagram of a Typical Metro Station

2. Methodology

The method begins by constructing similar 1D and 3D isothermal models of the station of interest. Figure 2 is an example of a typical station. The 1D model (solid black lines and dots) includes all the flow paths which exist in the 3D geometry as illustrated in Figure 3.

Utilizing the advantage of the simple 1D modelling capability of FDS 6.5.2 [5], 1D elements of known hydraulic resistance are added to represent tunnels connecting to the station. Identical elements are included in the 1D SES model. The resistances of the adjoining 'calibration' elements are set such that there is an approximately even balance of flow from the calibration tunnel side and station side of each ventilation shaft, in order to guarantee a reasonably sufficient air flow through all of the station stairways and calibration elements. The general exhaust flow directions are indicated in Figure 4.

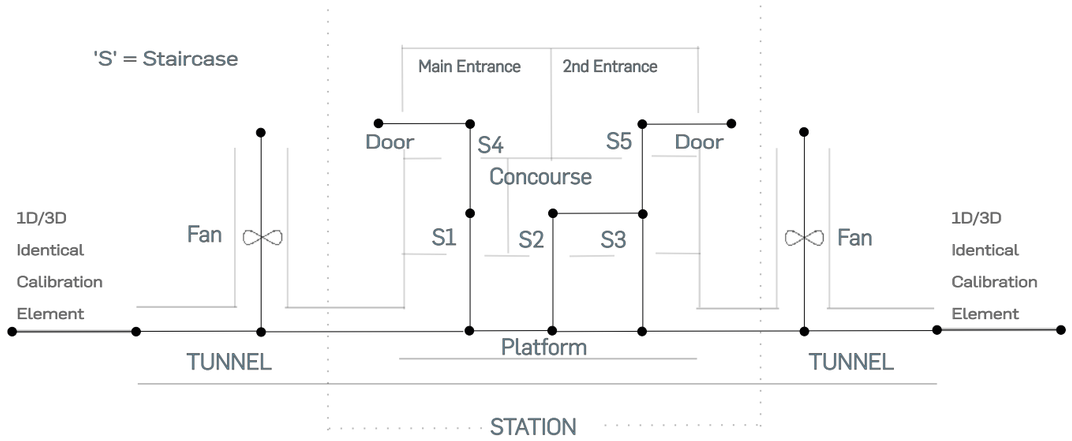

Figure 3: 1D Model Overlaid on a Simplified Schematic Representation of a Metro Station. The Dotted Line Indicates the Portion of the Station Shown in Figure 2

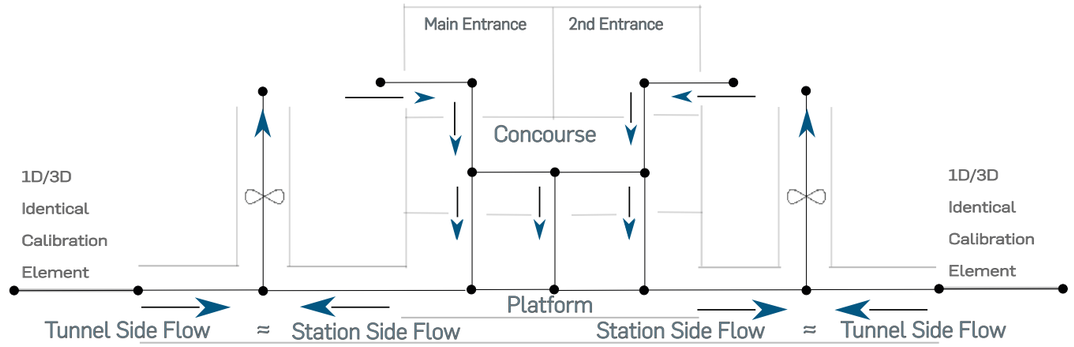

Figure 4: General Flow Directions in Each 1D Section When the Ventilation System Is Operating in Exhaust Mode

The inclusion of the calibration elements is important as it allows both the flow rate and pressure drop to be matched. If 1D air flow predictions were prescribed at the tunnel boundaries, the 1D model could match the flow rates of the 3D model with an arbitrary set of local loss coefficients which are correct relative to one another but too high or too low in an absolute sense, i.e. the overall pressure drop through the station could be over- or under-predicted.

The 3D model is used to simulate isothermal flow through the station with the ventilation system in supply or exhaust mode (as shown in Figure 4). The same scenario is then simulated in the 1D model with estimated local loss coefficients. In an automated routine, the flow rates along selected paths are compared, the corresponding loss coefficients are adjusted through a proportional-integral-derivative model, and the 1D simulation is repeated. Ultimately, loss coefficients are determined for each flow path in the 1D model, such that differences in the local flow rate are within a certain tolerance. The procedure is repeated with the ventilation system operating in the opposite mode (i.e. supply or exhaust) and then for each station in the metro network.

3. Demonstration and Discussion

3.1 Complexity of a Simple Geometry With Obstructions

To demonstrate that the pressure loss can be difficult to predict even for simple obstructions, two models are set up in SES and FDS as shown in Figure 5 and Figure 6.

Each model consists of an inlet with a steady inflow. The inlet path is then divided into two branches with identical cross section and length. The 'reference' branch has a wall friction loss and an exit loss. The obstructed branch is similar, but features additional unknown losses due to an elbow junction and several full-height rectangular column obstructions.

In the first model (Figure 5) the obstructed branch features three equi-spaced columns upstream of the elbow. The second model (Figure 6) features three additional equi-spaced columns downstream of the elbow.

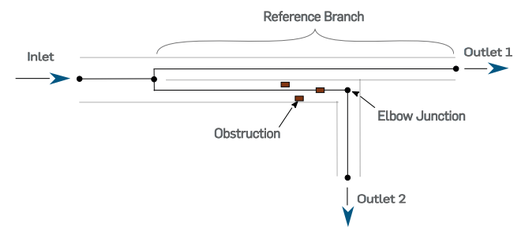

Figure 5: Simple Geometry Containing Three Obstructions

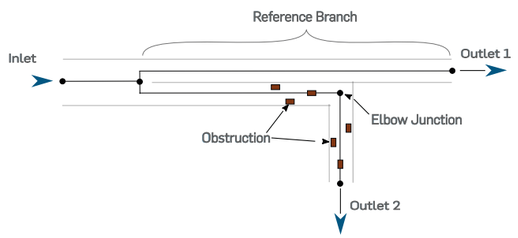

Figure 6: Simple Geometry Containing Six Obstructions

The new iterative coupling method is used to determine the pressure losses for the obstructed branch of each model. The corresponding loss coefficient, or K-factor, is defined as

$$K = \frac{\Delta p}{\frac{1}{2}\rho u^2} \quad (1)$$

where Δp is pressure change, ρ is density and u is velocity. *K*-factors of 1.74 and 3.3 are determined for the obstructed branch in the three-column and six-column case, respectively. For comparison, the branch loss is calculated from reference data as the sum of the separate friction, elbow, exit, and column losses in Table 1, which are significantly different to the numerical predictions.

Table 1: Calculation of Obstructed Branch K-Factor Based on Reference Data

Element	*K*-factor	Sources
Walls (friction)	0.13	Based on Darcy friction factor of 0.026
Elbow	1.5	SES User's Manual, Table 4.4 [1]
Single column	1.52	SES User's Manual, Table 4.3 [1]
Exit	1.0	SES User's Manual, Table 4.4 [1]
Total – 3 column case	7.19	
Total – 6 column case	11.75	

The situation in a metro station is more complex with columns, escalator shafts, fare gates, and smoke baffles in close proximity as shown in Figure 1. Hence a 3D CFD prediction of the pressure loss is expected to be more reliable than a simplified calculation in the style of Table 1.

3.2 Calibration Element

The 'calibration' element, the common element between the 1D and 3D models shown in Figure 4, ensures that flow rates and hydraulic resistance are matched. To demonstrate the concept, a simple symmetrical model was set up in both SES and FDS as shown in Figure 7. Flow rates of 50-100 m^3/s were specified at the ventilation shaft, and the K-factors in element 1 and 2 were varied. For cases where both K-factors are below approximately $K = 20$, SES and FDS predictions of flow rates Q_1 and Q_2 do not agree, due to modelling differences in the wall friction between 1D and 3D models. However, the pressure losses in metro stations are dominated by large-scale flow separations at stairways and other obstructions, and that wall friction is less significant. When $K_1 > 20$ and $K_2 > 20$, SES and FDS predictions of flow rate and pressure drop agree very well, with the error generally below 1%.

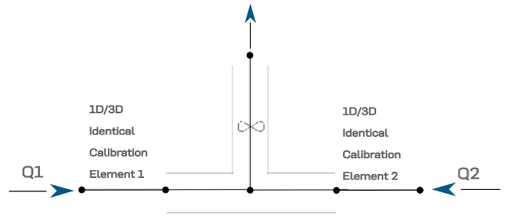

Figure 7: Simple Demonstration of the 1D/3D Calibration Elements

3.3 Application to Metro Stations

In this section, the effect of matched 1D and 3D models of a typical metro station (illustrated in Figure 2) is demonstrated. In the first case K-factors for the 1D model are prescribed based on guidance from the SES User's Manual [1]. This results in an approximately symmetrical air flow pattern on the platform level as indicated by the schematic vectors in Figure 8 (where arrow size indicates approximate relative flow rate).

The new coupling method is then used to determine the K-factors, such that the flow rates in each path are within 3% of the reference 3D simulation. An asymmetric flow pattern develops, as shown in Figure 9, reflecting geometrical differences in the various stairways and entrances.

Comparing Figure 8 and Figure 9, the magnitude and location of the highest air flow rate has changed, as well as the locations of flow split on the platform and the concourse. These changes can have significant effects on predicting both normal and emergency operations with the optimized model.

1. Normal Operation:

The optimized model can better predict where air velocity may exceed the criteria within stations. With better predictions of the air flow pattern, more reliable temperature predictions may be made.

2. Emergency Operation:

The optimized model can better predict the air flow pattern and hence smoke migration (indicated in SES by temperature). Tunnel emergency fire cases can also benefit from the coupled model, due to improved modelling of the hydraulic resistance of adjacent stations. Additionally, optimized 1D model is a fast and approximate indicator of potential design failures for station fire scenarios, which can subsequently be examined in detail using the 3D model.

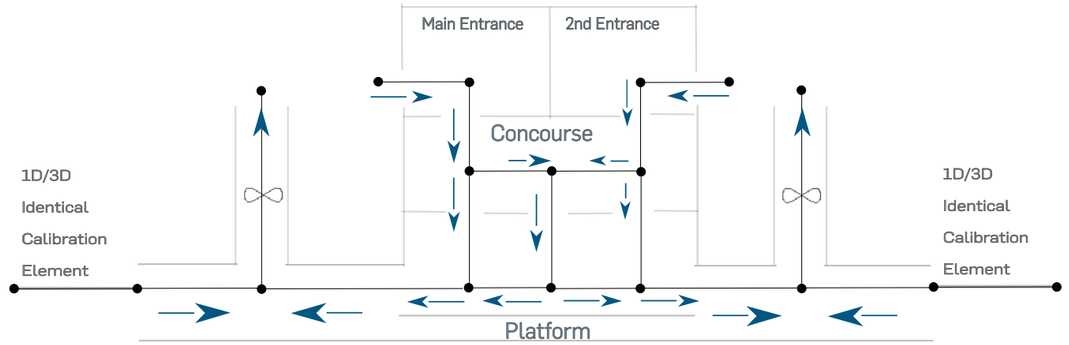

Figure 8: 1D Flow Pattern Based on K-Factors From Reference Data.

4. Conclusion

A new method of achieving consistency between 1D and 3D models of air flow in metro systems using standard versions of widely-used flow solvers was developed. Such consistency is necessary to adequately represent the hydraulic resistance of stations in network-scale 1D models, and to adequately represent network-scale effects in station-scale 3D models.

Other authors have addressed this issue by implementing 1D tunnel flow models within existing 3D flow solvers, thereby achieving fully-coupled 1D/3D simulation capabilities. However, these methods did not improve 1D modelling accuracy. Our method improves the accuracy of 1D network-scale models of normal operations and of tunnel fires with better representation of station resistances. The optimized 1D model is also used to determine boundary conditions for its 3D counterpart during a station fire scenario. Moreover, our method is based on standard versions of existing 1D and 3D software and hence avoids considerable development and validation efforts. The 3D flow solver FDS 6.5.2 was used to calculate the flow through a station in isothermal conditions, and this flow was matched by automatically adjusting the pressure loss coefficients of an equivalent 1D flow model designed in SES v4.1.

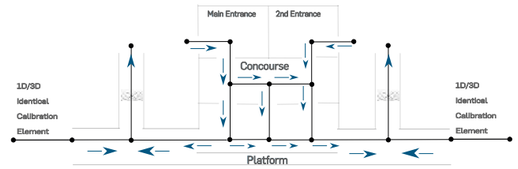

Figure 9: 1D Flow Pattern Based on K-Factors Determined by Matching the 3D Reference Simulation

As a final note, the 1D model could be tuned to match field measurements instead of 3D simulation results, which might be useful for modelling the impact of refurbishment or extension of existing systems.

References

[1] Subway Environmental Simulation Computer Program SES Version 4.1, Part I user's Manual, New York: US Department of Transportation, 2002.

[2] J Prince, M Tabarra, J Alexander, J Peiro, "On the prediction of pressure losses in complex flow scenarios using CFD," in 16th International Syposium on Aerodynamics, Ventilation & Fire in Tunnels, Seattle, USA, 2015.

[3] Francesco Colella, Vittorio Verda, Romano Vorchiellini, Guillermo Rein, "One-dimensional and multi-scale modelling of tunnel ventilation and fires," in Handbook of Tunnel Fire Safety, ICE Publishing, 2012, p. 541–554.

[4] J. Prince, "Coupled 1D-3D simulation of flow in subway transit networks," Imperial College London, 2016.

[5] K. McGrattan, S.Hostikka, R.McDermott, J.Floyd, C.Weinschenk, K.Overholt, Fire Dynamics Simulator User's Guide, 6th ed., National Institue of Standards and Technology, 2017.

[6] D. Miller, Internal Flow Systems., BHRA Fluid Engineering, 1978.

Acknowledgements

Originally presented and published as: Shi Y S, Fleming C, Sejekan C, Wong E, Samimi M, Duckhamby M. Automated coupling of standard one-dimensional and three-dimensional flow solvers for simulation of metro ventilation systems. The 17th International Symposium on Aerodynamics, Ventilation & Fire in Tunnels: BHR Group, Sep 2017, Lyon, France.

Mapping Geohazards in the Watersheds Above Leh, Ladakh: The Use of Publicly Available Remote Sensing to Assist Risk Management

Dr Andrew B. Hart

Chief Engineering Geologist
Engineering, Design and Project Management
Epsom, UK

Dr Gareth J Hearn

Hearn Geoserve Ltd
West Sussex, UK

Abstract

The town of Leh, capital of the Province of Ladakh, located in the Indian State of Jammu and Kashmir, suffered considerable damage and loss of life following floods and debris flows in 2010. Although the 2010 events have been the subject of a number of important geohazard-related studies, the town of Leh, as well as the rest of the province of Ladakh, lacks sufficient data with which to assess geohazards for purposes of preparedness, mitigation or future planning and development control. Publicly-available satellite imagery has been used to derive maps at various scales depicting geomorphology and geohazards and this has been supported by ground truthing in order to derive a prototype mapping technique for wider application.

Keywords

Geohazards; Remote Sensing; Risk Management

1. Introduction

Leh is the capital city of the province of Ladakh, in the Indian state of Jammu and Kashmir. Ladakh is a province of extremes in terms of topography, climate and geohazards [7], and Leh itself has been affected by major floods and debris flows in recent years and decades. As is the case with many remote mountain regions of the World, there is a general lack of background information with which to assess the risk posed by geohazards to land use and infrastructure. The situation in Leh is particularly acute, with rapid urbanisation taking place as a result of in-migration from the more remote parts of the province. This is forcing urban expansion into increasingly marginal areas, potentially at significant risk from floods, debris flows, rock falls and landslides.

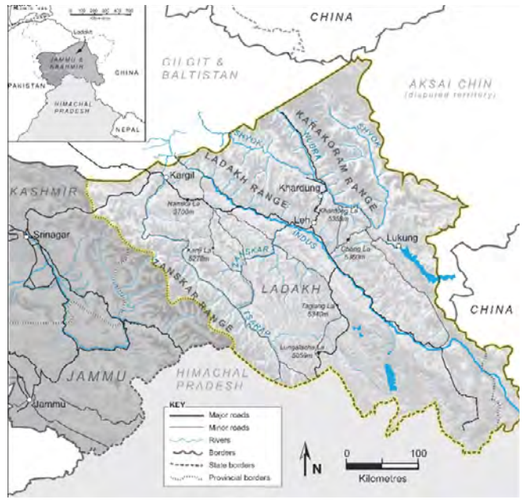

Figure 1: Leh and the Province of Ladakh (Hearn & Shilston (2017) With Permission From the Geological Society of London)).

To help bridge the geodata gap, and thereby provide a tool for rational land use planning, a desk study was undertaken utilising publicly-available satellite data in order to develop a geohazard map of Leh and the mountainous catchments upstream. This desk study was supported by a ground truthing (field checking) visit that allowed the interpretative map to be adjusted using ground observation. The result is not only a document that is of direct value to existing and future urban development in Leh, but also serves as a prototype for wider application in the Ladakh region and neighbouring provinces.

2. Geography, Geology and Geomorphology of Leh

2.1. Geography

The 16th Century town of Leh is located in the upper Indus valley between the Ladakh Range to the northeast and the Zanskar Range to the southwest (Figure 1). The town is at an elevation of 3500 m a.s.l. and, with an average annual precipitation of 100 mm and sub-zero temperatures for all but the spring and summer months, it is a true high altitude cold desert. The population is a little over 30,000, but this is increasing rapidly (by 25% in the last ten years [17]) due to an influx of low-skilled migrant labour, the migration of families from other parts of the province to take advantage of education facilities and employment prospects, and the boom in the tourist industry since the turn of the 21st Century.

The town is located on an outwash fan (Figure 2) above the terraces of the Indus River. This fan extends for a distance approximately 5 km upstream of the main town, with its apex at the confluence of several mountain streams. These streams drain five main catchments, the largest of which extends to the ridge line at Kardhung La, at an elevation of 5359 m a.s.l. and approximately 20 km to the north of Leh. While large parts of the town have been constructed on the fan surface, housing has progressively extended onto neighbouring mountain slopes (Figure 3).

Figure 2: Much of the Town of Leh Is Constructed on an Outwash Fan.

Figure 3: Urban Expansion Into Mountainous Areas.

2.2. Geology and Geomorphology

Ladakh is in the collision zone between the Ladakh block to the northeast and the Great Himalaya to the southwest, and is underlain by an assemblage of igneous, sedimentary and metamorphic rocks, with major structural zonation orientated northwest – southeast. Leh itself is located on the northern side of the Indus valley that forms part of the Indus-Tsangpo Suture Zone (ITSZ). The ITSZ occupies the boundary zone between the lithologies of the Indian plate to the south and the Eurasian plate to the north [16,18,8]. Researchers have identified five Quaternary glacial stages in the Ladakh Range [13] and at least four stages in the Zanskar Range [12]. The catchments that surround Leh have been exposed to cycles of glacial, periglacial and paraglacial processes during the Quaternary, with vast quantities of glaciogenic sediments deposited in moraines, fluvio-glacial terraces and outwash fans. The mountains above Leh are underlain by granitic rocks of the Ladakh Batholith (Ladakh Plutonic Complex) that are closely-jointed and frequently weakened by dyke intrusions. Slopes are inclined at angles of up to 40° or more. The jointed rock masses are especially prone to intense mechanical weathering and erosion, resulting in widespread rock fall deposits, scree slopes and debris fans (Figure 4). Further discussion on the Quaternary evolution of the landscape in general can be found in Pant et al. [14], Phartiyal et al. [15], Dortch et al. [5].."

2.3. Geohazards

Despite the very low average annual precipitation, heavy rainfall during the summer months has given rise to floods and debris flows, some of which have resulted in major damage and loss of life. The most significant of these events took place in the early hours of 6 August 2010, although it is unclear as to how much rainfall was responsible for triggering this event. The rain gauge at Leh airport recorded 13 mm of rainfall during 24 hours [2]. While this was high compared to the average rainfall of a little over 15 mm for the entire month of August, it could not have been representative at all of the rainstorm that generated the large-scale flooding and debris flows that ensued. Stolle et al. [17] report that the Geological Survey of India recorded 12 mm during a 30-min period near the most affected area, while Hobley et al. [9] consider that as much as 75 mm or more rainfall may have fallen during the same 30-min period. Thayyen et al. [19] use the geomorphological evidence of the flood itself to back-analyse rainfall intensities of 209 ± 35% mm in 12 min over small catchment areas. Whatever the size of the triggering rainfall, the geomorphological and human consequences of the floods and debris flows that this rainstorm generated were immense ([1,11,6,9,17,20] and others). Reports vary widely, but there were at least 200 and perhaps in excess of 600 fatalities [9]. Nevertheless, the 2010 event was not unique, with floods impacting the region in 2005, 2006, 2008, 2011 and 2015 [19,20,2,9].

Figure 3:
Urban Expansion Into Mountainous Areas.

3. Geohazard Assessment of Leh and Its Watersheds

3.1. Interpretation of Satellite Data

Much of the terrain surrounding Leh, as well as other towns and villages in Ladakh, is difficult and dangerous to access for geohazard assessment purposes. Furthermore, sources of geohazard can be very remote from the settlements and infrastructure that are ultimately at risk, and therefore maximum use should be made of satellite remote sensing in the development of datasets that can inform urban and infrastructure planning and the development of geohazard preparedness strategies. A pilot study was carried out to determine what level of geomorphological and geohazard detail could be derived from an interpretation of publicly accessible imagery and data, and thus maximise the potential take-up of the technique by those engaged in infrastructure and urban planning in Ladakh. Initially, ASTER GDEM and SRTM data [10] were used to develop a digital elevation model of the Leh area and its upstream watersheds (Figure 5), covering an area of 175 km2. Derivative slope angle, slope aspect and catchment area maps were also developed in order to assist terrain familiarisation.

There are no documented cases that the authors are aware of where large rock failures have impacted the town of Leh. Nevertheless, large landslides have occurred during the last 10,000 years [4] in the Ladakh region and they continue to pose a hazard to infrastructure and rural populations (e.g. [7]). It is not inconceivable that a large rock failure could occur on the slopes and in the watersheds above Leh, posing potentially serious consequences.

One of Juyal's [11] recommendations in 2010 was the development of a methodology to assess the impact of possible future events, especially given increasing development pressures on land. Despite the mapping undertaken by Bhatt et al. [3] and Hobley et al. [9] of the 2010 debris flow runout using Cartosat-1 and ASTER hillshade data respectively, this recommendation does not appear to have been addressed and there is little documentation available to facilitate geohazard management in urban planning and preparedness.

Figure 4: Steep Mountainsides Above Leh Formed in Closely-Jointed Rock Are the Sources of Rock Falls, Debris Flows and Debris Fans.

However, this information in itself provided little opportunity to interpret and classify the geomorphology of the area and neither did it allow sources of geohazard to be identified. To achieve this an onscreen interpretation was made of the 3D view of DigitalGlobe's WorldView 2 imagery -available through Google Earth and the 2D version of the same imagery available through the ESRI ArcGIS software. These data sets comprise cloud-free satellite imagery of multiple ages acquired by DigitalGlobe between 2010 and 2016. Interpretative maps were developed at scales ranging between 1:5,000 and 1:15,000 (Figure 6), with summary maps produced at 1:40,000 (Figure 7). The following landforms and processes were identified and delineated:

- Catchment boundaries, ridge lines, spurs, ephemeral and permanent stream channels;
- Terraces and other landforms consistent with glacial moraine;
- Alluvial fans and river terraces associated with Holocene and present-day fluvial activity
- Flood deposits and areas of potential flood damage
- Talus, taluvial and colluvial deposits
- Debris flow source areas and deposits

- Debris slides
- Rock fall and rock avalanche source areas and deposits
- Potential landslide dams
- Sand ramps derived from aeolian processes

Table 1 describes and summarises the geohazard implications of each of the terrain units identified. In total, the interpretation took between two and three weeks to complete, with just over a week of additional work after the ground truthing (see below).

One of the most striking features of the landscape is the abundance of mobile sediment on slopes and within drainage channels, and the proximity of urban and village areas to these sediment sources. From the imagery, it is apparent that settlements have expanded into flood-prone areas as populations have grown, and in some cases development has taken place in the immediate vicinity of ephemeral water courses or on currently dormant debris fans, placing them at heightened risk. Rock fall source areas were also very easily identifiable. Although most of these are located along ridge lines and cliffs in remote catchments, there are also significant source areas on slopes directly above areas of urban expansion

3.2. Ground Truthing

A programme of ground truthing (or field checking) was undertaken over a 3-day period. The purpose of this exercise was to observe a sample of the features identified from the remote sensing to confirm their validity and provide additional detail concerning the potential hazards they might pose. Equally importantly, the ground truthing was undertaken in order to determine the size and mechanism of geohazards not identified by the desk study. Ground truthing combined drive-over and walk-over inspections, recording observations by GPS.

3.3. Validation and Calibration of the Interpretation

Figs. 8 to 10 illustrate some of the outcomes of the ground truthing exercise. It is very clear from these illustrations how reliable the interpretation was in identifying mass movement and fluvial deposits within the landscape. Nevertheless, the ground truthing did identify some areas where minor reinterpretation was required and the maps were adjusted accordingly. These adjustments were applied to other parts of the mapping area, by way of calibration.

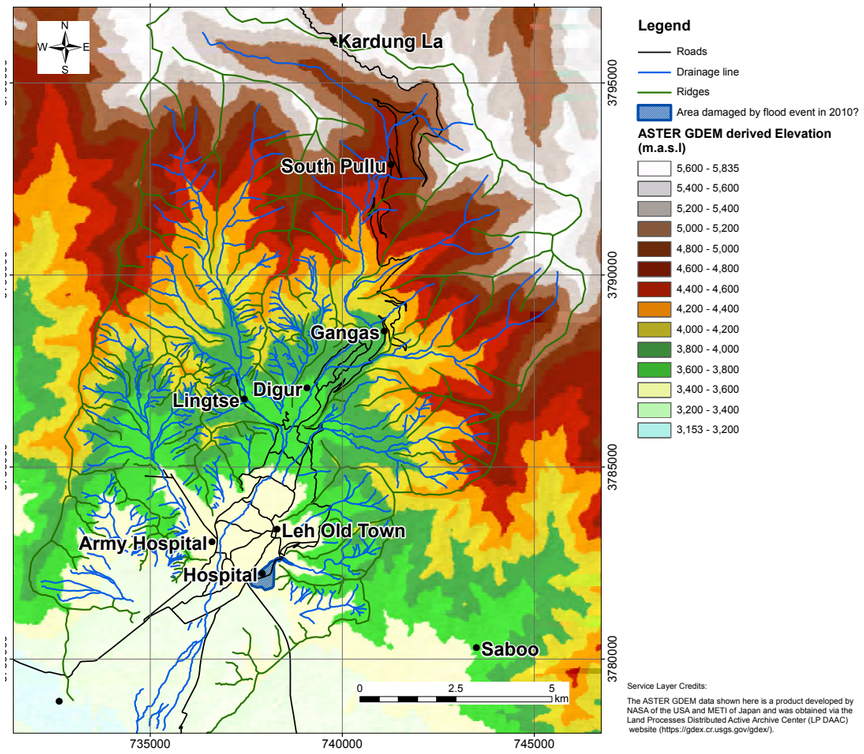

Figure 5:
Digital Elevation Model of the Mountain Watersheds Above the Town of Leh Using ASTER DEM.

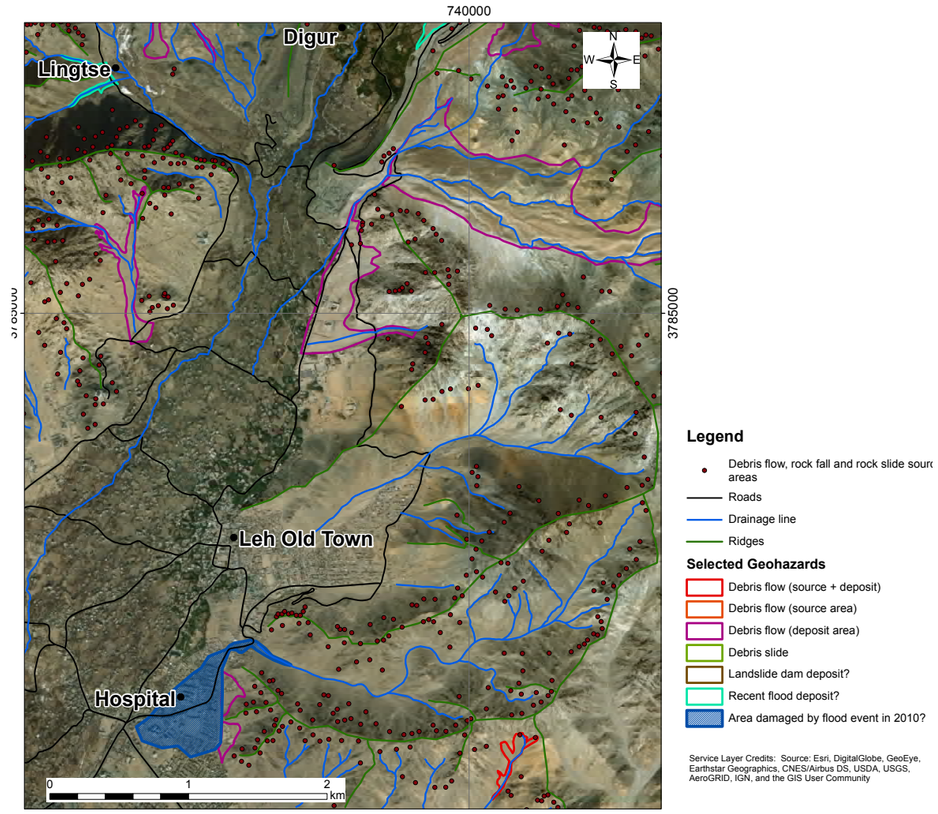

Figure 6: Extract From the Remote Sensing Interpretation at 1:15,000 Original Scale.

4. Important Geohazard Details Not Identified From the Remote Sensing

Generally, the limiting factor in the remote sensing was the resolution of the available satellite imagery compared to the size of the features being mapped, as well as the scale at which it was used. Features similar in size to a small car were generally identifiable. Any geological or geomorphological feature smaller than this could therefore not be observed, unless it was part of a larger collection or pattern of features. Shadows formed on north-facing mountain slopes can also influence how easily a geohazard (such as a rock fall source area) can be identified. Figure 11 illustrates some of the geohazard source areas identified on the ground that were not apparent from the imagery.

5. Discussion

The exercise described above was undertaken as a pilot study to determine the extent to which geohazard information could be obtained from the interpretation of satellite imagery available through online mapping databases. The value of such an approach is that it provides a technique that a) can be applied at minimal cost by other practitioners who have the appropriate interpretation skills and b) derives basic geomorphological and geohazard information for use by urban and infrastructure planners under conditions where no other relevant data exist. The ground truthing exercise allowed some of the satellite interpretation to be improved, thereby increasing its accuracy and providing important supplementary field information, including apparent depth and composition of deposits, activity of geohazard processes and observable impacts to land use, infrastructure and buildings.

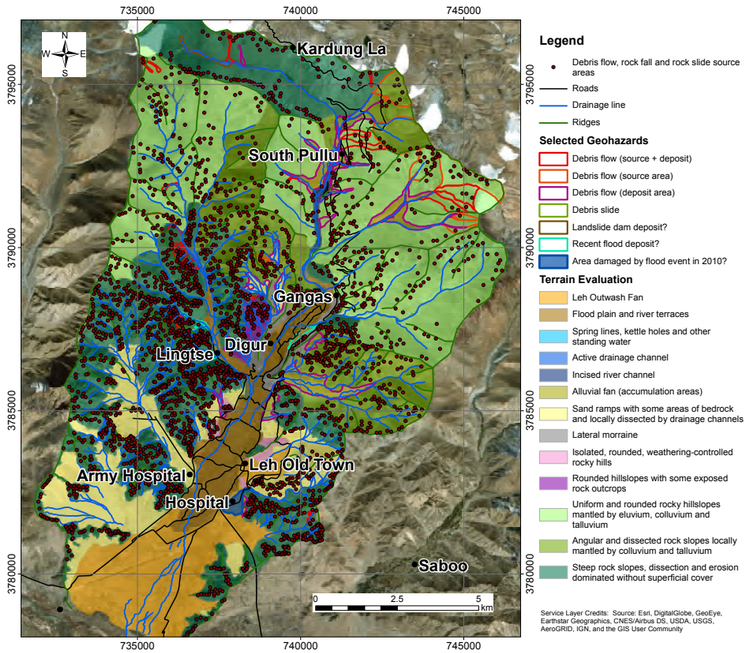

Figure 7: Summary Geomorphology at 1:50,000 Original Scale.

Discussions with residents and other local informants provided valuable historical and human context to the assessment of risk. The next stage in taking this pilot study forward will be to perform a more rigorous ground truthing exercise in order to be able to quantify the reliability of the satellite interpretation and develop a formalized set of guidelines for landform and geohazard identification, classification and delimitation. Importantly, however, one of the main constraints on the wider use of techniques such as these is the interpretation skills of available practitioners to carry out the work. This pilot study was undertaken by remote sensing and geohazard specialists with over twenty years of experience in mountain terrain, and it cannot be expected that such skills will be available to those seeking to extend the technique into other areas. However, any skill shortages can be addressed through training and selection of the most suitable personnel to carry out the work. Another issue concerns the interface between remote sensing and fieldwork. All too often (GIS-based) geohazard susceptibility mapping is carried out primarily from desk study with little or no regard to conditions on the ground and the factors that control levels of hazard. In the Leh study, the desk study provides very useful terrain classification and geomorphological mapping that allows a) broad identification of geohazard areas and b) more detailed field investigations to become focused. The Leh District Disaster Management Plan is currently in the process of being updated and expanded by the Leh District Disaster Management Authority. Similar plans will also be required for other parts of the province and the wider State of Jammu and Kashmir. Desk study interpretations, such as those outlined here, can provide vital supporting information for these plans, helping to focus attention on critical hazards and critical areas. One important point to bear in mind is the fact that localised sources of hazard, such as those illustrated in Figure 11, can usually only be identified in the field, and there is no substitute for 'experienced boots on the ground'.

Alluvial fans (coarse-grained - debris)

Figure 8: Debris Fans Mapped From Satellite Imagery and Confirmed by Ground Truthing.

6. Conclusions

Prior to the 2010 floods and debris flows there was very little published information concerning the geohazards affecting urban and rural populations, infrastructure and development in Ladakh. Since the 2010 event, there has been a flurry of publications on the subject, including this one. It takes a disaster such as the 2010 event to focus geohazard minds on the situation, and it is unfortunate that there seems to have been little research or even publicised awareness of these geohazards prior to the event. This situation must not be replicated elsewhere. Remote sensing must be used to its fullest capacity in the provision of data for geomorphological and geohazard interpretation, risk assessment and risk management. The studies described in this paper were based on rapid remote sensing and field assessment, but nevertheless have yielded extremely useful outputs for use in Leh and other districts through wider application. While the 2010 event itself would not have been predictable from this mapping, the mapping does allow potential geohazard source areas and vulnerable infrastructure and urban areas to be identified.

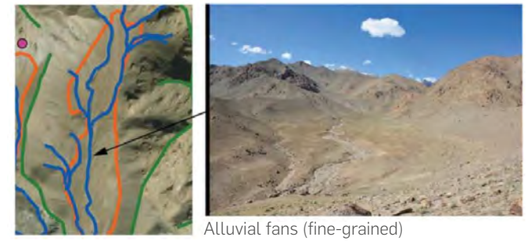

Alluvial fans (fine-grained)

Figure 9: Fine-Grained Alluvial Fans Mapped From Satellite Imagery and Confirmed by Ground Truthing.

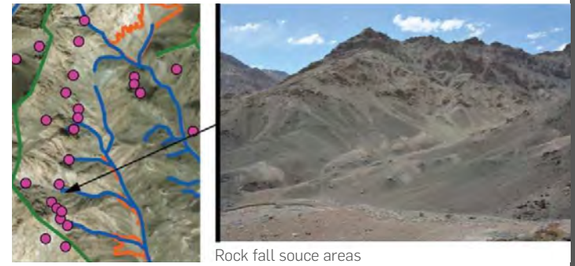

Rock fall souce areas

Figure 10: Rock Fall Source Areas Mapped From Satellite Imagery and Confirmed by Ground-Truthing

River scour and damage to roads and services

Loss of road access and high sediment loads

Wedge failure in rock slope below palace

Rock fall/debris flow - housing interface

Figure 11: Geohazard Details Not Identified From the Satellite Imagery

Table 1 Summary of the Terrain Unit Descriptions and Geohazard Implications

(Note That Some of the Small Hills Are a Source of Rock Fall/Slide Hazard (e.g. Figure 11).

Terrain Unit	Description	Primary Geohazard Sources & Exposure
Leh outwash fan	Large, relatively flat area that was formed by the building up of material washing out from the catchment area above Leh. Includes numerous drainage channels and flood plains, as well as some river terraces. Underlays much of the area on which the town of Leh is located, including the airport and hospitals, etc.	Impact from flood events initiating further up stream
Drainage channels and incised river channels	Predominantly ephemeral drainage channels. Vegetation often found along margins. Some sections appear to be incised, possibly due to tectonic and/or climate-controlled base level changes.	Flood events and debris flows within the channels, with impacts felt downstream from source areas (distance of impact depending on magnitude of events).
Flood plains and river terraces	Areas adjacent to drainage channel formed by sediment deposition. Areas higher up in the valleys often used for agriculture. Areas in the lower valleys are used for housing (e.g. northern parts of Leh) and agriculture.	Debris flows and flood events that overtop the drainage channel and travel over adjacent areas. Impact from floods or debris flows if located within or immediately adjacent to channels.
Alluvial fans (accumulation areas)	Mostly relatively large alluvial fan deposition areas, but may also contain some source areas, which sometimes can become difficult to differentiate as they erode or are built over. Often with very little or no vegetation.	Debris flows and rock falls. Impacts occur in fan accumulation areas. Much of the devastating impacts of the 2010 event were likely due to debris flows.
Sand ramps	Large areas of aeolian deposits, some containing distinct sand dunes. Undulating surface with drainage channels forming around the margins. Can be difficult to distinguish between these & alluvial fans. Usually very little or no vegetation.	Sand flows plus rock falls and debris flows from adjacent slopes.
Lateral moraines	Distinct linear ridge features within the valley areas, comprising debris formed by past glacial activity. Often seen truncating tributary valleys and occasionally diverting drainage channels. Little or no vegetation.	Impact from minor landslides occurring within the moraine materials.
Isolated, rounded, weathering-controlled rocky hills	A small number of rocky hills located within Leh. Often used for Stupas and other religious monuments.	Minor rock fall activity on slopes.
Rounded hillslopes with some exposed rock outcrops	Distinct area of relatively 'rounded' topography with areas of exposed bedrock, immediately to the north of Leh. Source areas for debris flows, showing characteristic debris flow features (source, channel, levees and fan areas). Dissected by drainage channels and erosion gullies. May contain a few 'sand ramps' and/or alluvial fans. Mixture of bare rock and talus slopes.	Debris flows, floods. Impact from floods or debris flows if located within or immediately adjacent to drainage channels.
Uniform rounded rock slopes mantled by eluvium, colluvium and taluvium	Mountain slopes with relatively uniform and rounded topography mantled by eluvium, colluvium and taluvium. Generally confined to the highest catchments. Some gullies on upper slopes are source areas for debris flows and other landslide activity (rock falls, rock slides, etc.). Some small areas of exposed rock but limited in extent. Some vegetation cover.	Rock falls, debris flows and snow avalanches. Impact from rock falls and avalanches immediately below rock faces. Impact from debris flows if within drainage channels and downstream from source areas.
Angular dissected rock slopes locally mantled by colluvium and taluvium	Mountain slopes with predominantly rocky topography, locally mantled by colluvium and taluvium, and heavily dissected by drainage channels and erosion gullies. These are the source areas for debris flows and other forms of landslide activity (e.g., rock falls, rock slides, etc.). Little or no vegetation.	Rock falls, rock avalanches, debris flows and snow avalanches. Impact from rock falls and avalanches immediately below rock faces. Impact from debris flows if within drainage channels and downstream from source areas.
Steep rock slopes, dissected and erosion dominated without superficial cover	Areas of steep rock slopes, dominated by erosion activity, including dissection by streams and erosion gullies. These are the source areas for debris flows and other forms of landslide activity (e.g., rock falls, rock slides, etc.). Lower slopes may be mantled by colluvium and taluvium. Close to Leh, these areas often contain large 'sand ramps'. Little or no vegetation.	

References

[1] R. Ashrit, Investigating the Leh 'cloudburst'. National Centre for Medium Range Weather Forecasting Ministry of Earth Sciences A50, Sector 62, NOIDA – 201307, India, 2010.

[2] S.C. Bhan, A.K. Devrani, V. Sinha, An analysis of monthly rainfall and the meteorological conditions associated with cloudburst over the dry region of Leh (Ladakh), India, Mausam 66 (1) (2015) 107–122.

[3] C.M. Bhatt, G.S. Rao, P. Manjusree, V. Bhanumurthy, Potential of high resolution satellite data for disaster management: a case study of Leh, Jammu & Kashmir (India) flash floods, 2010. in: Geomatics, Natural Hazards and Risk, 2, 4, 365-375. DOI:10.1080/19475705.2011.580014, 2011.

[4] J.M. Dortch, L.A. Owen, W.C. Haneberg, M.W. Caffee, C. Dietsch, U. Kamp, Nature and timing of mega-landslides in northern India, Quaternary Science. Reviews, 28 (2009) 1037–1056.

[5] J.M. Dortch, L.A. Owen, M.W. Caffee, Quaternary glaciation in the Nubra and Shyok valley confluence, northernmost Ladakh, India, Quaternary Research, 74 (2010) 132–144, https://doi.org/10.1016/j.yqres.2010.04.013.

[6] C. Ghosh, S. Parkash, Cloud burst induced debris flows on vulnerable establishments in Leh, Indian Land. 3 (2) (2010) 1–6.

[7] G.J. Hearn, D. Shilston, Terrain geohazards and sustainable engineering in Ladakh, India, Quarterly Journal of Engineering Geology and Hydrogeology, 50 (3) (2017) 231–238, https://doi.org/10.1144/qjegh2016-143.

[8] A.L. Henderson, Y. Najman, R. Parrish, D.F. Mark, G.L. Foster, Constraints to the timing of India-Eurasia collision: a re-evaluation of evidence from the Indus Basin sedimentary rocks of the Indus-Tsangpo Suture Zone, Ladakh, India, Earth-Science Reviews, 106 (3–4) (2011) 265–292, https://doi.org/10.1016/j.earscirev.2011.02.006.

[9] D.E.J. Hobley, H.D. Sinclair, S.M. Mudd, Reconstruction of a major storm event from its geomorphic signature: the Ladakh floods, 6 August 2010, Geology, 40 (6) (2012) 483–486, https://doi.org/10.1130/G32935.1.

[10] A. Jarvis, H.I. Reuter, A. Nelson, E. Guevara. Hole-filled seamless SRTM data V4. International Centre for Tropical Agriculture (CIAT), 2008.

[11] N. Juyal, Cloud burst-triggered debris flows around Leh, Current Science, 99 (9) (2010) 1166–1167.

[12] N. Orr, L. Owen, M.K. Murari, S. Saha, M.W. Caffee, The timing and extent of quaternary glaciation of Stok, northern Zanskar Range, Trans-Himalaya, northern India, Geomorphology, 284 (2017) 142–155, https://doi.org/10.1016/J.geomorph.2016.05.031.

[13] L.A. Owen, M.W. Caffee, K.R. Bovard, R.C. Finkel, M.C. Sharma, Terrestrial cosmogenic nuclide surface exposure dating of the oldest glacial successions in the Himalaya Orogen: Ladakh Range, Northern India, Geological Society of America Bulletin, 118 (2006) 383–392.

[14] R.K. Pant, N.R. Phadtare, L.S. Chamyal, N. Juyal, Quaternary deposits in Ladakh and Karakoram himalaya: a treasure trove of the palaeoclimate record, Current Science, 88 (11) (2005) 1789–1798.

[15] B. Phartiyal, A. Sharma, R. Upadhyay, Ram-Awatar, A.K. Sinha, Quaternary geology, tectonics and distribution of palaeo- and present fluvio/glacio lacustrine deposits in Ladakh, NW Indian Himalaya e a study based on field observations, Geomorphology 65 (2005) 241–256.

[16] M.P. Searle, K.T. Pickering, D.J.W. Cooper, Restoration and evolution of the intermontane Indus molasse basin, Ladakh Himalaya, India, Tectonophysics 174 (1990) 301–314.

[17] A. Stolle, M. Langer, J.H. Blothe, O. Korup, On predicting debris flows in arid mountain belts, Global and Planetary Change 126 (2015) 1–13, http://doi.org/10.1016/j.gloplacha.2014.12.005

[18] V.C. Thakur, Indus Tsangpo suture zone in ladakh—its tectonostratigraphy and tectonics, Proceedings of the Indian Academy of Sciences (Earth and Planetary Sciences) 99 (2) (1990) 169–185, https://doi.org/10.1007/BF02839388.

[19] R. Thayyen, A.P. Dimri, P. Kumar, G. Agnihotri, Study of cloudburst and flash floods around Leh, India during August 4-6, 2010, Natural Hazards 65 (2013) 2175–2204, https://doi.org/10.1007/s11069-012-0464-2.

[20] A.D. Ziegler, S.I. Cantarero, R.J. Wasson, P. Srivastava, S. Spalzin, W. Chow, J. Gillen, A clear and present danger: ladakh's increasing vulnerability to flash floods and debris flows: tourism and vulnerability to floods, Hydrological Processes, 30 (22) (2016) 4214–4223, https://doi.org/10.1002/hyp.10919.

Acknowledgements

The authors would like to thank the Institute for Risk and Disaster Reduction (University College London, UK), and in particular P. Sammonds, and the Institute of Energy Research and Training (University of Jammu, India), for organising the workshop and fieldwork associated with the Global Challenge Research Fund (GCRF) research programme 'Increasing Resilience to Environmental Hazards in Ladakh', which is jointly funded by the Natural Environment Research Council (NERC), the Arts & Humanities Research Council (AHRC) and the Economic & Social Research Council (ESRC) (grant no. NE/ P016138/1).

The authors acknowledge that the SRTM data used in this study was produced by the International Centre for Tropical Agriculture (CIAT) and obtained via the CGIAR-CSI website (http://srtm.csi.cgiar.org), and that the ASTER GDEM data used is a product developed by the United States National Aeronautics and Space Administration (NASA) and the Ministry of Economy, Trade, and Industry (METI) of Japan and was obtained via the Land Processes Distributed Active Archive Center (LP DAAC) website (https://gdex.cr.usgs.gov/gdex/).

A Hart would like to thank his employer (Atkins) for supporting his work on this project; the research undertaken by both authors was on a pro bono basis.

This paper has previously been published in the International Journal of Disaster Risk Reduction (volume 31, 2018, 789-798 - https://doi.org/10.1016/j.ijdrr.2018.07.021). The authors thank Elsevier for permission to reproduce the paper here. The authors also acknowledge that Figure 1 of this paper was originally published in the Quarterly Journal of Engineering Geology and Hydrogeology (Hearn & Shilston, 2017), and thank the Geological Society of London for permission to reproduce the figure here.

TBM U-Turning Method in an Underground Rock Cavern

Ray Chan

Technical Director
Engineering, Design and Project Management
Hong Kong, China

K.K. Cheung

Senior Engineer
Engineering, Design and Project Management
Hong Kong, China

The Association of Consulting Engineers of Hong Kong Annual Award 2018 WINNER

Abstract

This paper presents Hong Kong's first application of a Tunnel Boring Machine (TBM) U-turning method in an underground rock cavern (23m high x 22m width x 40m long), in order to excavate two tunnel tubes,whereby the normal practice is to relaunch the TBM from its original launching point which involves the tasks of dismantling, transporting and reassembly.

The scope of this project is to build 4.8km long, dual two-lane road tunnels in which an underground rock cavern is constructed in the middle of the tunnel for ventilation purposes. An innovative solution was devised to allow the large, 14.1m-diameter TBM to make a historical U-turn within the cavern. This operation involved the enlargement of the conforming underground rock cavern and tunnel section.

This paper discusses the technical issues associated with the construction of tunnels and of rock caverns to support a U-turning method along with the various ground conditions for future TBM relaunching projects, from planning stage to construction stage.

Keywords

Tunnel Boring Machine; U-Turning Cavern

1. Introduction

Effective and efficient cross-border transport infrastructure is believed to be essential in facilitating collaboration and economic growth of the Greater Bay area. A series of major transport infrastructure connecting Hong Kong and Mainland China is currently under construction, including the Liantang/Heung Yuen Wai Boundary Control Point, which is going to be the 7th land crossing facility between Hong Kong and Shenzhen. The aim of the project is to significantly shorten travel time within the region, supporting connectivity and accessibility.

Atkins (the Contractor's Designer) was appointed by Dragages Hong Kong Limited (the Contractor) and is proud to have been delivering a key section of the Liantang/Heung Yuen Wai project since December 2013. The major contract, with a total sum of GBP 1.03billon, has already set a number of records for the tunneling industry in Hong Kong: the 4.8 km Lung Shan Tunnel will be the longest twin tube land road tunnel in Hong Kong, and the project engages the largest earth pressure balance (EPB) TBM in Hong Kong, with a diameter of 14.1m. Following breakthrough of the southbound tunnel section on March 2017, the TBM went on to complete a 180-degree U-turn for the construction of the northbound section just three months later. It is the first time in Hong Kong that a TBM has completed a U-turn in a specially-designed rock cavern. The usual practice of a TBM drive to excavate twin tunnel tubes is to dismantle the TBM prior to being transported back and set up again at its original launching position. A TBM U-turn enabled the construction progress to remain in line with the tight programme. Also, work was conducted underground to minimize environmental impact to the public by eliminating TBM transportation and set up for relaunching. The innovative approach, which was applied for the first time in Hong Kong, brings overall savings to the project.

This challenging project demonstrates excellence and innovation in design and construction. Close collaboration between designer and contractor is another key success factor. This paper aims to showcase the technical challenges and innovative solutions for a TBM U-turn operation.

2. Project Background

The objective of the project is to construct 4.8km long dual two-lane carriageway tunnels, i.e. 2 tunnel tubes, with tunnel sizes from 13m to 18m in span/diameter. Due to extremely difficult ground conditions, the project has applied various tunnel excavation methods, including mining, drill-&-blast and TBM concurrently, at different work sites. Extensive site formation was required at tunnel portals which was beneficial to the programme.

Facing a tight project programme, a team of tunnel experts conceived numerous innovative construction methods and Atkins' international expertise in engineering and design allowed them to be put into practice.

One innovative idea was to design and construct the underground rock ventilation cavern for the 180-degree TBM U-turn operation, the first time this has been attempted in Hong Kong. This key milestone in Hong Kong's tunneling history was successfully achieved in mid-2017. Following the completion of the first TBM drive along the southbound tunnel from the North Portal (NP), the approach taken was to then U-turn the TBM within the cavern and start the second drive along the northbound tunnel towards the NP, as opposed to restarting the drive anew from NP. The TBM was successfully relaunched and the tunnel excavation was completed in April 2018. This innovative solution and design were vital to achieving completion within the tight programme. This feat also demonstrates that Hong Kong's tunneling expertise and design has reached world-class status.

3. Development of the Innovative TBM U-Turn Cavern

As the TBM section is the contractor's design and the tender allowed the contractor to propose an alternative design for the permanent tunnel section, the team made a critical decision to extend the TBM section close to the cavern location and plan for the TBM U-Turn in Cavern, i.e. Mid-Ventilation Junction (MVJ), to relaunch for the NB excavation, see Figure 2.

Figure 1: Site Location

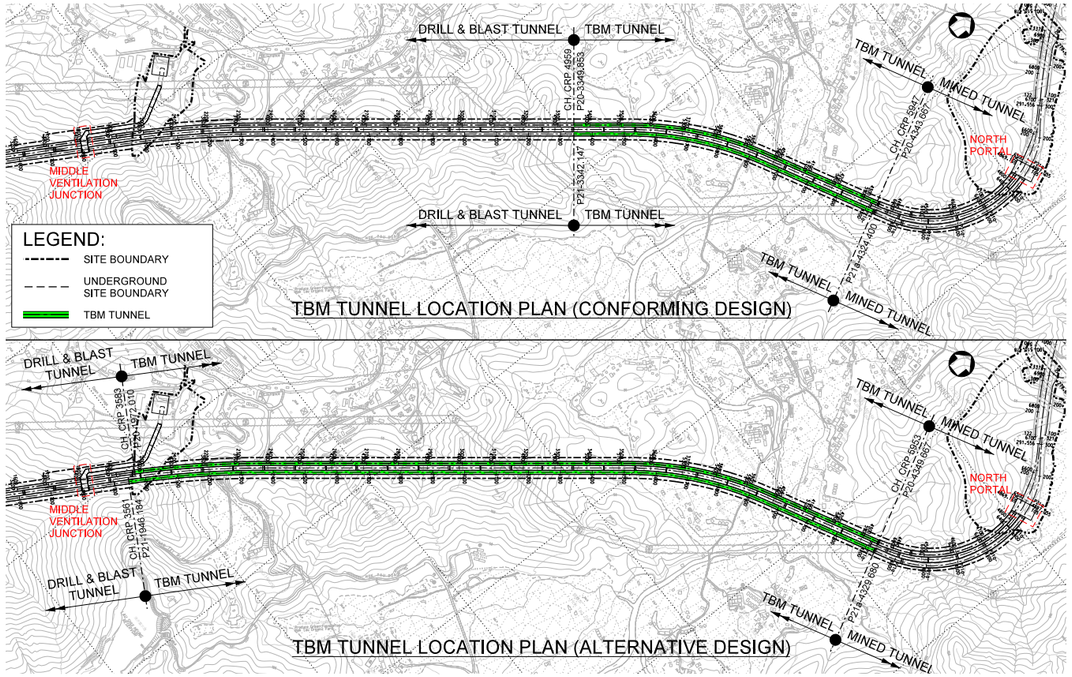

Figure 2: TBM Extent – Conforming Design (Upper) vs Alternative Design (Lower)

With this alternative solution, we can successfully achieve significant benefits for the project:

a) Mitigate adverse ground conditions - Poor ground conditions for the long tunnel section between MVJ and the conforming TBM tunnel end point were anticipated. If mined excavation were adopted, heavy temporary support with substantial grouting was expected. Our proposed engineering solution is to extend the TBM section. This eliminates the need for extensive temporary support and enhances work safety.

b) Permanent work space for TBM U-turning – The designer duly considered the spatial requirements for the U-turning scheme. We made use of the underground space to serve two key purposes i.e. permanent cavern lining and the TBM U-turn operation. The cavern excavation profile was optimized to meet functional requirements while preventing unnecessary excavation.

c) Critical path optimization - Significant time is saved because the second drive can be started earlier and it eliminates the need to disassemble, transport TBM components, and reassemble at the initial launching site.

d) Minimise public nuisance - Transporting the TBM components back to NP inevitably requires traveling on the rural Sha Tau Kok road. Transportation of large TBM components is usually permitted at midnight and is subject to approval by relevant authorities. The U-Turning method could avoid public nuisance and minimise liaisons with relevant authorities.

4. Alternative Design to Accommodate the TBM U-Turn Operation

The TBM U-Turn Cavern layout - a 23m high, 22m span, 40m long cavern - one of the largest caverns ever built in Hong Kong to accommodate the large TBM passing through. The first TBM drive was planned to breakthrough 90m away from the cavern. This 90m tunnel was excavated with an enlarged profile to sufficiently accommodate the TBM's passage.

To minimize the excavation profile of this 90m tunnel section, the designer worked out spatial requirements for creating a corridor to pull the TBM toward the cavern for the TBM U-turn from the breakthrough location. This allowed spaces for working access and logistics maintained on both sides of the TBM shield. The space required for TBM pulling was determined together with the

Figure 3b: TBM breakthrough at Southbound Tunnel

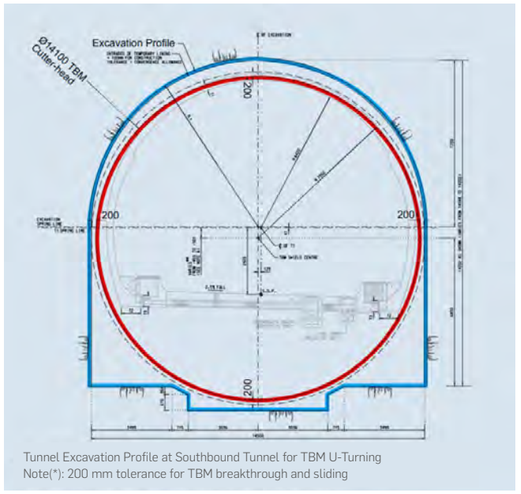

Tunnel Excavation Profile at Southbound Tunnel for TBM U-Turning
Note(*): 200 mm tolerance for TBM breakthrough and sliding

Figure 3a: Excavation Profile of Southbound Tunnel

permanent tunnel lining and thus the enlargement profile has been designed as a "best fit" for the giant TBM. Figures 3a and 3b present a typical excavation profile for the TBM sliding corridor and TBM breakthrough at the Southbound Tunnel (SB) after the completion of the TBM's first drive. A numbers of heavy supports on the TBM cradle were designed to facilitate the over 2400-ton TBM's sliding and jacking operation. A jacking system was installed on the support to allow the lateral movement of the TBM without having to build permanent segments behind it.. Therefore, the TBM does not need to be dismantled after the breakthrough. The overall sequence of the TBM U-turn operation is shown in Figures 4a and 4b.

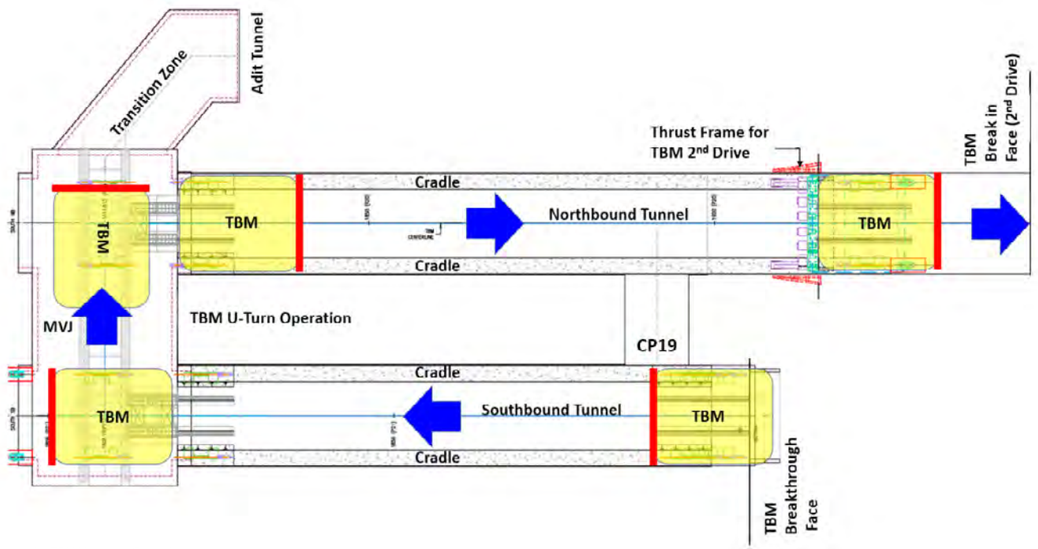

Figure 4a: TBM U-turning Operation

5. Excavation Work for the TBM U-Turn Operation

The excavation work was paramount to the TBM U-turn operation. The excavation profiles and sizes of MVJ, NB and SB tunnels were revised to suit the dimensions of the TBM and other necessary equipment to complete the U-turn operation. The excavation work commenced from the the Middle-Ventilation Adit (MVA) towards MVJ, and then to the TBM breakthrough face and break in face for the second drive at the SB and NB tunnels respectively, see Figure 5. Optimizing excavation profiles and temporary supports corresponding to various ground conditions were one of the designer's utmost challenges.

The designer studied and interpreted existing ground data such as mapping records of the MVA and drillhole records, to predict the ground conditions along the NB and SB tunnels to create cost-effective designs. Different temporary support provisions which include shotcrete with pattern rock bolts/lattice girders/steel ribs were designed to accommodate the varying ground conditions encountered, i.e. from hard rock to fault zone/sheared zone. The excavation profile, in particular the tunnel section within thefault zone, were revised to suit the latest scheme. The excavation profile of the side walls ofthe the tunnel were therefore revised from curvedd to straight which induced significant bending moment on the wall supports due to undesirable geometry.

Figure 4a: Photos of TBM U-turning Operation. Photo credits to DHK

The analysis was carried out with the aid of a finite-element computer programme PLAXIS in which the ground materials are modelled based on Mohr-Coulomb failure criteria. The convergence-confinement approach was adopted for the analysis which involves the interaction between ground relaxation and the timing of support installation.If we quite simply install the support immediately after tunnel excavation without permitting any ground movement, the required support pressure will be be the thesame as the in-situ ground stress. Conversely, if we allow certain ground movement before the the installation of temporary support, the required support pressure will be reduced to achieve a cost-effective design, see Figure 6. The timing of support installation could be correlated to the advance length for each round of excavation. The corresponding ground relaxation under specified advance length for analysis therefore could be determined, see Figure 7. Pre-supports such as canopy tubes or spile bars were installed around the tunnel roof before the commencement of excavation. The pre-supports had been extended along the tunnel during excavation and are used for stabilizing the excavated face, before the installation of temporary lining, in both transverse and longitudinal directions with an arch-like reinforced zone. Although staged excavation (i.e. 2 stages namely top heading and bottom bench) has been applied to the tunnel, the height of the tunnel for excavation is still over 7m where face nails were installed to stabilize the face.

The excavation sequence of twin tunnel tubes would affect stress distributions. The designer duly considered ground-structure interaction, the tunnel tubes excavation sequence and ground relaxation under specified unsupported length for each round of excavation in the numerical analysis to simulate as many situations as possible, see Figure 8

The temporary supports applied within the fault zone have been successfully installed and completed on time for theTBM U-turn and the second drive. The photo of the NB tunnel within the fault zone is shown in Figure 9.

Figure 4b: Photos of TBM U-turning Operation. Photo credits to DHK

The designer proactively reviewed the ground conditions given by the contractor and carried out real-time interaction with the contractor's site team. Tunneling, monitoring and design review were integrated throughout the excavation process so as to quickly resolve urgent site issues and streamline the overall construction programme.

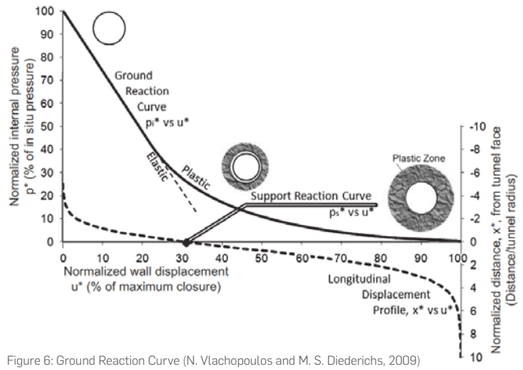

Figure 6: Ground Reaction Curve (N. Vlachopoulos and M. S. Diederichs, 2009)

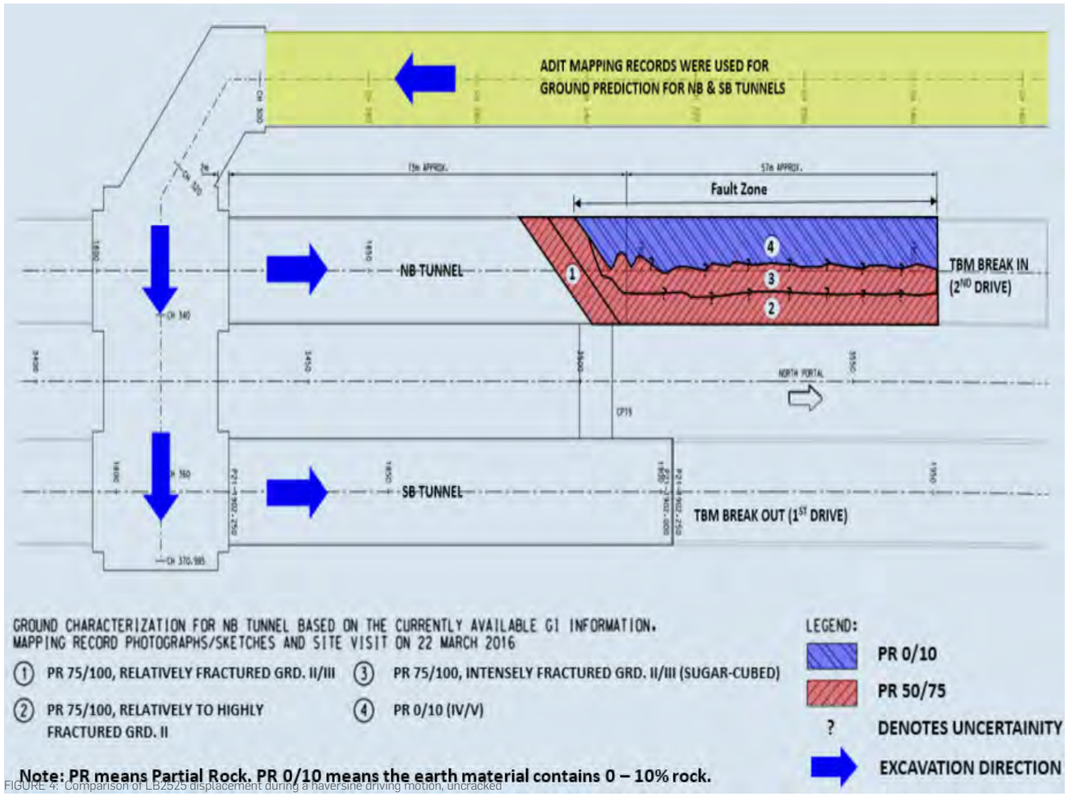

FIGURE 4: Comparison of LB2525 displacement during a haversine driving motion, uncracked

Figure 5: Excavation Sequence for the TBM U-Turn Operation

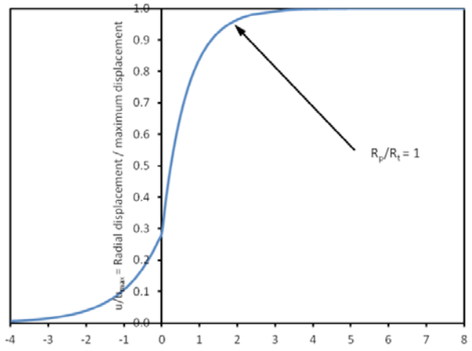

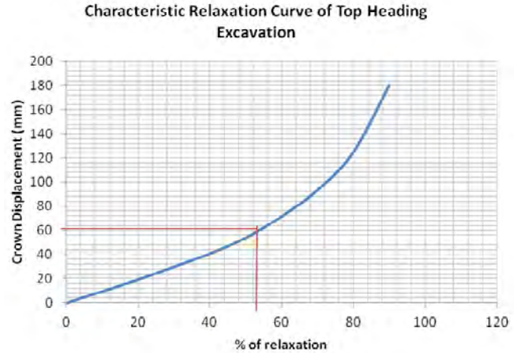

Figure 7: Longitudinal Displacement Profile (left); Characteristic Relaxation Curve (right)

6. The Narrow Rock-Pillar Design at Tunnel Cavern Junctions

Another key design challenge is to ensure the stability of the rock pillar located at the intersection of the MVA, the cavern and the NB tunnel, see Figure 10. In general, the width-to-height ratio of the rock pillar is designed within a range from 0.5 to 1.5 to avoid it from overstressing. After revising the profile for the TBM U-turn scheme, the overall tunnel height was substantially increased making the pillar over 12m high.. The width-to-height ratio became a minimum of only 0.2. This pillar ratio is extremely small and may cause significant tunnel stability issues.. Additionally, the rock pillar is subject to ground loading from the adjacent main tunnels, MVA and the large-span cavern.

As suggested by Hoek (2007), "...it is useful to consider the overall behaviour of a rock mass rather than the detailed failure propagation process... For example, when considering the strength of a pillar, it is useful to have an estimate of the overall strength of the pillar rather than a detailed knowledge of the extent of fracture propagation in the pillar". Therefore, the pillar stability is given as an average rock mass strength to induced stress ratio and a recommended Factor of Safety shall be achieved for the overall pillar stability.

The strength of the pillar is correlated to the in-situ stress using Generalised Hoek-Brown criterion for jointed rock mass as shown below::

$$\sigma_1' = \sigma_3' + \sigma_{ci}\,[m_b\,\sigma_3'/\,\sigma_{ci} + s]^a$$

where σ_1' and σ_3' are the maximum and minimum effective principal stresses at failure;
m_b is the value of the Hoek-Brown constant m for the rock mass;

s and a are constant which depend upon the rock mass characteristics; and

σ_{ci} is the uniaxial compressive strength of intact rock.

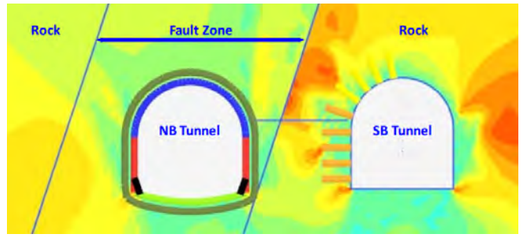

Figure 8: Numerical Analysis for Tunneling within Fault Zone

Figure 9: Photos of NB Tunnel – Top heading and bench

Furthermore, the strength of rock mass, σ_1', could be enhanced by confining pressure (σ_3') which could be contributed by the temporary support e.g. rock bolts apart from the in-situ stress.

The ground condition was reviewed, and the designer proposed to adopt a staged approach whereby excavation-induced stress-redistribution to surrounding rock mass would occur in a step-by-step fashion. Temporary rock pillar support is installed as soon as possible so that the ground load can be transferred onto to the support prior to substantial rock relaxation occurring. In addition, the designer also limited the maximum pull length in each excavation. A series of comprehensive computer analyses, using PHASE2 (for rock mass induced failure) and U-DEC (for rock joints induced failure), were performed to predict the pillar stability. Through bolt was finally proposed and the plan was successfully executed on site.

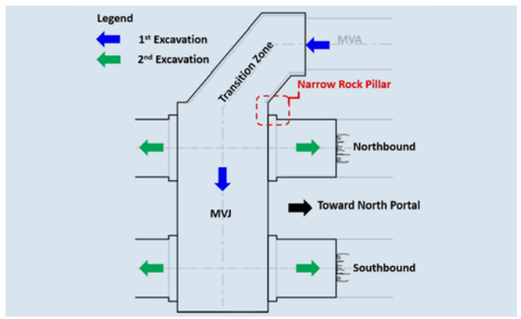

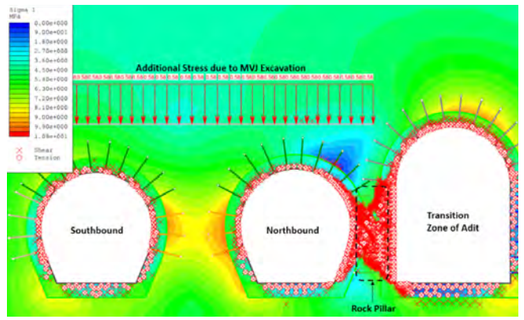

Figure 10a: Layout Plan of Narrow Rock Pillar (left); Figure 10b: Numerical Analysis for Rock Pillar – PHASE2 (right)

7. Detailed Permanent Cavern Design

The excavation profile was revised so as to facilitate the passage and U-turning of the mega TBM and the permanent cavern was redesigned to serve the needs of the operation. Both the permanent lining as well as the internal structures were redefined from the conforming design. The cavern acts as a ventilation junction with the MVA and complex ventilation duct geometry needs to be considered at the interface with the main tunnels. A number of E&M function rooms were properly reviewed and sized in accordance to permanent work requirements. Colossal efforts were made to ensure that the design had gone through lengthy discussions and coordination with various interested parties. Permanent linings of mega-sized caverns require a complicated sequence of construction works and temporary stability was a primary concern of the designer. A structural analysis was performed for different loading conditions, see Figure 11. To maximize work efficiency, the design allows the work teams performing tunnel construction and those preparing the TBM U-turn operation to work simultaneously. The project demonstrates how a contractor's designer benefits the construction process in detailed design-build work.

8. Cross Passage (CP) 19 Design

Apart from the MVJ and the associated tunnel sections for the TBM U-turn operation CP 19, a CP next to the MVJ, was enlarged for

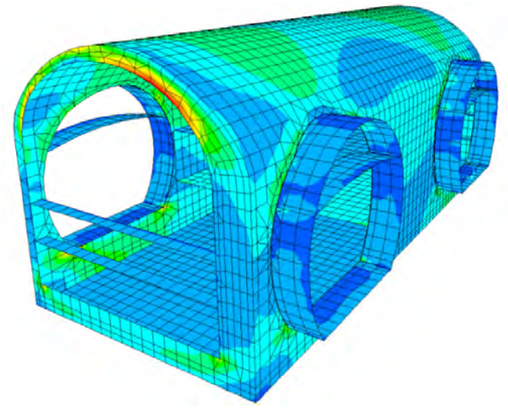

Figure 11: Numerical Analysis for MVJ

maintaining site logistics during the U-turn operation which is another key success factor.. CP 19 was envisaged to be located within rock according to Ground Investigation data. Cast-in-situ permanent lining was adopted for CP19 which was excavated using a drill-&-blast method. The internal size of this CP was 6m wide x 3.65m high and the original excavation size was planned to be 7m wide x 4.15m high (before enlargement). However, this CP was used for logistical purposes and to house both TBM traffic and the conveyor belt during construction, which resulted in an enlarged excavation profile of 9.3m wide x 8.6m high. The enlarged excavation profile is shown in Figures 12 and 13 below.

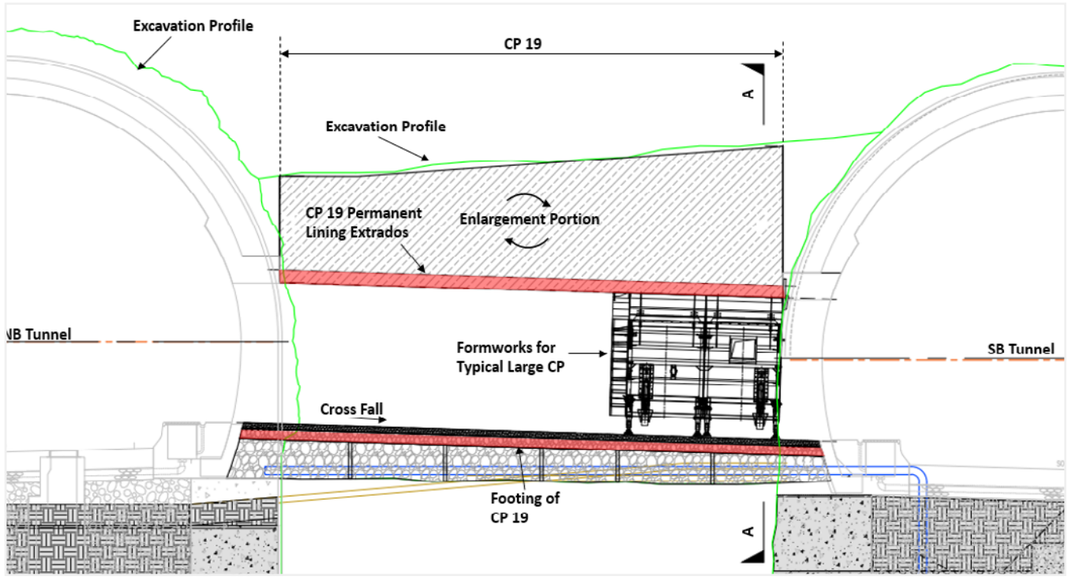

Figure 12: Excavation Profile along CP19

Various options were studied for the permanent case to accommodate this enlarged excavation profile, such as increasing the CP internal height or using low-density concrete to fill the void above the CP crown. In the end, it was decided to remain loyal to the original CP internal height of 3.65m with normal in-situ reinforced concrete permanent lining due to the following advantages:

1. Consistency of CP dimensions with all other large CPs;
2. Utilization of conventional CP formwork used for other large CPs; and
3. Eliminates the need to obtain approval from the engineer and future maintenance group that would result from a CP dimension/size change.

However, this option also came with the following challenges:

1. Large amounts of concrete are needed to fill the enlarged excavation;
2. A thick concrete section would require shrinkage control and early-age thermal cracks control; and
3. Robust formwork would be needed to cater to such a thick concrete section (up to 4m thick).

To overcome shrinkage and early age thermal cracks, it was proposed to divide the concrete pouring to a maximum of 1.0m thick sections above the crown. A252 wire mesh is provided between two concrete pours for early age thermal crack control. This splitting of concrete pours offered the added advantage of using CP formwork since the strength of the previously poured concrete can be used to support the next concrete pour.

Also, the structural lining thickness was increased by using the over-excavated space. This helped to optimize the level of reinforcement.

Using the above described measures, the CP19's permanent lining was successfully and cost-effectively constructed while still maintaining the same internal shape and dimensions as conventional CPs.

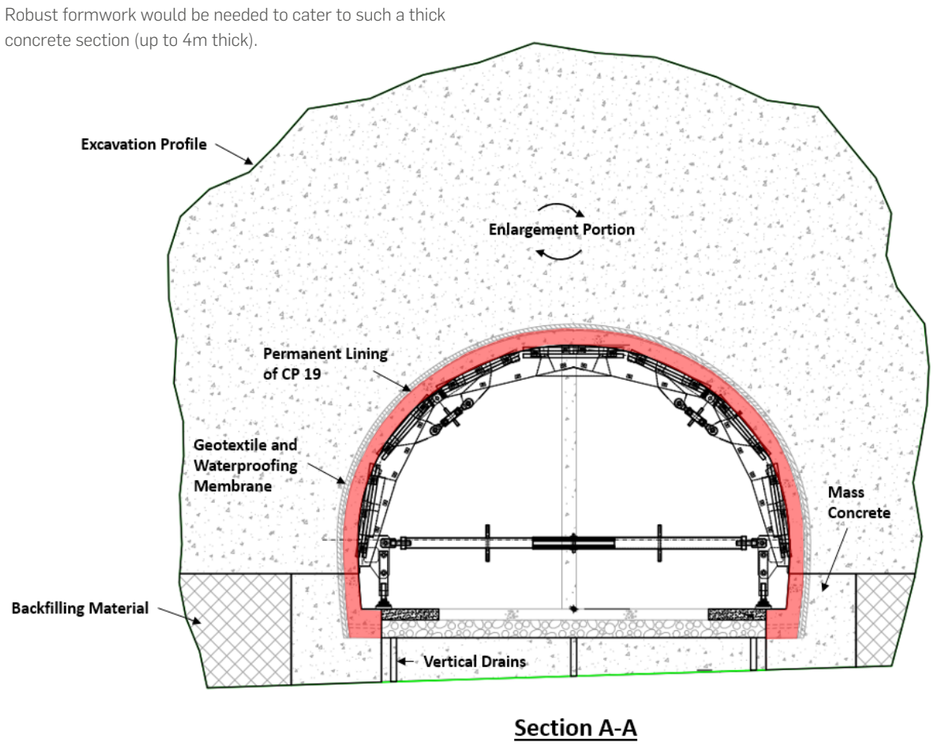

Figure 13: Cross Section of Enlarged CP19

References

Barton, Lien and Lund (1974) "Engineering Classification of Rock Masses for the Design of Tunnel Support".

Barton (2002). "Some new Q-value Correlations to assist in Site Characterisation and Tunnel Design".

Geotechnical Engineering Office (1988), GEOGUIDE 3, Guide to Rock and Soil Description; Civil Engineering Department, Hong Kong

Geotechnical Engineering Office (1992), GEOGUIDE 4, Guide to Cavern Engineering; Civil Engineering Department, Hong Kong

Grimstad and Barton (1993). "Updating the Q-system for NMT"

Hoek, E. (1999). "Support for Very Weak Rock Associated with Faults and Shear Zones". International Symposium on Rock Support and Reinforcement Practice in Mining, Kalgoorlie, Austria, 14-19 March, 1999.

Hoek, Carranza-Torres and Corkum (2002). "Hoek-Brown Failure Criteria – 2002 Edition" 5th North American Rock Mechanics Symposium and the 17th Tunnelling Association of Canada Conference, Toronto, Ontario, Canada, 2002.

Hoek: Practical Rock Engineering, 2007

Hoek et al. (2008), 'Integration of geotechnical and structural design in tunnelling'.

N. Vlachopoulos, M.S. Diederichs (2009) "Improved Longitudinal Displacement Profiles for Convergence Confinement Analysis of Deep Tunnels"

Yoshinao Muraki (1997), 'The Umbrella Method in Tunnelling'.

Z.T. Bieniawski (1984). "Rock Mechanics Design In Mining and Tunneling"

Summary and Conclusion

TBM U-turning work in a rock cavern is one of the greatest milestones in Hong Kong's construction industry and starts a new chapter for tunneling in Hong Kong. This innovative idea has been successfully proven and executed by a team of tunnel experts including both a design team and a site team together with the client's full support. To implement this idea, a series of project engineering challenges were resolved in sustainable and cost-effective ways. The joint communication, management and partnership among the Designer - Atkins, the Contractor -Dragages Hong Kong Limited and the ultimate client- CEDD, moved the project in the right direction, kept it on track, facilitated the exchange of real-time data, and fostered innovative solutions.

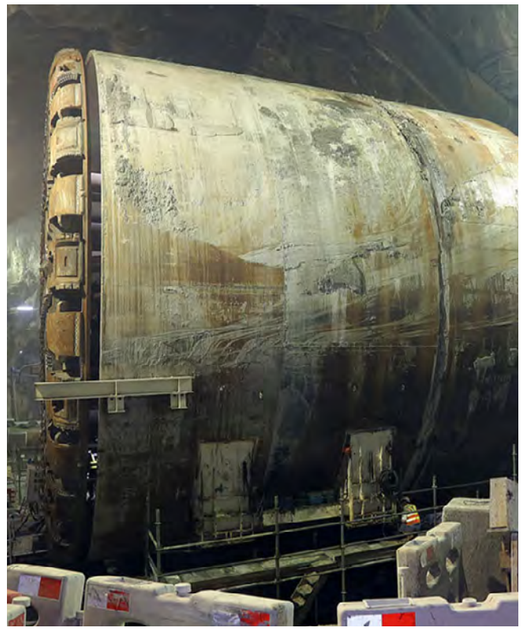

Continuous Monitoring and Adaptive Control: The “Smart” Stormwater Management Solution

Jeffrey Wright

PE, PH
Vice President, Water Practice Director
Engineering, Design and Project Management
Alexandria, VA, USA

Dayton Marchese

Water Resources Engineer
OptiRTC, Inc.
Boston, MA, USA

Abstract

Our approach to managing stormwater, and the implementation of stormwater infrastructure, hasn't kept pace with our digitally enabled environment. Since the first runoff systems designed in ancient times, moving stormwater away from our cities to protect life and property has been our primary concern—out of sight, out of mind. The engineering and science community agree: extreme weather events and climatic conditions like floods and droughts are more likely in the future. To keep up, the built environment is changing by integrating smart technologies and holistic approaches to infrastructure design and management. Regulations for the mitigation of pollution caused by urban runoff require more accuracy than in the past. Future water resources design must adapt to these new conditions. Adaptation includes using smart systems, such as continuous monitoring and adaptive control (CMAC), to repurpose our existing infrastructure and build modern systems that harness stormwater's latent value—changing what we once thought of as a liability into an asset.

Keywords

Containment Ponds, Reservoirs & Canals; Sewers & Drains; Hydrology & Water Resource

1. Introduction

Existing stormwater infrastructure is ordinarily passive and often serves a limited purpose. The design and construction of these systems rely on fixed site configurations and pre-determined static flow scenarios to provide a single management objective (e.g., flood risk mitigation, water quality improvement, or channel protection). Once constructed, the systems require perpetual operation and maintenance (O&M), with limited future benefit; in fact, they often act as a liability as communities continue to pay for antiquated benefits while modern-day costs increase. New stormwater management systems face these same design and construction limitations because they rely on the same passive design methodology and implementation to achieve current regulatory requirements, only to become substandard as environmental and regulatory conditions evolve (Barbosa et al., 2012).

Two of the dominant, and often opposing functions of stormwater infrastructure are conveyance (i.e., moving stormwater from one place to another) and storage (i.e., detaining or retaining water on-site). Stormwater conveyance infrastructure (e.g., pipe systems and channels) helps reduce localized flooding by removing water from developed areas as quickly as possible. Stormwater storage infrastructure (e.g., ponds and underground basins) provides downstream channel protection and flood risk mitigation by limiting discharge rates, and improves water quality by facilitating pollutant-removal processes prior to water being released. Developing infrastructure that meets these opposing functions has traditionally been a challenge.

Continuous monitoring and adaptive control (CMAC) systems provide a practical solution to enhance the performance and value of existing stormwater infrastructure, and increase the efficacy and efficiency of new infrastructure (Lefkowitz et al., 2016). CMAC stormwater systems leverage the communications technology known as Internet of Things (IoT) to integrate site data (e.g., water level and discharge) from field-deployed environmental sensors with real-time weather forecast information to directly monitor performance and actively control stormwater storage and flows (Figure 1). For example, a CMAC stormwater pond preparing for a future rain event would analyse the forecast storm size, compare the incoming runoff volume to the available storage capacity in the pond, and discharge water until the storm could be fully captured (Roman et al., 2017). CMAC systems are adaptive and more efficient, converting stormwater infrastructure into an asset, instead of a liability, even when considering the long-term O&M costs. Through CMAC, existing stormwater infrastructure can be enhanced or repurposed, new stormwater infrastructure can provide better benefits, and both can provide a higher return on investment (ROI) by managing more stormwater volume to the design standards.

Three significant challenges face current stormwater management systems. First, measurement and performance reporting—communities need accurate reports on performance to meet regulatory compliance requirements. Second, operations and maintenance—there is a need to reduce ongoing costs and achieve sustained performance. And third, multi-purpose management—communities need solutions that are adaptive and scalable to address changing watershed conditions and meet multiple desired stormwater management outcomes. CMAC provides a cost-effective and adaptive solution to all three challenges.

2. Measuring and Reporting Performance

Regulatory agencies will soon require communities to provide consistent, accurate and reliable data on the performance of their stormwater systems to demonstrate compliance, including metrics such as nutrient removal efficiency or peak discharge (National Research Council, 2009). Collecting, collating, and reporting this data is currently not feasible due to limited resources and technology. Common practice in stormwater management is to use design standards as proxies for performance metrics. For example, the static design volume of a stormwater detention pond can be used as a proxy for nutrient removal efficiency – larger capture volume yields a longer hydraulic residence time, resulting in a higher removal efficiency (Benjamin and Lawler, 2013). However, the use of design standards as proxies for performance assumes that after construction, stormwater infrastructure will function indefinitely as designed. Due to adverse site conditions, changing environments, and unidentified failures, this assumption of perfect functionality is often incorrect (Blecken et al., 2017), and introduces risk as the claimed level of performance is not delivered.

CMAC technology provides the necessary data for accurately recording and reporting on stormwater infrastructure performance. Because CMAC uses real-time site information – often one data point per minute per sensor (Lefkowitz, 2017) – these systems obtain high-quality performance data, efficiently collated and readily reported to regulators. CMAC's ability to provide accurate, real-time data for the performance of the system, and the source and concentration of pollutants, will give communities and regulators an unprecedented level of accuracy when evaluating the success of their stormwater infrastructure.

3. Operations and Maintenance

Current periodic or schedule-driven O&M activities are inefficient and typically result in higher maintenance costs. CMAC technology allows communities to manage their stormwater infrastructure more proactively and efficiently through targeted O&M activities. Because CMAC continuously monitors performance, anomalous behaviour (e.g., an underground basin losing water faster than expected) can be automatically identified, and targeted action (e.g., fixing an identified leak) can be taken before system failure. This targeted O&M makes CMAC systems more efficient and better maintained, thus reducing cost.

Another way in which CMAC improves O&M is through intelligent asset management. Data-driven analysis and decision making dramatically improve many routine O&M activities for managing stormwater assets, increasing uptime and decreasing O&M costs. Adaptive and proactive maintenance through the integration of asset management tracking systems allows the community to maintain assets, addressing their needs before they fail. System performance information is integrated into maintenance contractor work flows and work order management, which helps target maintenance requirements, minimizing unplanned maintenance and associated downtime by alerting staff when a facility is operating outside its expected performance limits or specifications.

4. Beyond Single-Purpose Management

One of the shortcomings of traditional stormwater infrastructure is that each facility functions for a limited purpose (flood control, channel protection, water quality, etc.), meaning that more resources (e.g., property, funding, and time) are required to meet the multiple objectives toward which many communities are now working. By installing smart technology and hardware, communities can enhance or convert existing stormwater infrastructure, improving water quality and significantly expanding capacity.

CMAC technology helps communities adapt to changing conditions, unlocking the potential to achieve multiple stormwater management goals and outcomes. Facilities that integrate CMAC can now meet many performance metrics, instead of one or two. For example, consider a dry stormwater detention pond that provides downstream channel protection and flood control, but little to no water quality benefit (Balascio and Lucas, 2009) due to having a relatively short hydraulic residence time. By implementing CMAC on a dry detention facility, water can be retained (e.g., by

automatically closing an actuated valve) during and after a storm event, thereby increasing hydraulic residence time and water quality performance, without compromising the flood control and channel protection benefits because the pond is automatically drained before the next incoming storm.

With CMAC, function and performance of stormwater infrastructure are easily modified, at minimal capital cost, thus adapting to changing climatic and hydrologic conditions. In many cases, functional modification is achieved by changing a setting in the CMAC software (e.g., programming a stormwater basin to have a longer post-event retention time or a shorter drawdown time) (Lefkowitz, 2017). Due to this programmable logic, CMAC allows the system to meet its intended performance measures and scale or adjust to new ones.

In new facilities, active and dynamic control of system performance meets stormwater management objectives more efficiently by simultaneously measuring quantity, volume and quality control. CMAC allows stormwater infrastructure to accomplish more with less—using a much smaller physical footprint, thus reducing land acquisition (or loss of developable space) and construction cost.

5. Relevant Application of CMAC

One such application of CMAC technology, developed and delivered by OptiRTC, Inc., has been successfully implemented in the City of Philadelphia, by the Philadelphia Water Department (PWD). Philadelphia is one of 860 U.S. municipalities with a combined sewer system (CSS) (see https://www.epa.gov/npdes/combined-sewer-overflows-csos), the overflows (i.e., discharge of stormwater combined with municipal waste to natural waters) from which represent a major source of water pollution. To address this issue of combined sewer overflow (CSO), Philadelphia implemented Green City, Clean Waters, a Long-Term Control plan to reduce stormwater pollution currently entering their CSS using green infrastructure. In particular, PWD, along with the Philadelphia Industrial Development Corporation (PIDC), incentivizes commercial property owners to implement stormwater mitigation solutions through the Stormwater Management Incentives Grant Program (SMIP).

In November 2016, PWD awarded SMIP grant funding for CMAC to be implemented on a 3.2-hectare commercial property within the city's combined sewer area (Lefkowitz, 2017). The property's existing retention pond was not meeting PWD's current stormwater management standards, thus contributing to potential CSOs. Implementation of CMAC included installing a real-time water level sensor in the pond, an actuated valve on the control structure, and a communications and control panel connecting the water level sensor and actuated valve to a cloud-computing platform. Programmable logic for the pond includes pre-event drawdown (i.e., opening the actuated valve before a storm to drawdown the water and create additional storage capacity) and post-event retention (i.e., closing the actuated valve during and after a storm).

A performance review of the installation after six months of operation revealed that the CMAC system exceeded PWD's criteria for wet weather discharge by completely avoiding wet weather outflow for nearly all rain events (see Lefkowitz, 2017 for supporting analysis). During the six-month period, a total 50.8 cm of precipitation fell, which is typical for Philadelphia. Using CMAC, PWD was able to keep 10,220 cubic meters of water out of the city's CSS during the storms, which accounted for 98.8 percent of total runoff on the property, while also controlling dry weather discharge effectively. By comparison, a passive system with the same hydraulic and hydrologic conditions would have only prevented 35 percent wet weather flow. The use of this technology has allowed PWD to reduce implementation time, cost, and risk while also providing the stakeholders with real-time performance data to help shape the design for future projects and increasing infrastructure resiliency in a changing environment.

7. Conclusion

Forecast-based real-time control technologies, such as CMAC, of both connected and distributed stormwater infrastructure allows for adaptive management by integrating information from field-deployed sensors with real-time weather forecast data to directly monitor performance and actively control storage and flows. Improved metrics and performance reporting via centralized, cloud-based control systems help communities predict and plan for O&M costs and comply with regulatory requirements. Moreover, CMAC allows communities to operate and maintain their infrastructure systems and components more efficiently, and achieve multiple stormwater management objectives and associated regulatory compliance targets while reducing capital and operating costs.

In the past, we designed stormwater management systems with only one purpose in mind—move the water away from our cities and structures as quickly as possible. It was an inelegant solution—short-sighted, but useful for a time. Now we can turn those "dumb" infrastructure solutions into "smart" systems—protecting our communities from flooding, increasing water quality and maintaining our stormwater systems more efficiently.

References

Balascio CC and Lucas WC (2009) A survey of storm-water management water quality regulations in four Mid-Atlantic States. Journal of Environmental Management 90(1):1-7.

Barbosa AE, Fernandes JN and David LM (2012) Key issues for sustainable urban stormwater management. Water Research 46(20): 6787-6798.

Benjamin MM and Lawler DF (2013) Water quality engineering: Physical/chemical treatment processes. John Wiley & Sons. New Jersey, USA.

Blecken GT, Hunt III WF, Al-Rubaei AM, Viklander M, and Lord WG (2017) Stormwater control measure (SCM) maintenance considerations to ensure designed functionality. Urban Water Journal 14(3):278-90.

Lefkowitz J (2017) From passive to dynamic storage. Water Environment and Technology 29(7).

Lefkowitz J, Sarmanian A and Quigley M (2016) Continuous monitoring and adaptive control—the internet of things transforms stormwater management. Journal of the New England Water Environment Association Journal 50(1): 44-51.

National Research Council (2009) Urban stormwater management in the United States. National Academies Press. Washington, D.C., USA.

Roman D, Braga A, Shetty N and Culligan P (2017) Design and modeling of an adaptively controlled rainwater harvesting system. Water 9(12): 974.

Acknowledgements

Originally presented and published as: Wright J, Marchese D. Briefing: Continuous monitoring and adaptive control: the 'smart' storm water

management solution. Proceedings of the Institution of Civil Engineers – Smart Infrastructure and Construction, 2018; 170(4): 86–89. https://doi.org/10.1680/jsmic.17.00017

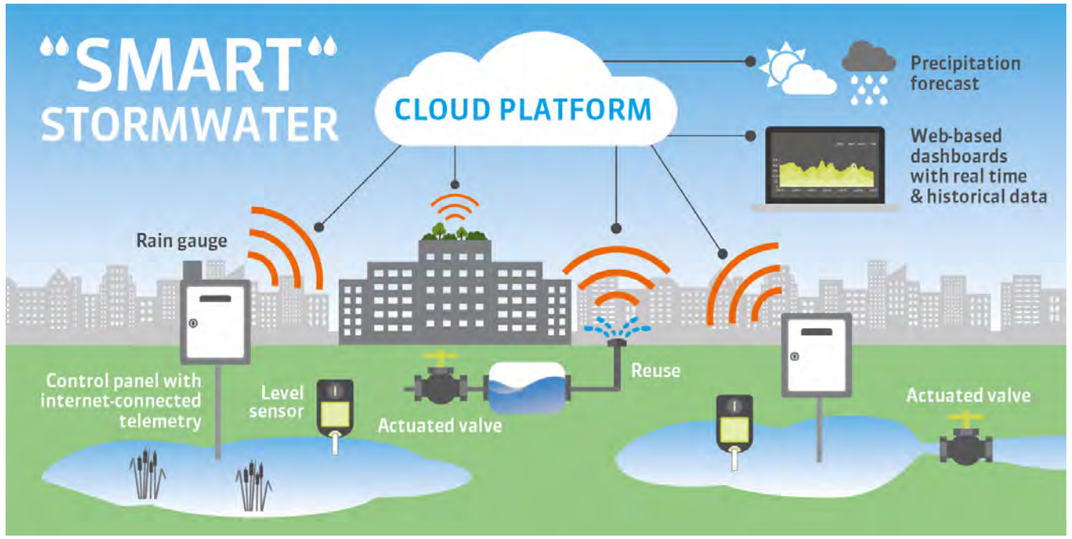

Figure 1: Continuous monitoring and adaptive control (CMAC) diagram. Information is integrated from field-deployed environmental and water-level sensors, actuated valves, telemetry-enabled control panels with cloud-based control systems, and real-time weather forecast data to directly monitor performance and actively control stormwater storage and flows. (Figure: Atkins)

Analysis of an Earth Fill Dam Affected by Potential Seepage From a Pressurized Power Tunnel Beneath

S. Mehdi Yousefi

PhD, PEng, PE
Senior Geotechnical Engineer
Clean Power
Vancouver, Canada

A. G. Dell
Lead Geotechnical Engineer
PEng
SNC-Lavalin
Vancouver, Canada
Tony.Dell@snclavalin.com.

Abstract

The purpose of this paper is to study the effect of seepage from a pressurized power tunnel excavated underneath an existing embankment dam. This study uses RS2 software to predict the seepage to the dam due to the potential water outflow from the power tunnel. Different alignments for the tunnel were studied and the final alignment was selected so as to minimize the potential increase of pore pressure in the dam foundation. Impact on the existing stability of the slopes and overloading the filter and drain layer capacity was also assessed.

The shotcrete liner and post grouting are designed as an effective liner for a rock mass with a hydraulic conductivity of 10-7 m/s or less. Measurement of the rock mass hydraulic conductivity was carried out using permeability tests in exploratory boreholes and probe holes during the tunnel construction. The results of analyses indicate a rock mass below the dam with a horizontal hydraulic conductivity (kh) of approximately 10-7 m/sec and a vertical hydraulic conductivity (kv) which varies from about 10-8 m/sec to about10-9 m/sec.

The results of the analyses indicate that the power tunnel in the proposed alignment during operation would slightly increase the pressure head on a potential slip surface in the dam foundation on the downstream side of the dam. However, slope stability calculations indicate that the factors of safety for the dam are not significantly changed.

Keywords

Dam Safety; Seepage; Power Tunnel

1. Introduction

This study uses RS2 software to predict the seepage to the underside of the earthfill dam (ED) due to the potential water outflow from the power tunnel beneath. This study confirms that exfiltration from the pressurized tunnel does not cause significant additional pore pressure on the base of the ED. The existing ED was constructed in the 1940s and upgraded in the 1980s because the dam was observed to have problems with potential piping of fine materials, settlement and local sloughing downstream.

Seepage analyses have been carried out in the proposed location of the power tunnel for three scenarios below.

Case 1: For the existing dam without a power tunnel
Case 2: For the power tunnel during the excavation
Case 3: For the power tunnel after pressurization

A 3D model of the dam and power tunnel is shown in Figure 1. For the purpose of comparison, all cases have the same boundary conditions and associated assumptions for hydraulic conductivity of the rock mass and overburden.

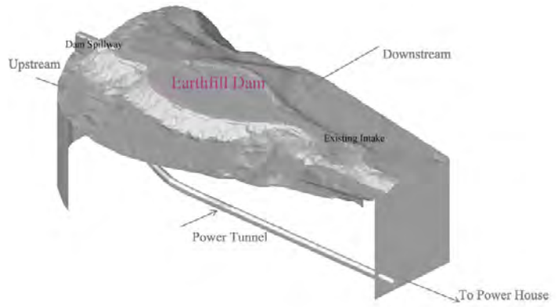

Figure 1. 3D Model of Dam and Power Tunnel

2. Current Groundwater Condition in the Earthfill Dam

The current groundwater conditions at the site are complex with two flow systems consisting of groundwater flow in the overburden sediments and a separate system within the bedrock. These two flow systems are somewhat isolated from each other due to the presence of a low vertical permeability layers overlaying the bedrock.

3. Stratigraphy

The foundation soils for the ED consist of glacial till, and interlayered sequence of clays, sands and silts. The stratigraphic section illustrates this sequence in the ED as shown in Figure 2.

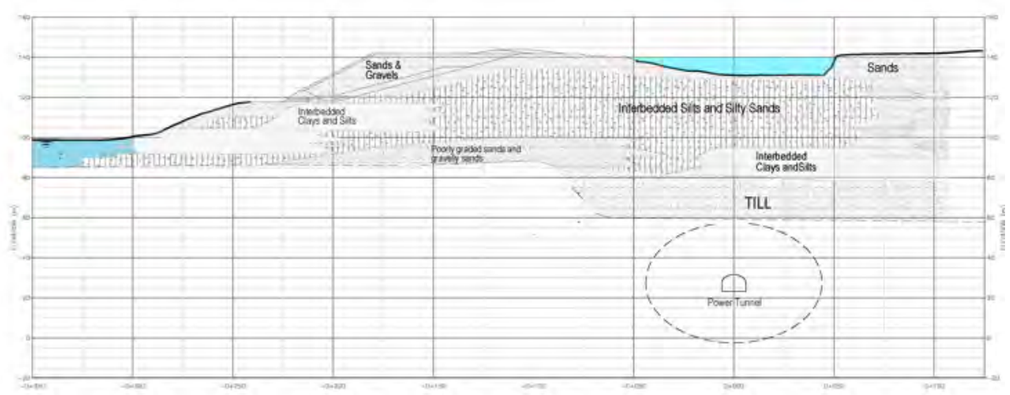

3.1 Overburden

Glacial till, silt and sand layers which overlies bedrock was estimated to have a horizontal hydraulic conductivity ranging from 10-8 m/s to 10-7 m/s.

3.2 Rock Mass

The bedrock along the tunnel alignment consisted of basalt that has been subjected to low grade metamorphism, but was generally fresh. Minor alteration (e.g. carbonate, epidote, chlorite) was observed on joints in some locations. An estimate of major joint sets was carried out prior the excavation of the power tunnel and three major joint sets namely two sub-vertical joint sets and one sub-horizontal joint set were identified based on logging data and Acoustic Televiewer (ATV) surveys collected from the boreholes located approximately at around the power tunnel.

The permeability of the rock mass around the power tunnel has been investigated using the data from packer tests done from the surface during the geotechnical investigation and in probe holes done during construction. The packer test results from the surface boreholes are summarized in Figure 3.

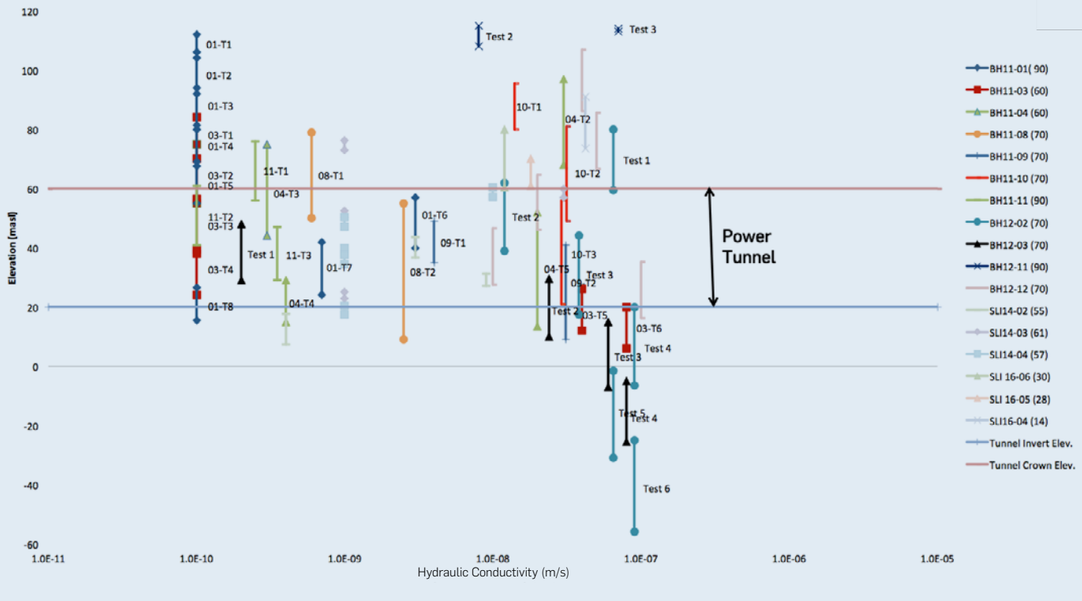

Figure 3. Hydraulic Conductivity Vs Elevation From Packer Tests in Exploratory Boreholes (2011, 2012, 2014, 2016 Data)

During construction of the power tunnel the observations suggest that the hydraulic conductivity in the horizontal direction is greater than in the vertical direction. Downward gradients were commonly observed in the site investigation surface drilled boreholes, which indicates that the bedrock has horizontal permeability greater than vertical permeability.

Figure 4 shows boreholes which were drilled to investigate permeability of the rock underneath of the dam. The result of the packer tests in the rock show a low permeablity rock mass. It is of note that the Packer test results in the faulted rock have lower permeability than the host rock.

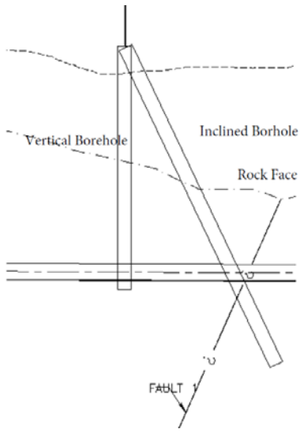

Figure 4. Sample Boreholes for Permeability Test

4. Methodology

For the initial calculations, the hydraulic conductivity for the basalt was assumed to be isotropic with a value of 10-7 m/sec. The assumed parameters for the overlying silt and sand layers and engineered fill materials are shown in Table 1 . The reservoir is assumed to be at maximum operation level Elevation 139.6 m and the creek/river level at Elevation 102.00 m. The tunnel shape was assumed to be circular in the analyses, which is assessed to be an acceptable approximation for the D-shaped tunnel for these seepage calculations.

Table 1. Hydraulic Conductivity Values Used in the RS2 Models for Overburden and Engineered Fill Material

							Overburden			
	Shell	Filter	Sand and Gravel	Slurry Wall	Jet Grouting	Rockfill	Lower Grey Silt	Interlayered Sand and Silt	Drain	Till Blanket
Hydraulic Conductivity kh (m/sec)	5E-6	1e-5	2e-5	7E-8	1e-8	2e-5	5e-8	1e-6	1e-3	5e-8
kv/kh	0.3	1	1	1	1	1	0.2	0.01	1	0.15

2D seepage analyses using the Finite Element software RS2 were carried out for four cross sections through the ED. The plan is shown in Figure 5 and the sections through the ED are shown in Figure 6, Figure 7 and Figure 8.

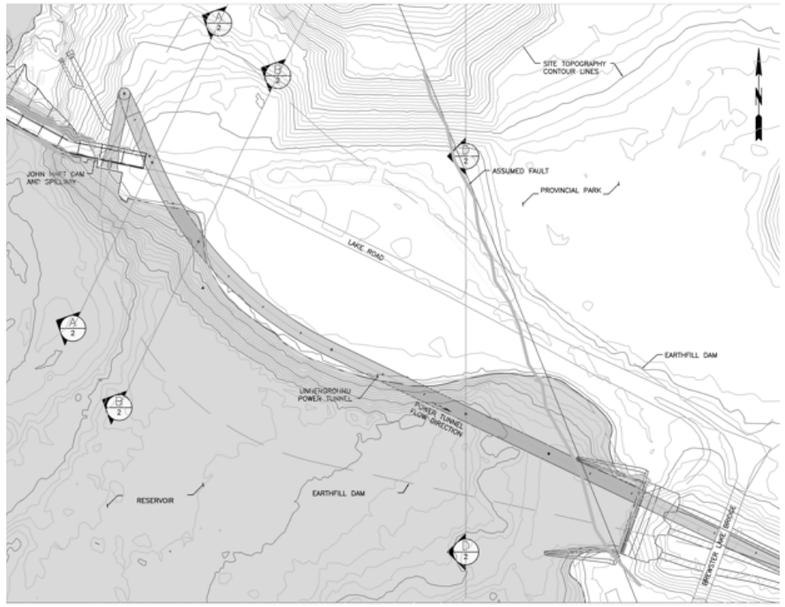

Figure 5. Plan of the Tunnel Under the Earthfill Dam

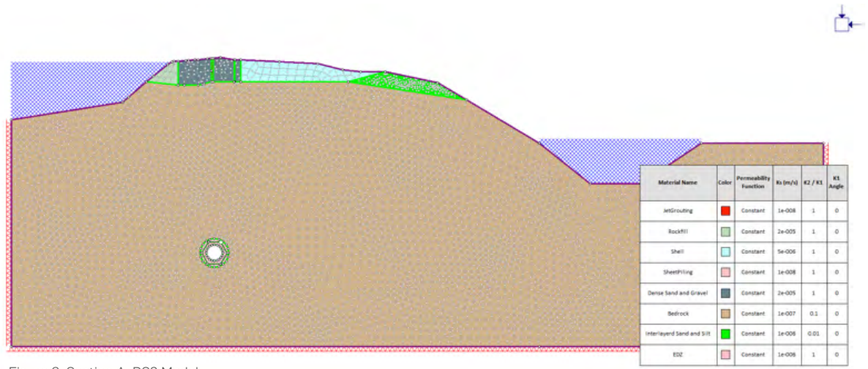

Figure 6. Section A, RS2 Model

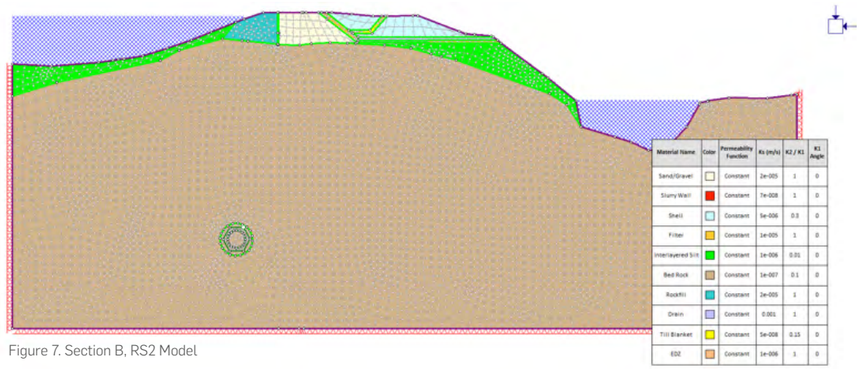

Figure 7. Section B, RS2 Model

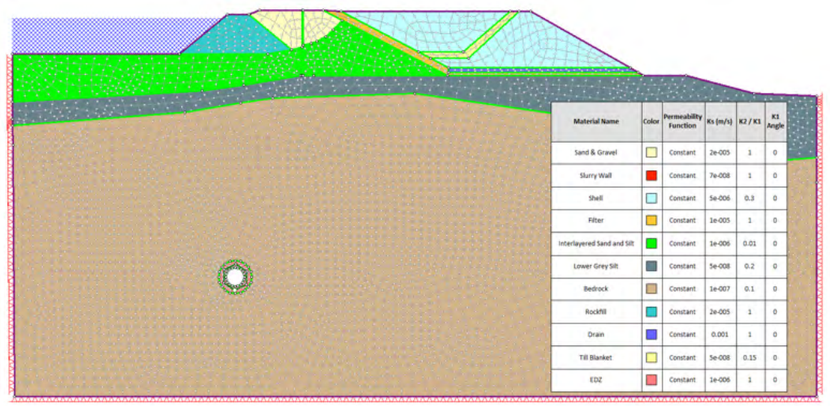

Figure 8. Section D, RS2 Model

5. Seepage Analyses for the Existing Dam Without the Power Tunnel

RS2 analysis for Sections A, B, and D were done using anisotropic permeability properties for the bedrock without the pressure tunnel. The analyses were carried out for a hydraulic conductivity in the horizontal direction (kh) equal to 1x10-7 m/s and the vertical hydraulic conductivity (kv) of 1x10-8 m/s.

The results are shown in Figure 9 to Figure 11. The results show a steady flow from the reservoir to the downstream pool and confirm the elevation measured in the downstream side of the dam.

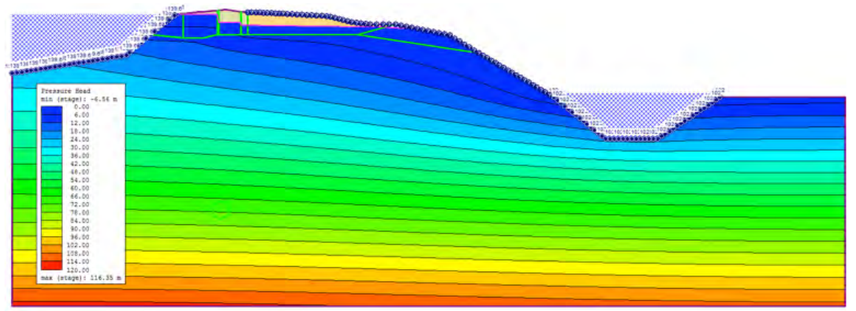

Figure 9. Section A, Pressure Head – Before Excavation, Bedrock Permeability Kh=1e-7 M/Sec, Kv=1e 8m/Sec

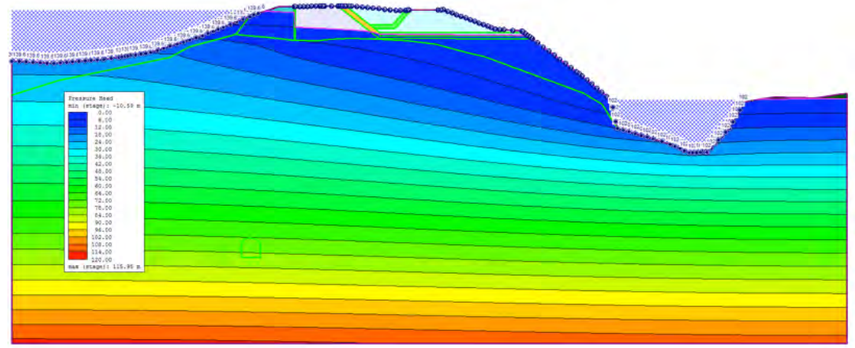

Figure 10. Section B, Pressure Head – Before Excavation, Bedrock Permeability Kh=1e-7 M/Sec, Kv=1e 8 M/Sec

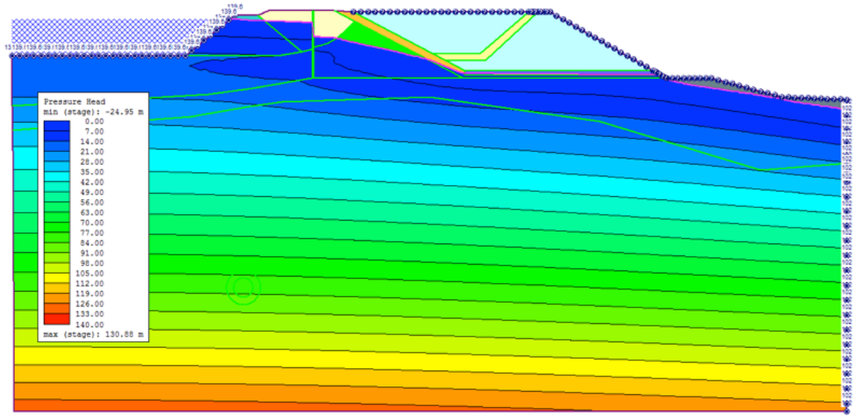

Figure 11. Section D, Pressure Head – Before Excavation, Bedrock Permeability Kh=1e-7m/Sec, Kv=1e-8 M/Sec

6. Seepage Analyses During the Power Tunnel Excavation

RS2 analyses were repeated after excavation of the power tunnel. The computed inflows to the power tunnel are shown in Table 2. The pore pressure distribution from these analyses for Sections A, B and D are given in Figure 12 to Figure 14. The results show the highest flow rate is 0.29 lit/min/m into the tunnel. The calculated values from the analyses are higher than the actual measured values during the tunnel excavation.

Table 2. Tunnel Discharge in to the Tunnel During Construction

Discharge into the Tunnel	Section A	Section B	Section D
Water Inflow (Lit/min/m)	0.28	0.27	0.29

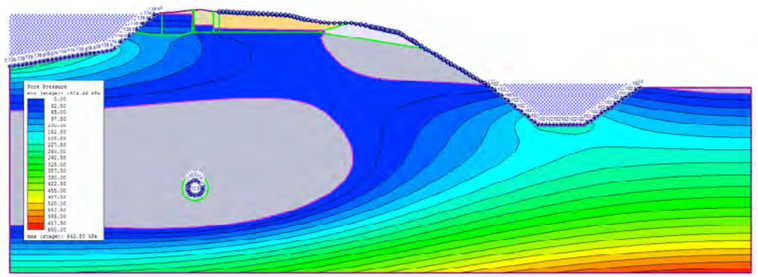

Figure 12. Section A, Seepage Flow Into the Power Tunnel, Bedrock Permeability Kh=1e-7 M/Sec, Kv=1e 8m/Sec

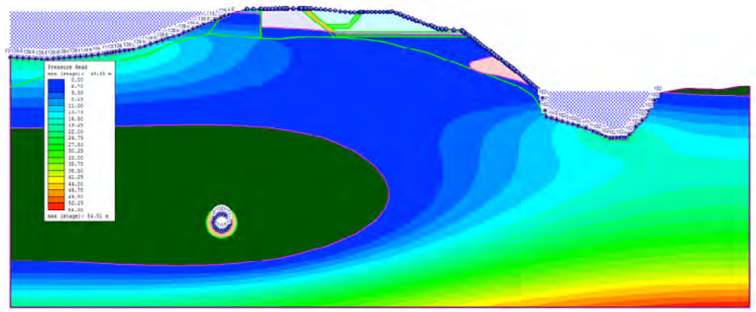

Figure 13. Section B, Seepage Flow Into the Power Tunnel, Bedrock Permeability Kh=1e-7 M/Sec, Kv=1e 8m/Sec

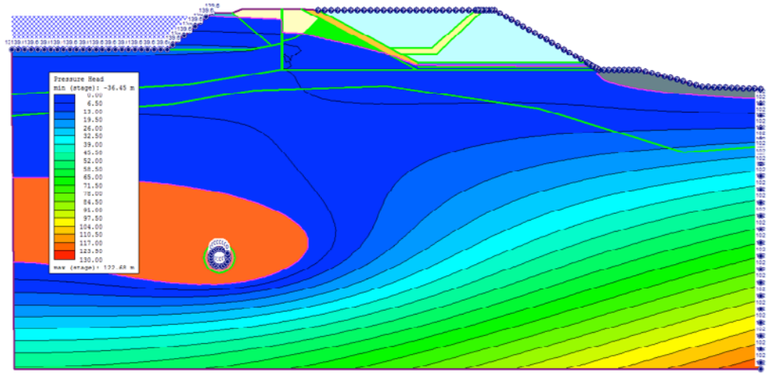

Figure 14. Section D, Seepage Flow Into the Power Tunnel, Bedrock Permeability Kh=1e-7 M/Sec, Ky=1e 8m/Sec

7. Seepage After Tunnel Pressurization

When the power tunnel is in operation the pressure head in the tunnel is assumed to be the same as the reservoir head. This increase in pressure head has the potential to increase the pressure at the rock-soil contact. A series of monitoring points were selected in the model at the dam downstream at the rock-soil contact to establish the maximum increase in the pressure head due to the power tunnel operation. The results from these analyses are summarized in Table 3 and the details of the results shown in Figure 15 to Figure 17.

Table 3. Maximum Pressure Head Excess at the Downstream Rock/Overburden Boundary of the Dam Assuming Anisotropic Permeability

Pressure Head Excess	Section A	Section B	Section D
Maximum Pressure Head Excess (m)	0.23	0.17	2.04

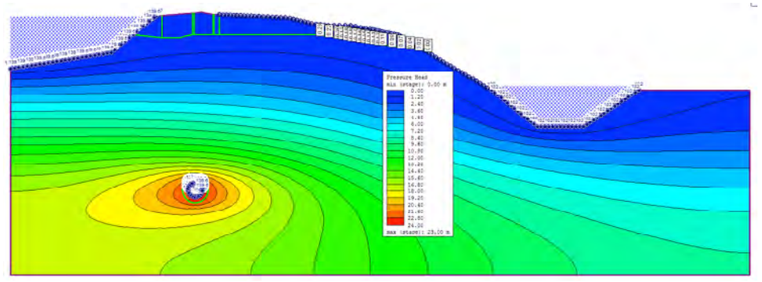

Figure 15. Section A, Excess Pressure Head, Bedrock Permeability Kh=1e-7 M/Sec, Kv=1e 8m/Sec

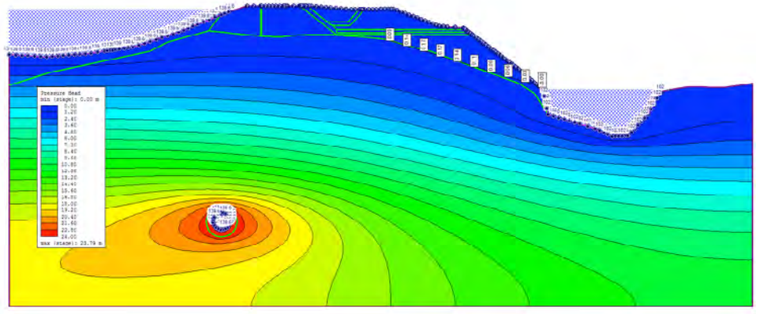

Figure 16. Section B, Excess Pressure Head, Bedrock Permeability Kh=1e-7 M/Sec, Kv=1e 8m/Sec

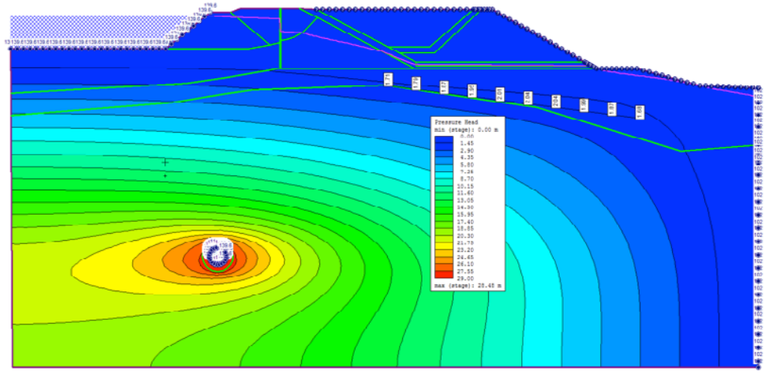

Figure 17. Section D, Excess Pressure Head, Bedrock Permeability Kh=1e-7 M/Sec, Kv=1e 8m/Sec

8. Pore Pressure Increase on the Sliding Surfaces

Two selected sections of the ED, namely Sections B and D were studied to estimate pore pressure increases along a potential sliding surface at the downstream side of the dam. Sections A and C are stable as there are no slope conditions on the downstream side of the dam. The results of the numerical study are plotted in Figure 18 and Figure 19.

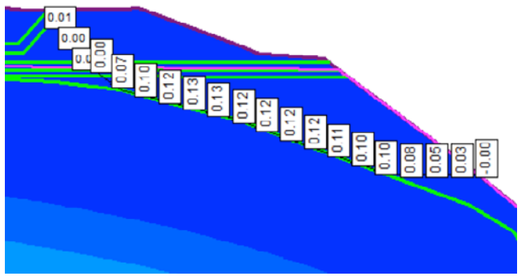

Figure 18. Pore Pressure Increase on the Sliding Surface of Section B, Anisotropic Rock Kh=1e 7 M/Sec, Kv=1e-8 M/Sec

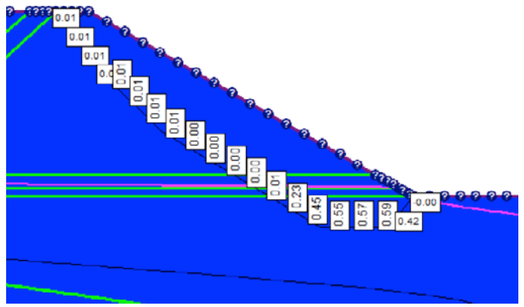

Figure 19. Pore Pressure Increase on the Sliding Surface of Section D, Anisotropic Rock Kh=1e 7m/Sec, Kv=1e-8 M/Sec

Figure 20 and Figure 21 present the pore pressure increase rate on the sliding face of the slope compare to the permeability value of the bedrock. The measured hydraulic conductivity during the tunneling showed that the excavation was largely done through tight rock. According to the packer tests data collected from probe holes during the excavation, it appears that the overall permeability in the rock is less than 1e-7 m/sec.

The calculations shows that, due to the pressurized tunnel, pore pressures at the downstream side of the dam on the potential sliding surface could increase up to 0.11 m for Section B and 0.6 m for Section D.

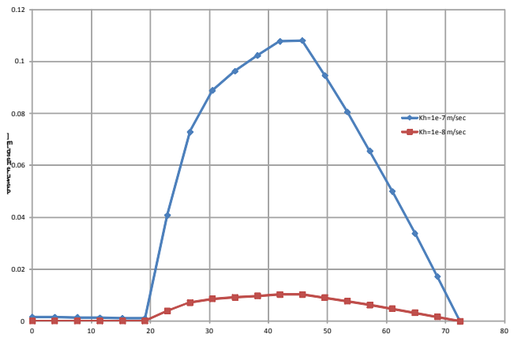

Figure 20. Comparison of the Pressure Head Excess on the Sliding Surface, Section-B Pressurized Tunnel, Kv=0.1 Kh

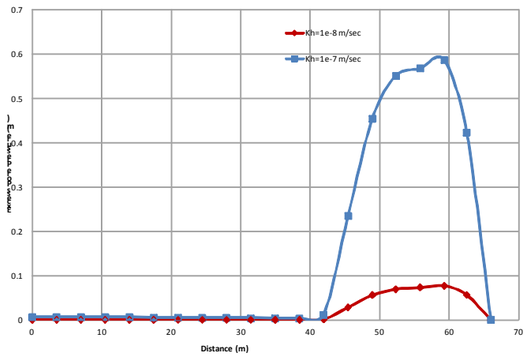

Figure 21. Comparison of the Pressure Head Excess on the Sliding Surface, Section-D Pressurized Tunnel, Kv=0.1 Kh

9. Piezometers

Observations of the responses of piezometers in the power tunnel bedrock within the ED zone, showed similar values to the numerical analyses: assuming rock with anisotropic hydraulic conductivity with kh=1e-7 m/sec and kv=1e-8 m/sec.

10. Conclusions

The results of these analyses indicate that seepage from the tunnel during operation using the proposed tunnel alignment will have limited impact on of the stability of the earthfill dam. The maximum pressure head increase will be 0.6 m on the critical sliding surface of the dam foundation downstream of the esrthfill dam at Section D.

The impact on the factor of safety of the earthfill dam due to the pressurized tunnel shows no significant difference before and after pressurization of the tunnel.

References

1. Design of Unlined and Lined Pressure Tunnels, Tunneling and Underground Space Technology, v4, n2, pp155-170, 1989, R.P. Benson.

2. Engineering Manual EM 1110-2-2104 (1992). Strength Design for Reinforced-Concrete Hydraulic Structures. Department of the Army, U.S. Army Corps of Engineers, Washington, DC 20314-1000.

3. Civil Engineering Guidelines for Planning and Designing Hydroelectric Developments, ASCE/EPRI, Volume 2, Waterways, Chapter 3.

4. Barton, Lien and Lunde, “Engineering Classifications of Rock Masses for the Design of Tunnel Support”, Journal of the International Society for Rock Mechanics, Vol. 6, No. 4, 1974

5. Updating the Q-system for NTM by Grimstad and Barton, Proceedings Int. Symp. On Sprayed Concrete - Modern Use of Wet Mix Sprayed Concrete for Underground Construction, Fagernes, 1993.

6. E. Broch “Unlined High Pressure Tunnels in Areas of Complex Topography”, Water Power, 1984.

7. T.L. Brekke, B.D. Ripley (1985): Leakage from pressure tunnels and shafts. Waterpower. In: Roluti, M. J. (ed.) ASCE, New York, pp 1228–1237.

8. Barton, N.R. and Bandis, S.C., Review of Predictive Capabilities of JRC-JCS model in Engineering Practice. In Rock Joints, Proc. Int. Symp. on Rock Joints, Loen, Norway, (ed. N. Barton and O. Stephansson), Rotterdam: Balkema, 1990.

9. ASTM D4879-08 “Standard Guide for Geotechnical Mapping of Large Underground Openings in Rock”.

10. Barton, N and Grimstad, E, “Tunnel and Cavern Support Selection in Norway, based on Rock Mass Classification with the Q-System”. Publication No. 23 Norwegian Tunnelling Society pp 45 – 77. 2014 Design Guidelines for Pressure Tunnels and Shafts, EPRI AP-5273.

Acknowledgements

The authors thank the Management of SNC-Lavalin for their approval and encouragement to publish this paper.

Originally presented and published as: Yousefi SM, Dell AG. Analysis of an Earth Fill Dam Affected by Potential Seepage from a Pressurized Power Tunnel Beneath. 38th Annual Conference of the United States Society on Dams, Apr 30-May 3, 2018: Miami, USA.

SNC·LAVALIN

snclavalin.com

Contact information
Akshaye Sikand
Manager, Knowledge Management
Akshaye.Sikand@snclavalin.com

4745_SL18